DTIC FILE COPY

UNCLASSIFIED

AD-A196 022

(2)

REPORT DOCUMENTATION PAGE

1a. REPORT SECURITY CLASSIFICATION: UNCASSIFIED	1b. RESTRICTIVE MARKINGS
2a. SECURITY CLASSIFICATION AUTHORITY	3. DISTRIBUTION/AVAILABILITY OF REPORT: Approved for public release, distribution unlimited
2b. DECLASSIFICATION/DOWNGRADING SCHEDULE	
4. PERFORMING ORGANIZATION REPORT NUMBER(S)	5. MONITORING ORGANIZATION REPORT NUMBER(S): AFOSR-TR- 88-0548
6a. NAME OF PERFORMING ORGANIZATION: Wayne State University; 6b. OFFICE SYMBOL (If applicable)	7a. NAME OF MONITORING ORGANIZATION: AFOSR
6c. ADDRESS (City, State and ZIP Code): College of Liberal Arts, Dept of Physics and Astronomy, Detroit, Michigan 48202	7b. ADDRESS (City, State and ZIP Code): same as 8c.
8a. NAME OF FUNDING/SPONSORING ORGANIZATION: AFOSR; 8b. OFFICE SYMBOL (If applicable): NP	9. PROCUREMENT INSTRUMENT IDENTIFICATION NUMBER: AFOSR-84-0143
8c. ADDRESS (City, State and ZIP Code): Bldg 410, Bolling AFB, Wash D.C. 20332-6448	10. SOURCE OF FUNDING NOS.: PROGRAM ELEMENT NO. 61102F; PROJECT NO. 2301; TASK NO. A7; WORK UNIT NO.
11. TITLE (Include Security Classification): "DISSOCIATIVE ELECTRON ATTACHMENT TO ROVIBRATIONALLY EXCITED MOLECULES" (U)	
12. PERSONAL AUTHOR(S): Wadehra	
13a. TYPE OF REPORT: FINAL; 13b. TIME COVERED: FROM 84/08/01 TO 87/8/31	14. DATE OF REPORT (Yr., Mo., Day); 15. PAGE COUNT: 135
16. SUPPLEMENTARY NOTATION	
17. COSATI CODES: FIELD / GROUP / SUB. GR.	18. SUBJECT TERMS (Continue on reverse if necessary and identify by block number): Rovibrationally, oscillators, Resonant

DTIC ELECTE MAY 18 1988 S E D

19. ABSTRACT (Continue on reverse if necessary and identify by block number)

The primary aim of our project has been to investigate the role played by the initial rovibrational excitation of a molecule in enhancing the cross sections and, therefore, the rates of dissociative electron attachment to the molecule. An echancement of the attachment rate results in the enhancement of the production of negative ion beams. The processes of dissociative electron attachment and of resonant vibrational excitation are complementary processes as the intermediate resonant anion state of the molecule, formed by electron impact, either can autodetach the electron or can dissociate itself. Therefore, as a further part of the present investigations we have explored excitation of the molecule. Our first project was to study the effect of initial vibrational excitation on the ratee of production of negative atomic lithium ions via the process of dissociative electron attachment to lithium dimers. The rate is enhanced by almost an order of magnitude if the molecule is initially vibrationally excited; however, the effect is certainly more dramatic for hydrogen

20. DISTRIBUTION/AVAILABILITY OF ABSTRACT: UNCLASSIFIED/UNLIMITED ☒ SAME AS RPT. ☒ DTIC USERS ☒	21. ABSTRACT SECURITY CLASSIFICATION: UNCLASSIFIED
22a. NAME OF RESPONSIBLE INDIVIDUAL: LT COLONEL BRUCE L. SMITH	22b. TELEPHONE NUMBER (Include Area Code): (202) 767-4907; 22c. OFFICE SYMBOL: NP

DD FORM 1473, 83 APR EDITION OF 1 JAN 73 IS OBSOLETE.

UNCLASSIFIED
SECURITY CLASSIFICATION OF THIS PAGE

molecules than for lithium dimers. In the second project we developed a simple model for the resonant vibrational excitation of a molecule. In this model the potential energy curves of the electronic states of the molecule and of its resonant anion are replaced by those of two simple harmonic oscillators of different frequencies and the width of the resonance is taken to be constant.

AFOSR-TR- 88-0548

THIRD AND FINAL ANNUAL TECHNICAL REPORT

Project Title: Dissociative Electron Attachment to Rovibrationally Excited Molecules.

Grant Number: AFOSR-84-0143

Principal Investigator: Professor J. M. Wadehra
Department of Physics and Astronomy
Wayne State University

Grant Period: September 1, 1984 - August 31, 1987.

88 6 16 130

ABSTRACT

The primary aim of our project has been to investigate the role played by the initial rovibrational excitation of a molecule in enhancing the cross sections and, therefore, the rates of dissociative electron attachment to the molecule. An enhancement of the attachment rate results in the enhancement of the production of negative ion beams. The processes of dissociative electron attachment and of resonant vibrational excitation are complementary processes as the intermediate resonant anion state of the molecule, formed by electron impact, either can autodetach the electron or can dissociate itself. Therefore, as a further part of the present investigations we have explored the contribution of the resonant state to the cross sections for vibrational excitation of the molecule. Our first project was to study the effect of initial vibrational excitation on the rate of production of negative atomic lithium ions via the process of dissociative electron attachment to lithium dimers. The rate is enhanced by almost an order of magnitude if the molecule is initially vibrationally excited; however, the effect is certainly more dramatic for hydrogen molecules than for lithium dimers. In the second project we developed a simple model for the resonant vibrational excitation of a molecule. In this model the potential energy curves of the electronic states of the molecule and of its resonant anion are replaced by those of two simple harmonic oscillators of different frequencies and the width of the resonance is taken to be constant. Simple recursion relations among excitation amplitudes are used for evaluation of vibrational excitation cross sections for any transition.

The principal aim of the investigations under the present Grant (number AFOSR-84-0143) has been to study the effect of vibrational excitation of a molecule (say, AB) on the production of light negative ion beams (for example, beams of Li^-, H^-, D^-, etc.) via the process of dissociative electron attachment. The intermediate resonant state AB^-, which as one possibility leads to dissociative attachment ($AB^- \rightarrow A + B^-$), can also lead to vibrational excitation ($AB^- \rightarrow AB(v_f) + e$) following the autodetachment of the electron. Thus the processes of dissociative attachment and resonant vibrational excitation are best investigated as two complementary projects of the same endeavor[1]. During the tenure of the Grant (September 1, 1984 - August 31, 1987) we concentrated on various different projects. The first project involved the investigations of the electron attachment to the lithium dimers. The second project concerned determination of the resonant as well as nonresonant vibrational excitation of lithium dimers. For the resonant vibrational excitation we developed a simple and reasonable model which allowed rapid evaluation of the vibrationally inelastic and superelastic amplitudes using recursion relations.

The details of various investigations carried out during the three years of our endeavor are as follows:

Dissociative Electron Attachment to Lithium Dimers

Previous theoretical[2] and experimental[3] studies have shown that in the case of molecular hydrogen the cross sections for dissociative attachment are strongly enhanced if the molecule H_2 is initially rovibrationally excited. In order to ascertain whether similar enhancement of attachment cross sections occurs for other molecules we investigated the process of electron attachment to lithium dimers which are isovalent with the molecular hydrogen. It is found that analogous to molecular hydrogen the rate of electron attachment to lithium dimers by the process of dissociative attachment is strongly enhanced if the dimers are initially vibrationally excited.

The fact that both the lithium dimers and the hydrogen molecules are isovalent leads to similarities between the two molecules as far as the configurations of the electronic states are concerned[4]. For example, the lowest electronic states of the negative molecular ions with configurations $(1\sigma_g)^2 (1\sigma_u)^2 (2\sigma_g)^2 (2\sigma_u)$ for Li_2^- and $(1\sigma_g)^2 (1\sigma_u)$ for H_2^- have similar symmetry, namely, $^2\Sigma_u^+$. However, unlike hydrogen molecule, the lithium dimers possess a large polarizability and a weak bond strength which makes the ground state of Li_2^- a true bound state. In the case of H_2^-, on the other hand, the $^2\Sigma_u^+$ state is a true bound state only for internuclear separations R larger than 2.9 a.u. and an autodetaching state for smaller values of R. The first excited state with symmetry $^2\Sigma_g^+$ and configurations $(1\sigma_g)^2 (1\sigma_u)^2 (2\sigma_g) (2\sigma_u)^2$ for Li_2^- and $(1\sigma_g) (1\sigma_u)^2$ for H_2^- is a partly Feshbach and a partly shape resonance in nature for both molecular anions. This resonance is the lowest-lying resonance of Li_2^- and because of its nature (namely Feshbach) the resonance is expected to have a small width and a long lifetime. This resonant state is essentially responsible for dissociative electron attachment to lithium dimers.

Potential curves of the electronic states of Li_2 and Li_2^- relevant to the attachment process are shown in Figure 1. Due to its autodetaching nature the A $^2\Sigma_g^+$ electronic state of Li_2^- exhibits a complex potential energy curve whose real part along with the potential curve of the ground $^1\Sigma_g^+$ electronic state of the neutral Li_2 is shown in the Figure. The two curves cross at R = 6.5 a.u. so that only for internuclear separations smaller than 6.5 a.u. the A state is autodetaching. Detailed orbital optimized CI calculations[4] reveal that the X and the A states have their respective potential minimum at 5.1

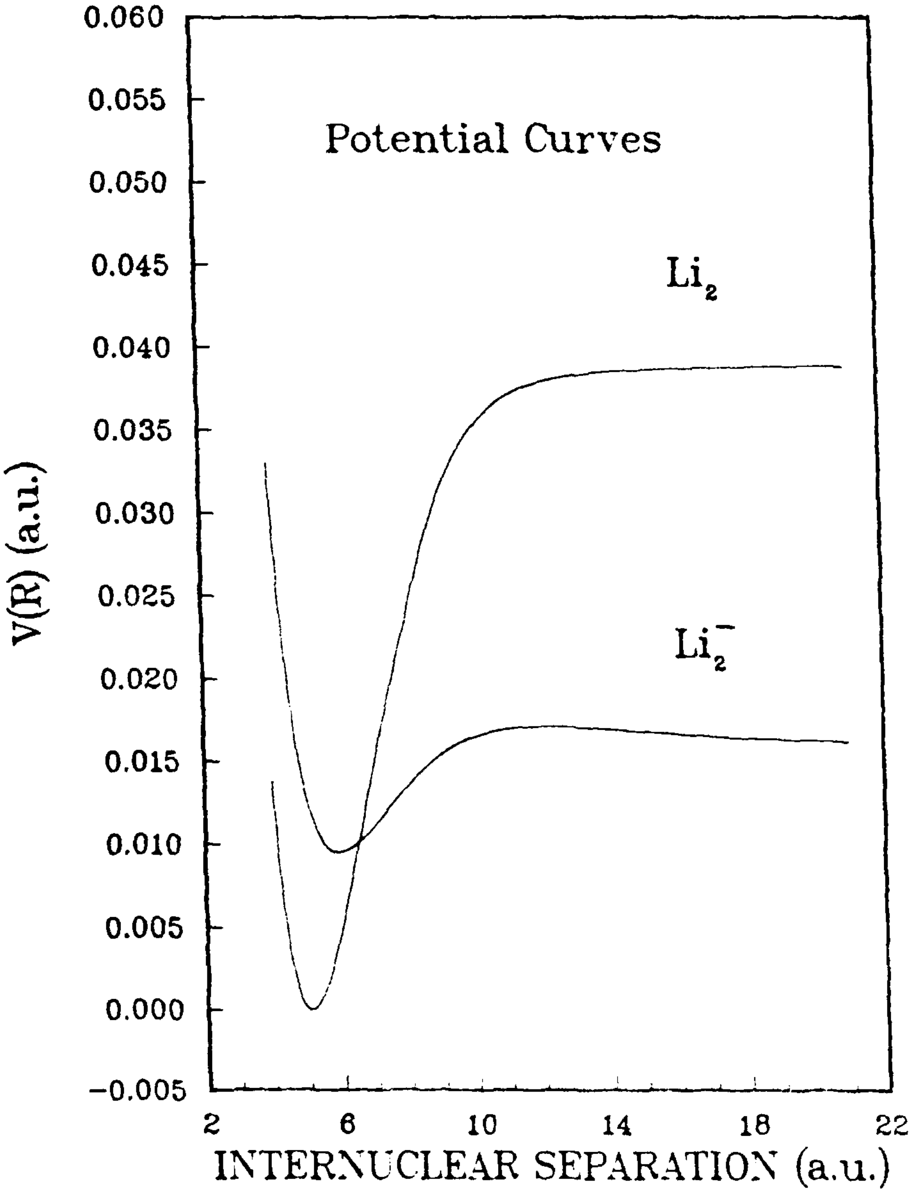

Figure 1. Potential curves of the ground $X\,^1\Sigma_g^+$ electronic state of Li_2 and the lowest $A\,^2\Sigma_g^+$ resonant state of Li_2^-.

a.u. and 5.9 a.u. The imaginary part of the complex potential energy curve of the A state of Li_2^- is related to the width of this resonant state. For internuclear separations smaller than 6.5 a.u. this resonant state can autodetach into Li_2 + e. In this autodetachment process [$^2\Sigma_g^+ \rightarrow {}^1\Sigma_g^+ + e$] the lowest contributing partial wave is an s-wave. Thus Wigner's threshold law for the width of this state implies $\Gamma(R) = c.k(R)$, where k(R) is the wave number of the electron emitted at internuclear separation R and c is a constant. To obtain this constant c the fully optimized orbital exponents of the CI wave functions were smoothly extrapolated from the variationally stable region ($R \gtrsim 6.5$ a.u.) into the autodetaching region ($R \lesssim 6.5$ a.u.) to obtain the matrix elements coupling the discrete and the continuum states. These matrix elements are related to the autodetachment width by Fermi's golden rule. This procedure yielded c = 0.0143 a.u. Thus the width of the A state of Li_2^- , which is primarily responsible for dissociative electron attachment to lithium dimers, as a function of internuclear separation is given, in atomic units, by $\Gamma(R) = 0.0143.k(R)$ and is shown in Figure 2. The small value of the width is characteristic of the Feshbach nature of the resonance.

The similarities between lithium dimers and hydrogen molecules suggest that theoretical approaches used successfully in the past for investigating the cross sections and rates for dissociative electron attachment to H_2 can be employed for similar investigations for Li_2. Thus local width resonant scattering theory is used for obtaining the cross sections as a function of the incident electron energy and the corresponding rates as a function of the electron temperature T (or, equivalently, the average electron energy $\bar{E}$ = 3kT/2.) for dissociative electron attachment to Li_2, $e + Li_2 \rightarrow Li + Li^-$. The contribution of only the $^2\Sigma_g^+$ resonance of Li_2^- is taken into account for

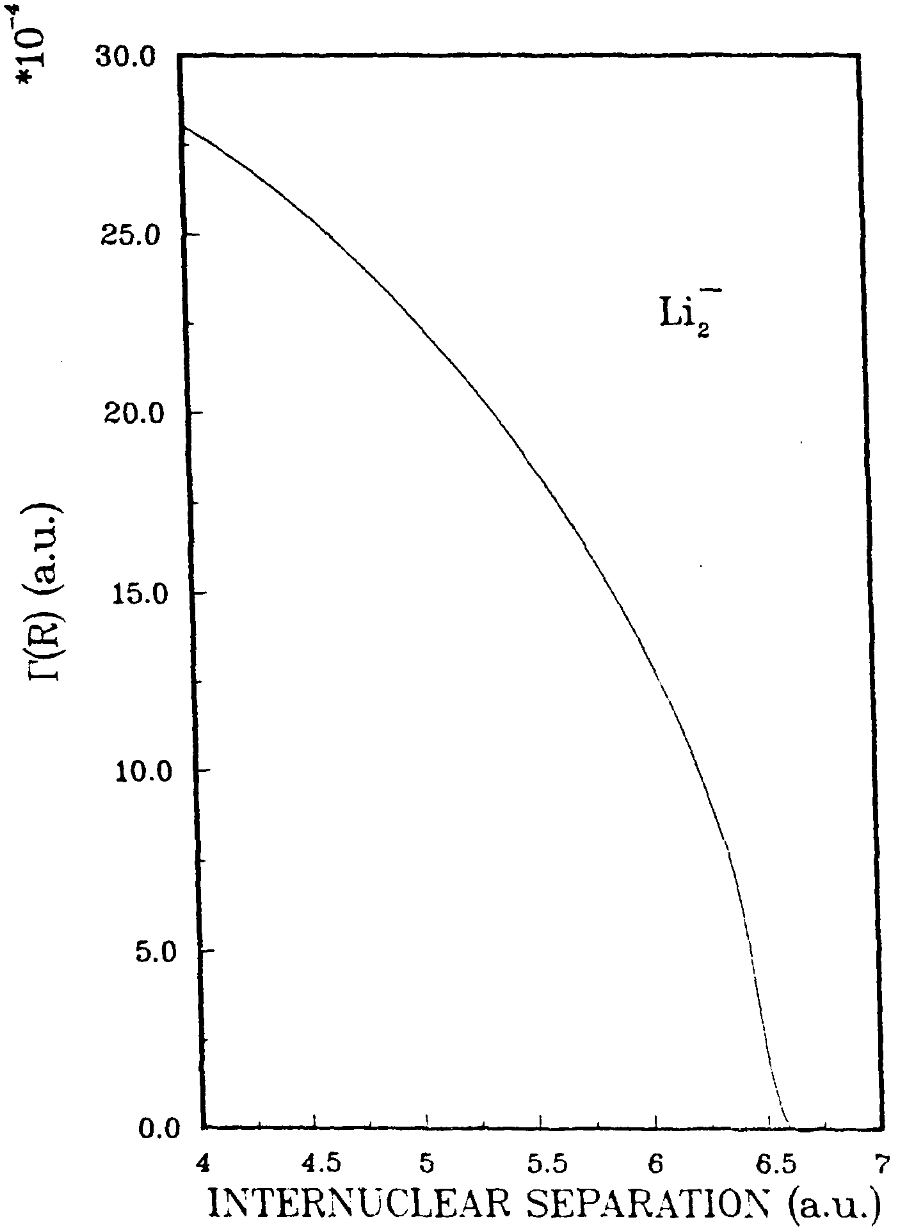

Figure 2. The width of the $A\,^2\Sigma_g^+$ resonant state of Li_2^- as a function of the internuclear separation R.

calculating the attachment cross sections. Figure 3 shows the results of such a calculation. The structure near the peak of the cross sections, as observed in this Figure, is possibly an artifact of the limited range of internuclear separations over which the resonant nuclear wave function is extended. Analogous to molecular hydrogen the cross sections for dissociative electron attachment to lithium dimers, as a function of the incident electron energy, show a rapid increase leading to a peak in the cross section, followed by a gradual decrease. The difference, however, is that the cross section peak is right at the energetic threshold in the case of hydrogen while the attachment cross section in the case of lithium peaks at an energy somewhat above the energetic threshold. This difference in behavior could be explained in terms of the Franck-Condon factors relating the vibrational levels of the neutral and the anion electronic states.

First part of the calculations involved computation of the energy values and the corresponding wave functions of various vibrational levels of the lithium dimers. Highly accurate potential curves of Li_2 and Li_2^- are available in published literature[4]. The energy values for various vibrational levels using these potential curves agree quite favorably, as shown in the Table I below, with the experimental energy values.

Recent measurements[6] of the rate constant k(T) for dissociative electron attachment to highly vibrationally excited lithium dimers indicate that this rate for thermal electrons is about $10^{-8} cm^3 sec^{-1}$. In order to convert the present attachment cross sections into attachment rates the cross sections are fitted to a simple analytical form:

$$\sigma_{DA}(E) = \sigma_{peak} \cdot \exp\{-(E-E_{peak})/E_o\} \qquad (1)$$

where σ_{peak} is the peak attachment cross section and E_o is a constant. Using this analytical form for the attachment cross sections it is possible to

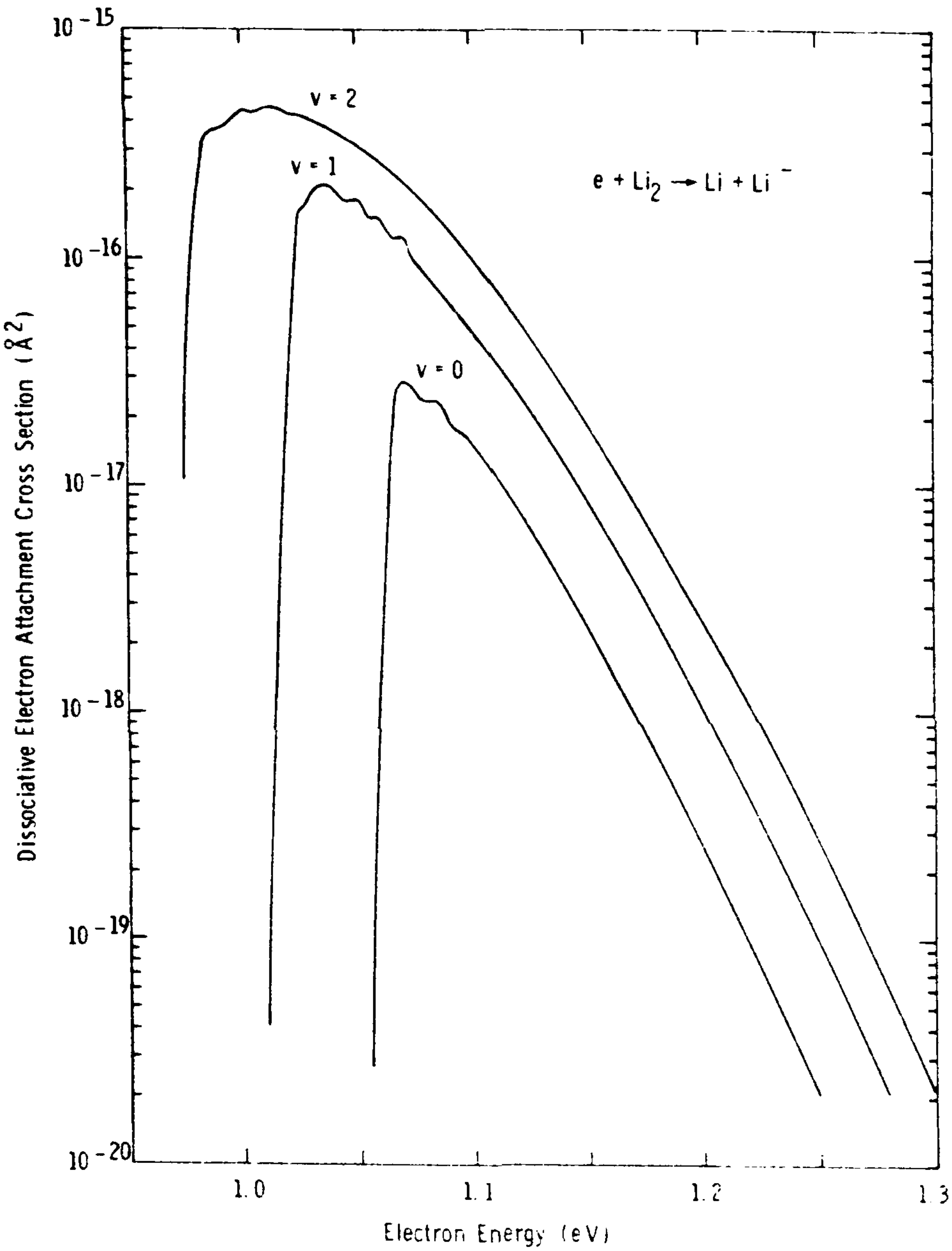

Figure 3. Cross sections for dissociative electron attachment to various vibrational levels of Li_2 as a function of the electron energy.

obtain the attachment rates as well in an analytical form if a Maxwellian distribution is assumed for the electron energies. The attachment rate as a function of the electron temperature is then given by

$$k(\bar{E}) = \left[\frac{27\bar{E}}{\pi m}\right]^{\frac{1}{2}} \sigma_{peak} \cdot \exp(-3E_{peak}/2\bar{E}) \left[1 + \frac{3E_{peak}}{2\bar{E}} + \frac{E_{peak}}{E_o}\right]\left[\frac{3}{2} + \frac{\bar{E}}{E_o}\right]^{-2} . \quad (2)$$

The average electron energy $\bar{E}$ is related to the electron temperature T by $\bar{E}$ = 3kT/2.

It is observed that the cross sections as well as the rates of Li^- formation are enhanced if the molecule Li_2 is initially vibrationally excited. The factors by which the peak attachment cross sections are enhanced, on vibrationally exciting the lithium molecule initially, are summarized and compared with the corresponding factors[7] for H_2 in the Table II below.

The reason for enhancement of the peak attachment cross section is that, as the internal energy of the molecule is initially increased via vibrational excitation, the range of internuclear separations R over which electron capture occurs is increased due to an increased vibrational amplitude.

Finally, the rates of electron attachment to Li_2 (that is, the rates of production of Li^- beams) are calculated as a function of the electron temperature T using Eq.(2) and are shown in Figure 4. The rate is as low as 10^{-11} $cm^3 sec^{-1}$ when the molecule is in its lowest vibrational level and the rate increases by almost an order of magnitude for each quantum of vibrational excitation of the molecular Li_2. It is thus plausible that the total attachment rate can approach the experimental value of 10^{-8} $cm^3 sec^{-1}$ as the initial excitation of the molecule is raised to the v = 10 level. The enhancement of the attachment rate, which is a direct consequence of the

TABLE I. Vibrational energy levels of Li_2.

Vibrational level (v) of Li_2	Energy value (eV)	
	Present calculation	Experimental value[5]
0	0.02170	0.02170
1	0.06459	0.06463
2	0.10683	0.10691
3	0.14836	0.14853
4	0.18914	0.18950
5	0.22910	0.22980
6	0.26806	0.26943
7	0.30556	0.30838

TABLE II. Enhancement factors for electron attachment to Li_2.

Initial vibrational level, v, the molecule is in.	Factor by which the peak attachment cross section is enhanced over that for v=0.		
	Li_2	H_2 (theory)[2]	H_2 (experiment)[3]
1	7.4	32.5	30 ± 10
2	16.4	465	500 ± 175

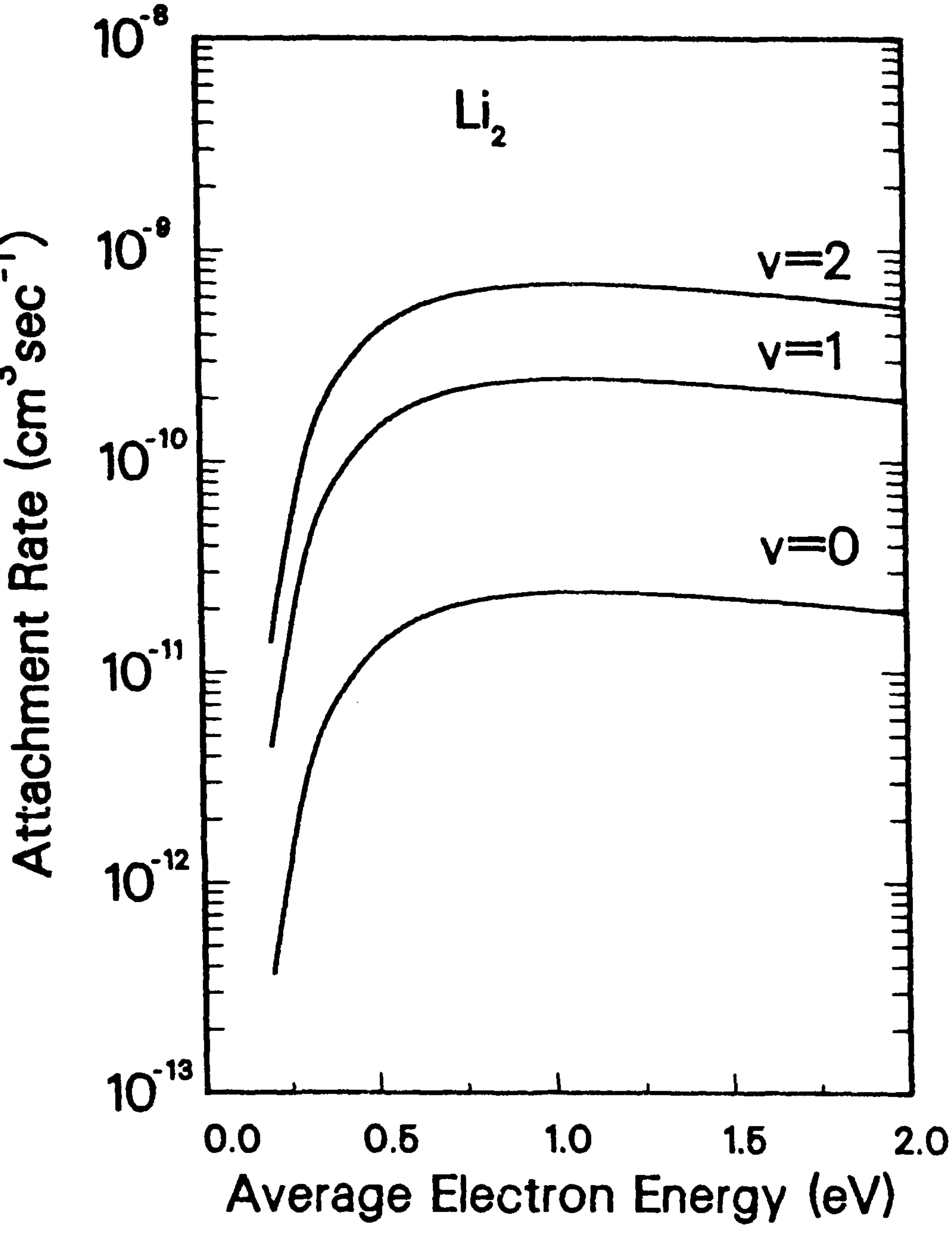

Figure 4. Rates of dissociative electron attachment to various vibrational levels of Li_2 as a function of the average electron energy $\bar{E}$ ($\bar{E}$ = 3kT/2).

TABLE III. Rates of dissociative electron attachment to vibrationally excited lithium dimers at various electron temperatures T. $\bar{E}$ is the average electron energy and v refers to the vibrational level of Li_2.

$\bar{E}$ = 3kT/2 (eV)	Attachment rate (in $cm^3 sec^{-1}$) v = 0	v = 1	v = 2
0.1	.285(-15)	.432(-14)	.157(-13)
0.2	.368(-12)	.445(-11)	.139(-10)
0.3	.311(-11)	.351(-10)	.104(-9)
0.4	.796(-11)	.869(-10)	.252(-9)
0.5	.130(-10)	.139(-9)	.399(-9)
0.6	.171(-10)	.181(-9)	.514(-9)
0.7	.201(-10)	.211(-9)	.596(-9)
0.8	.221(-10)	.230(-9)	.647(-9)
0.9	.233(-10)	.241(-9)	.677(-9)
1.0	.239(-10)	.246(-9)	.689(-9)
1.1	.241(-10)	.247(-9)	.690(-9)
1.2	.240(-10)	.245(-9)	.684(-9)
1.3	.236(-10)	.241(-9)	.671(-9)
1.4	.232(-10)	.236(-9)	.656(-9)
1.5	.226(-10)	.230(-9)	.638(-9)
1.6	.220(-10)	.223(-9)	.619(-9)
1.7	.213(-10)	.216(-9)	.599(-9)
1.8	.207(-10)	.209(-9)	.579(-9)
1.9	.200(-10)	.202(-9)	.559(-9)
2.0	.193(-10)	.195(-9)	.540(-9)

enhancement of the attachment cross section, is expected for any distribution of the electron energies. It is to be noted that for the isovalent molecule H_2 as well the maximum predicted rate for electron attachment via the process of dissociative attachment is[7] about 10^{-8} $cm^3 sec^{-1}$.

Analogous to molecular hydrogen, the lithium dimers exhibit an enhancement of the cross sections as well as of the rates of dissociative electron attachment if they are vibrationally excited. Detailed calculations have been carried out only for the lowest three vibrational levels of the dimers. In the immediate future these calculations will be extended to higher vibrational levels upto and including the endoergic regime. Experimental observations[6] of rates of electron attachment to lithium indicate that this rate can be as high as 10^{-8} $cm^3 sec^{-1}$ when the molecule Li_2 is in the vibrational level $v = 10$.

In the case of molecular hydrogen it has been established that the rotational excitation of the molecule also aids in the enhancement of the electron attachment rate; however, the enhancement factor is larger for initial vibrational excitation than for initial rotational excitation. Recent experimental observations[6] on the electron attachment to lithium dimers, on the other hand, seem to suggest that initial rotational excitation plays little role in controlling the attachment to Li_2. A theoretical investigation of the effect of initial rotational excitation on the rate of Li^- formation via the process of dissociative electron attachment to Li_2 will be made within the resonance scattering model.

Resonant Vibrational Excitation of Molecular Lithium

We have developed[8] a simple and reasonable model for resonant vibrational excitation of molecules. In this model the potential curves of the molecule and of its resonant anion state are replaced by those of one-dimensional simple harmonic oscillators of different frequencies and curvatures and the width of the resonance is taken to be constant. The model obviously works best for excitation of low lying levels. A schematic representation of the potential energy curves of an arbitrary molecule AB and of its resonant anion AB^- by linear harmonic oscillators is shown in Figure 5. In the earlier parts of our investigations we noted that for the case of equal frequency oscillators it is possible to obtain recursion relations among the excitation amplitudes. However, on realizing that the origin of the recursion relation among amplitudes, for the equal frequency case, is really a similar relation among the corresponding Franck-Condon factors, it became natural to investigate[9] in detail the recursion relations among the Franck-Condon factors for a two-center harmonic oscillator system. Using these recursion relations of two-center harmonic oscillator matrix elements we have been able to obtain recursion relations among the resonant vibrational excitation amplitudes even when the frequencies of the two harmonic oscillators are unequal. If the amplitude, $A(m\rightarrow n)$, for excitation from the initial level with vibrational quantum number m to the final level with vibrational quantum number n is written as

$$A(m\rightarrow n;\varepsilon) = -\frac{2\pi}{\omega_-}\left(\frac{\Gamma^2}{k_i k_f}\right)^{1/2} a(m\rightarrow n;\varepsilon)$$

then $a(m\rightarrow n)$ satisfies[8] the following recursion relations:

$$\begin{aligned}&[2n(\omega^2+\omega_-^2)-4\omega\omega_-(Q+1)+(\omega+\omega_-)^2+\frac{2\omega\omega_-^2}{\omega_0}]\,a(m\rightarrow n;\varepsilon)+4\omega\omega_-\delta_{m,n}\\&-2\omega_-^2(2\omega/\omega_0)^{1/2}\left[(n+1)^{1/2}a(m\rightarrow n+1)+n^{1/2}a(m\rightarrow n-1;\varepsilon)\right]\\&-(\omega^2-\omega_-^2)\left\{[(n+1)(n+2)]^{1/2}a(m\rightarrow n+2;\varepsilon)+[n(n-1)]^{1/2}a(m\rightarrow n-2;\varepsilon)\right\}=0\end{aligned}$$

with $\quad Q = [\varepsilon - \delta E + m\omega + (\omega - \omega_-)/2 - \Delta + i\Gamma/2]/\omega_-$.

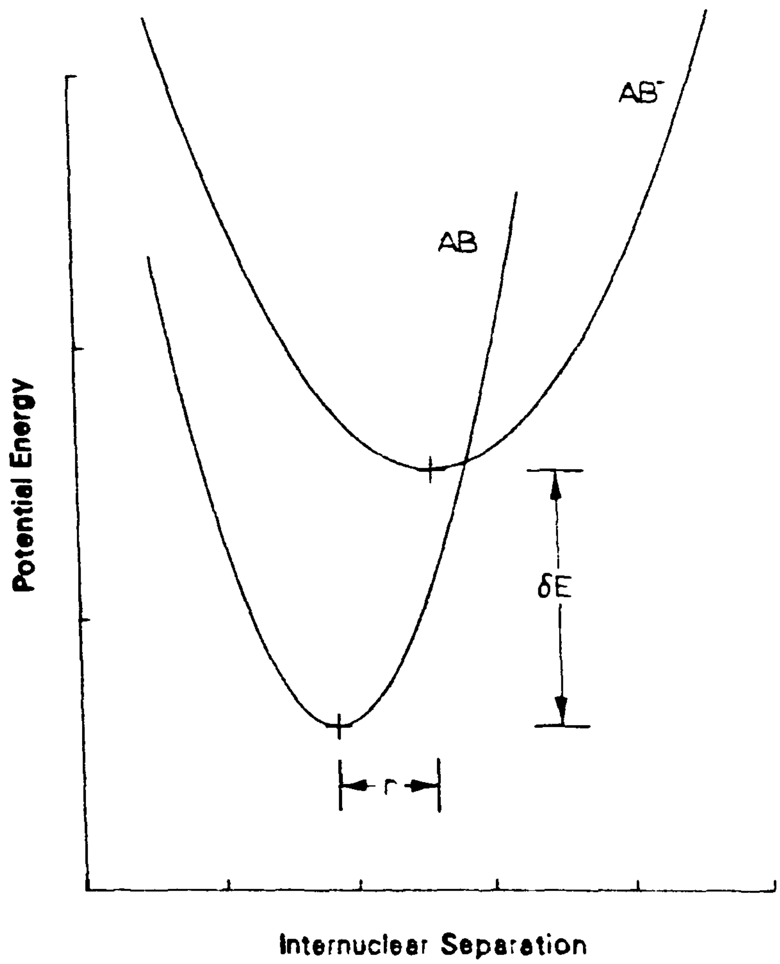

Figure 5. A schematic representation of the potential energy curves of the molecule AB and its resonant anion AB^- by linear harmonic oscillators.

Here ε is the energy of the incident electron, ω and ω_- are the frequencies of the two oscillators, Γ is the resonance width, r is the relative separation of the oscillators, μ is the reduced mass of the nuclei and $\omega_o = \hbar/\mu r^2$. δE is defined in Figure 5. The level shift Δ is taken to be zero in the present calculations. Note that when either n or m is zero the recursion relation among the excitation amplitudes reduces to a three-term recursion relation. Furthermore, amplitude for any transition -- inelastic or superelastic -- can be obtained from a mere knowledge of $a(0\rightarrow 0)$, $a(1\rightarrow 1)$ and $a(0\rightarrow 1)$ only. Figure 6 shows the results of such a calculation for the vibrational excitation of molecular nitrogen, which is treated as a test case in the present calculations. It is worth noting that the spectacular peaks in the excitation cross sections for molecular nitrogen are better reproduced by using unequal frequency oscillators. A similar calculation is done using this simple model to predict the cross sections for the vibrational excitation of Li_2. The vibrational excitation cross sections for molecular lithium are displayed in Figure 7. It is easy to verify that the first five vibrational levels of the simple harmonic oscillators utilized in the present calculations have the same energy levels, within 5%, as the actual vibrational levels of the ground electronic states of these two molecules. It is not surprising, based on the similarities between H_2 and Li_2, that the excitation cross sections for molecular lithium as shown in Figure 7 are almost structureless. All of the cross sections show only one peak, and the location of the peak is roughly the same for all transitions. We note in passing that in order to use the above recursion relation for obtaining the vibrational excitation cross sections it is necessary to know the amplitude for vibrationally elastic cross section which in turn could be obtained by summing the contributions of various partial waves for a given electron-molecule interaction. Recently

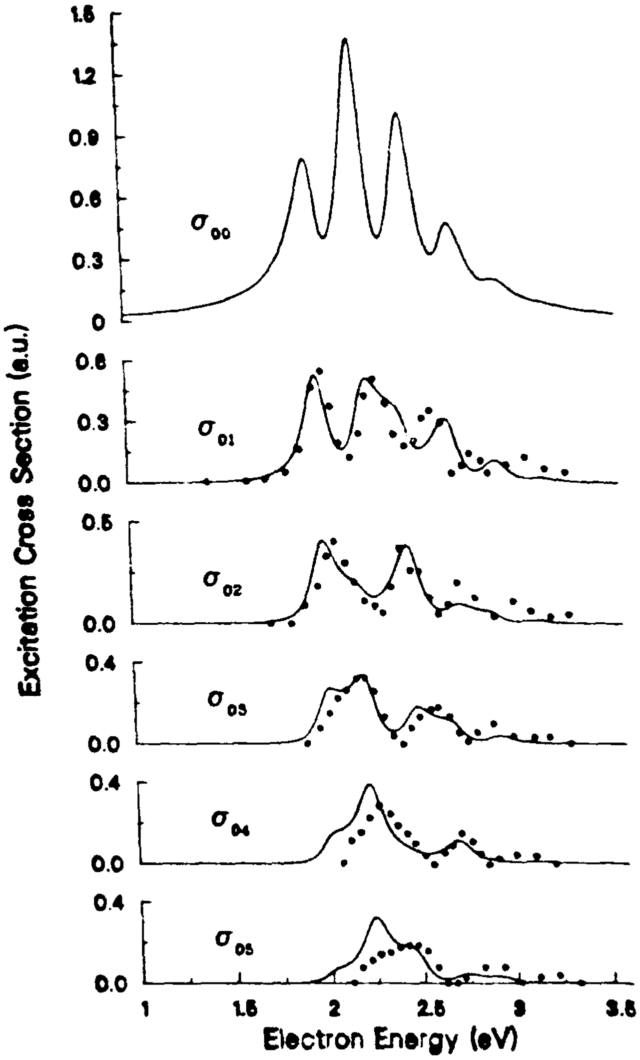

Figure 6. Cross sections for the resonant vibrational excitation of molecular nitrogen by the impact of low energy electrons. Solid circles represent the experimental values of the respective cross sections from G. J. Schulz, Phys. Rev. 135, A988 (1964).

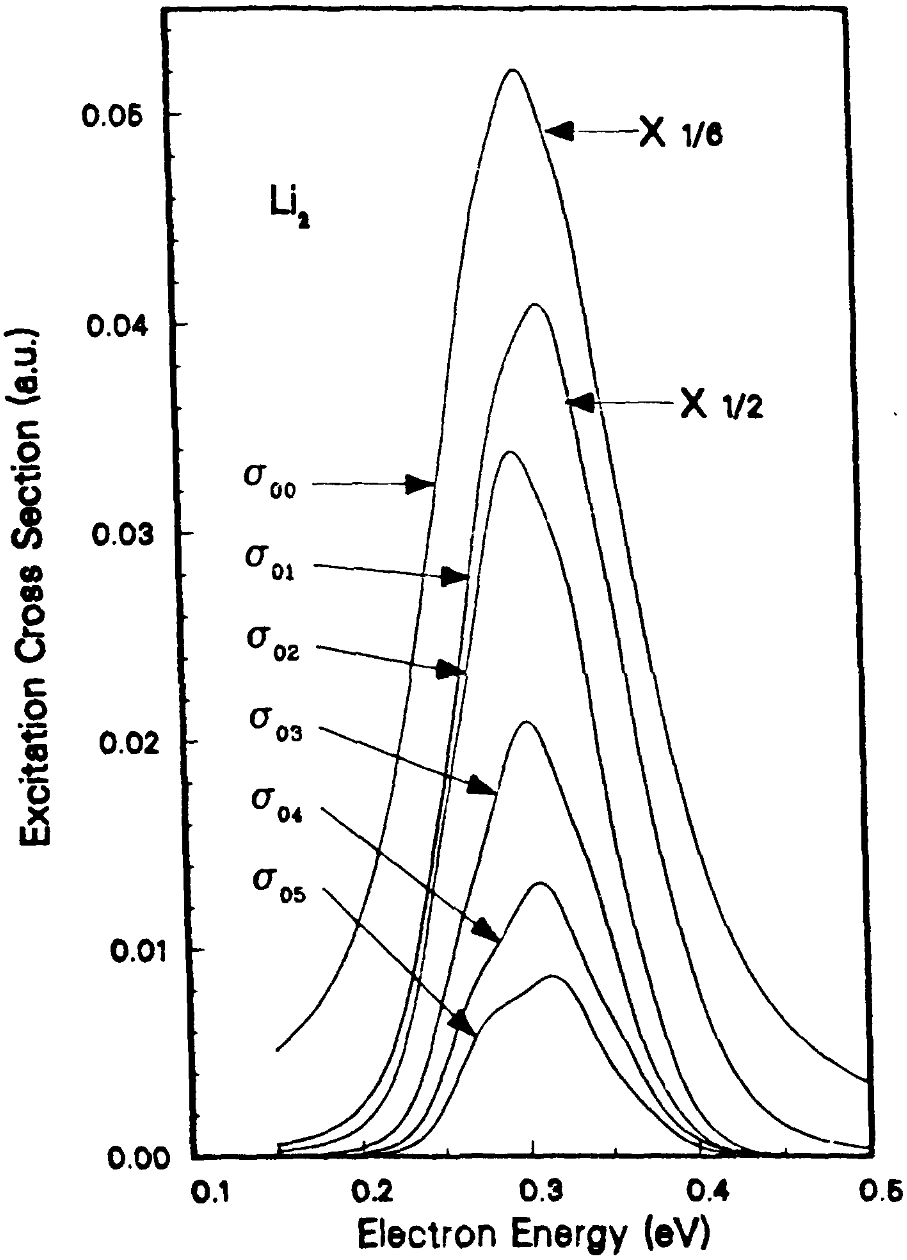

Figure 7. Cross sections for the resonant vibrational excitation of molecular lithium by the impact of low energy electrons.

during such an investigation[10] we calculated the second Born contribution of long range forces to higher partial wave phase shifts.

Nonresonant Vibrational Excitation of Molecular Lithium

As one possible nonresonant process for the vibrational excitation of a molecule we investigated the process of radiative decay from the excited electronic states of the molecule. For the excitation of the vibrational levels of the ground $X^1\Sigma_g^+$ state of lithium molecule we considered the following two step process. In the first step, the molecule is excited from its ground electronic state to a higher singlet electronic state either by electron impact or by photon pumping. Schematically,

$$e + Li_2\,(X^1\Sigma_g^+\;,\;v_i) \rightarrow Li_2\,(A\,^1\Sigma_u^+\;,\;B^1\Pi_u) + e$$
$$Li_2\,(X^1\Sigma_g^+\;,\;v_i) + h\nu \rightarrow Li_2\,(A\,^1\Sigma_u^+\;,\;B^1\Pi_u).$$

In the second step, the electronically excited molecule undergoes a rapid radiative decay to an excited vibrational level of the ground electronic state.

$$Li_2\,(A\,^1\Sigma_u^+\;,\;B^1\Pi_u) \rightarrow Li_2\,(X^1\Sigma_g^+\;,\;v_f) + h\nu\;.$$

Our calculations[11] of the relative cross sections for excitation of higher vibrational levels of the ground electronic state of molecular lithium by this nonresonant process indicate that in general the excitation occuring via the formation of the A electronic state is more efficient than via the formation of the B electronic state. Furthermore, this process populates all vibrational levels of the ground electronic state upto about v = 9 with high probability for both electron collisional excitation as well as the photon pumping of the A state. This fact has recently been utilized[12] by investigators for obtaining vibrationally excited molecular lithium in the laboratory.

Finally, an updated list of all the publications and presentations carried out under the tenure of the present Grant is provided in the appendices A and B.

A Personal Note

The kind support of the Air Force Office of Scientific Research, for which we are very grateful, has so far allowed us to investigate the role played by the initial vibrational excitation of molecular lithium in enhancing the rate of production of negative ions of atomic lithium via the process of dissociative elctron attachment. As part of these endeavors we also investigated the resonant and nonresonant vibrational excitation of lithium dimers. We are continuing our theoretical investigations, under Grant Number AFOSR-87-0342, on the production of light negative ions (hydrogen and its heavier isotopes) by dissociative attachment. Furthermore, with the aim of having an effective neutral particle beam, we are in the process of obtaining a realistic electron energy distribution in the hydrogen source. For this purpose we have developed a novel technique for solving the Boltzmann equation. We will soon be using this technique for numerically obtaining the electron energy distribution in a hydrogen source which contains a realistic mixture of atomic and molecular hydrogen.

REFERENCES

1. For a recent review see, J. M. Wadehra in Nonequilibrium Vibrational Kinetics, ed. M. Capitelli (Springer-Verlag, 1986).
2. J. M. Wadehra and J. N. Bardsley, Phys. Rev. Lett. 41, 1795 (1978).
3. M. Allan and S. F. Wong, Phys. Rev. Lett. 41, 1791 (1978).
4. H. H. Michels, R. H. Hobbs and L. A. Wright, Chem. Phys. Lett. 118, 67 (1985).
5. M. M. Hessel and C. R. Vidal, J. Chem. Phys. 70, 4439 (1979).
6. M. W. McGeoch and R. E. Schlier, Phys. Rev. A33, 1708 (1986).
7. J. M. Wadehra, Phys. Rev. A29, 106 (1984).
8. J. M. Wadehra and P. J. Drallos, Phys. Rev. A36, 1148 (1987).
9. P. J. Drallos and J. M. Wadehra, J. Chem. Phys. 85, 6524 (1986).
10. J. M. Wadehra, J. Phys. B19, L761 (1986).
11. J. M. Wadehra and H. H. Michels, Chem. Phys. Lett. 114, 380 (1985).
12. M. W. McGeoch, private communication (1986).

Appendix A: Publications

During the tenure of the present Grant, AFOSR 84-0143, the following papers were published in various refereed journals. Reprints of some of these papers follow this report.

A. Review Article

1. "Vibrational excitation and dissociative attachment", J.M. Wadehra, in Nonequilibrium Vibrational Kinetics, M. Capitelli, ed. (Springer-Verlag, New York, 1986) p. 191-232.

B. Refereed Journals

2. "Vibrational excitation of Li_2 ($X\,{}^1\Sigma_g^+$) via electron or photon excitation of the $A\,{}^1\Sigma_u^+$ and $B\,{}^1\Pi_u$ states", J. M. Wadehra and H. H. Michels, Chem. Phys. Lett. 114, 380 (1985).

3. "The second Born contribution of long-range forces to higher partial wave phaseshifts", J.M. Wadehra, J. Phys. B19, L761 (1986).

4. "Exact evaluation and recursion relations of two-center harmonic oscillator matrix elements", P.J. Drallos and J.M. Wadehra, J. Chem. Phys. 85, 6524 (1986).

5. "Elastic Scattering of positrons and electrons by argon", Sultana N. Nahar and J.M. Wadehra, Phys. Rev. A35, 2051 (1987).

6. "Positronium formation from Li and Na atoms using pseudopotential", Sultana N. Nahar and J.M. Wadehra, Phys. Rev. A35, 4533 (1987).

7. "Contributions of higher partial waves to the elastic scattering amplitude for various long range interactions", J.M. Wadehra and Sultana N. Nahar, Phys. Rev. A36, 1458 (1987).

8. "A simple model for the resonant vibrational excitation of molecules and its application to Li_2 and N_2", J.M. Wadehra and P.J. Drallos, Phys. Rev. A36, 1148 (1987).

C. Conference Proceedings

9. "Dissociative attachment to lithium dimers", J.M. Wadehra, Proceedings of the Fourth International Symposium on the Production and Neutralization of Negative Ions and Beams, J. Alessi, ed. pp. 547-554 (American Institute of Physics, 1987).

10. "Mutual neutralization - three body effects", J.M. Wadehra, Proceedings of the Fourth International Symposium on the Production and Neutralization of Negative Ions and Beams, J. Alessi, ed. pp. 59-68 (American Institute of Physics, 1987).

Appendix B: Presentations

During the tenure of the Grant, AFOSR 84-0143, the following presentations were made at various national and international meetings. Abstracts of some of these presentations follow this report.

A. Invited

1. "Mutual neutralization - three body effects"; presented at the Fourth International Symposium on the Production and Neutralization of Negative Ions and Beams, Upton, New York, October 27-31, 1986.

B. Contributed

2. "Dissociative Attachment in Low-Energy e+Li_2 Collisions", (with H.H. Michels); presented at the 37th Gaseous Electronics Conference, Boulder, Colorado, October 9-12, 1984.

3. "Dissociative electron attachement to molecular lithium", (with H.H. Michels); presented at the Fourteenth International Conference on the Physics of Electronic and Atomic Collisions, Palo Alto, California, July 24-30, 1985.

4. "Vibrational excitation of diatomic molecules during resonance scattering of electrons" (with P.J. Drallos); presented at the Thirty Eighth Annual Gaseous Electronics Conference, Monterey, California, October 15-18, 1985.

5. "Elastic scattering of positrons and electrons from argon", (with Sultana N. Nahar); presented at the 18th Annual Meeting of the Division of Electron and Atomic Physics, Eugene, Oregon, June 18-20, 1986.

6. "Dissociative electron attachment to the isotopes of molecular hydrogen"; presented at the Thirth-Ninth Annual Gaseous Electronics Conference, Madison, Wisconsin, October 7-10, 1986.

7. "Li^- production by dissociative electron attachment to Li_2"; presented at the Fourth International Symposium on the Production and Neutralization of Negative Ions and Beams, Upton, New York, October 27-31, 1986.

8. "Closed form expressions for the contributions of higher partial waves to the elastic scattering amplitude for various long range potentials", (with Sultana N. Nahar); presented at the 1987 annual meeting of the Division of Atomic, Molecular and Optical Physics, Cambridge, Massachusetts, May 18-20, 1987.

9. "Charge transfer processes during the collisions of positrons and protons with atomic hydrogen", (with Sultana N. Nahar) presented at the 1987 annual meeting of the Division of Atomic, Molecular and Optical Physics, Cambridge, Massachusetts, May 18-20, 1987.

10. "Elastic scattering of positrons from argon", (with Sultana N. Nahar); presented at the Fifteenth International Conference on the Physics of Electronic and Atomic Collisions, Brighton, United Kingdom, July 22-28, 1987.

11. "A simple model for the resonant vibrational excitation of molecules", (with P.J. Drallos); presented at the Fifteenth International Conference on the Physics of Electronic and Atomic Collisions, Brighton, United Kingdom, July 22-28, 1987.

12. "Elastic scattering of positrons from argon", (with Sultana N. Nahar) presented at the NATO Advanced Research Workshop on Atomic Physics with Positrons, University College London, United Kingdom, July 15-17, 1987.

13. "Positronium formation from atomic hydrogen", (with Sultana N. Nahar) presented at the NATO Advanced Research Workshop on Atomic Physics with Positrons, University College London, United Kingdom, July 15-17, 1987.

14. "A simple model for the resonant vibrational excitation of molecules", (with P.J. Drallos) presented at Satellite Meeting on Electron-molecule Scattering and Photoionisation, Daresbury, United Kingdom, July 18-19, 1987.

15. "Time evolution of electron and positron swarms in neon", (with P.J. Drallos) presented at the 40th Annual Gaseous Electronics Conference, Atlanta, Georgia, October 13-16, 1987.

Reprint from

Topics in Current Physics

Volume 39: **Nonequilibrium Vibrational Kinetics**

Editor: M. Capitelli

Springer-Verlag Berlin Heidelberg New York
London Paris Tokyo

Nonequilibrium Vibrational Kinetics

Editor: M. Capitelli

---

7. Vibrational Excitation and Dissociative Attachment

J. M. Wadehra

With 14 Figures

The process of dissociative electron attachment to molecules is known to be one of the main sources of production of negative ions in gaseous discharges, plasma switches, and gas lasers. In this process, a diatomic (or polyatomic) molecule, under the impact of an electron, dissociates into its component atoms (or smaller molecular species) while the incident electron attaches itself to one of the component products. The rate of negative ion production via dissociative attachment can be significantly increased, for both homonuclear molecules (for example, H_2) and heteronuclear molecules (for example, HCl), if the molecule initially has stored internal energy in the form of rovibrational excitation. Schematically, for electron impact on a molecule AB,

$$e + AB \rightarrow A + B^- \qquad \text{(dissociative electron attachment)},$$

$$e + AB(v_i) \rightarrow e + AB(v_f) \qquad \text{(vibrational excitation by electron impact)}.$$

This chapter reviews the resonance model in general and its application, in particular, to the process of dissociative attachment (DA) of electrons to various diatomic homonuclear and heteronuclear molecules like H_2, N_2, CO, and HCl. It also discusses the related problem of vibrational excitation (VE), via resonance formation, of these molecules by electron impact. No attempt will be made to present a paper-by-paper historical view of the topics since this has been accomplished in a number of other review articles. Rather, an attempt will be made to present the results in as simple a manner as possible so that the present review might serve as a starting point for an investigator new to this area. Emphasis will be placed on the most recent results.

Some of the comprehensive review articles and books dealing with DA are [7.1-8]. A popular account of the process of dissociative electron attachment is given in [7.9]. The recent review articles on VE of molecules by electron impact include [7.10-15].

7.1 The Resonance Model

7.1.1 Qualitative Remarks

One model that has been quite successful in explaining the DA and VE of diatomic molecules is the resonance model, in which the projectile electron is temporarily trapped by the target molecule. The molecular anion (or the resonant state) thus formed has a finite lifetime and it can either autodetach, leading to VE of the molecule or, if the lifetime is sufficiently large, it can lead to DA forming a neutral atom and an atomic anion. Thus

$$e + AB(v_i) \rightarrow AB^-(\text{res}) \begin{cases} \rightarrow A + B^- & \text{(DA)} \\ \rightarrow AB(v_f) + e & \text{(VE)} \end{cases} .$$

A schematic representation of the resonance model is shown in Fig.7.1, which shows the potential curves of the neutral molecule AB and its anion (resonant state) AB^-. The two curves cross at internuclear separation $R = R_s$ so that for $R > R_s$ the resonance turns into a bound state. The nuclei, initially rovibrating in state

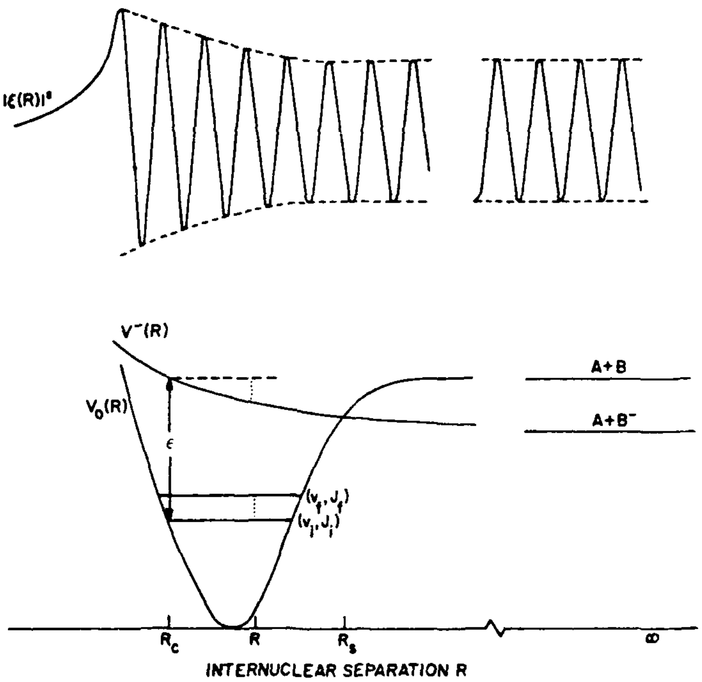

Fig.7.1. The resonance model. Here $V_0(R)$ and $V^-(R)$ are the potential curves of the neutral molecule AB and the resonant state AB^-. The resonant state is formed by capture of an electron with energy ϵ by the molecule AB

(v_i, J_i) under the influence of the potential $V_0(R)$, move under the influence of $V^-(R)$ after capturing the electron. The probability of capture of an electron with energy ε depends on the internuclear separation R and, classically speaking, it peaks at $R = R_c$ (known as the capture radius) where $V^-(R_c) - V_0(R_c) = \varepsilon$. After anion formation, the nuclei begin to separate if the potential curve $V^-(R)$ is repulsive and begin to gain kinetic energy at the expense of electronic energy. Due to its resonant nature, the anion, at any internuclear separation R, can autodetach the electron leaving the nuclei in one of the rovibrational states of the potential $V_0(R)$. The final rovibrational state (v_f, J_f) that the neutral molecule achieves depends on the kinetic energy gained by the nuclei (as indicated by the dotted line in Fig.7.1) and on the selection rules governing the transition. If, on the other hand, the nuclei in the anion state can separate to internuclear separations $R > R_s$ without autodetachment having occurred, the detachment of the electron becomes energetically impossible and the dissociative attachment becomes unavoidable. The internuclear separation R_s beyond which the molecular anion becomes stable against autodetachment is called the stabilization radius. The fact that the molecular anion is capable of autodetaching the electron implies that it has a complex potential energy curve, $E^-(R) = V^-(R) - \frac{1}{2} i\Gamma(R)$. The real part gives the usual potential energy curve of the anion (as shown in Fig.7.1) and the imaginary part is related to the lifetime of the resonant anion state. This can be seen by noting that the time dependence of the nuclear wave function $\xi(R)$ of the resonant state is given by

$$\xi(R) \propto \exp\left(\frac{-iE^-(R)t}{\hbar}\right) \quad ,$$

so that

$$|\xi(R)|^2 \propto \exp\left(\frac{-\Gamma(R)t}{\hbar}\right) \quad ,$$

where $\Gamma(R)$ is the width of the resonance, indicating that $\hbar/\Gamma$ is the lifetime of the resonant state. Figure 7.1 also shows the nuclear wave function ξ as a function of R. Note that for internuclear separations R between R_c and R_s, the envelope of $|\xi(R)|^2$ decreases with R because of the possibility of autodetachment. For $R > R_s$, since the autodetachment of the electron is energetically not allowed, the width of the resonance becomes zero and hence $|\xi(R)|^2$ has constant amplitude which determines the cross section for the dissociative electron attachment.

A few noteworthy points of this model are the following: first, the dissociative electron attachment and the vibrational excitation of the molecule are two possible decay channels, apart from electronic excitation etc., resulting from a particular resonance state. Thus a calculation of the cross sections for the dissociative electron attachment to a molecule will provide resonant contributions (of that particular resonant state) to the cross sections for vibrational excitation of the molecule as a bonus and vice versa. Second, in explaining the vibrational excitation by this resonance model, it was implicitly assumed that the transition from the resonant state $V^-(R)$ to the neutral state $V_0(R)$ after autodetachment is a Franck-Condon transition, that is, an instantaneous transition with no change in nuclear velocities or positions. This is a so-called *local* complex potential model. This is obviously true only if the energy of the projectile electron is much greater than the vibrational spacing. At very low impact energies or if the vibrational spacing of the molecule is relatively large, a description of the DA and VE processes using a *nonlocal* complex potential for the resonant state is essential since the neutral molecule must accept only quanta of vibrational energy for its vibrational excitation. Third, in the cases of some molecules it might be possible, for certain electron energies, to form more than one intermediate resonant state. Alternatively, the resonant anion state may decay into more than one electronic state of the neutral molecule. In such cases, the total width $\Gamma(R)$ is the sum of various partial widths — each partial width corresponding to a certain transition between the resonant anion state (or states) and the neutral molecular state (or states).

During a resonance formation, the time spent by the projectile electron in the vicinity of the target molecule is much larger — by several orders of magnitude — than the normal transit time. For example, a 10 eV electron, normally taking 10^{-17}s ($\sim a_B$/velocity) to transit a molecule, might be trapped for almost 10^{-14}s ($\sim\hbar/\Gamma$) if it forms a resonance with the target molecule with an average width of ~0.1 eV. The effect of the resonance formation is then to strongly distort the target wave function. There are several mechanisms by which the electron could be trapped by the molecular target to form the resonant anion state. For example, on impact the electron could excite the molecular target and thereby lose sufficient energy to hinder its own escape. The energy of the resonant state then lies below that of the excited target state. This is a type I or Feshbach or closed-channel resonance. Before autodetaching, the trapped electron must gain energy by reverting the target molecule back into its lower energy state. This type of resonance is relatively narrow (that is, has a long lifetime) since the trapped electron is forced to affect the electrons of the target molecule dynamically for autodetachment to occur. Another possibility is that the electron encounters the target in a configuration of nonzero angular momentum. The projectile electron then gets trapped in the centrifugal potential barrier of the target from which it eventually tunnels out. This trapping mechanism obviously depends on the shape of the potential of the target state. This is a type II or shape or open-channel resonance.

Whatever the mechanism of the electron trapping, the lifetime of the resonance is determined by its width. To classify the various limits of the resonances, one has to compare the lifetime $\hbar/\Gamma$ of the resonance, with the average vibrational period of the nuclei in the resonant state. If $\hbar\omega$ is the average energy of the vibrational quanta in the resonant state, then the condition $\hbar/\Gamma \ll 1/\omega$ implies that during the lifetime of the resonance, the nuclei hardly have an opportunity to vibrate. This is the *impulse limit* since the incoming electron effectively provides an impulse to the target without staying with it for a long time. Similarly, the condition $\hbar/\Gamma \gg 1/\omega$ implies the *compound state limit* since in this case the nuclei make a large number of vibrations during the lifetime of the resonance. Finally, if $\hbar/\Gamma \sim 1/\omega$, one has the *boomerang limit*. In the boomerang case, one needs to consider only the interference between the single outgoing and a single reflected nuclear wave. An important characteristic of the boomerang limit is that the resonance width Γ decreases on increasing the internuclear separation R [7.16].

7.1.2 Quantitative Discussion

A quantitative analysis using the nonlocal formalism of the application of the resonance model to the dissociative attachment and vibrational excitation of diatomic molecules has been given [7.17,18]. In this analysis, following *Fano* [7.19] one views a resonance as a discrete state embedded in and interacting with a continuum. If q represents the totality of all electronic coordinates, including those of the projectile, then in the Born-Oppenheimer approximation, the wave function of the discrete state representing the resonance can be written in the product form $\phi(q,R)\xi(\mathbf{R})$. Here ϕ is the normalized electronic wave function and ξ is the nuclear wave function of the resonant state. The internuclear separation R appears only parametrically in the electronic part ϕ. The total Hamiltonian $H(q,\mathbf{R})$ can be written as the sum of the electronic Hamiltonian $H_{el}(q,\mathbf{R})$ and the nuclear kinetic energy term $T_N(\mathbf{R})$,

$$H(q,\mathbf{R}) = H_{el}(q,\mathbf{R}) + T_N(\mathbf{R}) \quad . \tag{7.1.1}$$

A typical member of the set of continuum functions representing the nonresonant scattering, in the Born-Oppenheimer approximation, is $\psi_\varepsilon(q,R)\chi_v(\mathbf{R})$. Here χ_v is the vibrational wave function of the target and $\psi_\varepsilon(q,R)$ is the properly antisymmetrized electronic wave function that takes into account all the target electrons and the projectile electron. The energy of the projectile ε is part of the total energy E; $E = E_v + \varepsilon$, E_v being the vibrational energy of the target molecule. It is convenient to choose $E_{v=0} = 0$. Asymptotically, ψ_ε approaches a form that is the product of a plane wave [with amplitude A(k)], representing a free electron of energy ε, and the electronic state of the target molecule: $\psi_\varepsilon^{asy} = A(k)\exp(i\mathbf{k}\cdot\mathbf{r})\psi_t^{el}$.

The electronic parts of the discrete and the continuum states are orthonormalized as

$$\int dq\, \phi^*(q,R)\phi(q,R) = 1 \quad , \tag{7.1.2a}$$

$$\int dq\, \psi_\varepsilon^*(q,R)\psi_{\varepsilon'}(q,R) = \delta(\varepsilon - \varepsilon') \quad , \quad \text{and} \tag{7.1.2b}$$

$$\int dq\, \phi^*(q,R)\psi_\varepsilon(q,R) = 0 \quad , \tag{7.1.2c}$$

for all R since R appears only parametrically in the electronic wave functions.

The electronic energy $V^{-}(R)$ associated with the discrete state is

$$V^{-}(R) = \int dq\ \phi^{*}(q,R)H_{el}\phi(q,R) \quad , \tag{7.1.3a}$$

and that associated with the continuum set of states is

$$\int dq\ \psi^{*}_{\varepsilon'}H_{el}\psi_{\varepsilon} = [V_0(R) + \varepsilon]\delta(\varepsilon - \varepsilon') \quad , \tag{7.1.3b}$$

where $V_0(R)$ is the potential curve of the target molecule. The vibrational wave functions satisfy

$$[T_N(\mathbf{R}) + V_0(R)]\chi_v(\mathbf{R}) = E_v\chi_v(\mathbf{R}) \quad . \tag{7.1.4}$$

The total Hamiltonian is thus diagonalized in the subspace of the continuum functions,

$$\begin{aligned} \int d\mathbf{R} \int dq\ \chi^{*}_{v'}\ \psi^{*}_{\varepsilon'}H(q,\mathbf{R})\psi_{\varepsilon}\chi_v &= \int d\mathbf{R}\ \chi^{*}_{v'}[T_N + V_0(R) + \varepsilon]\delta(\varepsilon - \varepsilon')\chi_v \\ &= (E_v + \varepsilon)\delta(\varepsilon - \varepsilon') \int d\mathbf{R}\ \chi^{*}_{v'}\chi_v = E\delta_{vv'}\delta(\varepsilon - \varepsilon') \quad . \end{aligned} \tag{7.1.5}$$

The matrix element governing the interaction between the discrete state and the continuum states is

$$V(\varepsilon,R) = \int dq\ \phi^{*}(q,R)H_{el}\psi_{\varepsilon}(q,R) \quad . \tag{7.1.6}$$

The complete wave function of the electron-molecule system in the configuration interaction form can be written as

$$\Psi(q,\mathbf{R}) = \phi(q,R)\xi(\mathbf{R}) + \sum_v \int d\varepsilon\ f_v(\varepsilon)\psi_{\varepsilon}(q,R)\chi_v(\mathbf{R}) \quad . \tag{7.1.7}$$

It is required to satisfy the Schrödinger equation

$$[H(q,\mathbf{R}) - E]\Psi(q,\mathbf{R}) = 0 \quad . \tag{7.1.8}$$

The functional coefficients $f_v(\varepsilon)$ are determined from the expression obtained by premultiplying (7.1.8) by $\psi^{*}_{\varepsilon'}(q,R)\chi^{*}_{v'}(\mathbf{R})$ and integrating over all the electronic and nuclear coordinates, that is,

$$\int d\mathbf{R} \int dq\ \psi^{*}_{\varepsilon'}\chi^{*}_{v'}[H(q,\mathbf{R}) - E]\Psi(q,\mathbf{R}) = 0 \quad , \tag{7.1.9}$$

along with the boundary conditions. If χ_{v_i} is the initial vibrational state of the target molecule, then the incoming waves are possible only in the term $v = v_i$ of the sum in (7.1.7). Substituting for Ψ from (7.1.7) into (7.1.9) and using the incoming wave boundary conditions for $v = v_i$, one obtains

$$f_v(\varepsilon) = \delta_{vv_i}\delta(E - E_v - \varepsilon) + \frac{1}{E - E_v - \varepsilon + i0^{+}} \int d\mathbf{R}\ \chi^{*}_v V^{*}(\varepsilon,R)\xi \quad . \tag{7.1.10}$$

Next, the differential equation satisfied by the nuclear wave function $\xi(\mathbf{R})$ of the discrete state is derived from the expression obtained by premultiplying (7.1.8) by $\phi^*(q,R)$ and integrating over all electronic coordinates, that is, from

$$\int dq\ \phi^*(q,R)[H(q,\mathbf{R}) - E]\Psi(q,\mathbf{R}) = 0 \quad . \tag{7.1.11}$$

Again using (7.1.7) for Ψ in (7.1.11), one obtains

$$[T_N(\mathbf{R}) + V^-(\mathbf{R}) - E]\xi(\mathbf{R}) + \int d\mathbf{R}'\ K(\mathbf{R},\mathbf{R}')\xi(\mathbf{R}') = -V(E - E_{v_i},\mathbf{R})\chi_{v_i}(\mathbf{R}) \quad , \tag{7.1.12a}$$

where

$$K(\mathbf{R},\mathbf{R}') = \sum_v \chi_v^*(\mathbf{R}')\chi_v(\mathbf{R})[\Delta(R,R';E - E_v) - \frac{1}{2}\, i\Gamma(R,R';E - E_v)] \quad , \tag{7.1.12b}$$

with

$$\Delta(R,R';E - E_v) = P \int d\varepsilon\ \frac{V(\varepsilon,R)V^*(\varepsilon,R')}{E - E_v - \varepsilon} \quad ,$$

(where P indicates the principal value) and

$$\Gamma(R,R';E - E_v) = 2\pi V(E - E_v,R)V^*(E - E_v,R') \quad .$$

Equation (7.1.12a) for the resonant nuclear wave function $\xi(\mathbf{R})$ is an integrodifferential equation with a nonlocal kernel. Here, Δ and Γ are the level shift and the level width, respectively. Some of the assumptions made implicitly in arriving at the result (7.1.12a) are: (a) the orientation of the internuclear axis is fixed in space so that the rotation of the molecule is of little concern, (b) degeneracy arising from the different possible directions of the projectile electron relative to the internuclear axis is omitted, and (c) multiplicities of the molecular states are not considered. These assumptions were made to simplify our presentation and it is possible to obtain the most general results by relaxing these assumptions [7.18].

The nonlocal equation (7.1.12a) can be reduced to a local equation by the following assumption. The level shift and the level width functions Δ and Γ depend on $E - E_v \equiv \hbar^2 k_v^2/2m$, which is the energy of the scattered electron when the target molecule undergoes the transition $0 \to v$. The assumption is that if either the electron energy is large or the vibrational spacing is small, then during the vibrational excitation $v_i \to v_f$ the energy of the electron is not significantly changed. Under such circumstances one can either replace E_v by E_{v_i} (that is, $E - E_v$ by the incident electron energy ε_i) or $E - E_v$ by the local classical electron energy $V^-(R) - V_0(R) \equiv \hbar^2 k^2(R)/2m$. The first choice will maintain the unitarity of the S matrix but will give nonzero cross sections at the threshold and the second choice will give zero cross sections at the threshold while minimizing any possibility of unitarity violation [7.20]. In either case, Γ and Δ will become independent of the vibrational quantum number v. The sum in (7.1.12b) is over all open vibrational levels since the condition $E - E_v > 0$ is satisfied only for open channels.

If the contribution of all closed vibrational channels is negligible, then using the closure property

$$\sum_v \chi_v^*(\mathbf{R}')\chi_v(\mathbf{R}) = \delta(\mathbf{R}' - \mathbf{R})$$

in (7.1.12b), (7.1.12a) reduces to a local equation

$$[T_N(\mathbf{R}) + V^-(R) + \Delta(R,\varepsilon_i) - \tfrac{1}{2}\, i\Gamma(R,\varepsilon_i) - E]\xi(\mathbf{R}) = -V(\varepsilon_i,R)\chi_{v_i}(\mathbf{R}) \quad , \tag{7.1.13}$$

where

$$\Delta(R,\varepsilon_i) = P\int d\varepsilon \frac{|V(\varepsilon,R)|^2}{\varepsilon_i - \varepsilon} \quad \text{and}$$

$$\Gamma(R,\varepsilon_i) = 2\pi|V(\varepsilon_i,R)|^2 \quad .$$

Note that it is the coupling between the discrete and the continuum states that leads to a complex potential and thus turns a discrete state into an autodetaching resonant state. The term on the right-hand side of (7.1.13) is called variously the electron entry amplitude or the feeding term or the source term of the resonant state. The local equation (7.1.13) is the starting point for most of the semiempirical calculations of the dissociative attachment and vibrational excitation processes [7.16,21]. The validity and the range of applicability of the local complex potential approach have been analyzed in detail [7.22,23]. The complex potential appearing in (7.1.13), due to the assumptions made above, does not depend on the orientation of $\mathbf{R}$ but only on its magnitude. This observation suggests that $\chi(\mathbf{R})$ and $\chi_{v_i}(\mathbf{R})$ in (7.1.13) can be decomposed into partial waves to separate out the angular dependence:

$$\xi(\mathbf{R}) = \sum_{J_r m_r} \xi_{J_r}(R) Y_{J_r m_r}(\hat{R})/R \quad ,$$

$$\chi_{v_i}(\mathbf{R}) = \sum_{J_i m_i} \chi_{v_i J_i}(R) Y_{J_i m_i}(\hat{R})/R \quad .$$

Then $\xi_J(R)$ satisfies the radial equation

$$\left(-\frac{\hbar^2}{2M}\frac{d^2}{dR^2} + \frac{\hbar^2 J_i(J_i + 1)}{2MR^2} + V^-(R) + \Delta(R,\varepsilon_i) - \frac{1}{2}\, i\Gamma(R,\varepsilon_i) - E\right)\xi_{J_i}(R)$$

$$= -V(\varepsilon_i,R)\chi_{v_i J_i}(R) \quad , \tag{7.1.14}$$

where $\chi_{v_i J_i}$ is the wave function of the initial *rovibrational* state of the target molecule. The resonant nuclear wave function $\xi_J(R)$ is obtained by directly integrating (7.1.14) subject to the boundary conditions

$$\xi_J(R = 0) = 0 \quad , \quad \text{and} \tag{7.1.15a}$$

$$\begin{aligned} \xi_J(R \to \infty) &\to 0 && \text{if} \quad E < V^-(\infty) \\ &\to KRh_J^{(1)}(KR) && \text{if} \quad E > V^-(\infty) \quad , \end{aligned} \tag{7.1.15b}$$

with $\hbar^2K^2/2M = E - V^-(\infty)$, M being the reduced mass of the nuclei and $h_J^{(1)}$ the spherical Hankel function of the first kind.

Sometimes it is convenient to use electronic wave functions ψ_k that are momentum normalized rather than energy normalized as in (7.1.2b). The relationship between the two functions is

$$\psi_\varepsilon = (mk/\hbar^2)^{1/2}\psi_k$$

with $\varepsilon = \hbar^2k^2/2m$. Then, in the local formalism,

$$\Gamma(R,\varepsilon) = (2\pi mk/\hbar^2)|V(k,R)|^2 \quad ,$$

where V(k,R) is the electronic coupling matrix element evaluated by using the momentum-normalized electronic wave functions. A summary of the properties of the energy-normalized and the momentum-normalized continuum functions is given in the appendix to this chapter.

7.1.3 Cross Section for Dissociative Attachment

The cross section for the process of dissociative electron attachment

$$e + AB \rightarrow A + B^-$$

is obtained by comparing the flux of the outgoing ion-atom pairs with the flux of the incoming electrons [7.24]. The quantum mechanical expression for the flux *density* associated with a wave function ψ is

$$\mathbf{J} = (\hbar/m)\,\mathrm{Im}\{\psi^*\nabla\psi\} \quad .$$

For $R\rightarrow\infty$, the total outward flux of the ion-atom pairs scattered per unit solid angle is

$$(\hbar/M)\,\mathrm{Im}\{\xi^*(\mathbf{R})\nabla\xi(\mathbf{R})\}\cdot\hat{R}R^2 \quad .$$

This flux should be averaged over the orientation of the molecule since the direction of $\hat{R}$ is random. Thus the net outward flux becomes

$$\frac{1}{4\pi}\int d\hat{R}\,\frac{\hbar K}{M}\,|\xi(\mathbf{R})|^2R^2 = \frac{1}{4\pi}\,\frac{\hbar K}{M}\,|\xi_J(R)|^2 \quad ,$$

where $\xi_J(R)$ is the solution of (7.1.14) and J is the total angular momentum of the resonant state. The incident electron flux density is $A^2(k_i)\hbar k_i/m$, where A(k), the amplitude of the plane wave representing the electron, is $(1/8\pi^3)^{1/2}$ or $(mk/8\pi^3\hbar^2)^{1/2}$ for momentum-normalized or energy-normalized functions, respectively. The cross section for dissociative electron attachment then becomes

$$\sigma_{DA} = \frac{1}{A^2(k_i)}\,\frac{m}{\hbar k_i}\,\frac{1}{4\pi}\,\frac{\hbar K}{M}\,\lim_{R\to\infty}|\xi_J(R)|^2 \quad . \qquad (7.1.16)$$

7.1.4 Cross Section for Vibrational Excitation

As a prelude to deriving an expression for the cross section for the vibrational excitation of a molecule

$$e(k_i) + AB(v_i) \rightarrow e(k_f) + AB(v_f) \quad ,$$

we observe that the total electronic Hamiltonian can be written as

$$H_{el} = H_{el}^T + T_e(\mathbf{r}) + V_{eT} \quad , \tag{7.1.17a}$$

where H_{el}^T, T_e, and V_{eT} are, respectively, the electronic Hamiltonian of the target molecule, the kinetic energy of the projectile electron, and the interaction between the electron and the molecule. When the electron is far away from the target (that is, $V_{eT} \rightarrow 0$), the initial wave function of the system is

$$\Psi_i = A(k_i)e^{i\mathbf{k}_i \cdot \mathbf{r}} \psi_t^{el} \chi_{v_i} = \psi_{\epsilon_i}^{asy} \chi_{v_i} \quad ,$$

where ψ_t^{el} is the electronic wave function of the target and $A(k_i)$ is the amplitude of the plane wave representing the noninteracting projectile electron. Similarly, the final wave function after vibrational excitation is

$$\Psi_f = A(k_f)e^{i\mathbf{k}_f \cdot \mathbf{r}} \psi_t^{el} \chi_{v_f} = \psi_{\epsilon_v}^{asy} \chi_{v_f} \quad .$$

The target electronic wave function satisfies

$$[H_{el}^T - V_0(R)]\psi_t^{el} = 0 \quad . \tag{7.1.17b}$$

Conservation of energy implies

$$E = E_{v_i} + \frac{\hbar^2 k_i^2}{2m} = E_{v_f} + \frac{\hbar^2 k_f^2}{2m} \quad .$$

The total cross section for vibrational excitation is [7.25]

$$\sigma_{v_i \rightarrow v_f} = \frac{k_f}{k_i} \int d\hat{k}_f |T_{i \rightarrow f}|^2 \quad ,$$

where the transition matrix element is

$$T_{i \rightarrow f} = \mathscr{B} \int dR \int dq \; \Psi_f^* V_{eT} \Psi = T_{i\rightarrow f}^{res} + T_{i\rightarrow f}^{nr} \quad ,$$

with

$$\mathscr{B} = - \frac{m}{2\pi\hbar^2} \frac{1}{A(k_f)A(k_i)} \quad .$$

Recall that A(k) is $(1/8\pi^3)^{1/2}$ and $(mk/8\pi^3\hbar^2)^{1/2}$ for momentum-normalized and energy-normalized continuum functions, respectively. The resonant and the nonresonant part of the matrix element are, using (7.1.7),

$$T_{i\to f}^{res} = \mathscr{B}\int dR \int dq\ \Psi_f^* V_{eT}\phi\xi$$

$$T_{i\to f}^{nr} = \mathscr{B}\int dR \int dq\ \Psi_f^* V_{eT}\Big(\sum_v \int d\varepsilon\ f_v(\varepsilon)\psi_\varepsilon \chi_v\Big) \quad .$$

In the following discussion, it will be assumed that there is no interference between the resonant and the nonresonant scattering amplitudes and only the resonant part of the excitation cross section will be considered. Now, using (7.1.2c,17b,6),

$$T_{i\to f}^{res} = \mathscr{B}\int dR \int dq\ \Psi_f^*[H_{el} - H_{el}^T - T_e]\phi\xi$$

$$= \mathscr{B}\int dR\ \chi_{v_f}^* V^*(\varepsilon_f,R)\xi \quad .$$

The direction of the outgoing electron appears only in the coupling matrix element via the plane wave $\exp(i\mathbf{k}_f\cdot\mathbf{r})$. If the Lth partial wave in the expansion of this plane wave is the lowest term providing a nonzero contribution to the coupling matrix element and if one makes the approximation of retaining only this leading term, then the matrix element can be written as

$$V(\varepsilon_f,R) = \tilde{V}_f(R)Y_{Lm}(\hat{k}_f) \quad ,$$

where $\tilde{V}_f = [\int d\hat{k}_f|V(\varepsilon_f,R)|^2]^{1/2}$ is independent of the final direction of the electron. Then if J is the final rotational state of the molecule,

$$T_{i\to f}^{res} = \mathscr{B}Y_{Lm}^*(\hat{k}_f)\int_0^\infty dR\ \chi_{v_fJ}^*\tilde{V}_f^*\xi_J(R) \quad .$$

The function $\xi_J(R)$ can be expressed in terms of an integral over the Green's function G(R,R') corresponding to the operator on the left-hand side of (7.1.14)

$$\xi_J(R) = -\int_0^\infty G(R,R')\tilde{V}_i(R')Y_{Lm}(\hat{k}_i)\chi_{v_iJ}(R')dR' \quad .$$

The resonant contribution to the cross section for vibrational excitation now becomes

$$\sigma_{i\to f}^{res} = \frac{k_f}{k_i}\mathscr{B}^2|Y_{Lm}(\hat{k}_i)|^2\left|\int_0^\infty dR\int_0^\infty dR'\ \chi_{v_fJ}^*(R)\tilde{V}_f^*(R)G(R,R')\tilde{V}_i(R')\chi_{v_iJ}(R')\right|^2 \quad .$$

This expression for the VE cross section should be averaged over the direction $\hat{R}$ of the molecular axis with respect to the fixed direction of the incident electron beam. Equivalently, one may average over $\hat{k}_i$ while holding $\hat{R}$ fixed. The final expression for the VE cross section is

$$\sigma_{i\to f}^{res} = \frac{k_f}{k_i}\left(\frac{m}{2\pi\hbar^2}\right)^2 \frac{1}{A^2(k_i)A^2(k_f)} \frac{1}{4\pi}$$

$$\times \left|\int_0^\infty dR \int_0^\infty dR' \, \chi_{v_f J}^* \tilde{V}_f^* G(R,R') \tilde{V}_i \chi_{v_i J}\right|^2 \quad . \tag{7.1.18}$$

7.1.5 Semiclassical Approximation

The cross sections for both dissociative attachment and vibrational excitation involve the continuum ion-atom wave function $\xi_J(R)$ which is most easily obtained by numerically solving (7.1.14). However, the physical nature of the processes involved, within the resonance model, becomes most evident if the semiclassical approximation is used for $\xi_J(R)$ [7.26]. The WKB approximation to $\xi_J(R)$ contains a factor

$$\exp\left[-\mathrm{Im}\left\{\int_z^{R_s} \left(\frac{2M}{\hbar^2}[E - V^-(R) - \Delta(R,\varepsilon_i) + \frac{1}{2} i\Gamma(R,\varepsilon_i)]\right)^{1/2} dR\right\}\right] \quad ,$$

where z is the complex classical capture radius:

$$\varepsilon_i = V^-(z) + \Delta(z,\varepsilon_i) - \frac{1}{2} i\Gamma(z,\varepsilon_i) - V_0(z) \quad .$$

For a narrow resonance (small Γ), this factor (on neglecting Δ) reduces to

$$\exp\left(-\frac{1}{2}\int_{R_c}^{R_s} \frac{\Gamma(R)}{\hbar} \frac{dR}{v(R)}\right) \quad , \qquad v(R) = \sqrt{\frac{2[E - V^-(R)]}{M}} \quad ,$$

so that for the case of a *narrow resonance*, the attachment cross section can be written as the product

$$\sigma_{DA} = \sigma_{cap} S \quad . \tag{7.1.19}$$

The first factor is interpreted as the cross section for the formation of the resonant state by electron capture. The second factor

$$S = \exp\left(-\int_{R_c}^{R_s} \frac{\Gamma(R)}{\hbar} \frac{dR}{v(R)}\right) \quad ,$$

the so-called classical survival factor, is the probability that the nuclei in the resonant state separate from R_c to R_s without autodetachment, that is, the probability that the resonant state survives long enough to assure the occurrence of dissociative attachment.

The Green's function appearing in the vibrational excitation cross section can be written as $G(R,R') = U_1(R_<)U_2(R_>)/W$, where U_1 and U_2 are the solutions of homogeneous part of (7.1.14) and W is the corresponding Wronskian. The cross section for vibrational excitation can now be written as [7.27]

$$\sigma_{i\to f}^{res} = \text{"constant"}\ |I_i|^2 |I_f|^2 \quad , \tag{7.1.20}$$

where all the normalization constants and the kinematical factors have been absorbed in the "constant" and I_i and I_f are the integrals

$$I_i = \int_0^{R_s} U_1(R)\tilde{V}_i^*(R)\chi_{v_i J}(R)dR \quad ,$$

$$I_f = \int_0^{R_s} U_2(R)\tilde{V}_f^*(R)\chi_{v_f J}(R)dR \quad .$$

These can be easily evaluated by using the WKB approximations for U_1 and U_2. The first factor $|I_i|^2$ in the VE cross section is the probability of the formation of the molecular resonant state when the neutral molecule is initially in the i^{th} vibrational level. This factor is proportional to σ_{cap}. The second factor $|I_f|^2$ is the probability that the resonant state autodetaches leaving behind the neutral molecule in the f^{th} vibrational level.

7.2 Applications to Specific Molecules

In the following discussion, vibrational excitation and dissociative electron attachment to some specific homonuclear as well as heteronuclear diatomic molecules will be reviewed. The threshold energy for the electron attachment process, $e + AB \to A + B^-$ depends on the dissociation energy (D_{00}) of AB and on the electron affinity (EA) of B: $E_{th}^{DA} = D_{00} - EA$. At higher incident electron energies, the negative ions can also be produced by the process of polar dissociation (PD). In this process also, the molecule AB dissociates under the impact of the incident electron. However, both the dissociating fragments are charged rather than neutral, that is, $e + AB \to e + A^+ + B^-$. The threshold energy for this process obviously depends on the ionization potential (IP) of A: $E_{th}^{PD} = D_{00} - EA + IP$. Table 7.1 provides the details of E_{th}^{DA} and E_{th}^{PD} for some simple diatomic molecules [7.28-30].

The shape of the electron attachment cross section as a function of the electron impact energy depends on the nature of the potential curve $V^-(R)$ of the resonant molecular anion. If the anion curve is attractive in nature, the attachment cross section shows a vertical onset with a peak at the threshold [7.17,31]. If the anion curve is repulsive, the attachment cross section, above the threshold, increases gradually to a peak. In the case of a heteronuclear molecule AB there are two thresholds for attachment corresponding to the possibility of either A^- or B^- formation. Table 7.2 shows the peak cross sections, just above the threshold, for attachment to various molecules at room temperature [7.32-35].

Table 7.1. Threshold energies and relevant quantities for dissociative electron attachment and polar dissociation of various diatomic molecules

Atom	EA [eV][a]	IP [eV][b]
H	0.7542	13.60
N	<0 (-0.07)	14.53
Cl	3.615	12.97
C	1.268	11.26
O	1.462	13.62

Molecule	D_{00} [eV][c]	E_{th}^{DA} [eV] (products)	E_{th}^{PD} [eV] (products)
H_2	4.478	3.724 ($H + H^-$)	17.32 ($H^+ + H^-$)
N_2	9.759	9.759 ($N + N + e$)	24.29 ($N^+ + N + e$)
CO	11.09	9.628 ($C + O^-$)	20.89 ($C^+ + O^-$)
CO	11.09	9.822 ($C^- + O$)	23.44 ($C^- + O^+$)
HCl	4.433	0.818 ($H + Cl^-$)	14.42 ($H^+ + Cl^-$)
HCl	4.433	3.679 ($H^- + Cl$)	16.65 ($H^- + Cl^+$)

[a][7.28]; [b][7.29]; [c][7.30]

Table 7.2. The peak cross sections for dissociative electron attachment to various diatomic molecules

Molecule	*Negative ion formed*	Peak attachment cross section [cm^2]	*Ref.*
H_2	H^-	1.8 (-21)[a]	[7.32]
N_2	N^- (autodetaching)	2.5 (-18)	[7.33]
CO	O^-	2.0 (-19)	[7.34]
CO	C^-	7.0 (-23)	[7.34]
HCl	Cl^-	2.68 (-17)	[7.35]
HCl	H^-	2.05 (-18)	[7.35]

[a]1.8 (-21) = 1.8×10^{-21}

7.2.1 Molecular Hydrogen

a) Resonances

Atomic hydrogen has a stable anion H^- with configuration $1s^2$. The lowest g and u states of the hydrogen molecular anion, namely the $^2\Sigma_g^+$ and $^2\Sigma_u^+$ states that dissociate into $H(1s) + H^-(1s^2)$, are true bound states for asymptotically large internuclear separations R. However, for small values of R, the states $(1\sigma_g)^2(1\sigma_u)\ ^2\Sigma_u^+$ and $(1\sigma_g)(1\sigma_u)^2\ ^2\Sigma_g^+$ are the lowest resonant states of H_2^-. Calculations of the resonant states show [7.36,37] that $^2\Sigma_u^+$ is a shape resonance, with the X $^1\Sigma_g^+$ state of H_2 as its parent, for internuclear separations $R \lesssim 3.0$ a.u. and that it turns into a bound state for larger values of R. This resonance is mainly responsible for the sharp threshold peaks in the dissociative attachment cross sections. The $^2\Sigma_g^+$ state of H_2^-, on the other hand, is [7.37] a shape resonance for $R \lesssim 5.1$ a.u. with the

$(1\sigma_g)(1\sigma_u)$ $^3\Sigma_u^+$ state of H_2 as its parent; it is an electron-excited Feshbach resonance in the approximate range 5.1 a.u. $\lesssim R \lesssim$ 5.3 a.u. of internuclear separations lying just below the repulsive $(1\sigma_g)(1\sigma_u)$ $^3\Sigma_u^+$ state of H_2 and it is a bound state for larger values of R. This resonance contributes strongly to the attachment cross sections and to excitation of higher vibrational levels of the ground electronic state $^1\Sigma_g^+$ of H_2 in the energy range 6-13 eV [7.38].

In the energy range 11-14 eV, information about the resonant states of H_2^- has been obtained [7.39] by investigating the energy-loss spectrum for the scattering of electrons by H_2 and D_2. The differential cross section plotted as a function of the incident electron energy for various fixed energy losses (corresponding to the excitation energy of various vibrational levels of the ground electronic state of the neutral molecule) in both H_2 and D_2 provided two series of peaks. These series have energy spacings of 0.3 eV and ~0.15 eV and have been designated series a and series b, respectively. The peaks of series b appear only in the high vibrational exit channels. The energy dependence of the differential cross sections for D_2 at smaller scattering angles ($\lesssim 70^\circ$) exhibited a further series of peaks which was labeled series c. The energy spacing of peaks in series c is very similar to that in series a. These three series of peaks were attributed to the vibrational levels of the excited resonant states of H_2^-. In fact, by studying rovibrational excitation of the ground electronic state of H_2 occurring via these resonant states, it was possible to establish the symmetry of the resonances [7.40]. It was tentatively concluded that the series a, b, and c belonged to the $1\sigma_g\ 1\pi_u^2\ ^2\Sigma_g^+$, $1\sigma_g\ 1\sigma_u^2\ ^2\Sigma_g^+$, and $1\sigma_g\ 1\pi_u\ 2\sigma_g$ $^2\Pi_u$ electronic states of H_2^-. It was later argued [7.41] that the series c could belong to a resonance with the configuration $1\sigma_g\ 1\pi_u^2$ (same configuration as for series a) and symmetry $^2\Delta_g$. The fact that both the series a and c have similar vibrational energy spacing was taken as supporting evidence for the corresponding resonances having the same electronic configuration. Calculations of the potential curves of the resonant states of H_2^- in the energy range 11-14 eV indicates [7.37] that series a starting at 11.32 eV with a spacing of 0.3 eV could originate from the resonant state A $^2\Sigma_g^+$ with a mixture of configurations $1\sigma_g\ 2\sigma_g^2$ and $1\sigma_g\ 1\pi_u^2$. Series c, possibly starting at 11.19 eV with the same vibrational energy spacing of 0.3 eV, might belong either to the $1\sigma_g\ 2\sigma_g\ 1\pi_u\ ^2\Pi_u$ resonant state or to the $1\sigma_g\ 1\pi_u^2\ ^2\Delta_g$ resonant state. The first designation ($^2\Pi_u$) is favored by calculations of the resonant potential curves since the minimum of the $^2\Delta_g$ curve appears to be too high in energy (> 11.5 eV) to account for the 11.19 eV starting point of the series. The second designation ($^2\Delta_g$), however, is deemed likely as a result of the more recent experiments [7.42] in which dissociative attachment occurring via higher vibrational levels of the $^2\Delta_g$ resonant state is apparently observed and it is suggested that the minimum of the $^2\Delta_g$ curve might lie lower in energy than calculated.

The existence of a $^2\Sigma_g^+$ resonance leading to the b series has also been experimentally confirmed [7.43]. However, not much further information seems to be avail-

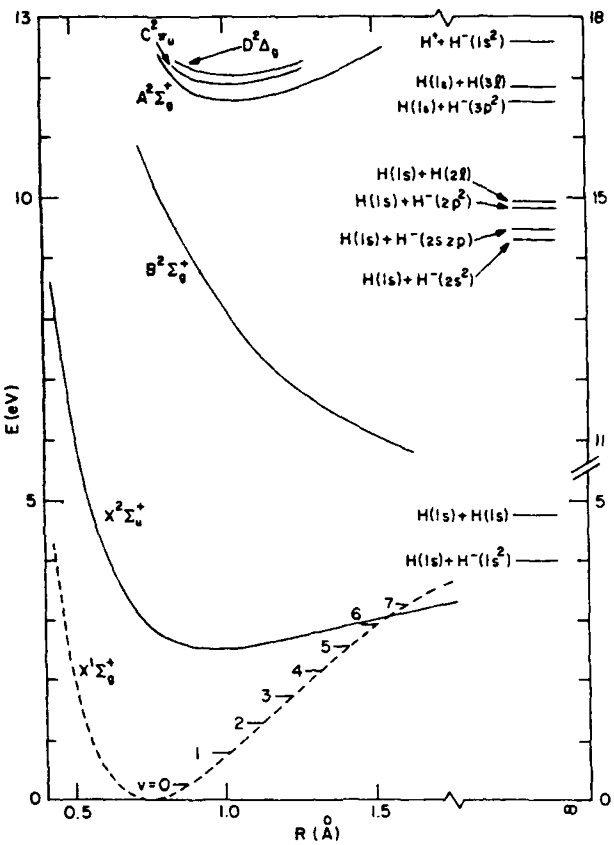

Fig.7.2. Potential curves of the ground and some excited electronic states of H_2^-. The dashed curve is the potential curve of the ground electronic state of H_2

able for series b. In fact, even the configuration of the electronic resonant state $^2\Sigma_g^+$ responsible for the b series does not appear to be firmly established.

A correlation diagram for various resonant states of H_2^- in the energy range 11-14 eV has been proposed [7.42,43]. The dominant configuration of the A $^2\Sigma_g^+$ resonance, which presumably is responsible for the a series, is $1\sigma_g\,2\sigma_g^2$ and it dissociates into H(1s) + $H^-(2s^2)$. The states $1\sigma_g\,2\sigma_g\,1\pi_u\ {}^2\Pi_u$ and $1\sigma_g\,1\pi_u^2\ {}^2\Delta_g$, which are possibly responsible for the c series, dissociate into H(1s) + H^-(2s2p) and H(1s) + $H^-(2p^2)$, respectively.

Finally, the real part of the potential curves of some of the resonant states of H_2^- [7.37] along with the potential curve for the ground electronic state of H_2 [7.44] are shown in Fig.7.2. The energy difference between the potential curves of the ground state of the neutral molecule and a particular resonant state, in the Franck-Condon region, is sometimes referred to as the energy of the resonance. As an example, the energy of the X $^2\Sigma_u^+$ and the B $^2\Sigma_g^+$ resonances of H_2^- are approximately 3.7 eV and 10.5 eV, respectively. The energetics of the potential curves imply, for example, that at an incident electron energy of ~9-11 eV the major contribution to the cross sections for the dissociative electron attachment as well as the vibrational excitation comes from the B $^2\Sigma_g^+$ resonance.

b) Vibrational Excitation

A somewhat superficial but easily understood approach is to think of the cross section for the vibrational excitation of a molecule as made up of two parts – a resonant part and a nonresonant (also potential or direct) part. A complete calculation of the vibrational excitation cross section should take into account both the resonant and the nonresonant contributions. The nonresonant part of the cross section is usually a smoothly varying function of the projectile energy. For any molecule it is possible to obtain the resonant contribution to the excitation cross section by using a resonance model in which an intermediate molecular anion resonant state is formed. For this purpose, one needs to know the complex potential energy curve of the resonant state. This can be obtained either by a separate ab initio calculation or by a semiempirical fit of some selected experimental data to the potential parameters. Close to the resonance energy, the resonant contribution to the excitation cross section can overwhelm, sometimes by orders of magnitude, the nonresonant part, while away from the resonance energy the resonant contribution is only a small fraction of the total excitation cross section. The overall excitation rate is then usually dominated by the resonant contribution. Alternatively, one could use various parts, static, exchange, polarization, etc., of the electron–molecule interaction to calculate low energy phase shifts and to obtain the relevant transition matrix elements either directly or by summing over various partial waves to calculate the excitation cross sections. If all the important parts of the interaction are taken into account properly, a resonance can reveal itself by making the phase shift of one of the partial waves, the one which leads the resonance formation, much larger than the other phase shifts [7.45].

The resonance contribution usually appears in the form of a bumplike structure in the excitation cross sections. If the resonance is short-lived (impulse limit), then during the lifetime of the resonance there is hardly any possibility of a nuclear wave packet reflecting at the turning points and the structure in the excitation cross sections is just a smooth broad bump. On the other hand, in the case of a long-lived resonance (compound limit) with an attractive curve, there is significant interference between the incident and reflected nuclear wave packets, which appears in the excitation cross sections [7.10] as a bump with substructure, corresponding to the vibrational levels of the resonance state.

Figure 7.3 shows the energy-loss spectrum of H_2 taken at 140° with 10.5 eV electrons [7.46]. The elastic peak at zero energy loss is normalized to 1. The energy separation between the peaks corresponds to the vibrational spacing of H_2. The ratio of the peak intensities gives the relative magnitude of the vibrational excitation

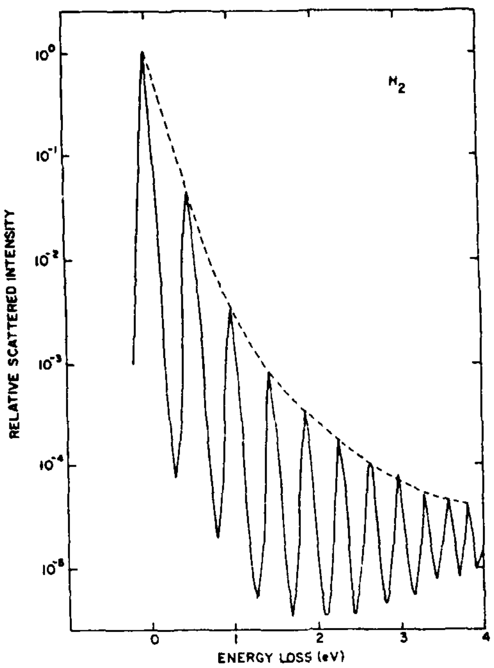

Fig.7.3. Energy-loss spectrum of H_2 at 10.5 eV and 140°. The elastic peak at zero energy loss is normalized to 1

cross sections for the incident electron energy of 10.5 eV. The important point is that at this incident energy, the vibrational excitation cross sections σ_{0v} relative to the elastic cross section σ_{00} decrease with increasing v by almost an order of magnitude for small v (v = 1,2,3) but become almost constant for large v (v = 8,9,10). This is a clear indication that the resonance responsible for the excitation of lower vibrational levels is different from the resonance responsible for excitation of the higher vibrational levels. This fact is also evident from Fig.7.4 where the individual contributions [7.38] of the lowest two (namely, $^2\Sigma_u^+$ and $^2\Sigma_g^+$) resonances of H_2^- to the vibrational excitation cross sections are shown, along with the experimental results [7.47,48]. Note that for incident electron energy ~10 eV, σ_{01} and σ_{02} are essentially dominated by the $^2\Sigma_u^+$ resonance while a tendency exists for the $^2\Sigma_g^+$ resonance to dominate the excitation of higher vibrational levels. The ab initio calculations [7.49] of the vibrational-excitation cross sections at low impact energies (≤ 10 eV) also agree with the experiments.

The excitation of higher vibrational levels can also be achieved very efficiently by a nonresonant process in which higher electronic states of the H_2 molecule are populated first by electron impact. The higher singlet electronic states will eventually decay radiatively leading to the repopulation of the vibrational levels of the X $^1\Sigma_g^+$ state of H_2. Above the threshold (~20 eV) the cross sections for vibrational excitation ($v_f \geq 3$) of H_2 via electron collisional excitation of the higher singlet states can be orders of magnitude larger than the resonant cross sections shown in Fig.7.4 [7.50].

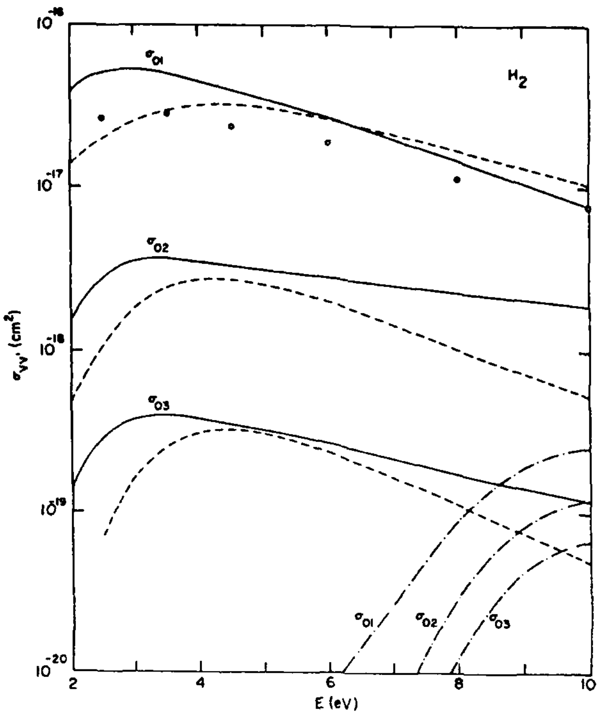

Fig.7.4. Contributions of the two lowest resonant states to the vibrational excitation cross sections of H_2 (---): $^2\Sigma_u^+$; (-·-·-): $^2\Sigma_g^+$. (——) are the experimental results of *Ehrhardt* et al. [7.47] and the circles are the observations for σ_{01} of *Linder* and *Schmidt* [7.48]

c) Dissociative Attachment

The production of H^- ions by electron impact on H_2 is caused either by the process of dissociative attachment,

$$e + H_2 \rightarrow H + H^-$$

or by polar dissociation

$$e + H_2 \rightarrow H^+ + H^- + e \quad .$$

Below an electron impact energy of 17.2 eV, polar dissociation of H_2 is energetically not possible and negative ions are produced only by dissociative attachment. A global view of the H^- production from H_2 in the lowest vibrational level of its ground electronic state is shown [7.51] in Fig.7.5. The structures around 3.5-4 eV and 8-12 eV are dominated by the $^2\Sigma_u^+$ and the $^2\Sigma_g^+$ resonances of H_2^-, respectively. The sharp peak around 14.2 eV is caused by the higher resonances [7.52] which result in dissociation into $H^* + H^-$. In fact, substructures corresponding to the vibrational levels of the higher resonant states have been observed [7.42,53] on the high-energy side of both the 10 eV and the 14 eV peaks.

Recent observations [7.54] of H^- production from H_2, in the energy range 1-5 eV, have revealed a dramatic increase in the attachment cross sections if the attaching

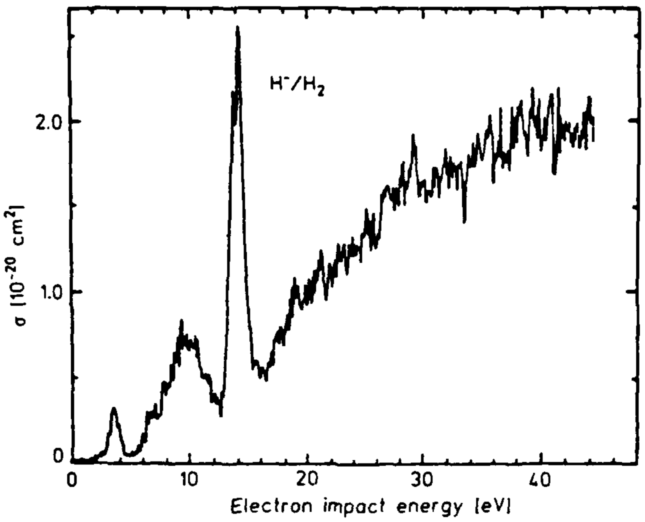

Fig.7.5. A global view of H^- production from H_2 by electron impact. From [7.51] with permission

H_2 molecule is rovibrationally excited. For example, an increase of four orders of magnitude in the cross section is observed if H_2 is excited from $v=0$ to $v=4$ and a fivefold increase for $J=0$ to $J=7$ excitation. These experimental observations can be completely accounted for within the resonance model by using semiempirical fits to the relevant potential curves of H_2 and H_2^-. These theoretical results [7.21, 38] are compared with experimental observations in Fig.7.6. The enhancement of the cross sections essentially arises from the $^2\Sigma_u^+$ resonance of H_2^- which is a short-lived resonance with an average width of about 8 eV. Figure 7.7 shows [7.55] the individual contributions of both the $^2\Sigma_u^+$ and the $^2\Sigma_g^+$ resonances of H_2^- to the dissociative attachment cross sections. The $^2\Sigma_g^+$ resonance, which dominates the attachment around 10 eV, does not exhibit a dramatic enhancement on vibrationally exciting the molecule. The $^2\Sigma_g^+$ contribution shows peaks which arise from the oscillations in the vibrational wave functions of H_2. This structure, which is apparently related to the Condon diffraction bands [7.56], clearly indicates that the $^2\Sigma_g^+$ resonance has a longer lifetime (and hence a smaller average width) than the $^2\Sigma_u^+$ resonance. This fact is indeed supported by the calculations [7.57].

The attachment rate at low electron temperatures is also essentially determined by the contribution of the $^2\Sigma_u^+$ resonance. The attachment rate is of course dramatically increased if the attaching molecule has internal energy (in the form of rovibrational excitation) built into it. At low internal energies, vibrational excitation is more effective in enhancing the attachment cross sections and rates than the rotational excitation, however, at high internal energies, the enhancement is basically determined by the total internal energy and not by its exact partitioning between the vibrational and rotational modes [7.58]. This strong enhancement of the attachment process on increasing the internal energy of the molecule is attributed to an increase in the range of internuclear separations over which the electron

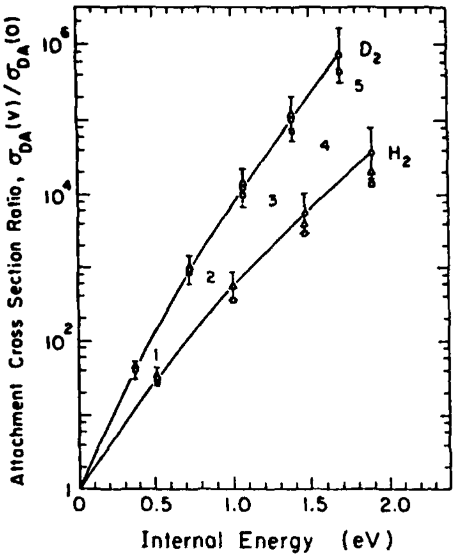

Fig.7.6

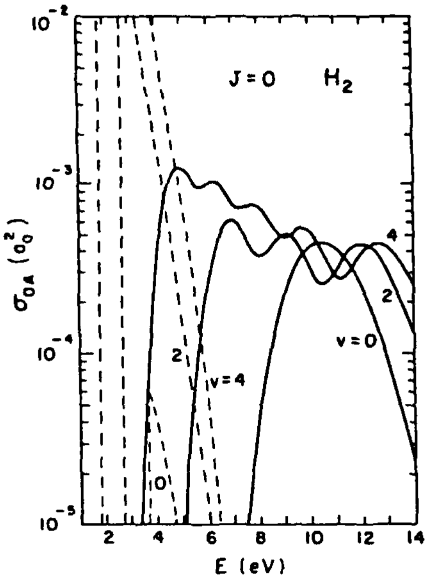

Fig.7.7

Fig.7.6. Internal energy dependence of the threshold cross sections for electron attachment to H_2 and D_2 via the lowest resonance. (○○○): experiment [7.54]; (□□□,△△△): theoretical results from [7.21 and 38], respectively. From [7.38] with permission

Fig.7.7. Contributions of the two lowest resonant states to the dissociative electron attachment cross sections for various rotationless vibrational levels of H_2. (——): $^2\Sigma_g^+$; (----): $^2\Sigma_u^+$. From [7.55] with permission

capture can occur. This increase occurs because of the larger amplitude of vibration for vibrational excitation and because of the centrifugal stretching of the molecule for rotational excitation.

The ground electronic state of H_2 supports at least 294 rovibrational levels. An investigation [7.59] of the contribution of the $^2\Sigma_u^+$ resonance to attachment to all these levels of H_2 revealed that the maximum possible rate of electron attachment to the ground electronic state of H_2 is about $10^{-8}\,cm^3s^{-1}$ and, furthermore, that the average energy carried by the H^- ions is almost always less than 0.5 eV.

From Fig.7.2 one notes that the real part of the potential curve of the $^2\Sigma_u^+$ state of H_2^- is slightly attractive, while that of the $^2\Sigma_g^+$ state is always repulsive. It has been argued [7.17,31] that, in general, an attractive resonance curve will result in a vertical onset of the attachment cross section at threshold while a repulsive resonance curve will give a gradual buildup of the cross section at the threshold. This behavior at the threshold in attachment cross sections is clearly noticeable in Fig.7.7 in the cases of the $^2\Sigma_u^+$ and the $^2\Sigma_g^+$ resonances of H_2^-.

Anomalously large densities of H^- ions observed [7.60] in a hydrogen plasma can be attributed to the production of these ions by dissociative electron attachment to either the ground electronic state or possibly to the excited electronic states of H_2 [7.61].

d) Isotope Effect

One can study the isotope effect for dissociative attachment and vibrational excitation by replacing either one or both of the nuclei by their isotopes. The effect is most striking for lighter molecules like hydrogen because of the greater change in the reduced mass on isotope substitution. It is observed [7.32,52] that the cross section for the production of H^- from H_2 exceeds that of D^- from D_2 by several orders of magnitude. However, ignoring the magnitude, the qualitative behavior of D^- production from D_2 is essentially similar to H^- from H_2. Table 7.3 provides cross sections, near threshold, for attachment to H_2 and D_2 in various rovibrational levels. This isotope effect in regard to the dissociative attachment can be understood [7.62] within the resonance model by noting, from the semiclassical expression (7.19) for the attachment cross section, that the classical survival factor

$$S = \exp\left(-\int_{R_c}^{R_s} \frac{\Gamma(R)}{\hbar}\,\frac{dR}{v(R)}\right)$$

is a strongly mass dependent quantity. In fact, S can be approximated by $\exp(-\bar{\Gamma}\tau/\hbar)$ where τ, the time taken for the separation of the nuclei to increase from the capture radius R_c to the stabilization radius R_s (see Fig.7.1), is inversely proportional to $M^{1/2}$, due to simple kinematical considerations. Thus nuclei of D_2, taking longer than nuclei of H_2 to separate out to R_s, experience a stronger competition from autodetachment which, in turn, reduces the probability of dissociative attachment.

It has been theoretically predicted [7.63] that the contribution of a short-lived (that is, impulse limit) resonance to the vibrational-excitation cross sections σ_{0v} behaves as $M^{-v/2}$. At low impact energies ($\lesssim 5$ eV) the dominant contribution to the excitation of the low vibrational levels of H_2 and D_2 comes from the $^2\Sigma_u^+$ resonance which is a broad, short-lived resonance. Both the experimental observations [7.54] and the theoretical calculations [7.38] indeed show $\sigma_{0v}(D_2) \approx 2^{-v/2}\sigma_{0v}(H_2)$ for $v = 1,2,3$.

7.2.2 Molecular Nitrogen

a) Resonances

It is rather curious that even though N_2 could be safely considered, in electron-molecule collisions, as the most investigated molecule, the complex potential energy curves of the first few resonant states of N_2^- have not yet been established over

Table 7.3. Dissociative electron attachment cross sections near threshold for various rovibrational levels of H_2 and D_2

v	J	H_2 E [eV]	H_2 σ_{DA} [cm^2]	D_2 E [eV]	D_2 σ_{DA} [cm^2]
0	0	3.73	1.6(-21)[a]	3.83	3.0(-24)
0	1	3.73	1.7(-21)	3.80	3.3(-24)
0	2	3.70	1.9(-21)	3.80	3.4(-24)
0	3	3.65	2.3(-21)	3.78	3.9(-24)
0	4	3.60	2.8(-21)	3.75	4.5(-24)
0	5	3.53	3.7(-21)	3.70	5.7(-24)
0	6	3.45	5.0(-21)	3.68	6.8(-24)
0	7	3.35	7.2(-21)	3.63	8.8(-24)
0	8	3.25	1.1(-20)	3.58	1.2(-23)
0	10	3.13	2.2(-20)	3.43	2.2(-23)
0	15	2.38	3.2(-19)	3.03	2.0(-22)
0	20	1.63	5.5(-18)	2.55	2.5(-21)
1	0	3.23	5.5(-20)	3.45	1.5(-22)
2	0	2.73	8.0(-19)	3.08	3.3(-21)
3	0	2.28	6.3(-18)	2.75	4.2(-20)
4	0	1.85	3.2(-17)	2.43	3.6(-19)
5	0	1.45	1.1(-16)	2.10	2.2(-18)
6	0	1.08	3.0(-16)	1.80	1.0(-17)
7	0	0.73	4.5(-16)	1.53	3.3(-17)
8	0	0.40	3.5(-16)	1.25	9.6(-17)
9	0	0.13	4.8(-16)	1.00	2.3(-16)
10	0			0.75	4.1(-16)
11	0			0.53	3.8(-16)
12	0			0.30	3.7(-16)
13	0			0.10	4.6(-16)

[a] $1.6(-21) = 1.6 \times 10^{-21}$

the complete range of internuclear separations R. In fact, the lowest resonance of N_2^-, namely, the $^2\Pi_g$ resonance at about 2.2 eV, has been traditionally used [7.16,25, 64-66] for testing many new ideas. The electron affinity of atomic nitrogen is slightly negative (-0.07 eV) indicating that N^- is an unstable anion capable of autodetaching the electron. The ground and the first excited electronic states of N_2, dissociating into N (^4S) + N (^4S), have configurations

$$1\sigma_g^2\ 1\sigma_u^2\ 2\sigma_g^2\ 2\sigma_u^2\ 1\pi_u^4\ 3\sigma_g^2\ X^1\Sigma_g^+ \quad \text{and}$$

$$1\sigma_g^2\ 1\sigma_u^2\ 2\sigma_g^2\ 2\sigma_u^2\ 1\pi_u^3\ 3\sigma_g^2\ 1\pi_g\ A^3\Sigma_u^+ \quad .$$

The two lowest resonant states of N_2^-, dissociating into $N(^4S) + N^-(^3P)$, are then obtained by adding an extra electron in the valence orbital π_g, that is,

$$1\sigma_g^2\ 1\sigma_u^2\ 2\sigma_g^2\ 2\sigma_u^2\ 1\pi_u^4\ 3\sigma_g^2\ 1\pi_g\ X^2\Pi_g \quad \text{and}$$

$$1\sigma_g^2\ 1\sigma_u^2\ 2\sigma_g^2\ 2\sigma_u^2\ 1\pi_u^3\ 3\sigma_g^2\ 1\pi_g^2\ A^2\Pi_u \quad .$$

The configuration and structure of these two resonant states of N_2^- are quite similar to the $X^2\Pi$ and $B^2\Pi$ states of the isoelectronic molecule NO [7.67].

Quite a few calculations have been made [7.16,66,68] just to establish the electronic resonance parameters of the $^2\Pi_g$ state. These calculations, by their very nature, provide reasonable values of the complex potential curve only in the vicinity of the equilibrium internuclear separations. The only calculation [7.69] of the absolute values of the potential curves of N_2^-, available over an extended range of internuclear separations R, is not able to correctly fix the N_2^- curves relative to the $X^1\Sigma_g^+$ curve of N_2. In Fig.7.8 these resonant curves for the $X^2\Pi_g$ and the $A^2\Pi_u$ states are shown over a large range of R and compared with the ab initio curves of the $X^1\Sigma_g^+$ and $A^3\Sigma_u^+$ states of N_2. The N_2^- curves in Fig.7.8 are positioned so that the potential minimum of the $^2\Pi_g$ curve matches that of the more elaborate ab initio calculation [7.66] done only in the vicinity of the equilibrium internuclear separation. The $X^2\Pi_g$ and the $X^1\Sigma_g^+$ curves shown in the figure cross at 1.48 Å which is larger than the internuclear separation at which the ab initio curves are seen to

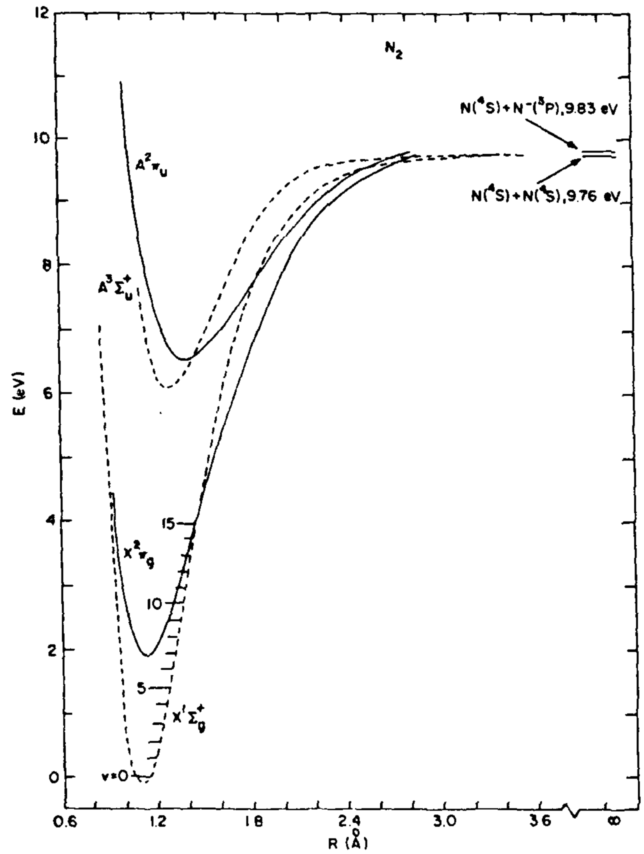

Fig.7.8. Potential curves of the lowest two electronic states of N_2^- (——) and N_2 (----)

cross. Interestingly, however, the curves in Fig.7.8 indicate that the $A^2\Sigma_u$ state of N_2^- turns into a true bound state for 1.8 Å $\lesssim R \lesssim$ 2.5 Å. It has also been argued independently [7.70] that this bound state behavior of the $^2\Sigma_u$ state exists over a larger range of internuclear separations than the one shown in Fig.7.8.

b) Vibrational Excitation

In the case of nitrogen, the lifetime of the lowest resonance, $^2\Pi_g$, is comparable to the vibrational period of the nuclei in N_2^-. This is an example of the boomerang limit of the resonance model. The strong interference between the initial and the single reflected nuclear wave packets results in spectacular peaks in the energy dependence of the vibrational excitation cross sections [7.10,71] at low impact energies ($\leqslant$ 4 eV). The positions of these peaks shift to higher energies for excitation to higher vibrational levels. More than forty clearly resolvable peaks in the cross sections are observed for excitation from $v = 0$ to $v = 1 - 7$ levels. A global view [7.10] of the vibrational-excitation cross sections of N_2 in the energy range 1 to 30 eV reveals at least three broad maxima at electron impact energies larger than 7 eV. The broadest and the largest of these maxima extends from roughly 15 eV to 30 eV.

A number of calculations have been carried out to explain the positions and the shifts of the peaks at low energies in the experimental vibrational excitation cross sections. These include an ab initio close-coupling hybrid calculation [7.64], a calculation using the R-matrix formulation [7.65], and calculations using the resonance model with both ab initio [7.66] and semiempirically fitted parameters [7.25] for the complex resonance potential curves. Various calculations differ in computational complexity, however, all calculations are able to reproduce at least qualitatively, and in some cases even quantitatively, the experimentally observed peaks in the excitation cross sections.

The essential difference [7.72] between the ab initio hybrid theory approach and the resonance model approach lies in the choice of the basis functions used for representing the electron-molecule system (with N + 1 electrons). In the hybrid theory, the system wave function is expanded, in a close-coupling manner, in terms of the complete set of vibrational states of the N-electron target molecule. In the boomerang model, on the other hand, the system wave function is written in terms of the electronic-nuclear wave functions of the (N + 1)-electron resonant state. If carried to completeness, either procedure would provide the same, and presumably the exact, result. However, computer limitations necessitate the truncation of the basis set which forces a finite number of N-electron functions, in the hybrid theory, to mimic the behavior of the (N + 1)-electron system. For this reason, even though the hybrid theory takes the complete physics of the process into account, the rate of convergence in the calculations using this theory is quite slow [7.64].

Therefore, in processes like the vibrational excitation of N_2 around 2-3 eV, where a resonance formation is evident, the resonance model approach will clearly give more rapidly converging results.

As mentioned earlier, an important feature of the boomerang limit of the resonance model is that the resonance width is a decreasing function of the internuclear separation R [7.16]. After resonance formation, the nuclei separate out until a reflection occurs at the outer turning point. Now as the nuclei come closer together, the resonance width increases and the resonance lifetime decreases with the net result that the resonance effectively "dies out" leading to the autodetachment of the electron or the vibrational excitation of the molecule. Thus it is the interference between the single incident and a single reflected nuclear wave in the resonant state that leads to the shifting peaks in the vibrational-excitation cross sections.

In two separate endeavors [7.25,66] the resonance model has been used to calculate the cross sections for the vibrational excitation of N_2 at low energies. In one case, the resonance parameters – the electronic potential curve of the molecular anion and its resonance width – are obtained from an ab initio calculation. In the other case, a semiempirical approach is used in which about half-a-dozen parameters are adjusted to obtain agreement with a selected subset of the experimental data. Either calculation is able to reproduce almost all of the peaks in the excitation cross sections. Figure 7.9 shows a comparison of the experimentally observed excitation cross sections [7.71] with those obtained by the semiempirical resonance model approach [7.25]. It is interesting that even though the ab initio resonance parameters differ substantially from the semiempirical ones, both sets of parameters provide similar results for the vibrational-excitation cross sections. This clearly suggests [7.73] that there may not be a unique set of resonance parameters which lead to the correct cross sections.

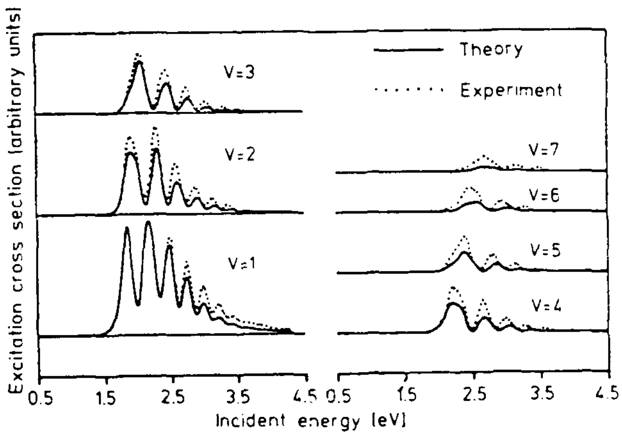

Fig.7.9. Relative cross sections for vibrational excitation of N_2. (····): experiment [7.71]; (——): theoretical results [7.25]. From [7.25] with permission

The peak in the vibrational excitation cross sections in the energy range 15 to 30 eV is quite broad; its full width at half maximum is larger than 5 eV. It is proposed [7.74] that this broad peak arises from a shape resonance which corresponds to the trapping of the incident electron in the $3\sigma_u$ molecular orbital.

c) "Dissociative Attachment"

The ground state of the atomic anion $N^-(^3P)$ is an autodetaching state. Thus the traditional process of dissociative attachment which would normally lead to a stable atomic negative ion is not possible for N_2. However, an analogous process, via the formation of an intermediate molecular resonant state, is possible for N_2 which results in the dissociation of the molecule plus a free electron with kinetic energy equal to the magnitude of the atomic electron affinity ($\sim$0.07 eV). This process is appropriately termed [7.33] "resonant dissociation by electron impact". Schematically

$$e + N_2 \rightarrow N_2^-(\text{resonance}) \rightarrow N(^4S) + N^-(^3P) \quad \text{and}$$

$$N^-(^3P) \rightarrow N(^4S) + e \quad .$$

That the dissociation is indeed occurring via the formation of $N^-(^3P)$ has been confirmed [7.75] by studying the energy distribution of the emitted electrons. This energy distribution is observed to be independent of the incident electron energy and is essentially determined by the energy and the lifetime (or the width) of the $N^-(^3P)$ resonant state. The measured current of the ejected electrons indeed peaks at the residual electron energy of 0.07 eV. Also, the molecular resonance responsible for $N^-(^3P)$ formation is argued [7.75] to be the $^2\Sigma_u$ state of N_2^-.

Both the differential and the integral (or total) cross section for "dissociative attachment" to N_2 have been measured [7.33,70] and are seen to be compatible with the calculations [7.70] of the same using the local resonance model. Figure 7.10 shows the total cross section for production of N atoms from the reaction $e + N_2 \rightarrow N + N + e$ (0.07 eV) as a function of incident electron energy. The resonance model calculations can, of course, be extended to determine whether the attachment cross section is dependent on the initial rovibrational state of the neutral molecule. Unlike hydrogen, the effect of temperature on the cross section for attachment to N_2 is not very dramatic. An increase by at most a factor of four of the attachment cross section is predicted [7.76] if the molecule is vibrationally excited from $v = 0$ to $v = 4$. An estimate of the dissociation rate suggests [7.33] that the resonant dissociation mechanism could be an important source of superthermal N atoms from N_2.

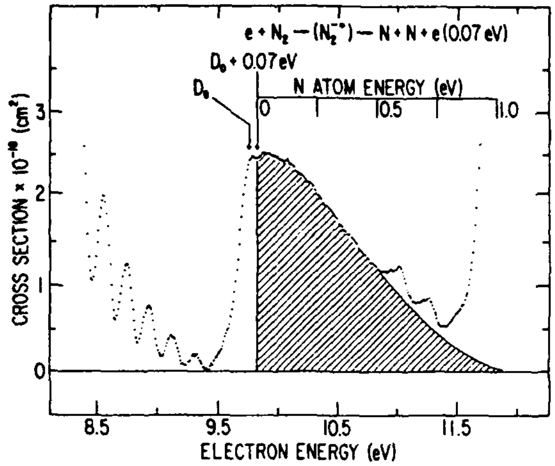

Fig.7.10. Total cross section for production of N atoms (*shaded area*) from the reaction $e + N_2 \rightarrow (N_2^{-*}) \rightarrow N + N + e$ (0.07 eV) as a function of incident electron energy. From [7.33] with permission

7.2.3 Carbon Monoxide

a) Resonances

Some information about the resonances of CO^- could certainly be gleaned from the resonances of the isoelectronic system N_2^-. However, unlike N_2, it is possible, in the case of CO, to obtain two stable negative ions, C^- and O^-. The lowest-energy state of CO, dissociating into $C(^3P) + O(^3P)$, has the configuration

$$(\sigma 1s)^2(\sigma^* 1s)^2(\sigma 2s)^2(\sigma^* 2s)^2(\pi 2p)^4(\sigma 2p)^2$$

which in the united-atom limit can be expressed as

$$(1s\sigma)^2(2s\sigma)^2(2p\sigma)^2(2p\pi)^4(3s\sigma)^2(3p\sigma)^2 \; {}^1\Sigma^+ \quad .$$

[The standard notation [7.77] of an asterisk is used to indicate an antibonding orbital.] The next vacant orbital is the antibonding π^*2p orbital and the lowest resonance of CO^- is thus obtained by placing the extra electron in this orbital. This results in the $^2\Pi$ shape resonance of CO^- which is analogous to the $^2\Pi_g$ resonance of N_2^-. The electron affinity of atomic oxygen is larger than the affinity of atomic carbon [7.28] and therefore the lowest resonance of CO^-, namely $^2\Pi$, dissociates into $C(^3P) + O^-(^2P)$. It might also be instructive to compare the resonant states of CO^- with another isoelectronic system, the heteronuclear diatomic molecule NO [7.67]. The $X\,^2\Pi$ ground state of NO has the same configuration as the lowest $^2\Pi$ resonance of CO^- mentioned above. The lowest excited $^2\Pi$ state of NO, the B state at 5.7 eV, is bound in the Franck-Condon region. This state of NO has the dominant configuration ... $(\pi 2p)^3(\sigma 2p)^2(\pi^* 2p)^2$. The analogous excited $^2\Pi$ resonance of CO^- is also expected to be attractive in the Franck-Condon region and is proposed [7.78] to be responsible for the vertical onset of the O^--production curve at the threshold.

The resonance most probably responsible for $C^-(^4S)+O(^3P)$ production is the $^2\Sigma^+$ Feshbach resonance with the dominant configuration

$$(\sigma 1s)^2(\sigma^* 1s)^2(\sigma 2s)^2(\sigma^* 2s)^2(\pi 2p)^4(\sigma 2p)(\sigma 3s)^2 \ ^2\Sigma^+ \quad .$$

This resonance was first observed [7.79] at 10.02 eV during investigations of the energy dependence of the differential cross sections for scattering of low-energy electrons (9.5-11.5 eV) by CO. The width of this resonance is expected to be small, due to its closed-channel nature. In fact, ab initio calculations [7.80] give a width of 71 meV compared with the experimental value [7.79] of 45 meV. An analogous Feshbach $^2\Sigma_g^+$ resonance of N_2^-, with a similar configuration, is observed [7.81] at 11.48 eV.

b) Vibrational Excitation

Experimental observations [7.47] of the energy dependence of low-energy cross sections for the vibrational excitation of CO reveal characteristics which are very similar to those shown by the cross sections for N_2. The vibrational-excitation cross sections show peaks which shift toward higher energies with increasing final vibrational quantum number. These characteristics are once again understood in terms of the boomerang limit of the lowest resonance of CO, namely, the $^2\Pi$ shape resonance. As shown in Fig.7.11, the semiempirical calculations [7.82,83] using the local width resonance model are able to explain the experimental observations [7.47] in a satisfactory manner. The average width of the $^2\Pi$ resonance, as obtained by this semiempirical fit, is indeed comparable to the vibrational period of the resonant state as expected for the boomerang limit. Even the semiclassical calculations [7.84] of the vibrational excitation cross sections using semiempirically derived resonance parameters are in fairly good agreement with the experimental observations.

The energy position of the $^2\Pi$ resonance of CO, which is essentially responsible for the oscillatory structure in the vibrational excitation cross sections at low energies (~1-4 eV), is 1.8 eV [7.47,85]. Figure 7.11 shows that, for electron impact energies either less than 1 eV or larger than 3.5 eV, the resonant contribution to the excitation is negligible and the excitation in these energy ranges is completely via nonresonant processes. In fact, on comparing the cross section σ_{01} for electron impact energies less than 1 eV for isoelectronic molecules CO and N_2 (from Figs.7.11 and 9, respectively), it is observed that the nonresonant contribution to the excitation persists below 1 eV for CO while for N_2 there is almost no background nonresonant contribution. This is understood [7.47] by the fact that, unlike N_2, carbon monoxide has a permanent dipole moment which is responsible for a considerable nonresonant contribution.

The angular dependences of the excitation cross sections at low energies ($\lesssim$5 eV) for isoelectronic molecules CO and N_2 are observed [7.47,86] to be different in

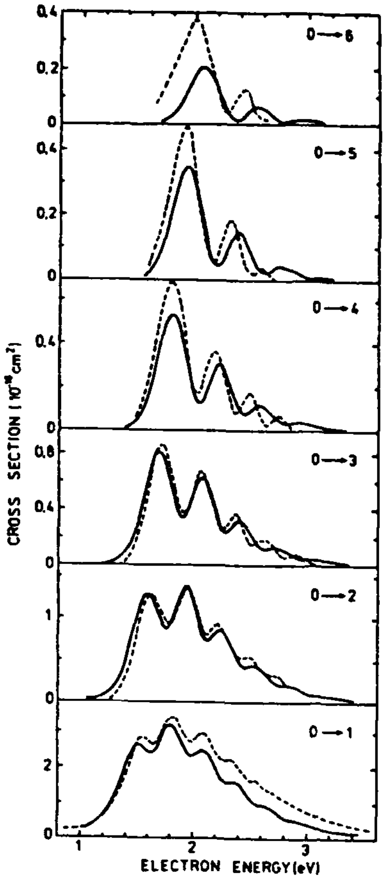

Fig.7.11. Energy dependence of the total cross sections for the vibrational excitation of CO from the lowest level v = 0. (----): experiment [7.47]; (——): theoretical results [7.83]. From [7.83] with permission

shape. At these low energies the excitation cross sections are dominated by shape resonances – $^2\Pi$ for CO^- and $^2\Pi_g$ for N_2^-. The temporarily bound electrons in these resonances are trapped in the molecular orbitals $p\pi$ for CO^- and πg for N_2^- which, in the united-atom limit, coalesce into p- and d-type atomic orbitals, respectively. Thus the angular momentum quantum number of the autodetaching electron is $l = 1$ for CO and 2 for N_2, which, of course, influences the angular distribution.

c) Dissociative Attachment

Dissociative electron attachment to CO can lead to two possible stable negative ions C^- and O^-. Due to the difference in the electron affinities of C and O, the thresholds for production of the two ions are different. For example, the process

$$e + CO \rightarrow C + O^-$$

is possible only for electron impact energies ≥9.63 eV, while the process

$$e + CO \rightarrow C^- + O$$

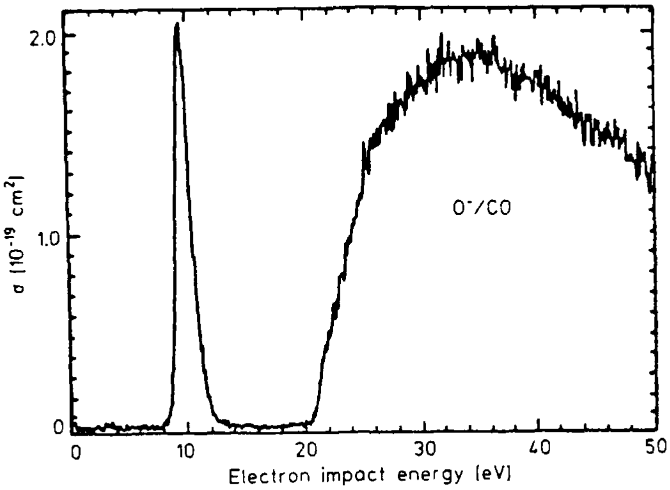

Fig.7.12. A global view of O^- production from CO by electron impact. From [7.51] with permission

has a higher threshold of 9.82 eV. Moreover, the cross section for the formation of C^- via dissociative attachment is smaller than the cross section for O^- formation [7.87,88]. Figure 7.12 shows [7.51] the global behavior of O^- production from CO. The threshold peak at 9.6 eV results from the lowest excited B $^2\Sigma$ shape resonance of CO^- and gives a maximum cross section of 2×10^{-19} cm^2. The vertical onset of the attachment cross section indicates that this $^2\Pi$ resonance of CO^- must be attractive in the Franck-Condon region. The structure on the high-energy side is related to the formation of $C^*(^1D)$ [7.78].

The sharp rise in O^- production from CO for electron impact energy larger than 20 eV arises from the process of polar dissociation [7.51]. The threshold for this process

$$e + CO \rightarrow C^+ + O^- + e$$

is 20.89 eV. The threshold for polar dissociation leading to C^-, namely,

$$e + CO \rightarrow C^- + O^+ + e$$

is 23.44 eV. Note that even though the peak cross section for O^- formation by polar dissociation is comparable to that by dissociative electron attachment, the relatively high threshold of polar dissociation makes that process a less efficient source of negative ions.

The cross section for C^- formation by attachment to CO, at its peak, is approximately a factor of 3000 smaller than the cross section for O^- formation [7.88]. An almost vertical onset at 10.26 eV gives a peak cross section of only 7×10^{-23} cm^2. The difference between the observed onset and the expected threshold is interpreted [7.34] as due to the predissociation of the $^2\Sigma^+$ resonant state of CO^- by another resonant state leading to the $C^-(^4S) + O(^3P)$ dissociation limit. This interpretation is further reinforced by the observation [7.34] of peaks in the variation of C^- ion current with the incident electron impact energy. The first two peaks at 10.27 eV and 10.50 eV are clearly related in their energy position to the vibrational levels v = 1 and 2 of the $^2\Sigma^+$ resonant state of CO^- at 10.04 eV.

7.2.4 Hydrogen Chloride

a) Resonances

The structure of the resonances of HCl is of special interest because of the highly polar nature of this molecule. The permanent dipole moment of HCl (1.11 D) is slightly smaller than the critical value (1.625 D) needed to bind an electron to a polar molecule [7.89]. The role played by the quasi-bound virtual state of the projectile electron in the dipolar field of the molecule in explaining the observations of the vibrational excitation still remains a matter of discussion [7.90]. The fact that both the constituent fragments of hydrogen chloride have positive electron affinities implies that, asymptotically, the potential curves of the resonant states of HCl^- are bound relative to the ground X $^1\Sigma^+$ state of HCl. In the united-atom limit the configuration of the ground state of HCl is

$$(1s\sigma)^2(2s\sigma)^2(2p\sigma)^2(2p\pi)^4(3s\sigma)^2(3p\sigma)^2(3p\pi)^4 \ X\ ^1\Sigma^+ \quad .$$

The lowest resonant state is obtained by placing the extra electron in the $4s\sigma$ molecular orbital. Also, noting that the electron affinity of the Cl atom (3.615 eV) is larger than the electron affinity of the H atom (0.754 eV) and that both H^- and Cl^- have no known excited states [7.28], the lowest resonant state asymptotically correlates with the limit $H + Cl^-$. In fact, using the Wigner-Witmer correlation rules [7.91], it is easy to infer that the only resonant state of HCl^- dissociating into $H(^2S) + Cl^-(^1S)$ has symmetry $^2\Sigma^+$. The other resonant states, dissociating into $H^-(^1S) + Cl(^2P)$, have possible symmetries of $^2\Sigma^+$ and $^2\Pi$.

It has been pointed out [7.92] that because of the highly polar nature of the molecule HCl, "electron trapping states" can also arise due to the dipolar field of the molecule. As the internuclear separation increases, the dipolar field tends to zero and these quasi-bound states merge into continuum states. Indeed, ab initio calculations [7.92-95] of the potential curves of HCl^- show several states of $^2\Sigma^+$ symmetry which exist only in the region of equilibrium internuclear separation (1.27 Å) and cannot be followed at larger values of R. The second-lowest state of HCl^- with $^2\Sigma^+$ symmetry exhibits an attractive potential curve that runs parallel to the X $^1\Sigma^+$ curve of HCl for internuclear separations less than ~2 Å and merges into a continuum state for larger separations. The mechanism responsible for the trapping of the incoming electron cannot be the centrifugal barrier since the dominant component of angular momentum is an s wave. The dipolar field of the molecule HCl is on the verge of binding an s electron; small displacements of the nuclei can cause an s wave bound state to appear or disappear. Such states are referred to as the virtual states of the system [7.96]. The virtual states merging into continuum states, in the case of HCl^-, would not be dissociating into atomic anions but rather into H + Cl + e. Whether these quasi-bound states in the dipolar field can be construed as bona fide resonances remains a topic of current discussion [7.95].

The lowest state of HCl^- with $^2\Sigma^+$ symmetry does indeed correlate, at infinite separations, with $H + Cl^-$. The potential curve for this resonant state is calculated to be an attractive one; however, the location of the potential minimum is not well established. The two ab initio calculations for the resonant states of HCl^- dissociating into $H^- + Cl$ provide conflicting results. For example, one calculation [7.93] gives a purely repulsive potential curve for the $^2\Pi$ state of HCl^-, while the other [7.94] shows a weakly attractive curve for the same state. An experimentally derived potential curve for the $^2\Pi$ state is repulsive at least in the Franck-Condon region [7.97].

b) Vibrational Excitation

Experimental observations [7.98,99] of the total cross sections for the excitation of the low-lying vibrational levels of HCl reveal some interesting features. First, the cross sections show a pronounced peak, about 0.2 eV wide, at the threshold, for excitation to each final vibrational level $v_f = 1,2,\ldots$. A small cusp is observed in the cross section σ_{01} at an impact energy which corresponds to the opening of the second vibrational level. Second, all the excitation cross sections show a broad peak at electron impact energy of ~2.5 eV. Third, the absolute magnitudes of the total excitation cross sections are about one or two orders of magnitude larger than expected from the Born approximation calculations [7.100]. The polarization effects are estimated to be small so that inclusion of the polarization interaction would not be sufficient to resolve this discrepancy. It is thus inferred that the excitation to $v_f = 1$ and $v_f = 2$ levels of HCl is not a direct (or potential) excitation. An isotropic distribution of the scattered electrons further supports this conclusion.

These experimental observations have inspired a number of calculations and interpretations of the vibrational excitation cross sections [7.90,92,101-104]. Stabilization calculations of the $^2\Sigma^+$ states of HCl^-, for fixed nuclei, indicate a state whose potential curve, running parallel to the potential curve of the ground electronic state of HCl, can be followed only for small values of R. (In the stabilization procedure, roots of the Hamiltonian matrix that remain stable on increasing the size of the basis set are interpreted to mimic the true energy eigenvalues of the Hamiltonian [7.105]. This procedure, however, does not provide information, for positive roots, as to whether the stable root is a resonance or a virtual state.) The curve of this second-lowest $^2\Sigma^+$ state of HCl^- is displaced by at most 0.32 eV from the X $^1\Sigma^+$ state of HCl. This $^2\Sigma^+$ state has been proposed [7.92] to be respon-

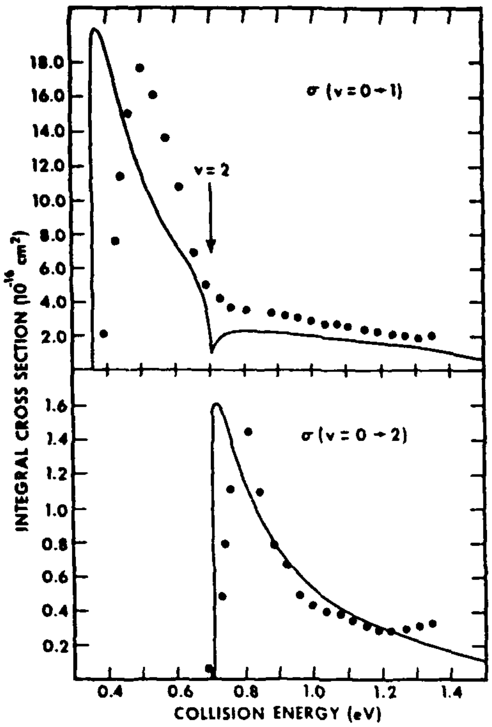

Fig.7.13. Total cross sections for vibrational excitation of HCl by electron impact. (——): theoretical results [7.101]; (····): experiment [7.99]. From [7.101] with permission

sible for the strong threshold peak in the vibrational excitation cross sections of HCl. The facts that the peak in the cross sections occurs about 0.32 eV above the threshold and that the angular distribution of the scattered electron is isotropic are consistent with the energy position as well as the $^2\Sigma^+$ symmetry of this state of HCl^-. Subsequently, it has been shown [7.106] that the two lowest $^2\Sigma^+$ states of HCl^- exhibit characteristics which are expected of virtual states. It is further shown that on taking nuclear motion into account, a virtual state in the fixed nuclei approximation leads to a separate virtual state associated with each vibrational excitation threshold. That would account for the sharp peak observed at the threshold for excitation to each final vibrational level $v_f = 1,2,\dots$. The results of a model calculation [7.101], for the vibrational excitation cross sections employing two adjustable parameters, are shown in Fig.7.13. These calculations invoke the idea of a virtual state to account for the enhancement of the departing electron's wave function near the molecule. The main threshold features of the observations for both σ_{01} and σ_{02} are satisfactorily explained by these calculations.

The s wave virtual state model is not the only one that explains the threshold structure in vibrational excitation functions of HCl. For example, the threshold peaks can also be qualitatively explained [7.102] by assuming a discrete electronic state of HCl^- coupled to a continuum distorted by a long-range strong dipole potential. It is, however, to be noted that a permanent dipole moment of the molecule is not essential for the occurrence of threshold peaks since a number of nonpolar molecules, for example CO_2 and SF_6, also exhibit [7.107] threshold peaks. Recent ab initio calculations, using static, exchange, and parameter-free correlation-polarization interactions, provided vibrational excitation cross sections which were about a factor of ten smaller in magnitude but had the semblance of a threshold peak [7.100]. Thus it is rather difficult to decide unambiguously about the merits of various calculations of the vibrational excitation cross sections of HCl.

c) Dissociative Attachment

Dissociative electron attachment to HCl can result in the formation of either Cl^- or H^-. Due to the larger electron affinity of the Cl atom, the threshold for production of Cl^- is lower than that for H^-. Furthermore, the peak attachment cross section leading to Cl^- production is about an order of magnitude larger than that for H^- production [7.35,108]. Experimental observations of cross sections for electron attachment to HCl are summarized in Fig.7.14. Detailed observations reveal the following features: (a) The cross section for Cl^- production has an almost vertical onset at an electron impact energy of 0.82 eV. Regularly spaced decreasing step structures, with an energy spacing of 0.3 eV, are observed on the higher-energy side of the peak [7.109,110]. (b) The cross section for H^- production, as a function of the incident electron energy, shows two peaks [7.111]. The first peak has a steep but nonvertical onset at 7.1 eV while the second peak gradually rises to a

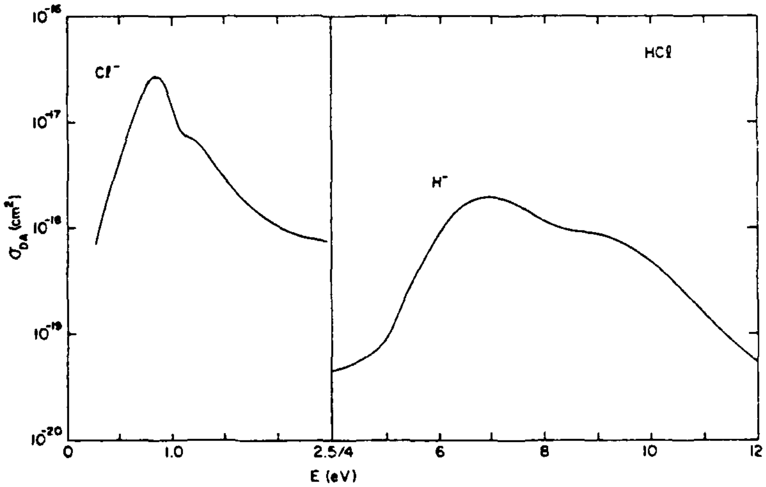

Fig.7.14. Total cross sections for the production of Cl^- and H^- by dissociative electron attachment to HCl

maximum at 9.3 eV. (c) Internal heating of the HCl molecule in the form of rovibrational excitation enhances the attachment cross section, analogously to H_2, by several orders of magnitude [7.112].

A number of calculations as well as further experiments have been carried out to understand these features. The step structure on the higher-energy side of the Cl^- peak is seen to occur at energies coincident with the vibrational thresholds of HCl. At the threshold for Cl^- formation, the energy of the incident electron is comparable to the vibrational spacing of HCl and thus the use of nonlocal formalism [see (7.1.12) and recall that the summation contains all *open* channels only] is essential for the computation of attachment cross sections. Now as the incident electron energy is increased, every time a new vibrational level is reached a new exit channel for the electron detachment opens up, which results in a reduction in the electron attachment cross section. This explains [7.113] the step structure observed on the higher-energy side of the Cl^- formation cross section.

Angular distributions of H^- ions produced by electron attachment to HCl provide clues about the nature of the peaks in the H^- production cross sections at 7.1 eV and at 9.3 eV [7.97]. For example, at an incident electron energy of 7.1 eV, the angular distribution of H^- ions shows a maximum at 90° and a minimum at 55° which is characteristic of a dσ wave. Similarly, at an incident electron energy of 9.3 eV, the angular distribution of H^- shows a behavior that is characteristic of a d- wave. These observations clearly indicate that the peaks at 7.1 eV and 9.3 eV are associated with the production of H^- ions via intermediate HCl^- states of symmetries $^2\Sigma^+$ and $^2\Pi$, respectively. Observations also reveal [7.97] fine structures superimposed on the higher-energy side of the broad 9.3 eV peak. These structures are believed to occur due to the interaction of the $^2\Pi$ repulsive state of HCl^- with the X $^2\Pi$ state of HCl^+ as the grandparent.

Finally, observations of the temperature dependence of the attachment cross sections reveal [7.112] a dramatic dependence of the cross sections on the initial rovibrational energy of the molecule. For example, the threshold cross section is enhanced by factors of 38 and 880 for HCl and by factors of 32 and 580 for DCl when the attaching molecule is excited to $v = 1$ and $v = 2$ levels, respectively. Applications of a nonlocal resonant scattering model to electron attachment to HCl and DCl have met with only partial success [7.114]. These semiempirical calculations show only qualitative agreement with the experimental observations; further improvements in the calculations are necessary for any quantitative predictions [7.115].

7.3 Applications of the Attachment Process Under Nonequilibrium Conditions

The process of dissociative electron attachment has been important in many practical applications. In particular, the process plays a key role in the production of high-energy beams for neutral injection in fusion plasmas, the kinetics of plasma switches, the analysis of attachment-induced instabilities in laser plasmas, the selection and application of gaseous dielectrics, etc. The rovibrational excitation of the attaching molecule enhances the rate of electron attachment. The degree of enhancement differs from one species to another and, depending upon the nature and the internal energy of the attaching molecule, can be as much as several orders of magnitude compared to the unexcited gas.

7.3.1 Neutral Beam Injection in Fusion Plasma

For future production of high-energy beams of neutral atomic hydrogen and deuterium, the fusion community has become aware of the possibility of using the negative ion beams as intermediaries [7.116]. In the past, production of high-energy neutral beams has been achieved by neutralizing the accelerated positive ion beams. However, due to their low efficiency of neutralization, the positive ion beams technology is quite difficult. The negative ion beams can be very efficiently produced by dissociative electron attachment to H_2 or D_2. The rovibrational excitation of the neutral molecule aids the production of the negative ion beams. After acceleration, the negative ion beam can be neutralized, with high efficiency, using photodetachment techniques. The high-energy neutral beam can be used to heat the fusion plasma as well as to provide the fuel. Presently both H^- and D^- are being considered for neutral beam injection in different experimental reactor designs [7.117].

7.3.2 Electron-Beam Switches

The feasibility of using a discharge ionized by an electron beam, for use as an on-off plasma switch is presently under consideration [7.118]. It has been demonstrated that electron beams of current densities as low as 10 mA/cm^2 are capable of producing discharge (or switched) currents as high as 1-10 A/cm^2. Thus, it seems possible to have current gains, that is, the ratio of discharge-switched current to the electron-beam current, as high as 1000 or so. For high repetition switching rates it is desirable to have as small a decay (or switch-off) time as possible. This can be most effectively achieved by introducing an electron attaching gas into the discharge plasma [7.119]. The rate of dissociative electron attachment to this gas then controls the decay time of the switch. The rovibrational excitation of the attaching molecule helps in two ways: first, it enhances the attachment rate and thus lowers the decay time. Second, the rovibrational excitation lowers the threshold of electron energy for dissociative electron attachment to occur. It is important, however, that the attachment should not introduce too high a loss in the on condition. Several polyatomic attaching gases are successfully used in plasma switches. Among diatomic molecules, HCl seems to be a prime candidate.

7.3.3 Laser Plasma Instabilities

Plasma instabilities in the form of striations (or ionization waves) often have been observed in self-sustained discharges used for CO_2 lasers [7.120]. In general, these instabilities arise due to the presence of a gas that is capable of producing negative ions via dissociative electron attachment and are referred to as the attachment instabilities of the laser plasma. The conditions necessary for the occurrence of instability are (i) that the rate of dissociative electron attachment increases with electron temperature and (ii) that the attachment and ionization rates are comparable in magnitude. If the effects of other processes governing the gain or loss of electrons, for example electron detachment and electron recombination, are negligible, then during any positive fluctuation of the electron temperature, more electrons are lost by dissociative attachment than are gained by ionization. The net loss of low-energy electrons thus leads to a still higher electron temperature and a smaller electron density. The fluctuation in electron temperature thus grows and leads to attachment instability. In CO_2 and CO laser discharges, the dissociative electron attachment rates are strongly increasing functions of the electron temperature and the ionization and the attachment rates are comparable so that the conditions for the attachment-induced instability are easily met.

7.3.4 Gaseous Dielectrics

For a gas to act as an efficient dielectric, it should be able to sustain large applied electric fields without causing gaseous breakdown. As the applied electric field is increased, a large fraction of the free electrons in the gas attain sufficient energy to cause ionization which eventually leads to the breakdown of the gas. The optimum dielectric efficiency of the gas is thus achieved by lowering both the energy and the number density of free electrons in the gas. Both of these parameters are controlled by introducing, in the dielectric medium, a gas with large cross sections for dissociative attachment and vibrational excitation by electron impact. The vibrational excitation reduces the average energy of the free electrons while dissociative attachment reduces their number density. Basic information about dissociative electron attachment and vibrational excitation is thus important for the development of gaseous dielectrics [7.121].

7.A Appendix: Normalization of Continuum Functions

The expressions for cross sections for DA and VE, as given by various authors, appear to differ depending upon the normalization of the continuum functions used. In this appendix we summarize the properties of momentum-normalized and energy-normalized continuum functions.

Consider the functions

$$\psi(\mathbf{k},\mathbf{r}) = \left(\frac{1}{8\pi^3}\right)^{1/2} e^{i\mathbf{k}\cdot\mathbf{r}} \quad ,$$

$$\phi(E,\mathbf{r}) = \left(\frac{mk}{8\pi^3\hbar^2}\right)^{1/2} e^{i\mathbf{k}\cdot\mathbf{r}} = \left(\frac{mk}{\hbar^2}\right)^{1/2} \psi(\mathbf{k},\mathbf{r}) \quad ,$$

with

$$E = \left(\frac{\hbar^2 k^2}{2m}\right)\hat{\mathbf{k}} \quad .$$

Then the orthonormality relations among these functions are

$$\int \psi^*(\mathbf{k},\mathbf{r})\psi(\mathbf{k}',\mathbf{r})d\mathbf{r} = \delta(\mathbf{k}-\mathbf{k}') = \frac{\delta(k-k')}{kk'}\delta(\hat{k}-\hat{k}') \quad ,$$

$$\int \psi^*(\mathbf{k},\mathbf{r})\psi(\mathbf{k},\mathbf{r}')d\mathbf{k} = \delta(\mathbf{r}-\mathbf{r}') \quad ,$$

$$\int \phi^*(E,\mathbf{r})\phi(E',\mathbf{r})d\mathbf{r} = \delta(E-E') = \delta(E-E')\delta(\hat{k}-\hat{k}') \quad ,$$

$$\int \phi^*(E,\mathbf{r})\phi(E,\mathbf{r}')dE = \delta(\mathbf{r}-\mathbf{r}') \quad .$$

The probability flux densities associated with $\psi(\mathbf{k},\mathbf{r})$ and $\phi(E,\mathbf{r})$ are $(\hbar k/8\pi^3 m)\,\hat{k}$ and $(k^2/8\pi^3\hbar)\,\hat{k}$, respectively. The asymptotic forms of the momentum- and energy-normalized functions are obtained by using plane wave expansions. These are

$$\psi(\mathbf{k},\mathbf{r}) = \sum_{\ell m} i^\ell \psi_\ell(k,r) Y^*_{\ell m}(\hat{k}) Y_{\ell m}(\hat{r}) \quad \text{and}$$

$$\phi(\mathbf{E},\mathbf{r}) = \sum_{\ell m} i^\ell \phi_\ell(E,r) Y^*_{\ell m}(\hat{k}) Y_{\ell m}(\hat{r}) \quad ,$$

where, for $r \to \infty$,

$$\psi_\ell(k,r) \to \left(\frac{2}{\pi k^2}\right)^{1/2} \frac{\sin(kr - \ell\pi/2)}{r} \quad \text{and}$$

$$\phi_\ell(E,r) \to \left(\frac{2m}{\pi\hbar^2 k}\right)^{1/2} \frac{\sin(kr - \ell\pi/2)}{r} \quad .$$

Acknowledgment. It is a pleasure to thank J.N. Bardsley, A. Garscadden, and T.S. Stein for a critical reading of the manuscript and for many valuable suggestions. Appreciation is also extended to various authors for permission to reproduce figures from their papers. Support of Air Force Wright Aeronautical Laboratory through subcontract F33615-81-C-2013 and of Air Force Office of Scientific Research through grant number AFOSR-84-0143 is gratefully acknowledged.

References

7.1 J.N. Bardsley, F. Mandl: Rep. Prog. Phys. **31**, 471 (1968)
7.2 H.S. Taylor: Adv. Chem. Phys. **18**, 91 (1970)
7.3 G.J. Schulz: Rev. Mod. Phys. **45**, 423 (1973)
7.4 F. Fiquet-Fayard: Vacuum **24**, 533 (1974)
7.5 Sir Harrie Massey: *Negative Ions* (Cambridge University Press, Cambridge 1976)
7.6 D.E. Golden: Adv. At. Mol. Phys. **14**, 1 (1978)
7.7 R.S. Berry, S. Leach: Adv. Electron. Electron Phys. **57**, 1 (1981)
7.8 B.M. Smirnov: *Negative Ions* (McGraw Hill, New York 1982)
7.9 H.S.W. Massey: Endeavour **4**, 78 (1980)
7.10 G.J. Schulz: In *Principles of Laser Plasmas*, ed. by G. Bekefi (Wiley, New York 1976) p.33
7.11 P.G. Burke, J.F. Williams: Phys. Rep. **34**, 325 (1977)
7.12 N.F. Lane: Rev. Mod. Phys. **52**, 29 (1980)
7.13 D.W. Norcross, L.A. Collins: Adv. At. Mol. Phys. **18**, 341 (1982)
7.14 S. Trajmar, D.F. Register, A. Chutjian: Phys. Rep. **97**, 219 (1983)
7.15 A. Herzenberg: In *Electron-Molecule Collisions*, ed. by I. Shimamura, K. Takayanagi (Plenum, New York 1984)
7.16 D.T. Birtwistle, A. Herzenberg: J. Phys. B4, 53 (1971)
7.17 T.F. O'Malley: Phys. Rev. **150**, 14 (1966)
7.18 J.N. Bardsley: J. Phys. B1, 349 (1968)
7.19 U. Fano: Phys. Rev. **124**, 1866 (1961)
7.20 J.N. Bardsley: In *Electron-Molecule and Photon-Molecule Collisions*, ed. by T. Rescigno, V. McKoy, B. Schneider (Plenum, New York 1979) p.267
7.21 J.M. Wadehra, J.N. Bardsley: Phys. Rev. Lett. **41**, 1795 (1978)
7.22 R.J. Bieniek: J. Phys. B13, 4405 (1980)
7.23 L.S. Cederbaum, W. Domcke: J. Phys. B**14**, 4665 (1981)
7.24 J.N. Bardsley, A. Herzenberg, F. Mandl: Proc. Phys. Soc., London **89**, 321 (1966)
7.25 L. Dube, A. Herzenberg: Phys. Rev. A20, 194 (1979)
7.26 J.N. Bardsley, A. Herzenberg, F. Mandl: *Proc. 3rd Int. Conf. Atomic Collisions 1963* (North-Holland, Amsterdam 1964) p.415
7.27 I.S. Elets, A.K. Kazanskii: Sov. Phys.-JETP **53**, 499 (1981)
7.28 H. Hotop, W.C. Lineberger: J. Phys. Chem. Ref. Data **4**, 539 (1975)
7.29 C.E. Moore: *Atomic Energy Levels*, Natl. Bur. Std. Circ. No. 467 (Washington D.C. 1949)
7.30 K.P. Huber, G. Herzberg: *Constants of Diatomic Molecules* (Van Nostrand, New York 1979)
7.31 D. Rapp, D.D. Briglia: J. Chem. Phys. **43**, 1480 (1965)
7.32 G.J. Schulz, R.K. Asundi: Phys. Rev. **158**, 25 (1967)
7.33 D. Spence, P.D. Burrow: J. Phys. B12, L179 (1979)
7.34 R. Abouaf, D. Teillet-Billy, S. Goursaud: J. Phys. B**14**, 3517 (1981)
7.35 O.J. Orient, S.K. Srivastava: Private communication (1984)
7.36 B.D. Buckley, C. Bottcher: J. Phys. B10, L635 (1977)
7.37 J.N. Bardsley, J.S. Cohen: J. Phys. B11, 3645 (1978)
7.38 J.N. Bardsley, J.M. Wadehra: Phys. Rev. **A20**, 1398 (1979)
7.39 J. Comer, F.H. Read: J. Phys. B**4**, 368 (1971)
7.40 G. Joyez, J. Comer, F.H. Read: J. Phys. B**6**, 2427 (1973)
7.41 E.S. Chang: Phys. Rev. A12, 2399 (1975)
7.42 M. Tronc, R.I. Hall, C. Schermann, H.S. Taylor: J. Phys. B**12**, L279 (1979)
7.43 A. Huetz, J. Mazeau: J. Phys. B16, 2577 (1983)
7.44 W. Kolos, L. Wolniewicz: J. Chem. Phys. **43**, 2429 (1965)
7.45 R.J.W. Henry, E.S. Chang: Phys. Rev. **A5**, 276 (1972)
7.46 F. Gresteau: Private communication to J.N. Bardsley (1977)
7.47 H. Ehrhardt, L. Laughans, F. Linder, H.S. Taylor: Phys. Rev. **173**, 222 (1968)
7.48 F. Linder, H. Schmidt: Z. Naturforsch. **26a**, 1603 (1971)
7.49 A. Klonover, U. Kaldor: J. Phys. B**12**, 323 (1979)
7.50 J.R. Hiskes: J. Appl. Phys. **51**, 4592 (1980)
7.51 S.K. Srivastava, O.J. Orient: In *Production and Neutralization of Negative Ions and Beams*, ed. by K. Prelec (American Institute of Physics, New York 1984) p.56

7.52 D. Rapp, T.E. Sharp, D.D. Briglia: Phys. Rev. Lett. **14**, 533 (1965)
7.53 M. Tronc, F. Fiquet-Fayard, C. Schermann, R.I. Hall: J. Phys. B**10**, 305 (1977)
7.54 M. Allan, S.F. Wong: Phys. Rev. Lett. **41**, 1791 (1978)
7.55 J.M. Wadehra: Appl. Phys. Lett. **35**, 917 (1979)
7.56 E.U. Condon: Phys. Rev. **32**, 858 (1928)
7.57 C.W. McCurdy, R.C. Mowrey: Phys. Rev. A**25**, 2529 (1982)
7.58 J.M. Wadehra: In *Production and Neutralization of Negative Ions and Beams*, ed. by K. Prelec (American Institute of Physics, New York 1984) p.46
7.59 J.M. Wadehra: Phys. Rev. A**29**, 106 (1984)
7.60 M. Bacal, G.W. Hamilton: Phys. Rev. Lett. **42**, 1538 (1979)
7.61 C. Bottcher, B.D. Buckley: J. Phys. B**12**, L497 (1979)
7.62 Y.N. Demkov: Phys. Lett. **15**, 235 (1965)
7.63 E.S. Chang, S.F. Wong: Phys. Rev. Lett. **38**, 1327 (1977)
7.64 N. Chandra, A. Temkin: Phys. Rev. A**13**, 188 (1976)
7.65 B.I. Schneider, M. Le Dourneuf, Vo Ky Lan: Phys. Rev. Lett. **43**, 1926 (1979)
7.66 A.U. Hazi, T.N. Rescigno, M. Kurilla: Phys. Rev. A**23**, 1089 (1981)
7.67 F.R. Gilmore: J. Quant. Spectrosc. Radiat. Transfer **5**, 369 (1965)
7.68 A. Lofthus, P.H. Krupenie: J. Phys. Chem. Ref. Data **6**, 113 (1977)
7.69 E.W. Thulstrup, A. Andersen: J. Phys. B**8**, 965 (1975)
7.70 A. Huetz, F. Gresteau, J. Mazeau: J. Phys. B**13**, 3275 (1979)
7.71 H. Ehrhardt, K. Willmann: Z. Phys. **204**, 462 (1967)
7.72 B.I. Schneider: Phys. Rev. A**14**, 1923 (1976)
7.73 A.U. Hazi: In *Electron-Atom and Electron-Molecule Collisions*, ed. by J. Hinze (Plenum, New York 1983)
7.74 J.L. Dehmer, J. Siegel, J. Welch, D. Dill: Phys. Rev. A**21**, 101 (1980)
7.75 J. Mazeau, F. Gresteau, R.I. Hall, A. Huetz: J. Phys. B**11**, L557 (1978)
7.76 A. Huetz, F. Gresteau, R.I. Hall, J. Mazeau: J. Chem. Phys. **72**, 5297 (1980)
7.77 M. Karplus, R.N. Porter: *Atoms and Molecules* (Benjamin, Menlo Park, California 1970)
7.78 R.I. Hall, I. Cadez, C. Schermann, M. Tronc: Phys. Rev. A**15**, 599 (1977)
7.79 J. Comer, F.H. Read: J. Phys. B**4**, 1678 (1971)
7.80 P.K. Pearson, H. Lefebvre-Brion: Phys. Rev. A**13**, 2106 (1976)
7.81 J. Comer, F.H. Read: J. Phys. B**4**, 1055 (1971)
7.82 M. Zubek, C. Szmytkowski: J. Phys. B**10**, L27 (1977)
7.83 M. Zubek, C. Szmytkowski: Phys. Lett. **74**A, 60 (1979)
7.84 I.S. Elets, A.K. Kazanskii: Sov. Phys.-JETP **55**, 258 (1982)
7.85 G.J. Schulz: Phys. Rev. **135**, A988 (1964)
7.86 M. Tronc, R. Azria, Y. Le Coat: J. Phys. B**13**, 2327 (1980)
7.87 P.J. Chantry: Phys. Rev. **172**, 125 (1968)
7.88 A. Stamatovic, G.J. Schulz: J. Chem. Phys. **53**, 2663 (1970)
7.89 J.E. Turner, K. Fox: Phys. Lett. **23**, 547 (1966)
7.90 F.A. Gianturco, N.K. Rahman: Chem. Phys. Lett. **48**, 380 (1977)
7.91 G. Herzberg: *Spectra of Diatomic Molecules* (Van Nostrand, New York 1950)
7.92 H.S. Taylor, E. Goldstein, G.A. Segal: J. Phys. B**10**, 2253 (1977)
7.93 E. Goldstein, G.A. Segal, R.W. Wetmore: J. Chem. Phys. **68**, 271 (1978)
7.94 M. Krauss, W.J. Stevens: J. Chem. Phys. **74**, 570 (1981)
7.95 M. Bettendorff, R.J. Buenker, S.D. Peyerimhoff: Mol. Phys. **50**, 1363 (1983)
7.96 J.R. Taylor: *Scattering Theory* (Wiley, New York 1972)
7.97 R. Azria, Y. Le Coat, D. Simon, M. Tronc: J. Phys. B**13**, 1909 (1980)
7.98 K. Rohr, F. Linder: J. Phys. B**8**, L200 (1975)
7.99 K. Rohr, F. Linder: J. Phys. B**9**, 2521 (1976)
7.100 N.T. Padial, D.W. Norcross: Phys. Rev. A**29**, 1590 (1984)
7.101 L. Dube, A. Herzenberg: Phys. Rev. Lett. **38**, 820 (1977)
7.102 W. Domcke, L.S. Cederbaum: J. Phys. B**14**, 149 (1981)
7.103 J.P. Gauyacq, A. Herzenberg: Phys. Rev. A25, 2959 (1982)
7.104 W. Domcke, L.S. Cederbaum: In *Electron-Atom and Electron-Molecule Collisions*, ed. by J. Hinze (Plenum, New York 1983)
7.105 A.U. Hazi, H.S. Taylor: Phys. Rev. A**1**, 1109 (1970)
7.106 R.K. Nesbet: J. Phys. B**10**, L739 (1977)
7.107 K. Rohr: In *Symposium on Electron-Molecule Collisions*, ed. by I. Shimamura, M. Matsuzawa (University of Tokyo, Tokyo 1979)

7.108 R. Azria, L. Roussier, R. Paineau, M. Tronc: Rev. Phys. Appl. **9**, 469 (1974)
7.109 J.P. Ziesel, I. Nenner, G.J. Schulz: J. Chem. Phys. **63**, 1943 (1975)
7.110 R. Abouaf, D. Teillet-Billy: J. Phys. B**10**, 2261 (1977)
7.111 M. Tronc, R. Azria, Y. Le Coat, D. Simon: J. Phys. B12, L467 (1979)
7.112 M. Allan, S.F. Wong: J. Chem. Phys. **74**, 1687 (1981)
7.113 F. Fiquet-Fayard: J. Phys. B**7**, 810 (1974)
7.114 J.N. Bardsley, J.M. Wadehra: J. Chem. Phys. **78**, 7227 (1983)
7.115 D. Teillet-Billy, J.P. Gauyacq: J. Phys. B**17**, 4041 (1984)
7.116 J.R. Hiskes: J. Phys. (Paris) **40**, C7-179 (1979)
7.117 M. Bacal: Phys. Scr. **T2/2**, 467 (1982)
7.118 M.R. Hallada, P. Bletzinger, W.F. Bailey: IEEE Trans. PS-10, 218 (1982)
7.119 A. Garscadden: In *Proceedings of the Fourth Pulsed Power Conference*, ed. by T.H. Martin, M.F. Rose (IEEE, New York 1983)
7.120 W.L. Nighan: In *Principles of Laser Plasma*, ed. by G. Bekefi (Wiley, New York 1976) p.257
7.121 L.G. Christophorou: In *Electrical Breakdown and Discharges in Gases*, ed. by E.E. Kunhardt, L.H. Luessen (Plenum, New York 1983) p.133

VIBRATIONAL EXCITATION OF $Li_2(X\,^1\Sigma_g^+)$ VIA ELECTRON OR PHOTON EXCITATION OF THE $A\,^1\Sigma_u^+$ AND $B\,^1\Pi_u$ STATES ☆

J.M. WADEHRA
Department of Physics, Wayne State University, Detroit, MI 48202, USA

and

H.H. MICHELS
United Technologies Research Center, East Hartford, CT 06108, USA

Received 10 December 1984

Cross sections for vibrational excitation (VE) of the $X\,^1\Sigma_g^+$ state of Li_2 via formation of the excited $A\,^1\Sigma_u^+$ or $B\,^1\Pi_u$ electronic states are reported. For VE through the $A\,^1\Sigma_u^+$ state, the cross sections are nearly constant for forming $X\,^1\Sigma_g^+$ $(3 \leq v'' \leq 9)$ via electron collisional excitation. For photon pumping $(660 \leq \lambda \leq 700$ nm) of the $A\,^1\Sigma_u^+$ state, levels $v'' \leq 9$ are predominantly formed. VE via the $B\,^1\Pi_u$ state has a lower probability.

1. Introduction

The negative ions of light atoms are currently being studied for their possible applications in gaseous discharges, fusion plasmas and gas lasers [1]. A possible source for the volume production of atomic anions is the process of dissociative electron attachment to molecules [2]. The rate of negative ion production by this process is enhanced, sometimes by orders of magnitude, if the molecule is initially rovibrationally excited [3–5]. Vibrational excitation of the molecule can be achieved either via a resonance (molecular anion) formation or via excitation of the higher electronic states of the neutral molecule. In this paper, we present cross sections for excitation of vibrational levels of the ground $X\,^1\Sigma_g^+$ electronic state of Li_2 via electronic excitation to the $A\,^1\Sigma_u^+$ and the $B\,^1\Pi_u$ states of Li_2.

In the processes under consideration, the electronic excitation of Li_2 to higher singlet states occurs either by electron impact or by photon pumping. Schematically,

$$e + Li_2(X\,^1\Sigma_g^+) \to Li_2^*(A\,^1\Sigma_u^+, B\,^1\Pi_u) + e\,, \tag{1}$$

or

$$Li_2(X\,^1\Sigma_g^+) + h\nu \to Li_2^*(A\,^1\Sigma_u^+, B\,^1\Pi_u)\,. \tag{2}$$

The excited molecule undergoes rapid radiative decay which returns the molecule to an excited vibrational level of the ground electronic state:

$$Li_2^*(A\,^1\Sigma_u^+, B\,^1\Pi_u) \to Li_2^\ddagger(X\,^1\Sigma_g^+) + h\nu\,. \tag{3}$$

In order to obtain the cross sections for vibrational excitation by these processes, one needs the potential energy curves and the vibrational manifold of the $X\,^1\Sigma_g^+$, $A\,^1\Sigma_u^+$ and $B\,^1\Pi_u$ states of Li_2. Fortunately, these states have been extensively studied and accurate potential curves are available [6–8]. Using these data, the band strengths (or transition moments), Franck–Condon factors and transition probabilities (or Einstein A coefficients) have been calculated for both the $X \to A$ and $X \to B$ transitions. From this information, the fraction of electronically excited molecules decaying into a particular vibrational level v'' of the ground electronic state can be calculated. The absolute cross sections for vibrational excitation are then obtained by multiplying this fraction by the total

☆ Supported in part by AFOSR under Contract F49620-83-C-0094 and Grant AFOSR-84-0143.

cross section for electronic excitation. We are able to obtain only the relative cross sections for vibrational excitation via electron collisions since information is not presently available on the electronic excitation cross sections of Li_2.

2. Theoretical considerations

We consider here the vibrational excitation of the ground $X\,^1\Sigma_g^+$ state of the Li_2 molecule by radiative decay from either the $A\,^1\Sigma_u^+$ or $B\,^1\Pi_u$ excited states. Population of these excited states can be achieved by either electron collisions with ground-state molecules or by photon pumping, via lasers as an example. The resultant vibrational distribution, in either case, is governed primarily by the product of the probability for electronic excitation and the transition probability for radiative decay back to the ground state of Li_2.

For either mechanism, we take the probability for electronic excitation to be proportional to the band strength for optical absorption. This is accurate for photon excitation and has been shown by Rudge [9] and Hiskes [10] to be a reasonable approximation for electron excitation, provided the vibrational dependence of the excitation cross section can be factored using the Franck–Condon approximation.

2.1. Electron excitation

The probability for electron excitation from the ground vibrational level of $Li_2(X\,^1\Sigma_g^+)$ to the v' level of either the $A\,^1\Sigma_u^+$ or $B\,^1\Pi_u$ excited state can be taken as

$$\mathcal{P}_{X,v_i''=0}^{A(B),v'} \simeq P_{X,v_i''=0}^{A(B),v'} \Big/ \sum_{v'} P_{X,v_i''=0}^{A(B),v'} , \tag{4}$$

where the band strength, $P_{X,v''}^{A(B),v'}$ is defined as the matrix element of the electronic dipole moment $D(R)$:

$$P_{X,v''}^{A(B),v'} = |\langle\psi(X,v'')|D(R)|\psi(A(B),v')\rangle|^2 , \tag{5}$$

and an average over rotational motion is assumed. The fraction decaying back to any discrete vibrational level v'' of the ground $X\,^1\Sigma_g^+$ state, from a particular vibrational level v' of the excited state, can be obtained by summing the appropriate Franck–Condon factors,

$$Q_X^{A(B)}(v') = \sum_{v''} q_{X,v''}^{A(B),v'} . \tag{6}$$

We shall see that this fraction is nearly unity for the states considered here. Any deviation from unity arises from the possibility of radiative decay to the continuum of $X\,^1\Sigma_g^+$. The probability for a transition from the excited electronic state back to the ground state is given by the Einstein A coefficient. The fraction of transitions from level v' of A(B) back to level v'' of X can be written as:

$$y_{X,v''}^{A(B),v'} = A_{X,v''}^{A(B),v'} \Big/ \sum_{v''} A_{X,v''}^{A(B),v'} . \tag{7}$$

The total cross section for populating a particular vibrational level v'' of the ground $X\,^1\Sigma_g^+$ state via electron excitation of $A\,^1\Sigma_u^+$ and $B\,^1\Pi_u$ can then be written as

$$\begin{aligned}\sigma_T(v_i''=0, v_f, \epsilon) &= \sigma_A(v_i''=0, v_f, \epsilon) + \sigma_B(v_i''=0, v_f, \epsilon)\\ &= \sigma_X^A(\epsilon) F_X^A(v_i''=0, v_f'') + \sigma_X^B(\epsilon) F_X^B(v_i''=0, v_f'') ,\end{aligned} \tag{8}$$

where

$$F_X^{A(B)}(v_i''=0, v_f'') = \sum_{v'} \mathcal{P}_{X,v_i''=0}^{A(B),v'} Q_X^{A(B)}(v') y_{X,v_f''}^{A(B),v'} \tag{9}$$

and $\sigma_X^{A(B)}(\epsilon)$ is the total cross section for electronic excitation from $X\,^1\Sigma_g^+$ to the A(B) state of Li_2. Since we are interested only in relative cross sections, we have for electron excitation via either $A\,^1\Sigma_u^+$ or $B\,^1\Pi_u$,

$$\begin{aligned}\mathcal{R}_X^{A(B)}(v_i''=0, v_f'') &= \sigma_{A(B)}(v_i''=0, v_f'', \epsilon)/\sigma_{A(B)}(v_i''=0, v_f''=0, \epsilon)\\ &= F_X^{A(B)}(v_i''=0, v_f'')/F_X^{A(B)}(v_i''=0, v_f''=0) .\end{aligned} \tag{10}$$

2.2. Photon excitation

The cross section for photon excitation of the $A\,^1\Sigma_u^+$ or $B\,^1\Pi_u$ states from the ground vibrational state of $Li_2(X\,^1\Sigma_g^+)$ can be written as

$$\sigma_X^{A(B)}(v_i''=0, v') = (4\pi^2/3\hbar c) P_{X,v_i''=0}^{A(B),v'} . \tag{11}$$

The total cross section for populating a particular vibrational level v_f'' of the ground $^1\Sigma_g^+$ state via photon excitation of either $A\,^1\Sigma_u^+$ or $B\,^1\Pi_u$ is

$$\sigma_T^{A(B)}(v_i''=0, v', v_f'') = \sigma_X^{A(B)}(v_i''=0, v') Q_X^{A(B)}(v') y_{X,v_f''}^{A(B),v'} . \tag{12}$$

Eq. (12) exhibits an implicit photon energy dependence through the $X(v'') \rightarrow A(v')$ or $B(v')$ transition wavelength.

3. Results and discussion

The ratio of cross sections, defined by eq. (10), for vibrational excitation of $Li_2(X\,^1\Sigma_g^+)$ by electron impact excitation of the $A\,^1\Sigma_u^+$ and $B\,^1\Pi_u$ states is shown in fig. 1 as a function of the internal vibrational energy of Li_2. Excitation via the $A\,^1\Sigma_u^+$ state yields a relatively flat final vibrational level distribution in the range $3 \lesssim v'' \lesssim 9$. Excitation via the $B\,^1\Pi_u$ state leads to a vibrational level distribution that falls off rapidly for increasing vibrational energy in the product Li_2. Fig. 1 suggests that excitation of $A\,^1\Sigma_u^+$ by electron impact energies $1.80 \lesssim \epsilon \lesssim 2.5$ eV should produce a ground-state vibrational distribution well suited for efficient dissociative attachment of low-energy electrons:

$$e + Li_2^{\ddagger} \rightarrow Li + Li^- . \quad (13)$$

In contrast, the $B\,^1\Pi_u$ state of Li_2 appears to be less efficient for populating the vibrational levels of $Li_2(X\,^1\Sigma_g^+)$ with $v'' \gtrsim 4$.

The cross sections for vibrational excitation of $Li_2(X\,^1\Sigma_g^+)$ via photon pumping of $A\,^1\Sigma_u^+$ and $B\,^1\Pi_u$ are shown in figs. 2 and 3, respectively. The largest cross sections are found to occur for excitation of $v' = 1$–4 of either the $A\,^1\Sigma_u^+$ state or $B\,^1\Pi_u$ state. The

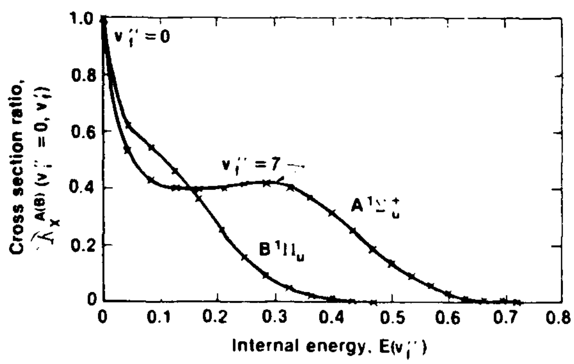

Fig. 1. Relative cross section for the excitation of the vibrational levels of $Li_2(X\,^1\Sigma_g^+)$ by electron collisional excitations through the A and B states.

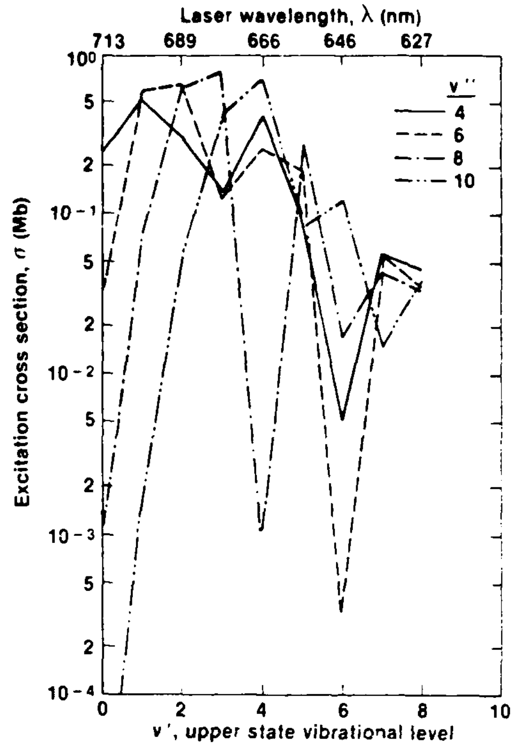

Fig. 2. Cross section for the excitation of the vibrational levels of $Li_2(X\,^1\Sigma_g^+)$ by photon excitation of the $A\,^1\Sigma_u^+$ state.

resultant vibrational distribution of $X\,^1\Sigma_g^+$ is rather flat for excitation via the $A\,^1\Sigma_u^+$ state but exhibits a rapid fall-off for $B\,^1\Pi_u$ excitation.

4. Conclusions

Analysis of the band strengths for excitation of the $A\,^1\Sigma_u^+$ and $B\,^1\Pi_u$ states and their subsequent radiative decay indicates that nearly 100% of the original excitations through either the A or B state return to the discrete vibrational levels of the ground $X\,^1\Sigma_g^+$ state. By summing eq. (9) over all final states, v_f'', we find the decay to the continuum to be less than 0.1%. This result for Li_2 is thus significantly different from that reported by Hiskes [10] in a similar study of $e + H_2$ collisional excitation, where there is nearly a 40% loss to the continuum upon radiative deexcitation.

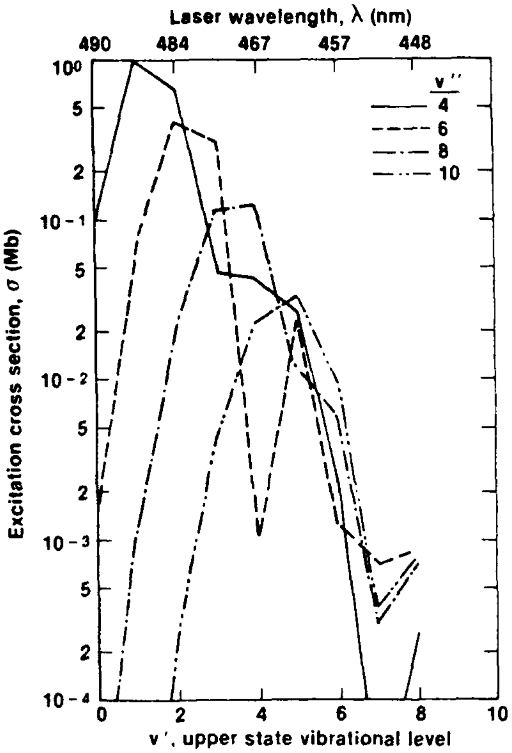

Fig. 3. Cross section for the excitation of the vibrational levels of $Li_2(X\,^1\Sigma_g^+)$ by photon excitation of the $B\,^1\Pi_u$ state.

Although we do not yet report absolute cross sections for vibrational excitation by electron collisions, clearly the Li_2 system has advantages from the standpoint of efficiency of vibrational excitation and from the relative location of the excited states, which should permit efficient selective excitation of $A\,^1\Sigma_u^+$ with a properly conditioned electron beam. Recent studies by McGeoch [11,12] of dissociative attachment (DA) in this system, via eq. (13), indicate that vibrational excitation of Li_2 by photon excitation produces a final Li_2 distribution which exhibits a large DA rate for collisions with low-energy electrons.

Further studies of the electronic excitation cross sections and dissociative electron attachment rates for this system are in progress.

Acknowledgement

We wish to extend our thanks to Ms. J.B. Addison for assistance in carrying out the computations and to Drs. M. McGeoch and J.R. Hiskes for valuable discussions. Use of the computational facilities at AFWL in Albuquerque and at AFWAL in Dayton is also acknowledged. This study was carried out while the authors were guests at the Aero Propulsion Laboratory at Wright–Patterson Air Force Base and we extend thanks to Dr. Alan Garscadden for his hospitality and interest in this research.

References

[1] K. Prelec, ed., Proceedings of the Third International Symposium on the Production and Neutralization of Negative Ions and Beams, AIP Conf. Proc. 111 (AIP, New York, 1984).
[2] M. Bacal, Physica Scripta T2/2 (1982) 467.
[3] J.M. Wadehra, Phys. Rev. A29 (1984) 106.
[4] M. Allan and S.F. Wong, Phys. Rev. Letters 41 (1978) 1791.
[5] J.M. Wadehra and J.N. Bardsley, Phys. Rev. Letters 41 (1978) 1795; Phys. Rev. A20 (1979) 1398.
[6] P. Kush and M.M. Hessel, J. Chem. Phys. 67 (1977) 586.
[7] M.M. Hessel and C.R. Vidal, J. Chem. Phys. 70 (1979) 4439.
[8] H.H. Michels, R.H. Hobbs and L.A. Wright, Electronic Structure of the Lithium Molecular Anion, Li_2^-, Chem. Phys. Letters, submitted for publication.
[9] M.R.H. Rudge, Proc. Phys. Soc. (London) 85 (1965) 607; 86 (1965) 763.
[10] J.R. Hiskes, J. Appl. Phys. 51 (1980) 4592.
[11] M.W. McGeoch and R.E. Schlier, in: Proceedings of the Third International Symposium on the Production and Neutralization of Negative Ions and Beams, AIP Conf. Proc. 111, ed. K. Prelec (AIP, New York, 1984) p. 291.
[12] M.W. McGeoch and R.E. Schlier, Abstracts 37th Gaseous Electronics Conference (1984).

J. Phys. B: At. Mol. Phys. 19 (1986) L761-L764. Printed in Great Britain

LETTER TO THE EDITOR

The second Born contribution of long-range forces to higher partial-wave phaseshifts

J M Wadehra

Department of Physics and Astronomy, Wayne State University, Detroit, Michigan 48202, USA

Received 1 August 1986

Abstract. An exact analytic evaluation of the second Born contribution of the long-range potentials, which fall off as r^{-n} as $r\to\infty$, to the phaseshifts of higher partial waves $(2l>2n-5)$ is presented. This expression agrees, for $n=4$, with the second term in the energy expansion of the phaseshifts obtained previously by Ali and Fraser. The expression can be used for predicting higher partial-wave phaseshifts as well as for determining the phaseshifts from experimental scattering data.

The scattering of a particle of energy $E=\hbar^2k^2/2\mu$ by a spherically symmetric potential can be best described in terms of phaseshifts, of various partial waves, which are functions of the wavenumber k. For long-range potentials which fall off as r^{-n} when $r\to\infty$, the computation of the phaseshifts for any angular momentum l requires special consideration. For example, in the scattering of a charged projectile by a neutral polarisable system, where the dominant long-range effect is the $1/r^4$ interaction arising from the adiabatic dipole polarisability of the target, it is known that the leading term in the energy expansion of the higher phaseshifts is proportional to k^2 independent of l (O'Malley *et al* 1961). The l-dependent coefficient of this leading term was obtained analytically by O'Malley *et al*. The next term, proportional to k^4, in the energy expansion of the higher phaseshifts $(l\geqslant 2)$ for the $1/r^4$ interaction was obtained analytically by Ali and Fraser (1977). Using mathematical arguments it has been shown (Levy and Keller 1963) that the leading term of O'Malley *et al* is identical to the first Born contribution of the long range $1/r^4$ potential to the higher phaseshifts. In this paper we show explicitly that the next term obtained by Ali and Fraser is essentially the second Born contribution of the $1/r^4$ potential to the higher phaseshifts. Thus, our analysis will provide an alternative derivation of the second term in the low-energy expansion of the higher phaseshifts. In fact, the procedure given below can easily be extended to obtain explicitly higher Born contributions to the phaseshifts for any long-range interaction.

Since long-range potentials of various inverse powers of r appear in several applications in atomic and molecular physics, we consider a general long-range spherically symmetric potential of the form

$$V(r)=C_n a_0^{n-1}\,e^2/r^n \tag{1}$$

where the constants in the coefficient (e is the electronic charge, $a_0=\hbar^2/me^2$ is the

Bohr radius and m is the mass of the electron) have been chosen so that the C_n are dimensionless. The final result will be simplified only for $n=4$. The second Born contribution to the phaseshift of the lth partial wave for a spherically symmetric potential $V(r)$ is (Joachain 1975)

$$(\tan \delta_l)_{11} = -k^2 \int_0^\infty dr\, r^2 j_l(kr)(2\mu V(r)/\hbar^2) \times \int_0^\infty dr'\, r'^2 j_l(kr')(2\mu V(r')/\hbar^2) j_l(kr_<) n_l(kr_>). \tag{2}$$

Substituting for $V(r)$ from (1) into (2), one gets

$$(\tan \delta_l)_{11} = -8[C_n(\mu/m)(ka_0)^{n-2}]^2 I \tag{3a}$$

where

$$I = \int_0^\infty dy\, y^{5-2n} j_l(y) n_l(y) \int_0^1 dx\, x^{2-n} j_l^2(xy). \tag{3b}$$

Note that, for given n, the k dependence of the phaseshift can be determined trivially since I is independent of k. For the evaluation of I, it is most convenient to work in terms of Meijer's G function (Luke 1975). Using

$$j_l^2(x) = \frac{\pi^{1/2}}{2x} G_{13}^{11}\left(x^2 \,\middle|\, \begin{matrix} \tfrac{1}{2}; \\ L; 0, -L \end{matrix}\right) \tag{4a}$$

$$j_l(x) n_l(x) = (-1)^{l+1} \frac{\pi^{1/2}}{2x} G_{13}^{11}\left(x^2 \,\middle|\, \begin{matrix} \tfrac{1}{2}; \\ 0; L, -L \end{matrix}\right) \tag{4b}$$

and equation (22) on p 190, equation (4) on p 176 and equation (5) on p 187 of Luke (1975), the integral I can be written in the following closed form:

$$I = \frac{(-1)^{l+1}\pi}{16} G_{55}^{23}\left(1 \,\middle|\, \begin{matrix} -1+n, \tfrac{1}{2}n, \tfrac{1}{2}; -L-1+n, L-1+n \\ -\tfrac{3}{2}+n, L; 0, -L, \tfrac{1}{2}n-1 \end{matrix}\right) \tag{5}$$

with $L = l + \frac{1}{2}$. The conditions of validity of this expression are

$$n > 1 \qquad \text{and} \qquad 2l+5 > 2n. \tag{6}$$

For a given n, the G function appearing in equation (5) can be evaluated using standard reduction techniques for these functions (Luke 1975). The fact that the above G function has unit argument further assists in the simplification. We illustrate this reduction technique for the case of $n=4$ which corresponds to the adiabatic dipole polarisation potential. The relevant G function is

$$G_4 \equiv G_{55}^{23}\left(1 \,\middle|\, \begin{matrix} 3, 2, \tfrac{1}{2}; -L+3, L+3 \\ \tfrac{5}{2}, L; 0, -L, 1 \end{matrix}\right) \tag{7}$$

where, as before, $L = l + \frac{1}{2}$. Using the recursion relations and some elementary properties of G functions (equations (1) and (2) on p 176 and equation (9) on p 177 of Luke 1975), one can reduce G_4 of equation (7) above to a combination of G functions of lower indices:

$$G_4=\frac{1}{L(L+1)^2(L+2)}G_{33}^{21}\left(1\left|\begin{matrix}\frac{1}{2};-L+3,L+3\\ \frac{5}{2},L;-L\end{matrix}\right.\right)$$
$$+\frac{2(2L+1)}{(L+2)(L+1)^2L^2(L-1)}G_{33}^{21}\left(1\left|\begin{matrix}\frac{1}{2};-L+3,L+2\\ \frac{5}{2},L;-L\end{matrix}\right.\right)$$
$$+\frac{2(5L^2-2)}{(L+2)(L+1)^2L^2(L-1)^2(L-2)}G_{33}^{21}\left(1\left|\begin{matrix}\frac{1}{2};-L+3,L+1\\ \frac{5}{2},L;-L\end{matrix}\right.\right)$$
$$+\frac{2(5L^2-2)}{(L+2)(L+1)^2L^2(L-1)^2(L-2)}G_{33}^{12}\left(1\left|\begin{matrix}1,\frac{1}{2};-L+3\\ \frac{5}{2};0,-L\end{matrix}\right.\right)$$
$$+\frac{2(3L^2-L-1)}{(L+1)^2L^2(L-1)^2(L-2)}G_{33}^{12}\left(1\left|\begin{matrix}2,\frac{1}{2};-L+3\\ \frac{5}{2};0,-L\end{matrix}\right.\right)$$
$$+\frac{3}{(L+1)L(L-1)(L-2)}G_{33}^{12}\left(1\left|\begin{matrix}3,\frac{1}{2};-L+3\\ \frac{5}{2};0,-L\end{matrix}\right.\right)$$
$$+\frac{1}{(L+1)L(L-1)}G_{44}^{13}\left(1\left|\begin{matrix}3,2,\frac{1}{2};-L+3\\ \frac{5}{2};0,-L,1\end{matrix}\right.\right). \tag{8}$$

At any stage, the G functions can be written in terms of the generalised hypergeometric functions ${}_pF_q$. However, if the last four terms in equation (8) are reduced further, by using recursion relations, to G functions of still lower indices and then these functions are expressed in terms of Gaussian hypergeometric functions ${}_2F_1$ of unit argument, it can be easily seen that the contribution of the last four terms in equation (8) is zero. The first three terms in equation (8) can be expressed in terms of hypergeometric functions ${}_3F_2$ of unit argument which can be evaluated by using Dixon's and Saalschütz's formulae (pp 163-4 of Luke 1975). The final result is

$$G_4=[(-1)^l/16(L+2)(L+1)^3L^3(L-1)^3(L-2)](15L^4-35L^2+8). \tag{9}$$

Thus the second Born contribution of the $1/r^4$ interaction to the phaseshifts of higher partial waves ($l\geq 2$) is

$$(\tan\delta_l)_{11}=\frac{\pi}{32}\left(C_4\frac{\mu}{m}(ka_0)^2\right)^2\frac{15L^4-35L^2+8}{(L+2)(L+1)^3L^3(L-1)^3(L-2)} \tag{10}$$

with $L=l+\frac{1}{2}$. This agrees with the expression given by Ali and Fraser (1977).

For large separations between a charged projectile (of mass μ) and a neutral atomic or molecular target, the first two terms of the interaction energy, in the adiabatic approximation, are

$$V(r)=-\tfrac{1}{2}\alpha_d a_0^3e^2/r^4-\tfrac{1}{2}\alpha_q a_0^5e^2/r^6 \tag{11}$$

where α_d and α_q are the static dipole and the quadrupole polarisability, in atomic units, of the target, respectively. The first Born contribution of the r^{-4} and r^{-6} terms of equation (11) to the phaseshift of the lth partial wave ($l\geq 2$) is (Levy and Keller 1963)

$$(\tan\delta_l)_1=\frac{\mu\pi}{m}\frac{(ka_0)^2}{(2l+3)(2l+1)(2l-1)}\left(\alpha_d+\frac{3\alpha_q(ka_0)^2}{(2l+5)(2l-3)}\right). \tag{12}$$

The first term is, of course, the one also given by O'Malley *et al* (1961). In many previous investigations, equation (12) has been used for obtaining phaseshifts of higher partial waves from known values of α_d and α_q or for experimental determinations of the phaseshifts by fitting the experimental scattering data. However, the second Born term of equation (10) should also have been included in such analyses since it has the same k dependence as the quadrupole term in (12). Numerical applications of (10), clearly showing the importance of this term, have been provided by Ali and Fraser (1977).

This research is supported, in part, by the Air Force Office of Scientific Research under Grant Number AFOSR-84-0143.

References

Ali M K and Fraser P A 1977 *J. Phys. B: At. Mol. Phys.* **10** 3091-104
Joachain C J 1975 *Quantum Collision Theory* (Amsterdam: North-Holland) p 172
Levy B R and Keller J B 1963 *J. Math. Phys.* **4** 54-64
Luke Y L 1975 *Mathematical Functions and their Approximations* (New York: Academic)
O'Malley T F, Spruch L and Rosenberg L 1961 *J. Math. Phys.* **2** 491-8

Exact evaluation and recursion relations of two-center harmonic oscillator matrix elements

P. J. Drallos and J. M. Wadehra
Department of Physics and Astronomy, Wayne State University, Detroit, Michigan 48202

(Received 16 July 1986; accepted 21 August 1986)

Using vibrational wave functions of two relatively displaced harmonic oscillators of arbitrary frequencies, Franck–Condon overlap integrals and matrix elements of x^l, $\exp(-2cx)$, and $\exp(-cx^2)$ (x is the internuclear separation) are obtained. Useful three-term, four-term, and five-term recursion relations among these matrix elements are derived. It is shown that all of the relevant matrix elements can be obtained from a mere knowledge of the lowest two Franck–Condon overlap integrals. Results are illustrated by computation of Franck–Condon factors for the $A\,{}^1\Sigma_u^+ - X\,{}^1\Sigma_g^+$ and the $B\,{}^1\Pi_u - X\,{}^1\Sigma_g^+$ systems of ${}^7\mathrm{Li}_2$.

I. INTRODUCTION

A quantitative description of transition probabilities for various vibrational levels (that is, vibrational excitation) as well as of intensities of various lines in the spectra of diatomic and polyatomic molecules requires matrix elements of various powers of the internuclear separation x between vibrational levels belonging to two different electronic states of the molecule.[1] A Franck–Condon overlap integral is a special example of such a matrix element. For low-lying vibrational levels, the potential curves of the molecular electronic states can be represented with reasonable accuracy by those of linear harmonic oscillators. For higher vibrational levels, where anharmonicity becomes important, the potential of a Morse oscillator is a better representation of the true potential curve. Even in such a case as the Morse oscillator, if one were to use first-order perturbation theory with the linear harmonic oscillator as the zero-order approximation, the matrix elements of powers of x would appear in the correction factors. With this spirit in mind, an attempt is made in this paper to obtain general analytic expressions and simple recursion relations for two-center harmonic oscillator matrix elements of various functions (powers, exponential, and Gaussian) of x. In fact, a general five-term recursion relation to be derived below [Eq. (32)], is valid for *any* analytical function of x that could be expanded as a power series in x.

The evaluation of Franck–Condon factors, which essentially involves an overlap integral between wave functions of vibrational levels belonging to two different electronic states of a molecule, using linear harmonic oscillator wave functions has been carried out in a number of investigations, and proper kudos have been distributed by Waldenstrøm and Razi Naqvi.[2] Various theoretical methods for obtaining the Franck–Condon factors have been reviewed more recently by Kuz'menko *et al.*[3] Overlap matrix elements of various functions of x using, once again, vibrational wave functions of two different harmonic oscillators, have been analytically obtained in some recent papers.[4,5] In Sec. IV of the present paper we will obtain some general recursion relations among these matrix elements. A single and double ket notation (for example, $|m\rangle$ and $|n\rangle\rangle$) will be used to distinguish between the vibrational eigenfunctions belonging to two different electronic states.

II. THE FRANCK–CONDON OVERLAP INTEGRAL

The relevant potential energy curves are replaced by those of one-dimensional harmonic oscillators of frequency ω_1 and ω_2, with a relative separation of r. For convenience, define $\omega_0 = \hbar\,(\mu r^2)$, where μ is the reduced mass of the nuclei. The two-center Franck–Condon overlap integral is then defined as $\langle m|n\rangle\rangle$, where

$$\langle x|m\rangle = (2^m m!)^{-1/2}[\omega_1/(\pi\omega_0 r^2)]^{1/4} \times\exp[-\omega_1 x^2/(2\omega_0 r^2)]H_m[(\omega_1/\omega_0)^{1/2}x/r] \quad (1)$$

is the wave function of the mth level of the harmonic oscillator associated with the potential $V_1 = \frac{1}{2}\mu\omega_1^2 x^2$, and

$$\langle\langle x|n\rangle\rangle = (2^n n!)^{-1/2}[\omega_2/(\pi\omega_0 r^2)]^{1/4} \times\exp[-\omega_2(x-r)^2/(2\omega_0 r^2)] \times H_n[(\omega_2/\omega_0)^{1/2}(x-r)/r] \quad (2)$$

is the wave function of the nth level of the harmonic oscillator associated with the potential $V_2 = \frac{1}{2}\mu\omega_2^2(x-r)^2$. Thus,

$$\langle m|n\rangle\rangle = \frac{(\omega_1\omega_2)^{1/4}}{[\pi\omega_0 r^2(2^{m+n}m!n!)]^{1/2}}\exp\left[\frac{-\omega_1\omega_2}{2\omega_0(\omega_1+\omega_2)}\right] \times\int_{-\infty}^{\infty}\exp\left\{-\left[\left(\frac{\omega_1+\omega_2}{2\omega_0 r^2}\right)^{1/2}x - \frac{\omega_2}{[2\omega_0(\omega_1+\omega_2)]^{1/2}}\right]^2\right\}H_m[(\omega_1/\omega_0)^{1/2}x/r] \times H_n[(\omega_2/\omega_0)^{1/2}(x-r)/r]dx. \quad (3)$$

Now, on changing the integration variable from x to $t = x[(\omega_1+\omega_2)/(2\omega_0 r^2)]^{1/2}$,

$$\langle m|n\rangle\rangle = N_{mn}\pi^{-1/2}\int_{-\infty}^{\infty}\exp[-(t-y)^2] \times H_m\left[\left(\frac{2\omega_1}{\omega_1+\omega_2}\right)^{1/2}t\right] \times H_n\left[\left(\frac{2\omega_2}{\omega_1+\omega_2}\right)^{1/2}t - \left(\frac{\omega_2}{\omega_0}\right)^{1/2}\right]dt, \quad (4)$$

where

$$N_{mn} = (\omega_1\omega_2)^{1/4}[(\omega_1+\omega_2)2^{m+n-1}m!n!]^{-1/2} \times\exp(-y^2\omega_1/\omega_2)$$

and

$$y = \omega_2/[2\omega_0(\omega_1+\omega_2)]^{1/2}. \tag{5}$$

The integral in Eq. (4) is of the same form as the integral defined in the Appendix. A direct use of Eq. (A8) yields a closed-form expression for the Franck–Condon integral:

$$\langle m|n\rangle\rangle = N_{mn}\sum_{k=0}^{[m,n]}\binom{m}{k}\binom{n}{k}\left(\frac{\omega_1-\omega_2}{\omega_1+\omega_2}\right)^{(n-k)/2} \times\left(\frac{\omega_2-\omega_1}{\omega_1+\omega_2}\right)^{(m-k)/2}\left[\frac{4(\omega_1\omega_2)^{1/2}}{\omega_1+\omega_2}\right]^k k! \times H_{m-k}\left[\left(\frac{\omega_1\omega_2^2}{\omega_0(\omega_2^2-\omega_1^2)}\right)^{1/2}\right] \times H_{n-k}\left[-\left(\frac{\omega_1^2\omega_2}{\omega_0(\omega_1^2-\omega_2^2)}\right)^{1/2}\right]. \tag{6}$$

This expression has been obtained, using various procedures, by a number of investigators.[6-8] It is interesting to note that for the two special cases, $m=0$ or $n=0$, the above sum reduces to a single term containing only one Hermite polynomial. [We note parenthetically that the above sum (6) also reduces to a single term for the case of equal frequency oscillators.] From the recursion relation for Hermite polynomials (A3), it follows:

$$\langle 0|n+2\rangle\rangle = \frac{-\omega_1}{\omega_1+\omega_2}\left[\frac{2\omega_2}{\omega_0(n+2)}\right]^{1/2}\langle 0|n+1\rangle\rangle - \left(\frac{\omega_1-\omega_2}{\omega_1+\omega_2}\right)\left(\frac{n+1}{n+2}\right)^{1/2}\langle 0|n\rangle\rangle, \tag{7}$$

$$\langle m+2|0\rangle\rangle = \frac{\omega_2}{\omega_1+\omega_2}\left[\frac{2\omega_1}{\omega_0(m+2)}\right]^{1/2}\langle m+1|0\rangle\rangle + \left(\frac{\omega_1-\omega_2}{\omega_1+\omega_2}\right)\left(\frac{m+1}{m+2}\right)^{1/2}\langle m|0\rangle\rangle. \tag{8}$$

In fact, on using the one-term expressions for $\langle 0|n\rangle\rangle$ and $\langle m|0\rangle\rangle$, Eq. (6) can be rewritten as

$$\langle m|n\rangle\rangle = \sum_{k=0}^{[m,n]}\left[\frac{2(\omega_1\omega_2)^{1/2}}{\omega_1+\omega_2}\right]^k\binom{m}{k}^{1/2}\binom{n}{k}^{1/2} \times\frac{\langle m-k|0\rangle\rangle\langle 0|n-k\rangle\rangle}{\langle 0|0\rangle\rangle}. \tag{9}$$

Equivalent expressions have been obtained previously by Manneback[6] and Smith.[9] It is remarkable—and this fact has apparently not been appreciated earlier in the literature—that the complete Franck–Condon matrix $\langle m|n\rangle\rangle$ can be determined using Eqs. (7), (8), and (9) from the mere knowledge of either $\langle 0|0\rangle\rangle$ and $\langle 0|1\rangle\rangle$, or $\langle 0|0\rangle\rangle$ and $\langle 1|0\rangle\rangle$.

III. MATRIX ELEMENTS OF SOME FUNCTIONS

Now let us consider the two-center matrix elements of x^l, $\exp(-2cx)$, and $\exp(-cx^2)$ in the harmonic oscillator basis. Various matrix elements can be written in terms of integrals of the form

$$I[f(t);m,n;a,b,y,z] = \int_{-\infty}^{\infty} f(t)\exp[-(t-y)^2]H_m(at)H_n(bt-z)dt, \tag{10}$$

which is derived in detail for the case $f(t)=1$ in the Appendix [see, for example, Eq. (A8)].

A. Powers of the coordinate *x*

The required matrix elements can be written as

$$\langle m|x^l|n\rangle\rangle = \frac{N_{mn}}{\pi^{1/2}}\left(\frac{2\omega_0 r^2}{\omega_1+\omega_2}\right)^{1/2} \times\int_{-\infty}^{\infty} t^l\exp[-(t-y)^2] \times H_m(at)H_n(bt-z)dt, \tag{11}$$

where

$$a=[2\omega_1/(\omega_1+\omega_2)]^{1/2},\quad b=[2\omega_2/(\omega_1+\omega_2)]^{1/2},\quad \text{and } z=(\omega_2/\omega_0)^{1/2}. \tag{12}$$

N_{mn} and y are defined in Eq. (5). Using Eq. (A13), the matrix elements of x^l can be written as a sum of Franck–Condon integrals,

$$\langle m|x^l|n\rangle\rangle = \left[\frac{\omega_0 r^2}{2(\omega_1+\omega_2)}\right]^{l/2} l! \times\sum_{p=0}^{[m,l]}\sum_{q=0}^{[n,l-p]}\left[\frac{m!n!}{(m-p)!(n-q)!}\right]^{1/2} \times\frac{(4\omega_1)^{p/2}(4\omega_2)^{q/2}}{(\omega_1+\omega_2)^{(p+q)/2}p!q!} \times\frac{(-i)^{l-p-q}}{(l-p-q)!}H_{l-p-q}(iy) \times\langle m-p|n-q\rangle\rangle. \tag{13}$$

This expression was obtained earlier by Morales *et al.*,[5] though there appears to be an error in the constants of their expression.

B. Exponential function exp(–2*cx*)

Here, in obtaining the relevant integral, we follow exactly the same steps as in the Appendix, Eqs. (A4)–(A6), except there now is an extra factor of $\exp(-2ct)$ in the integrand. It leads to the following result for the integral:

$$I[\exp(-2ct);m,n;a,b,y,z] = \pi^{1/2}\exp(c^2-2cy)\left(\frac{\partial}{\partial t_2}\right)^n_{t_2=0}\left(\frac{\partial}{\partial t_1}\right)^m_{t_1=0} \times\exp\{-(1-a^2)t_1^2-(1-b^2)t_2^2 + 2a(y-c)t_1+2[b(y-c)-z]t_2+2abt_1t_2\}. \tag{14}$$

Except for the constant $\exp(c^2-2cy)$, Eq. (14) looks just like Eq. (A6), and we can immediately write down the final result:

$$I[\exp(-2ct);m,n;a,b,y,z] = \exp(c^2-2cy)I[1;m,n;a,b,y-c,z]. \tag{15}$$

The matrix element $\langle m|\exp(-2cx)|n\rangle\rangle$ is related to $I[\exp(-2ct);m,n;a,b,y,z]$ and by using Eq. (15) one can write

$$\langle m|\exp(-2cx)|n\rangle\rangle = N_{mn}\exp(\alpha^2 - 2\alpha y) \times I[1;m,n;a,b,y-\alpha,z]/\pi^{1/2}, \quad (16)$$

where $\alpha = c[(2\omega_0 r^2)/(\omega_1+\omega_2)]^{1/2}$ is introduced by a change of the integration variable from x to the dimensionless $t = x(\omega_1+\omega_2)^{1/2}/(2\omega_0 r^2)^{1/2}$.

C. Gaussian function $\exp(-cx^2)$

The case $f(t) = \exp(-ct^2)$ can be worked out in a fashion very similar to the case of the exponential above. Following the same steps as Eqs. (A4) and (A5), we obtain

$$I[\exp(-ct^2);m,n;a,b,y,z] = \beta\exp(-c\beta^2y^2)\left(\frac{\partial}{\partial t_2}\right)^n_{t_2=0}\left(\frac{\partial}{\partial t_1}\right)^m_{t_1=0} \times\exp(-t_1^2 - t_2^2 - 2zt_2 - \beta^2y^2) \times\int_{-\infty}^{\infty}\exp[-t^2 - 2(a\beta t_1 + b\beta t_2 + \beta y)t]dt, \quad (17)$$

where $\beta = (1+c)^{-1/2}$.

The expression in Eq. (17) has essentially the same form as Eq. (A5), and we can immediately write down the result by inspection,

$$I[\exp(-ct^2);m,n;a,b,y,z] = \beta\exp(-c\beta^2y^2)I[1;m,n;a\beta,b\beta,y\beta,z]. \quad (18)$$

The matrix elements $\langle m|\exp(-cx^2)|n\rangle\rangle$ are related to the above integral by

$$\langle m|\exp(-cx^2)|n\rangle\rangle = N_{mn}\gamma\exp[-(1-\gamma^2)y^2] \times I[1;m,n;\gamma a,\gamma b,\gamma y,z]/\pi^{1/2}, \quad (19)$$

where $\gamma = [1 + 2c\omega_0 r^2/(\omega_1+\omega_2)]^{-1/2}$ is once again introduced by the change of integration variable.

Summarizing this section, the integral for $f(t) = t^l$ can be written as a finite sum of integrals for $f(t) = 1$. The integrals for the exponential and Gaussian functions can each be obtained by a simple scaling of an $f(t) = 1$ integral.

IV. RECURSION RELATIONS

Four-term recursion relations among Franck–Condon overlap integrals were derived by Ansbacher[7] and, in equivalent form, by Manneback.[6] These recursion relations are special cases of the more general recursion relations, to be obtained below, for the integral $I[t^l;m,n;a,b,y,z]$. In the preceding section it was shown that the integrals for the exponential and Gaussian functions could be written in terms of $I[1;m,n;a,b,y,z]$ so that the recursion relations for the integrals for these functions are also obtained from the recursion relations for $I[t^l;m,n;a,b,y,z]$.

For brevity, define $I_l(m,n) \equiv I[t^l;m,n;a,b,y,z]$ in the following discussion. Thus,

$$I_l(m,n) = \int_{-\infty}^{\infty}\exp[-(t-y)^2]t^lH_m(at)H_n(bt-z)dt \quad (20)$$

$$= 2aI_{l+1}(m-1,n) - 2(m-1)I_l(m-2,n) \quad (21)$$

or equivalently,

$$2aI_{l+1}(m,n) = I_l(m+1,n) + 2mI_l(m-1,n). \quad (22)$$

In going from Eq. (20) to Eq. (21), the recursion relation for Hermite polynomials (A3) was applied to $H_m(at)$. Using the recursion relation for Hermite polynomials on the $H_n(bt-z)$ term in Eq. (20), on the other hand, gives

$$2bI_{l+1}(m,n) = I_l(m,n+1) + 2zI_l(m,n) + 2nI_l(m,n-1). \quad (23)$$

It is important to note that from Eq. (22) or (23), the complete matrix of any power of t (for example, t^l) can be obtained from the knowledge of the matrix of the next lower power (namely, t^{l-1}). We reemphasize that the matrix of Franck–Condon overlap integrals can be completely determined from a mere knowledge of only two matrix elements, $\langle 0|0\rangle\rangle$ and $\langle 0|1\rangle\rangle$ (or $\langle 0|0\rangle\rangle$ and $\langle 1|0\rangle\rangle$), so, in principle, the complete matrix of any power of x can be built up from only two overlap matrix elements.

Using, in the integrands of the terms on the left-hand sides of Eqs. (22) and (23),

$$t\exp[-(t-y)^2] = -\tfrac{1}{2}\left(\frac{d}{dt}\right)\exp[-(t-y)^2] + y\exp[-(t-y)^2],$$

then performing integration by parts and the necessary derivatives we obtain

$$alI_{l-1}(m,n) = I_l(m+1,n) - 2nabI_l(m,n-1) + 2m(1-a^2)I_l(m-1,n) - 2ayI_l(m,n) \quad (24)$$

and

$$blI_{l-1}(m,n) = I_l(m,n+1) - 2mabI_l(m-1,n) + 2n(1-b^2)I_l(m,n-1) - 2(by-z)I_l(m,n). \quad (25)$$

The recursion relations for these integrals can easily be adapted to the matrix elements $\langle m|x^l|n\rangle\rangle$, using Eq. (11):

$$2lr(\omega_1\omega_0)^{1/2}\langle m|x^{l-1}|n\rangle\rangle = [2(m+1)]^{1/2}(\omega_1+\omega_2)\langle m+1|x^l|n\rangle\rangle - (8n\omega_1\omega_2)^{1/2}\langle m|x^l|n-1\rangle\rangle + (2m)^{1/2}(\omega_2-\omega_1)\langle m-1|x^l|n\rangle\rangle - (\omega_1/\omega_0)^{1/2}2\omega_2\langle m|x^l|n\rangle\rangle, \quad (26)$$

$$2lr(\omega_2\omega_0)^{1/2}\langle m|x^{l-1}|n\rangle\rangle = [2(n+1)]^{1/2}(\omega_1+\omega_2)\langle m|x^l|n+1\rangle\rangle - (8m\omega_1\omega_2)^{1/2}\langle m-1|x^l|n\rangle\rangle + (2n)^{1/2}(\omega_1-\omega_2)\langle m|x^l|n-1\rangle\rangle + (\omega_2/\omega_0)^{1/2}2\omega_1\langle m|x^l|n\rangle\rangle. \quad (27)$$

Equations (26) and (27) are generalized forms of Ansbacher's[7] recursion relations for Franck–Condon overlap integrals which are obtained by letting $l=0$.

Equations (22) and (23) can be adapted to the integrals for the exponential and Gaussian functions by multiplying the equations by $(-2c)^l/l!$ or $(-ct)^l/l!$, respectively, and then summing over l. This yields, for the exponential case (suppressing the constants a, b, y, and z):

$$\begin{aligned}2aI&[t\exp(-2ct);m,n]\\&=I[\exp(-2ct);m+1,n]\\&\quad+2mI[\exp(-2ct);m-1,n],\end{aligned}\tag{28}$$

$$\begin{aligned}2bI&[t\exp(-2ct);m,n]\\&=I[\exp(-2ct);m,n+1]\\&\quad+2zI[\exp(-2ct);m,n]\\&\quad+2nI[\exp(-2ct);m,n-1].\end{aligned}\tag{29}$$

Note that these equations relate the $f(t)=\exp(-2ct)$ integral to the $f(t)=t\exp(-2ct)$ integral. Analogous relations for the Gaussian case can be obtained in a similar manner.

Equations (24) and (25) [or Eqs. (26) and (27)] can be similarly adapted for integrals for the exponential and Gaussian functions. For the exponential case, Eqs. (24) and (25) are transformed into

$$\begin{aligned}2a(y-c)&I[\exp(-2ct);m,n]\\&=I[\exp(-2ct);m+1,n]\\&\quad-2nabI[\exp(-2ci);m,n-1]\\&\quad+2m(1-a^2)I[\exp(-2ct);m-1,n],\end{aligned}\tag{30}$$

$$\begin{aligned}2[b(y-c)-z]&I[\exp(-2ct);m,n]\\&=I[\exp(-2ct);m,n+1]\\&\quad-2mabI[\exp(-2ct);m-1,n]\\&\quad+2n(1-b^2)I[\exp(-2ct);m,n-1].\end{aligned}\tag{31}$$

Equations (30) and (31) could have been obtained by an alternative method using the results of Sec. III B, in which it was shown that the integrals for the exponential and Gaussian functions were related by simple scaling to the $f(t)=1$ integral. Thus setting $l=0$ in Eqs. (24) and (25) or in Eqs. (26) and (27), and using Eq. (15) for the scaling property of the exponential case, the recursion relations (30) and (31) are immediately obtained. This alternative procedure provides a self-consistent check on the present results. A similar check can be easily verified for the Gaussian case using the scaling property (18).

Equations (22) and (23) or Eqs. (24) and (25) can be combined to eliminate the integral on the left side in each case, and obtain a five-term recursion relation valid for the matrix elements of powers of x. It turns out that the recursion relation thus obtained is very general; since it is good for any power of x, it will be valid for any analytic function of x which can be expanded in a power series. Thus,

$$\begin{aligned}\langle m|f(x)|n\rangle\rangle=\left(\frac{\omega_0}{2\omega_1}\right)^{1/2}&\{(m+1)^{1/2}\langle m+1|f(x)|n\rangle\rangle\\&+m^{1/2}\langle m-1|f(x)|n\rangle\rangle\}-\left(\frac{\omega_0}{2\omega_2}\right)^{1/2}\\&\times\{(n+1)^{1/2}\langle m|f(x)|n+1\rangle\rangle\\&+n^{1/2}\langle m|f(x)|n-1\rangle\rangle\},\end{aligned}\tag{32}$$

where $f(x)$ can be a power, exponential, Gaussian, trigonometric function, etc.

V. DISCUSSION AND CONCLUSIONS

For the special case of equal frequency oscillators ($\omega_1=\omega_2$), expression (6) for the Franck–Condon overlap integral reduces to a series which can be identified as a representation of an associated Laguerre polynomial.[10] Explicitly, for $\omega_1=\omega_2=\omega$,

$$\begin{aligned}\langle m|n\rangle\rangle=(-1)^{n-m}&\left[\frac{m!}{n!}\left(\frac{\omega}{2\omega_0}\right)^{n-m}\right.\\&\left.\times\exp\left(-\frac{\omega}{2\omega_0}\right)\right]^{1/2}L_m^{n-m}\left(\frac{\omega}{2\omega_0}\right).\end{aligned}\tag{33}$$

During their numerical evaluation of integrals of the form $\langle m|x^l|n\rangle\rangle$ for the first positive system of N_2, Fraser[11] and Nicholls and Jarmain[12] observed that under certain conditions the following equality nearly holds:

$$\frac{\langle m|x^2|n\rangle\rangle}{\langle m|x|n\rangle\rangle}\approx\frac{\langle m|x|n\rangle\rangle}{\langle m|x^0|n\rangle\rangle}.\tag{34}$$

That this should be true is easily seen by using the recursion relation (22). For the case $\omega\gg\omega_0$ and $(\omega/\omega_0)\gg m,n$ [which are equivalent[11,12] to the conditions necessary for equality (34) to hold], it is readily seen that the ratios in Eq. (34) are approximately equal to $\frac{1}{2}r$, independent of m or n.

In order to illustrate the results of the recursion relations derived above, we have numerically evaluated the Franck–Condon factors for the $A\,^1\Sigma_u^+$–$X\,^1\Sigma_g^+$ and the $B\,^1\Pi_u$–$X\,^1\Sigma_g^+$ systems of $^7Li_2$ using Eqs. (7), (8), and (9). The harmonic oscillators representing the potential curves of the X, A, and B electronic states have frequencies 351.43, 255.45, and 269.69 cm^{-1}, respectively, and potential minimum at 2.672, 3.107, and 2.936 Å, respectively. It is easy to verify that the first five vibrational levels of the above three simple harmonic oscillators have the same energy levels, within 5%, as the actual vibrational energy levels of the three electronic states, indicating that the harmonic oscillator approximation is reasonable for these levels. The computed numbers for Franck–Condon factors are compared, in Table I, with the experimentally obtained values of these factors for the above transitions in Li_2 by Hessel and coworkers.[14,15] To make comparison easy, we use a double ket notation, $|m\rangle\rangle$, to indicate the mth vibrational level of the ground state (analogous to the double prime, v'', notation of Hessel) and a single ket notation, $|n\rangle$, to indicate the nth vibrational level of the excited A or B states (analogous to the single prime, v', notation of Hessel). The results shown in Table I indicate that the agreement between computed factors, $|\langle m|n\rangle\rangle|^2$, and experimental values is not encouraging even for the low vibrational levels where the harmonic oscillator is supposed to be a good approximation. However, we note that the agreement becomes reasonable when the designation of the vibrational quantum numbers of two relevant levels are *interchanged, that is, when the experimental* $|\langle m|n\rangle\rangle|^2$ is compared with $|\langle\langle m|n\rangle|^2$. For ease of comparison, we have displayed $|\langle m|n\rangle\rangle|^2$ and $|\langle\langle m|n\rangle|^2$ side-by-side in Table I. We do not yet understand the reason for this puzzling observation.

TABLE I. A comparison of the Franck–Condon factors for the $A\,^1\Sigma_u^+-X\,^1\Sigma_g^+$ system (multiplied by 10^3) and the $B\,^1\Pi_u-X\,^1\Sigma_g^+$ system (multiplied by 10^4) of $^7Li_2$. A double ($|\rangle\rangle$) and a single ($|\rangle$) ket notation refers to the vibrational levels of the ground and the excited electronic state, respectively.

Vibrational quantum number	$A\,^1\Sigma_u^+-X\,^1\Sigma_g^+$			$B\,^1\Pi_u-X\,^1\Sigma_g^+$		
	experiment (Ref. 14)			experiment (Ref. 15)		
m , n	$\lvert\langle m\|n\rangle\rangle\rvert^2$	$\lvert\langle m\|n\rangle\rangle\rvert^2$	$\lvert\langle\langle m\|n\rangle\rvert^2$	$\lvert\langle m\|n\rangle\rangle\rvert^2$	$\lvert\langle m\|n\rangle\rangle\rvert^2$	$\lvert\langle\langle m\|n\rangle\rvert^2$
0 , 0	53	52	53	3267	3188	3267
0 , 1	131	176	)	3149	3827	4104
0 , 2	182	270	,8	1961	2103	2065
0 , 3	187	250	254	969	698	507
0 , 4	158	156	153	413	156	55
1 , 0	180	134	131	4104	3340	3149
1 , 1	191	197	191	39	77	39
1 , 2	78	58	54	844	1511	2042
1 , 3	4	9	12	1692	2711	3127
1 , 4	15	134	145	1516	1657	1395
2 , 0	277	187	182	2065	2008	1961
2 , 1	54	79	78	2042	942	844
2 , 2	13	15	13	1110	1345	1110
2 , 3	9	127	120	0.5	63	329
2 , 4	88	56	51	622	1834	2826
3 , 0	254	190	188	507	918	969
3 , 1	12	3	4	3127	1884	1692
3 , 2	120	98	90	329	1	0.5
3 , 3	46	45	46	1391	1508	1391
3 , 4	2	25	20	423	303	28
4 , 0	153	157	158	55	358	413
4 , 1	145	18	15	1395	1585	1516
4 , 2	51	90	89	2826	711	622
4 , 3	20	4	2	28	550	423
4 , 4	84	92	84	800	661	800

To summarize, we have obtained explicit expressions for the matrix elements of x^l, $\exp(-2cx)$, and $\exp(-cx^2)$, x being the internuclear separation, in the two-center simple harmonic basis. It is shown that in principle, the complete matrices of combinations of these functions could be determined in terms of only the lowest two Franck–Condon overlap matrix elements. Furthermore, a very general five-term recursion relation (32) is obtained which is valid for the matrix elements of *any* analytic function of x.

ACKNOWLEDGMENTS

It is a pleasure to thank Professor H. B. Schlegel for bringing some useful references to our attention. This research is supported by the Air Force Office of Scientific Research under Grant No. AFOSR-84-0143.

APPENDIX

The integral

$$I[f(t);m,n;a,b,y,z] = \int_{-\infty}^{\infty} f(t)\exp[-(t-y)^2]H_m(at)H_n(bt-z)\,dt \tag{A1}$$

with a, b, y, and z constant, is very useful in the evaluation of the Franck–Condon factors, and the matrix elements of powers of the coordinate x. The matrix elements of exponential and Gaussian functions, $\exp(-2cx)$ and $\exp(-cx^2)$, respectively, can also be easily obtained with only slight modifications in the solution of the integral for the case $f(t)=1$. To this end, a detailed derivation of the integral, $I(1;m,n;a,b,y,z)\equiv I_0$, is given in this Appendix. Some formulas, useful in the evaluation of the integral, and in obtaining recursion relations for it are presented first.

From the generating function of Hermite polynomials,

$$\sum_{n=0}^{\infty} H_n(x)t^n/n! = \exp(-t^2+2xt),$$

the following representation for Hermite polynomials is obtained:

$$H_n(B/A) = A^{-n}\left(\frac{\partial}{\partial t}\right)^n_{t=0}\exp(-A^2t^2+2Bt). \tag{A2}$$

The three-term recursion relation for Hermite polynomials is

$$2xH_n(x) = H_{n+1}(x) + 2nH_{n-1}(x). \tag{A3}$$

The integral to be evaluated is

$$I_0 = \int_{-\infty}^{\infty} \exp[-(t-y)^2]H_m(at)H_n(bt-z)\,dt. \tag{A4}$$

Using Eq. (A2) for the Hermite polynomials in Eq. (A4) we obtain

$$I_0 = \left(\frac{\partial}{\partial t_1}\right)^m_{t_1=0}\left(\frac{\partial}{\partial t_2}\right)^n_{t_2=0}\exp(-t_1^2-t_2^2-2zt_2-y^2) \times\int_{-\infty}^{\infty}\exp[-t^2+2(at_1+bt_2+y)t]\,dt \tag{A5}$$

$$= \pi^{1/2}\left(\frac{\partial}{\partial t_1}\right)^m_{t_1=0}\left(\frac{\partial}{\partial t_2}\right)^n_{t_2=0} \exp[-(1-a^2)t_1^2 - (1-b^2)t_2^2 + 2abt_1t_2 + 2ayt_1 + 2(by-z)t_2]. \tag{A6}$$

Carrying out the t_2 derivatives, and using the definition (A2) of the Hermite polynomials leads to

$$I_0 = \pi^{1/2}\sum_{k=0}^{n}\binom{n}{k}(1-b^2)^{(n-k)/2}H_{n-k}\left[\frac{by-z}{(1-b^2)^{1/2}}\right] \times \sum_{j=0}^{m}\binom{m}{j}\left(\frac{\partial}{\partial t_1}\right)^j_{t_1=0}(2abt_1)^k\left(\frac{\partial}{\partial t_1}\right)^{m-j}_{t_1=0} \times \exp[-(1-a^2)t_1^2 + 2ayt_1] \tag{A7}$$

$$= \pi^{1/2}\sum_{k=0}^{[m,n]}\binom{n}{k}\binom{m}{k}(1-b^2)^{(n-k)/2}(1-a^2)^{(m-k)/2} \times (2ab)^k k!H_{m-k}\left[\frac{ay}{(1-a^2)^{1/2}}\right] \times H_{n-k}\left[\frac{by-z}{(1-b^2)^{1/2}}\right] \tag{A8}$$

since, on setting $t_1 = 0$, the only nonzero term in the j sum is $j = k$. Thus the k sum runs from zero to the smaller of m or n, indicated by $[m,n]$.

We can evaluate $I[t^l;m,n;a,b,y,z] \equiv I_l$ by following the same procedure as above, through Eq. (A6), and using the standard integral,[13]

$$\int_{-\infty}^{\infty} t^l \exp(-t^2 + 2ut)dt = \pi^{1/2}\exp(u^2)(2i)^{-l}H_l(iu).$$

We obtain

$$I_l = (2i)^{-l}\pi^{1/2}\left(\frac{\partial}{\partial t_2}\right)^n_{t_2=0}\left(\frac{\partial}{\partial t_1}\right)^m_{t_1=0} \times H_l(iu)A(t_1,t_2) \tag{A9}$$

$$= (2i)^{-l}\pi^{1/2}\sum_{p=0}^{m}\sum_{q=0}^{n}\binom{m}{p}\binom{n}{q} \times \left[\left(\frac{\partial}{\partial t_2}\right)^q_{t_2=0}\left(\frac{\partial}{\partial t_1}\right)^p_{t_1=0}H(iu)\right] \times \left[\left(\frac{\partial}{\partial t_2}\right)^{n-q}_{t_2=0}\left(\frac{\partial}{\partial t_1}\right)^{m-p}_{t_1=0}A(t_1,t_2)\right], \tag{A10}$$

where

$$A(t_1,t_2) = \exp[-(1-a^2)t_1^2 - (1-b^2)t_2^2 + 2ayt_1 + 2(by-z)t_2 + 2abt_1t_2],$$
$$u = at_1 + bt_2 + y \text{ and } i = (-1)^{1/2}. \tag{A11}$$

Using Eq. (A6) and

$$\left(\frac{\partial}{\partial t_2}\right)^q_{t_2=0}\left(\frac{\partial}{\partial t_1}\right)^p_{t_1=0}H_l(iu) = \frac{l!a^pb^q(2i)^{p+q}}{(l-p-q)!}H_{l-p-q}(iy); \quad p+q\leqslant l \tag{A12}$$

we obtain the final result:

$$I[t^l;m,n;a,b,y,z] = \sum_{p=0}^{[m,l]}\sum_{q=0}^{[n,l-p]}\binom{m}{p}\binom{n}{q} \times \frac{l!a^pb^q}{(2i)^{l-p-q}(l-p-q)!}H_{l-p-q}(iy) \times I[1;m-p,n-q;a,b,y,z]. \tag{A13}$$

[1] G. Herzberg, *Molecular Spectra and Molecular Structure*, 2nd ed. (Van Nostrand, Princeton, 1950), Vol. I; J. I. Steinfeld, *Molecules and Radiation*, 2nd ed. (MIT, Cambridge, 1985).
[2] S. Waldenstrøm and K. Razi Naqvi, Chem. Phys. Lett. **85**, 581 (1982).
[3] N. E. Kuz'menko, L. A. Kuznetsova, and Yu. Ya. Kuzyankov, Sov. Phys. Usp. **26**, 425 (1983).
[4] K. Nishikawa, Int. J. Quantum Chem. **12**, 859 (1977).
[5] J. Morales, A. Palma, and M. Berrondo, Int. J. Quantum Chem. Symp. **18**, 57 (1984).
[6] C. Manneback, Physica **17**, 1001 (1951).
[7] F. Ansbacher, Z. Naturforsch. Teil A **14**, 889 (1959).
[8] T. Terasaka and T. Matsushita, Chem. Phys. Lett. **80**, 306 (1981).
[9] W. L. Smith, J. Phys. B **2**, 1 (1969).
[10] I. S. Gradshteyn and I. M. Ryzhik, *Table of Integrals, Series and Products* (Academic, New York, 1980), p. 1037.
[11] P. A. Fraser, Can. J. Phys. **32**, 515 (1954).
[12] R. W. Nicholls and W. R. Jarmain, Proc. Phys. Soc. A **69**, 253 (1955).
[13] I. S. Gradshteyn and I. M. Ryzhik, Ref. 10, p. 338.
[14] P. Kusch and M. M. Hessel, J. Chem. Phys. **67**, 586 (1977).
[15] M. M. Hessel and C. R. Vidal, J. Chem. Phys. **70**, 4439 (1979).

PHYSICAL REVIEW A VOLUME 35, NUMBER 5 MARCH 1, 1987

Elastic scattering of positrons and electrons by argon

Sultana N. Nahar and J. M. Wadehra
Department of Physics and Astronomy, Wayne State University, Detroit, Michigan 48202
(Received 15 September 1986)

Differential and integrated cross sections for the elastic scattering of low- and intermediate-energy (3–300 eV) positrons and electrons by argon atoms are calculated. Higher transport cross sections, representing moments of $1-(\cos\theta)^n$, for these systems are also obtained for $n=1$–4. Model potentials are used to represent the interactions between positrons or electrons and argon atoms. For each impact energy, the phase shifts of the lower partial waves are obtained exactly by numerical integration of the radial equation. The Born approximation is used to obtain the contribution of the higher partial waves to the scattering amplitude. The phase shifts of the seven lowest partial waves are tabulated for various impact energies of positrons and electrons.

I. INTRODUCTION

Since the pioneer work of Ramsauer,[1] the study of electron scattering by noble gases has been of considerable theoretical and experimental interest. Observations and calculations of both the total collisional as well as elastic differential and integrated cross sections for the scattering of electrons by rare-gas atoms have been made. In particular, low-energy total collisional cross sections, for electron scattering, exhibit a Ramsauer-Townsend (RT) minimum for Ar, Kr, and Xe. Observations of the scattering of positrons by rare-gas atoms are relatively recent. "First generation experiments" on positron scattering included observations of the total collisional cross sections.[2] It was then observed that the scattering of positrons by only the lighter rare-gas atoms He, Ne, and possibly Ar, exhibited the RT minimum. Thus argon may play a unique role in exhibiting the RT minimum for the scattering of both the electrons and the positrons. With the advent of high-intensity positron beams, it has now become feasible to carry out "second generation experiments" for measurements of angular distribution of positrons elastically scattered by rare-gas atoms. The impetus for the present paper is provided by the recent measurement[3] of differential cross sections for elastic scattering of intermediate-energy positrons by argon atoms. In the present calculations of elastic scattering of electrons and positrons by argon, an attempt is made to use as similar (within physical consistency) potential for the two projectiles as is possible.

Elastic and total collisional scattering of *electrons* by argon has been given considerable attention, both experimentally as well as theoretically, during the past sixty years.[1,4–55] Webb[4] has summarized the electron-argon scattering results prior to 1935. The later experiments on integrated elastic and total collisional cross sections were performed by Aberth *et al.*[5] (15–25 eV), Golden and Bandel[6] (0.1–21.6 eV), Kauppila *et al.*[7] (1.5–15.7 eV), Wagenaar and de Heer[8] (25–750 eV), Wagenaar and de Heer[9] (20–100 eV), Kauppila *et al.*[10] (15–800 eV), Nickel *et al.*[11] (4–300 eV), Jost *et al.*[12] (0.08–54.423 eV), Ferch *et al.*[13] (0.08–20 eV), Charlton *et al.*[14] (2–50 eV), and Gus'kov *et al.*[15] (0.025–1.0 eV). The differential cross sections (DCS) for the elastic scattering of electrons by argon have been measured by Mehr[16] (5–1000 eV, 20°–155°), Schackert[17] (40–150 eV, 30°–150°), Bromberg[18] (200–700 eV, 2°–30°), Williams and Willis[19] (20–400 eV, 20°–150°), Jansen *et al.*[20] (100–3000 eV, 5°–55°), Lewis *et al.*[21] (15–200 eV, 20°–140°), Vušković and Kurepa[22] (60–150 eV, 5°–150°), DuBois and Rudd[23] (20–800 eV, 2°–150°), Gupta and Rees[24,25] (100 eV, 10°–150°), Williams[26] (0.5–20 eV, 15°–150°), Srivastava *et al.*[27] (3–100 eV, 20°–135°), Andrick[28] (1–20 eV, 0°–180°), Qing *et al.*[29] (10–50 eV, 40°–110°), and Filipović[30] (10–100 eV, 20°–150°). From experimental angular distribution measurements, integrated elastic cross sections have also been calculated in some cases. Semiempirical cross sections for elastic and inelastic scattering of electrons from argon in the energy range 20 to 3000 eV have been obtained by de Heer *et al.*[31] Momentum transfer cross sections for electron-argon scattering have been measured or derived from experimental parameters by McPherson *et al.*[32] (0.08–4 eV), Golovanivsky and Kabilan[33] (0.005–0.6 eV), and Haddad and O'Malley[34] (0–4 eV). Theoretical studies of electron- or positron-argon scattering are characterized by the method used as well as by the potential used in the calculations. Theoretical calculations for electron scattering by argon have been performed by Walker[35] and by Fink and Yates[36] using the relativistic approximation; Thompson,[37] Garbaty and LaBahn,[38] Yau *et al.*,[39] and Dasgupta and Bhatia[40] using the polarized orbital method; Fon *et al.*,[41] and Bell *et al.*[42] using the R-matrix method; Pindzola and Kelly,[43] Amusia *et al.*,[44] McCarthy *et al.*,[45] Joachain *et al.*,[46,47] and Staszewska *et al.*[48] using optical model potentials; Berg *et al.*[49] and Datta *et al.*[50] using model potentials; Khare and Shobha[51] using the first Born approximation; McEachran and Stauffer[52] using adiabatic exchange approximation; and Haberland *et al.*[53] using Kohn-Sham-type one-particle theory. Momentum transfer cross sections for electron-argon scattering are obtained by Frost and Phelps[54] from transport coefficients and by Milloy *et al.*[55] by a swarm technique.

All measurements of *positron* scattering by argon have been made in the last decade or so. Measurements of total collisional cross sections for positron scattering from argon include those by Canter *et al.*[56] (2–400 eV), Jaduszliwer and Paul[57] (4–9 eV), Kauppila *et al.*[58] (0.4–18 eV), Coleman *et al.*[59] (2–960 eV), Griffith *et al.*[60] (30–800 eV), Tsai *et al.*[61] (25–300 eV), Brenton *et al.*[62] (200–1000 eV), Sinapius *et al.*[63] (1–6 eV), Coleman *et al.*[64] (2–50 eV), and Kauppila *et al.*[10] (15–800 eV). A recent summary of positron-gas scattering is given by Stein and Kauppila.[65] Measurements of the angular distribution for positron-argon elastic scattering have been made by Coleman and McNutt[66] (2.2–8.7 eV, 20°–60°) and by Hyder *et al.*[3] (100–300 eV, 30°–135°). On the theoretical side, positron-argon scattering calculations have been carried out by Joachain *et al.*[46] and Khare *et al.*[67] using optical model potentials; McEachran *et al.*[68] and McEachran and Stauffer[69] using the polarized orbital method; and Datta *et al.*[50] and Arifov and Zhuravleva[70] using a model potential. In the present study of elastic scattering of low- and intermediate-energy positrons and electrons from argon atoms, model static and Buckingham-type polarization potentials for the positron scattering and the same static (albeit with opposite sign) and polarization potentials along with an exchange potential for electron scattering have been used. The results of the present calculation are compared with the recent experimental observations of positrons and electrons elastically scattered from argon.

II. THEORY

Consider a projectile of charge e_p, with laboratory-frame impact energy E, being scattered elastically by a target with central potential $V(r)$. The scattering can be described by the radial part, $u_l(r)$, of the lth partial wave of the wave function which satisfies (in atomic units)

$$\left[\frac{d^2}{dr^2}-\frac{l(l+1)}{r^2}+2\mu[E-V(r)]\right]u_l(r)=0 . \qquad (1)$$

Here μ is the reduced mass of the system. The asymptotic form of the radial part of the wave function is

$$u_l(r) \underset{r\to\infty}{\longrightarrow} kr[j_l(kr)-(\tan\delta_l)n_l(kr)] , \qquad (2)$$

where $k^2=2\mu E$. j_l and n_l are the spherical Bessel functions of the first and the second kind, respectively. (For their numerical evaluation, see Appendix A.) For positron and electron impact, $\mu=1$. δ_l is the energy-dependent phase shift caused by the potential $V(r)$. From the values of the wave function at two adjacent points r and $r+h$ ($h \ll r$), in the asymptotic domain, one can extract the phase shift

$$\tan\delta_l=-\frac{(r+h)u_l(r)j_l(k(r+h))-ru_l(r+h)j_l(kr)}{ru_l(r+h)n_l(kr)-(r+h)u_l(r)n_l(k(r+h))} . \qquad (3)$$

Various phase shifts are used to obtain the scattering amplitude as

$$f(\theta)=\frac{1}{2ik}\sum_{l=0}^{\infty}(2l+1)(e^{2i\delta_l}-1)P_l(\cos\theta) , \qquad (4)$$

where θ is the scattering angle. Equation (1) is solved by using the Numerov procedure and the first L phase shifts are obtained exactly. L depends on the energy of the incident projectile. For large l ($>L$) the exact phase shifts δ_l are approximately equal to the Born phase shifts δ_{Bl},

$$\exp(i\delta_{Bl})\sin\delta_{Bl}\equiv T_{Bl}=-2k\int_0^\infty r^2 j_l^2(kr)V(r)dr . \qquad (5)$$

The typical values of L corresponding to the impact energies of 3 and 300 eV are 4 and 20, respectively.

The infinite sum in Eq. (4) is then approximated by

$$f(\theta)=\frac{1}{2ik}\sum_{l=0}^{L}(2l+1)[\exp(2i\delta_l)-1-\exp(2i\delta_{Bl})+1] \times P_l(\cos\theta)+f_B(\theta) , \qquad (6)$$

where f_B is the scattering amplitude in the Born approximation. For a spherically symmetric potential $V(r)$,

$$f_B(\theta)=\frac{1}{2ik}\sum_{l=0}^{\infty}(2l+1)[\exp(2i\delta_{Bl})-1]P_l(\cos\theta) = -2\int_0^\infty r^2\frac{\sin(qr)}{qr}V(r)dr , \qquad (7)$$

where $q=2k\sin(\theta/2)$ is the momentum transfer. The differential and the integrated elastic cross sections are

$$\frac{d\sigma}{d\Omega}=|f(\theta)|^2 , \qquad (8)$$

$$\sigma_I=2\pi\int_0^\pi\left[\frac{d\sigma}{d\Omega}\right]\sin\theta\, d\theta . \qquad (9)$$

The transport cross sections (including the momentum transfer, $n=1$, cross section) are

$$\sigma^{(n)}=2\pi\int_0^\pi(1-\cos^n\theta)\left[\frac{d\sigma}{d\Omega}\right]\sin\theta\, d\theta . \qquad (10)$$

TABLE I. Range of the values and the value used for the parameter d (in units of a_0) for various impact energies.

E (eV)	d (in units of a_0) Range of values	Value used
3	1.38–1.4	1.39
5	1.25–1.45	1.35
10	1.65–1.8	1.7
15	1.6 –1.8	1.6
20	1.7 –2.75	1.75
30	1.3 –1.7	1.65
40	1.35–1.7	1.6
50	1.3 –2.0	1.5
75	1.65–2.35	2.0
100	1.5 –2.5	2.0
150	1.5 –3.0	2.0
200	1.5 –3.0	2.0
250	1.5 –3.0	2.0
300	1.7 –3.0	2.0

The optical theorem

$$\sigma_I = \frac{4\pi}{k}\operatorname{Im} f(0) \tag{11}$$

is used as a self-consistent check on the present calculations. In the present calculations of elastic scattering of electrons and positrons by argon atoms, the potentials used are

$$V(r) = V_s(r) + V_p(r) \text{ for positron impact} \tag{12}$$

$$= V_s(r) + V_p(r) + V_{ex}(r) \text{ for electron impact .} \tag{13}$$

Here $V_s(r)$ is the static potential of the target atom, obtained by averaging over the motion of the target electrons:

$$V_s(\mathbf{r}) = \frac{Ze_p}{r} - \sum_{i=1}^{Z} e_p \int |\Psi(\mathbf{r}_1,\mathbf{r}_2,\ldots,\mathbf{r}_Z)|^2 \times \frac{1}{|\mathbf{r}-\mathbf{r}_i|} d\mathbf{r}_1 \cdots d\mathbf{r}_Z , \tag{14}$$

where Z is the nuclear charge of the target atom. $\Psi(\mathbf{r}_1,\ldots,\mathbf{r}_Z)$ is the antisymmetrized Hartree-Fock wave function of the target and is expanded in terms of the Slater-type orbitals:

$$\Phi_{\lambda p}(\mathbf{r}) = \sum_{i=1}^{M} A(\lambda,p,i) r^{n(p,i)-1} \exp[-\zeta(p,i) r] Y_{lm}(\hat{\mathbf{r}})$$

$$\equiv \phi_{\lambda p}(r) Y_{lm}(\hat{\mathbf{r}})$$

with

$$A(\lambda,p,i) = c(\lambda,p,i)[2\zeta(p,i)]^{n(p,i)+1/2} / \{[2n(p,i)]!\}^{1/2} . \tag{15}$$

The values of $c(\lambda,p,i)$, $\zeta(p,i)$, and $n(p,i)$ are taken from the tables of Clementi and Roetti.[71] Defining, for convenience,

$$v = n(p,i) + n(p,j),\quad z = \zeta(p,i) + \zeta(p,j),\quad a = A(\lambda,p,i) A(\lambda,p,j) v!,\quad s = z^{-v-1},\quad m = [1/(t+1)! - 1/(t!v)]/z^{v-t} , \tag{16}$$

where i, j, and t are integers, the static potential for argon atom is given by

$$V_s(r) = e_p \sum_{\lambda=1}^{N} \sum_{p=0}^{\lambda-1} N_{\lambda p} \sum_{i=1}^{M} \sum_{j=1}^{M} a \exp(-zr) \left[\frac{s}{r} + \sum_{t=0}^{v-2} m r^t \right] , \tag{17}$$

where N is the number of occupied shells in the atom and $N_{\lambda p}$ is the number of electrons in the orbital (λ,p). V_p is taken to be a model polarization potential of the Buckingham type,

$$V_p(r) = -\tfrac{1}{2} \alpha r^2 / (r^2 + d^2)^3 , \tag{18}$$

where α is the static dipole polarizability. d is an energy-dependent adjustable parameter determined by fitting the calculated differential and integrated cross sections for the elastic scattering of electrons by argon atoms with the experimental values of the same at a particular energy. The same value of d is then used for positron-argon scattering calculations at that energy. The values of the parameter d for various impact energies are given in Table I. Khare *et al.*,[67,72] who have used a very similar polarization potential, have expressed the parameter d as a linear function of k in their work. The exchange potential, $V_{ex}(r)$, for a closed-shell atom is taken to be[73]

$$V_{ex}(r) = \tfrac{1}{2} \left[[E - V_D(r)] - \left\{ [E - V_D(r)]^2 + \sum_{\lambda=1}^{N} \sum_{p=0}^{\lambda-1} N_{\lambda p} |\phi_{\lambda p}(r)|^2 \right\}^{1/2} \right] , \tag{19}$$

where V_D is the direct interaction potential, namely, $V_D = V_s + V_p$. $\phi_{\lambda p}(r)$ is the radial part of the Slater-type orbital as in Eq. (15). $V_{ex}(r)$ is a shorter range and much weaker potential than the static potential. Hence it is excluded from the computation of the phase shifts of higher partial waves using the Born approximation. For the polarization potential, the integral for the lth Born phase shift, Eq. (5), defined by T_{pBl}, is (for its derivation see Appendix B)

$$T_{pBl} = \tfrac{1}{4} \alpha k^2 \{ -(2l+3) i_{l+1}(kd) k_l(kd) + \pi(2l+3)/(4k^2 d^2) - [kd + (2l+1)(2l+3)/(2kd)] i_l(kd) k_l(kd) + kd\, i_{l+1}(kd) k_{l+1}(kd) \} , \tag{20}$$

where i_l and k_l are the modified spherical Bessel functions of the first and the third kind, respectively. (For their numerical evaluation see Appendix A.) The Born amplitude, Eq. (7), for the polarization potential defined above, is

$$f_{Bp} = \pi\alpha(3 - qd)\exp(-qd)/(16d) . \tag{21}$$

For the static potential, the lth Born phase shift, Eq. (5), defined to be T_{sBl}, is (for details see Appendix C)

$$T_{sBl} = -\frac{e_p}{k} \sum_{\lambda=1}^{N} \sum_{p=0}^{\lambda-1} N_{\lambda p} \sum_{i=1}^{M} \sum_{j=1}^{M} a \left[s Q_l \left[1 + \frac{z^2}{2k^2} \right] + \sum_{t=0}^{v-2} (-1)^{t+1} m \frac{d^{t+1}}{dz^{t+1}} Q_l \left[1 + \frac{z^2}{2k^2} \right] \right] , \tag{22}$$

where v, z, a, s, and m are defined in (16). Q_l is the Legendre function of the second kind. The corresponding Born scattering amplitude, f_{Bs}, is

$$f_{Bs} = -2e_p \sum_{\lambda=1}^{N} \sum_{p=0}^{\lambda-1} N_{\lambda p} \sum_{i=1}^{M} \sum_{j=1}^{M} a \left[\frac{s}{z^2+q^2} + \sum_{t=0}^{\nu-2} (-1)^{t+1} m \frac{d^{t+1}}{dz^{t+1}} \frac{1}{z^2+q^2} \right] . \tag{23}$$

For a given impact energy, the polarization potential provides the major contribution and the static potential a non-negligible contribution to the phase shifts of higher partial waves especially for the case of positron impact. The reason is that due to the opposite nature of the static and polarization interactions for the positron case, the first part of the scattering amplitude obtained from the first L exact phase shifts [see Eq. (6)] is smaller for positron impact than for electron impact and thus the relative contribution of the Born-approximation part with static interaction is more significant for positron impact than for electron impact.

III. RESULTS AND DISCUSSION

The differential and integrated cross sections for the elastic scattering of electrons from argon are shown in

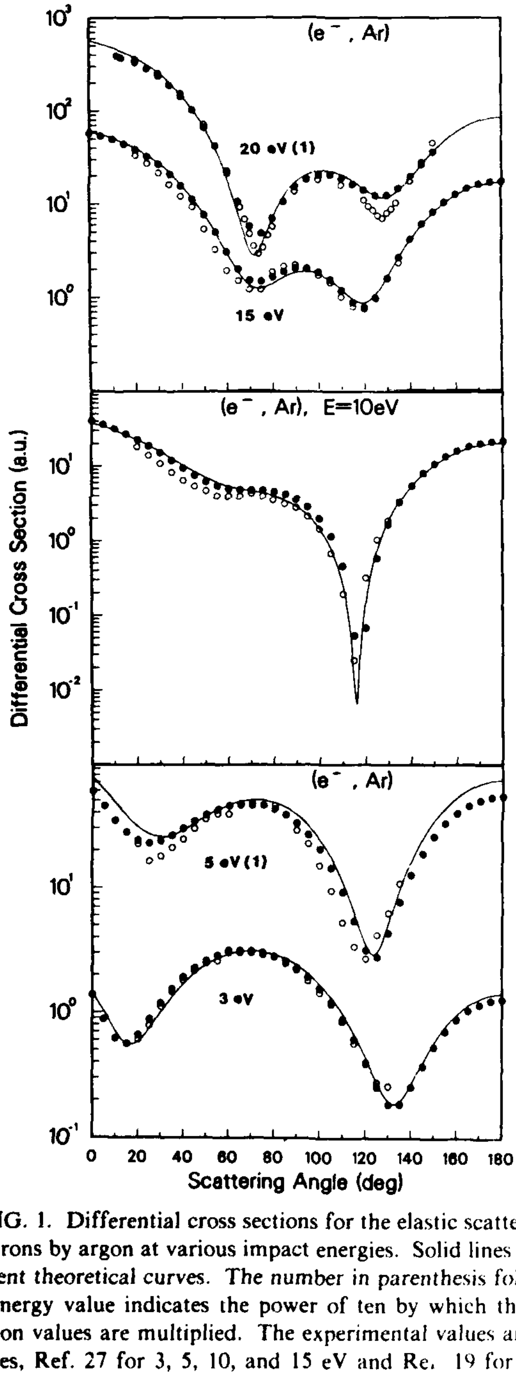

FIG. 1. Differential cross sections for the elastic scattering of electrons by argon at various impact energies. Solid lines are the present theoretical curves. The number in parenthesis following an energy value indicates the power of ten by which the cross section values are multiplied. The experimental values are open circles, Ref. 27 for 3, 5, 10, and 15 eV and Re. 19 for 20 eV; closed circles, Ref. 28 for 3, 5, 10, and 15 eV and Ref. 23 for 20 eV.

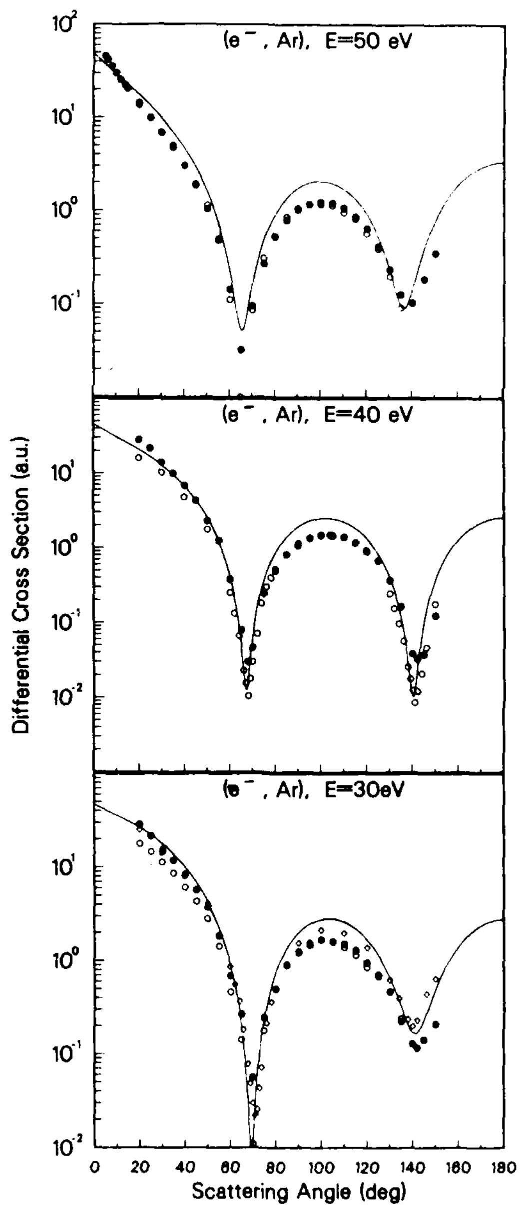

FIG. 2. Same as Fig. 1 except the experimental values are open circles, Ref. 27 for 30 and 50 eV and Ref. 19 for 40 eV; closed circles, Ref. 30 for 30 and 40 eV and Ref. 23 for 50 eV; diamonds, Ref. 19 for 30 eV.

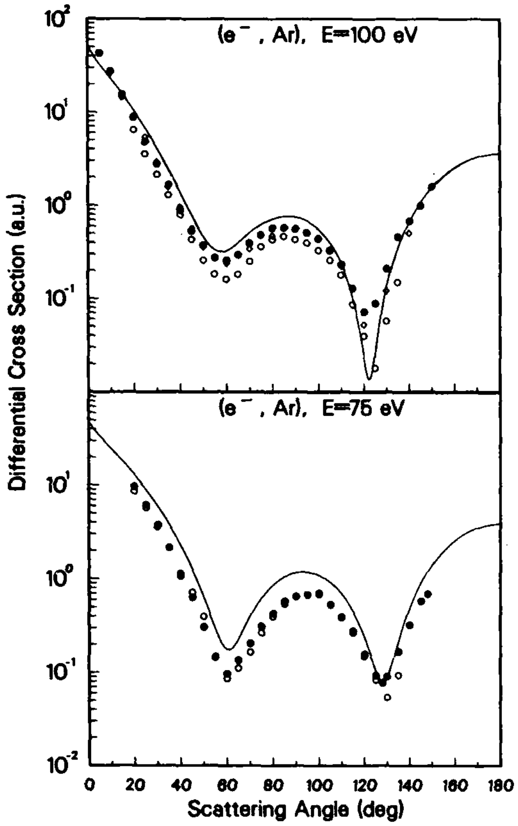

FIG. 3. Same as Fig. 1 except the experimental values are open circles, Ref. 27 for 75 and 100 eV; closed circles, Ref. 30 for 75 eV and Ref. 22 for 100 eV; diamonds, Ref. 25 for 100 eV.

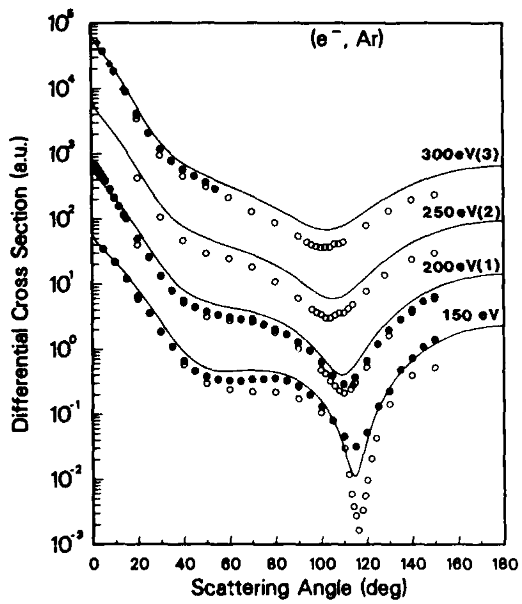

FIG. 4. Same as Fig. 1 except the experimental values are open circles, Ref. 19 for 150, 200, 250, and 300 eV; closed circles, Ref. 22 for 150 eV, Ref. 23 for 200 eV, and Ref. 20 for 300 eV; diamonds, Ref. 18 for 300 eV.

Figs. 1–4. The single adjustable parameter d in the polarization potential has been varied, for each impact energy, to fit, as closely as possible, the experimentally observed differential as well as integrated cross sections for elastic scattering of electrons from argon. It was noticed that a finite range of values of d could be used for such a fitting procedure. Table I gives the range of values of d along with the final value of d used for computing the present cross sections. It is seen by observing the size of the range of values of d from Table I that the cross sections are more sensitive to the value of d at lower energies

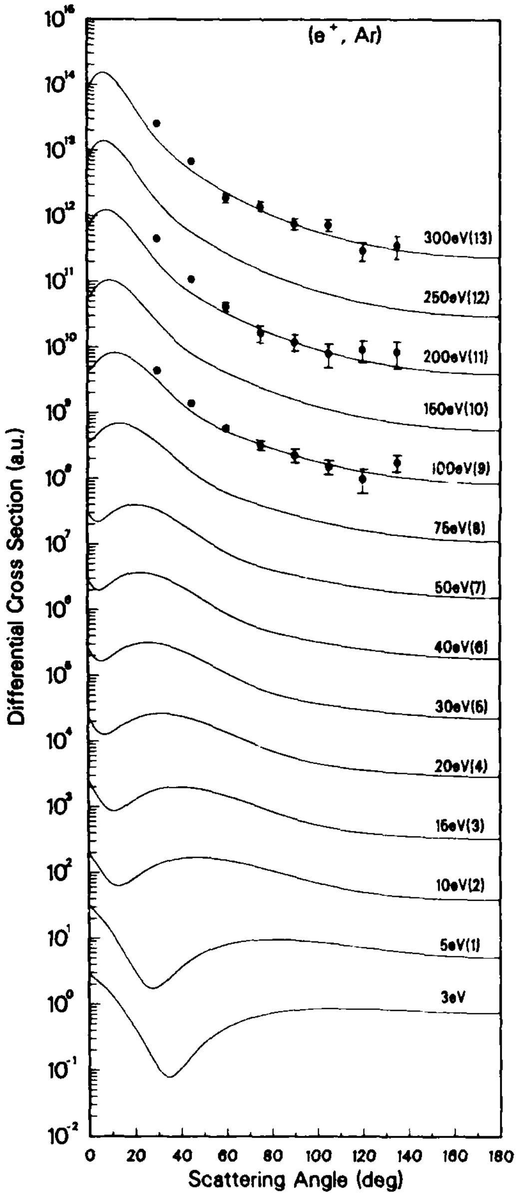

FIG. 5. Differential cross sections for the elastic scattering of positrons by argon at various impact energies. Solid lines are the present theoretical curves. The number in parentheses following an energy value indicates the power of ten by which the cross section values are multiplied. The experimental values are from Ref. 3.

TABLE II. Differential and integrated cross sections ($a_0^2\,sr^{-1}$) for elastic scattering of *electrons* from argon at $E=3-300$ eV.

θ (deg) \ E (eV)	3	5	10	15	20	30	40
0	0.147[1][a]	0.760[1]	0.377[2]	0.602[2]	0.571[2]	0.472[2]	0.460[2]
5	0.102[1]	0.608[1]	0.341[2]	0.557[2]	0.523[2]	0.409[2]	0.373[2]
10	0.717	0.481[1]	0.300[2]	0.509[2]	0.476[2]	0.359[2]	0.308[2]
15	0.560	0.379[1]	0.262[2]	0.455[2]	0.426[2]	0.312[2]	0.254[2]
20	0.585	0.311[1]	0.224[2]	0.396[2]	0.371[2]	0.267[2]	0.208[2]
25	0.742	0.271[1]	0.189[2]	0.335[2]	0.314[2]	0.222[2]	0.166[2]
30	0.101[1]	0.257[1]	0.156[2]	0.274[2]	0.256[2]	0.179[2]	0.129[2]
35	0.133[1]	0.265[1]	0.127[2]	0.215[2]	0.200[2]	0.138[2]	0.955[1]
40	0.170[1]	0.291[1]	0.103[2]	0.161[2]	0.149[2]	0.101[2]	0.673[1]
45	0.207[1]	0.330[1]	0.843[1]	0.115[2]	0.104[2]	0.685[1]	0.440[1]
50	0.242[1]	0.377[1]	0.699[1]	0.777[1]	0.673[1]	0.422[1]	0.257[1]
55	0.272[1]	0.424[1]	0.599[1]	0.496[1]	0.391[1]	0.225[1]	0.125[1]
60	0.295[1]	0.466[1]	0.534[1]	0.302[1]	0.196[1]	0.916	0.423
65	0.310[1]	0.498[1]	0.491[1]	0.187[1]	0.808	0.198	0.492[−1]
70	0.315[1]	0.513[1]	0.461[1]	0.134[1]	0.322	0.110[−1]	0.619[−1]
75	0.310[1]	0.510[1]	0.433[1]	0.125[1]	0.341	0.238	0.368
80	0.295[1]	0.488[1]	0.397[1]	0.140[1]	0.686	0.739	0.859
85	0.273[1]	0.447[1]	0.350[1]	0.164[1]	0.118[1]	0.137[1]	0.142[1]
90	0.243[1]	0.390[1]	0.290[1]	0.183[1]	0.168[1]	0.198[1]	0.193[1]
95	0.208[1]	0.322[1]	0.220[1]	0.187[1]	0.205[1]	0.247[1]	0.231[1]
100	0.171[1]	0.248[1]	0.145[1]	0.176[1]	0.224[1]	0.275[1]	0.250[1]
105	0.134[1]	0.177[1]	0.771	0.151[1]	0.222[1]	0.279[1]	0.247[1]
110	0.990	0.113[1]	0.252	0.121[1]	0.204[1]	0.259[1]	0.223[1]
115	0.685	0.643	0.120[−1]	0.951	0.174[1]	0.219[1]	0.183[1]
120	0.446	0.358	0.150	0.864	0.144[1]	0.168[1]	0.134[1]
125	0.281	0.311	0.741	0.106[1]	0.122[1]	0.114[1]	0.843
130	0.199	0.519	0.182[1]	0.164[1]	0.117[1]	0.663	0.412
135	0.197	0.980	0.339[1]	0.264[1]	0.137[1]	0.321	0.119
140	0.269	0.166[1]	0.539[1]	0.407[1]	0.185[1]	0.172	0.103[−1]
145	0.403	0.252[1]	0.773[1]	0.586[1]	0.261[1]	0.234	0.101
150	0.581	0.350[1]	0.103[2]	0.793[1]	0.358[1]	0.495	0.375
155	0.781	0.451[1]	0.128[2]	0.101[2]	0.469[1]	0.912	0.791
160	0.985	0.548[1]	0.152[2]	0.122[2]	0.583[1]	0.141[1]	0.128[1]
165	0.117[1]	0.633[1]	0.173[2]	0.141[2]	0.688[1]	0.192[1]	0.177[1]
170	0.131[1]	0.700[1]	0.190[2]	0.156[2]	0.773[1]	0.236[1]	0.219[1]
175	0.141[1]	0.742[1]	0.200[2]	0.166[2]	0.828[1]	0.265[1]	0.247[1]
180	0.144[1]	0.755[1]	0.204[2]	0.169[2]	0.847[1]	0.275[1]	0.257[1]
σ_I	0.207[2]	0.393[2]	0.763[2]	0.866[2]	0.728[2]	0.511[2]	0.396[2]

θ (deg) \ E (eV)	50	75	100	150	200	250	300
0	0.488[2]	0.474[2]	0.505[2]	0.555[2]	0.595[2]	0.630[2]	0.661[2]
5	0.374[2]	0.332[2]	0.334[2]	0.337[2]	0.341[2]	0.344[2]	0.347[2]
10	0.293[2]	0.244[2]	0.232[2]	0.218[2]	0.208[2]	0.201[2]	0.194[2]
15	0.229[2]	0.180[2]	0.161[2]	0.138[2]	0.123[2]	0.111[2]	0.102[2]
20	0.177[2]	0.129[2]	0.107[2]	0.824[1]	0.679[1]	0.581[1]	0.509[1]
25	0.134[2]	0.896[1]	0.685[1]	0.470[1]	0.363[1]	0.300[1]	0.259[1]
30	0.986[1]	0.597[1]	0.419[1]	0.262[1]	0.198[1]	0.166[1]	0.147[1]
35	0.699[1]	0.380[1]	0.246[1]	0.149[1]	0.119[1]	0.105[1]	0.963
40	0.471[1]	0.228[1]	0.140[1]	0.911	0.809	0.760	0.713
45	0.294[1]	0.126[1]	0.789	0.632	0.627	0.605	0.564
50	0.162[1]	0.629	0.465	0.508	0.532	0.506	0.460
55	0.729	0.290	0.332	0.463	0.476	0.435	0.382
60	0.221	0.175	0.324	0.457	0.437	0.378	0.319
65	0.516[−1]	0.228	0.394	0.467	0.404	0.329	0.267
70	0.162	0.395	0.504	0.475	0.370	0.283	0.223
75	0.475	0.621	0.620	0.470	0.330	0.239	0.183

TABLE II. (*Continued*).

θ (deg) \ E (eV)	50	75	100	150	200	250	300
80	0.902	0.853	0.713	0.445	0.282	0.195	0.149
85	0.135[1]	0.105[1]	0.760	0.397	0.229	0.154	0.119
90	0.174[1]	0.116[1]	0.749	0.327	0.173	0.117	0.948[−1]
95	0.199[1]	0.118[1]	0.678	0.244	0.121	0.869[−1]	0.778[−1]
100	0.208[1]	0.109[1]	0.555	0.158	0.769[−1]	0.668[−1]	0.691[−1]
105	0.198[1]	0.921	0.400	0.818[−1]	0.485[−1]	0.593[−1]	0.697[−1]
110	0.172[1]	0.693	0.239	0.286[−1]	0.412[−1]	0.668[−1]	0.804[−1]
115	0.135[1]	0.449	0.103	0.113[−1]	0.592[−1]	0.904[−1]	0.101
120	0.925	0.238	0.236[−1]	0.401[−1]	0.105	0.131	0.133
125	0.532	0.104	0.263[−1]	0.121	0.180	0.187	0.173
130	0.237	0.869[−1]	0.130	0.257	0.282	0.257	0.221
135	0.971[−1]	0.210	0.343	0.444	0.408	0.339	0.276
140	0.145	0.482	0.662	0.676	0.552	0.429	0.334
145	0.387	0.889	0.107[1]	0.939	0.706	0.524	0.395
150	0.799	0.140[1]	0.154[1]	0.122[1]	0.864	0.617	0.454
155	0.133[1]	0.198[1]	0.204[1]	0.150[1]	0.102[1]	0.706	0.509
160	0.192[1]	0.256[1]	0.252[1]	0.176[1]	0.115[1]	0.786	0.558
165	0.249[1]	0.309[1]	0.295[1]	0.198[1]	0.127[1]	0.853	0.599
170	0.296[1]	0.352[1]	0.329[1]	0.215[1]	0.136[1]	0.903	0.630
175	0.327[1]	0.379[1]	0.351[1]	0.226[1]	0.142[1]	0.934	0.649
180	0.338[1]	0.388[1]	0.358[1]	0.230[1]	0.144[1]	0.945	0.655
σ_I	0.333[2]	0.234[2]	0.192[2]	0.150[2]	0.128[2]	0.114[2]	0.103[2]

[a]The notation $a[b]$ means $a\times10^b$.

than at higher energies. The reason possibly is that the polarization interaction plays a more significant role at lower energies. It was also noticed that variation of d has a significant effect on the location of the minima and the maxima of the DCS curves and on the value of the DCS at those locations, especially at low energies. Variation of d also affected the DCS in the forward direction at all energies. Hence the DCS curves could be moved up and down near the forward direction by changing the value of d whereas the shape of the DCS curves at higher angles stayed about the same.

Within the range of values of d, shown in Table I for various electron-impact energies, the computed DCS curves and the integrated elastic cross sections remain close to the corresponding experimentally measured values. The value of d that, in our judgment, gave the best fitting was used for final computation of differential and integrated elastic cross sections for the scattering of both the electrons as well as the positrons. The DCS curves in the forward direction for positron impact are more sensitive to the value of d than the corresponding curves for electron impact due to the tendency of cancellation between the static and polarization interactions for the positrons. The differential cross sections for the elastic scattering of positrons from argon are shown in Fig. 5. Numerical values of the differential and integrated elastic cross sections for the scattering of electrons and positrons from argon are provided in Tables II and III.

A comparison of the various cross sections calculated here, for *electron* scattering, with corresponding measured values is given in Figs. 1—4 and in Tables IV and V. The calculated DCS curves for elastic scattering of electrons from argon are in good agreement with the measured values of Srivastava *et al.*,[27] Andrick,[28] DuBois and Rudd,[23] and Filipović[30] at lower energies (<50 eV) and with Vušković and Kurepa,[22] and DuBois and Rudd[23] at higher energies ($100\leq E\leq200$ eV). However, the agreement with Srivastava *et al.*[27] and Filipović[30] at larger angles becomes progressively poorer as the electron-impact energy becomes large. The differential cross sections measured by Williams and Willis[19] are almost always lower than our calculated cross sections at the minimum points. The integrated elastic cross sections given in Table IV are consistent with the available experimental values except with those of Srivastava *et al.*[27] which are lower than our calculated values. The transport cross sections, which represent the moments of $1-(\cos\theta)^n$, and which are related to the momentum transfer or diffusion cross section (for $n=1$), viscosity and thermal conductivity cross section (for $n=2$), etc.,[74] for both electrons and positrons are tabulated in Table V. Comparison in Table V of the present momentum transfer cross sections for the electron-argon system with the corresponding experimental values shows reasonable agreement except with the results of Ref. 27. Phase shifts of the seven lowest partial waves ($l=0-6$) for various impact energies of electrons and positrons are presented in Table VI and compare favorably with the available measured values.

The DCS curves for the elastic scattering of *positrons* by argon at various energies are shown in Fig. 5. These

TABLE III. Differential and integrated cross sections ($a_0^2\ \mathrm{sr}^{-1}$) for elastic scattering of *positrons* from argon at $E=3-300$ eV.

θ (deg) \ E (eV)	3	5	10	15	20	30	40
0	0.295[1][a]	0.335[1]	0.212[1]	0.263[1]	0.239[1]	0.276[1]	0.302[1]
5	0.209[1]	0.210[1]	0.114[1]	0.127[1]	0.134[1]	0.167[1]	0.199[1]
10	0.140[1]	0.122[1]	0.676	0.875	0.135[1]	0.193[1]	0.252[1]
15	0.795	0.626	0.651	0.983	0.176[1]	0.253[1]	0.325[1]
20	0.441	0.321	0.832	0.128[1]	0.220[1]	0.299[1]	0.365[1]
25	0.220	0.189	0.109[1]	0.160[1]	0.251[1]	0.318[1]	0.364[1]
30	0.108	0.183	0.133[1]	0.185[1]	0.263[1]	0.309[1]	0.332[1]
35	0.795[−1]	0.252	0.153[1]	0.198[1]	0.259[1]	0.281[1]	0.284[1]
40	0.107	0.364	0.165[1]	0.201[1]	0.242[1]	0.244[1]	0.232[1]
45	0.170	0.488	0.171[1]	0.195[1]	0.218[1]	0.204[1]	0.184[1]
50	0.256	0.615	0.170[1]	0.182[1]	0.191[1]	0.167[1]	0.143[1]
55	0.348	0.724	0.165[1]	0.166[1]	0.164[1]	0.135[1]	0.112[1]
60	0.445	0.819	0.156[1]	0.148[1]	0.138[1]	0.109[1]	0.888
65	0.536	0.890	0.144[1]	0.131[1]	0.116[1]	0.888	0.722
70	0.617	0.937	0.132[1]	0.114[1]	0.981	0.737	0.605
75	0.689	0.968	0.120[1]	0.990	0.833	0.626	0.523
80	0.747	0.976	0.108[1]	0.861	0.716	0.545	0.464
85	0.796	0.973	0.967	0.753	0.626	0.485	0.419
90	0.830	0.954	0.869	0.665	0.556	0.441	0.384
95	0.855	0.929	0.782	0.594	0.504	0.407	0.355
100	0.870	0.896	0.707	0.538	0.464	0.379	0.330
105	0.877	0.860	0.645	0.493	0.432	0.357	0.309
110	0.879	0.823	0.592	0.459	0.408	0.337	0.289
115	0.873	0.783	0.549	0.432	0.388	0.320	0.272
120	0.865	0.746	0.514	0.411	0.371	0.304	0.257
125	0.853	0.709	0.486	0.394	0.357	0.291	0.244
130	0.841	0.676	0.463	0.381	0.345	0.279	0.232
135	0.826	0.645	0.445	0.370	0.335	0.268	0.222
140	0.812	0.618	0.431	0.361	0.326	0.259	0.213
145	0.799	0.594	0.420	0.354	0.318	0.251	0.206
150	0.785	0.572	0.411	0.348	0.311	0.243	0.200
155	0.775	0.557	0.404	0.343	0.305	0.238	0.195
160	0.763	0.541	0.399	0.339	0.300	0.233	0.191
165	0.757	0.531	0.395	0.336	0.297	0.230	0.188
170	0.750	0.523	0.392	0.334	0.294	0.227	0.186
175	0.747	0.518	0.391	0.333	0.293	0.226	0.184
180	0.749	0.520	0.390	0.332	0.292	0.225	0.184
σ_I	0.842[1]	0.927[1]	0.118[2]	0.113[2]	0.117[2]	0.109[2]	0.104[2]

θ (deg) \ E (eV)	50	75	100	150	200	250	300
0	0.334[1]	0.365[1]	0.426[1]	0.532[1]	0.623[1]	0.704[1]	0.777[1]
5	0.219[1]	0.493[1]	0.640[1]	0.903[1]	0.113[2]	0.132[2]	0.149[2]
10	0.286[1]	0.653[1]	0.809[1]	0.104[2]	0.119[2]	0.129[2]	0.136[2]
15	0.364[1]	0.680[1]	0.778[1]	0.875[1]	0.901[1]	0.892[1]	0.865[1]
20	0.396[1]	0.602[1]	0.630[1]	0.618[1]	0.573[1]	0.522[1]	0.473[1]
25	0.379[1]	0.477[1]	0.459[1]	0.397[1]	0.339[1]	0.292[1]	0.255[1]
30	0.331[1]	0.352[1]	0.314[1]	0.248[1]	0.202[1]	0.171[1]	0.148[1]
35	0.270[1]	0.251[1]	0.211[1]	0.159[1]	0.129[1]	0.110[1]	0.958
40	0.211[1]	0.177[1]	0.144[1]	0.109[1]	0.894	0.768	0.673
45	0.162[1]	0.127[1]	0.104[1]	0.798	0.665	0.571	0.497
50	0.123[1]	0.950	0.789	0.620	0.517	0.439	0.377
55	0.947	0.746	0.632	0.500	0.411	0.344	0.292
60	0.751	0.612	0.524	0.411	0.333	0.275	0.230
65	0.616	0.519	0.445	0.343	0.273	0.222	0.184
70	0.524	0.450	0.383	0.289	0.226	0.182	0.150
75	0.459	0.395	0.332	0.245	0.190	0.152	0.124
80	0.410	0.350	0.290	0.211	0.161	0.128	0.104

TABLE III. (*Continued*).

θ (deg) \ E (eV)	50	75	100	150	200	250	300
85	0.372	0.312	0.256	0.183	0.138	0.109	0.886[−1]
90	0.340	0.280	0.227	0.160	0.120	0.943[−1]	0.762[−1]
95	0.313	0.252	0.202	0.141	0.106	0.824[−1]	0.664[−1]
100	0.290	0.229	0.182	0.126	0.937[−1]	0.728[−1]	0.584[−1]
105	0.269	0.209	0.166	0.114	0.839[−1]	0.649[−1]	0.520[−1]
110	0.250	0.192	0.151	0.103	0.757[−1]	0.584[−1]	0.467[−1]
115	0.234	0.178	0.140	0.944[−1]	0.690[−1]	0.530[−1]	0.423[−1]
120	0.220	0.166	0.130	0.871[−1]	0.633[−1]	0.485[−1]	0.387[−1]
125	0.208	0.156	0.121	0.808[−1]	0.586[−1]	0.448[−1]	0.357[−1]
130	0.197	0.147	0.114	0.756[−1]	0.546[−1]	0.417[−1]	0.332[−1]
135	0.188	0.140	0.108	0.712[−1]	0.513[−1]	0.391[−1]	0.311[−1]
140	0.180	0.133	0.103	0.675[−1]	0.485[−1]	0.369[−1]	0.293[−1]
145	0.174	0.128	0.982[−1]	0.644[−1]	0.462[−1]	0.351[−1]	0.279[−1]
150	0.168	0.124	0.946[−1]	0.619[−1]	0.443[−1]	0.336[−1]	0.267[−1]
155	0.164	0.120	0.917[−1]	0.598[−1]	0.427[−1]	0.325[−1]	0.258[−1]
160	0.160	0.117	0.894[−1]	0.582[−1]	0.415[−1]	0.315[−1]	0.250[−1]
165	0.158	0.115	0.877[−1]	0.569[−1]	0.406[−1]	0.308[−1]	0.245[−1]
170	0.156	0.114	0.864[−1]	0.561[−1]	0.400[−1]	0.303[−1]	0.241[−1]
175	0.155	0.113	0.857[−1]	0.556[−1]	0.396[−1]	0.300[−1]	0.238[−1]
180	0.155	0.113	0.855[−1]	0.554[−1]	0.395[−1]	0.299[−1]	0.238[−1]
σ_I	0.973[1]	0.102[2]	0.956[1]	0.861[1]	0.791[1]	0.736[1]	0.690[1]

[a]The notation $a[b]$ means $a\times10^b$.

curves show a minimum at low energies which shifts toward the forward direction with increasing impact energy. The increasing depth of this minimum on lowering the impact energy suggests the existence of the critical point for the positron-argon system. The critical points represent the points of minimum scattering, where a small change in either the incident projectile energy or the scattering angle is associated with an appreciable increase in the differential scattering cross section. The low-energy critical points for various positron—rare-gas-atom systems have been predicted by Wadehra *et al.*[75] So far the measurements of the angular distributions of elastic

TABLE IV. Comparison of calculated integrated elastic cross sections (in units of a_0^2) with the experimental values.

Projectile	E (eV)	Present value of σ_I	Experimental value of σ_I
e^-	3	20.66	20.83(7),[a] 19.48(12), 17.3(13), 20.64(14), 20.12(26), 19.65(27), 20.51(28)
	5	39.31	33.95(7), 32.1(11), 32.59(12), 30.87(13), 36.76(14), 36.09(26), 30.02(27), 34.73(28)
	10	76.33	70.75(10), 73.47(11), 74.33(12), 67.54(13), 69.3(14), 83.4(26), 64.32(27), 77.29(28)
	15	86.57	85.5(26), 75.04(27), 85.48(28)
	20	72.79	71.31(19), 68.4(23), 70.65(26), 44.67(27), 71.18(28)
	30	51.08	47.21(19)
	40	39.61	32.28(19)
	50	33.28	26.48(19), 25.61(23), 21.8(27)
	75	23.37	14.29(27)
	100	19.21	18.66(19), 16.51(20), 17.33(22), 17.1(23), 18.04(24), 9.29(27)
	150	15.02	11.86(19), 13.21(20), 13.33(22), 14.83(24)
	200	12.8	11.51(18), 9.81(19), 10.9(23), 12.68(24)
	300	10.32	8.74(18), 7.82(19), 8.81(20), 10.19(24)
e^+	3	8.42	12.57(56), 9.11(58), 8.56(64)
	5	9.27	12.56(55), 10.8(57), 9.68(58), 8.73(64)

[a]The notation $a(b)$ for experimental values of σ_I means the measured value of a taken from Ref. b.

TABLE V. The higher transport cross sections $\sigma^{(n)}$ (in units of a_0^2) and comparison of $\sigma^{(1)}$ with the experimental values.

Projectile	E (eV)	$\sigma^{(4)}$	$\sigma^{(3)}$	$\sigma^{(2)}$	$\sigma^{(1)}$	Experimental momentum transfer, $\sigma^{(1)}$
e^-	3	18.19	19.41	15.89	16.56	16.72(26),[a] 14.65(27), 16.08(28)
	5	30.45	38.97	25.98	34.67	32.45(26), 22.87(27), 29.5(28)
	10	42.15	66.37	31.61	58.97	67.65(26), 53.6(27), 62.4(28)
	15	40.84	58.57	28.41	49.56	51.2(26), 53.6(27), 51.28(28)
	20	34.83	41.82	24.44	33.65	33.66(26), 23.58(27), 34.8(28)
	30	26.18	26.52	19.40	21.33	13.22(27)
	40	20.20	20.82	15.38	17.49	
	50	16.12	18.05	12.38	15.67	8.58(27)
	75	9.98	13.40	7.60	11.90	6.79(27)
	100	7.39	11.03	5.48	9.78	5.72(27)
	150	5.24	7.96	3.74	6.95	
	200	4.26	6.08	2.99	5.22	
	250	3.63	4.86	2.53	4.09	
	300	3.16	4.01	2.19	3.31	
e^+	3	6.87	9.02	5.89	9.71	
	5	7.87	9.39	6.80	9.44	
	10	9.67	10.40	8.01	8.95	
	15	8.85	9.33	7.15	7.64	
	20	8.63	8.92	6.79	7.01	
	30	7.51	7.62	5.78	5.79	
	40	6.73	6.73	5.10	5.00	
	50	6.04	5.98	4.55	4.38	
	75	5.38	5.19	3.95	3.63	
	100	4.62	4.40	3.36	2.30	
	150	3.64	3.40	2.60	2.22	
	200	3.01	2.77	2.12	1.74	
	250	2.56	2.33	1.77	1.43	
	300	2.22	2.00	1.52	1.20	

[a]The notation $a(b)$ for experimental values of $\sigma^{(1)}$ means the measured value of a taken from Ref. b.

scattering of positrons by argon have been made only for a limited range of energies. The only available measured relative values of differential cross sections of Hyder *et al.*[3] at energies 100, 200, and 300 eV, have been normalized to the present calculated DCS curves at 90°. In this energy range, other calculations of elastic cross sections are those of McEachran and Stauffer[69] using the polarized orbital method and some limited results by Joachain[47] using the optical model potential. At higher energies and at larger angles the present calculations of DCS agree with those of McEachran and Stauffer and with the measurements of Hyder *et al.* When normalized separately at 90°, the measurements of Hyder *et al.* at 300 eV agree well both with the present calculation as well as with the calculations of Joachain.[47] At low energies and near the forward scattering direction, where unfortunately no experimental information for positron-argon elastic scattering is available, our DCS curves differ significantly from the calculated results of McEachran and Stauffer. It would certainly be worthwhile to carry out experiments on the elastic differential scattering of positrons by argon in this energy and angular range. For positron energies smaller than the positronium formation threshold in Ar (8.96 eV), the integrated elastic cross sections are compared in Table IV with the measured total positron-argon collisional cross sections. Higher transport cross sections and the lowest seven phase shifts for positron-argon elastic scattering are given in Tables V and VI, respectively. No comparison of these numbers is possible due to the lack of measurements of these quantities.

Finally, an attempt was made to obtain the cross sections for the elastic scattering of ultralow (≤ 2.5 eV) energy electrons and positrons by argon. In this energy range, no experimental numerical values of differential cross sections for electron impact are available. Thus it was not possible to obtain the low-energy parameters such as the scattering length and effective range for the positron-argon system using the present procedure.

In the present paper we have obtained various cross sections—differential, integrated, momentum transfer, etc.—and the corresponding phase shifts for the elastic scattering of positrons and electrons by argon. These cross sections compare favorably with the recent measurements of elastic differential scattering of intermediate-energy positrons by argon. With the anticipation that similar measurements will be made for other rare-gas targets in the near future, we are presently calculating the cross sections for the elastic scattering of low- and intermediate-energy positrons by He, Ne, Kr, and Xe by a similar procedure.

TABLE VI. Phase shifts (rad) of the first seven partial waves for elastic scattering of electrons and positrons by argon.

Projectile	E (eV)	$l=0$	$l=1$	$l=2$	$l=3$	$l=4$	$l=5$	$l=6$
e^-	3	−0.490	−0.132	0.130	0.0241	0.0106	0.0057	0.003 46
		−0.457	−0.134	0.142	0.021(26)[a]			
		−0.548	−0.140	0.125	0.035(27)			
		−0.493	−0.142	0.120	0.025(28)			
	5	−0.747	−0.272	0.306	0.042	0.0175	0.0094	0.0057
		−0.685	−0.205	0.317	0.031(26)			
		−0.747	−0.256	0.254	0.102(27)			
		−0.733	−0.277	0.260	0.044(28)			
	10	−1.283	−0.688	0.751	0.084	0.0321	0.0172	0.0106
		−1.098	−0.528	0.936	0.093(26)			
		−1.243	−0.430	0.805	0.171(27)			
		−1.143	−0.562	0.840	0.10(28)			
	15	−1.569	−0.867	1.131	0.140	0.0497	0.0255	0.0156
		−1.394	−0.750	1.451	0.154(26)			
		−1.365	−0.506	1.593	0.2(27)			
		−1.443	−0.782	1.39	0.165(28)			
	20	−1.826	−1.064	1.519	0.186	0.064	0.032	0.0194
		−1.653	−0.935	1.747	0.241(26)			
		−1.818	−0.871	1.679	0.262(27)			
		−1.683	−0.962	1.670	0.232(28)			
	30	−2.154	−1.296	1.817	0.306	0.104	0.0496	0.0288
	40	−2.40	−1.47	1.929	0.421	0.147	0.0682	0.0386
	50	−2.583	−1.595	2.008	0.539	0.196	0.0909	0.0503
	75	0.122	1.207	−1.184	0.645	0.250	0.116	0.0622
	100	−0.146	1.014	−1.166	0.773	0.330	0.159	0.0858
	150	−0.532	0.735	−1.168	0.929	0.460	0.241	0.135
	200	−0.809	0.535	−1.185	1.013	0.552	0.311	0.182
	250	−1.027	0.38	−1.207	1.064	0.619	0.368	0.225
	300	−1.205	0.253	−1.229	1.096	0.668	0.415	0.263
e^+	3	−0.334	0.0839	0.0528	0.0219	0.0105	0.005 72	0.003 46
	5	−0.496	0.0505	0.0703	0.0341	0.0169	0.009 39	0.005 72
	10	−0.878	−0.139	0.0455	0.0456	0.0278	0.0167	0.0106
	15	−1.06	−0.251	0.0173	0.0509	0.0368	0.0235	0.0152
	20	−1.245	−0.384	−0.0427	0.0371	0.0378	0.027	0.0185
	30	−1.455	−0.545	−0.126	0.0132	0.0385	0.0335	0.0248
	40	1.529	−0.674	−0.206	−2.081	0.0306	0.0354	0.0291
	50	1.423	−0.765	−0.267	−0.0506	0.0217	0.036	0.0326
	75	1.115	−1.044	−0.487	−0.196	−0.0598	−0.0038	0.0154
	100	0.967	−1.185	−0.606	−0.284	−0.115	−0.0344	0.000 64
	150	0.789	−1.365	−0.774	−0.420	−0.214	−0.986	−0.0374
	200	0.690	−1.474	−0.884	−0.519	−0.294	−0.158	−0.778
	250	0.631	−1.543	−0.960	−0.593	−0.359	−0.209	−0.116
	300	0.596	1.552	−1.015	−0.651	−0.412	−0.254	−0.151

[a]Numbers in parentheses denote reference from which the measured phase shift was taken.

ACKNOWLEDGMENTS

We thank Dr. D. Andrick, Dr. A. K. Bhatia, Dr. D. Filipović, Dr. W. E. Kauppila, Dr. A. D. Stauffer, and Dr. T. S. Stein for providing unpublished data. Support of the National Science Foundation (Grant No. PHY 83-11705) and the Air Force Office of Scientific Research (Grant No. AFOSR-84-0143) is gratefully acknowledged.

APPENDIX A: GENERATION OF SPHERICAL BESSEL FUNCTIONS

The standard recursion relations[76] can be used for the generation of the spherical Bessel functions $n_l(x)$ and $k_l(x)$ for any value of the argument x and for increasing l as well as for the generation of $j_l(x)$ for increasing l and for argument $x>50$. However, due to a numerical instability, these recurrence relations cannot be used for the generation of $j_l(x)$ for increasing l if $x\leq 50$ and for the generation of $i_l(x)$ for increasing l for any value of the argument x. In these cases $i_l(x)$ and $j_l(x)$ can be evaluated using hypergeometric function ${}_0F_1$:

$$i_l(x)=\sqrt{\pi/2x}\,(x/2)^{l+1/2}{}_0F_1(l+\tfrac{3}{2};x^2/4)/\Gamma(l+\tfrac{3}{2})\,, \tag{A1}$$

$$j_l(x)=\sqrt{\pi/2x}\,(x/2)^{l+1/2}{}_0F_1(l+\tfrac{3}{2};-x^2/4)/\Gamma(l+\tfrac{3}{2})\,. \tag{A2}$$

The function $_0F_1$ can be evaluated using the rational approximation.[77] When the argument x of j_l is large (>50), the rational approximation for $_0F_1$ becomes unstable.

APPENDIX B: DERIVATION OF PHASE SHIFT FOR POLARIZATION POTENTIAL IN BORN APPROXIMATION

For the polarization potential, Eq. (18), the Born phase-shift integral T_{Bl}, Eq. (5), is defined to be T_{pBl} and is given by

$$T_{pBl}=\alpha k \int_0^\infty r^4 j_l^2(kr)/(r^2+d^2)^3 dr \;. \tag{B1}$$

After some simplifications, Eq. (B1) can be written as

$$T_{pBl}=\alpha k^2 \left[\int_0^\infty x^2 j_l^2(x)/(x^2+a^2)^2 dx - a^2 \int_0^\infty x^2 j_l^2(x)/(x^2+a^2)^3 dx \right] , \tag{B2}$$

where $a=kd$. Using Eq. (6.535) of Ref. 78 and the recurrence relations for the spherical Bessel functions $i_l(x)$ and $k_l(x)$ one can derive

$$\int_0^\infty x^2 j_l^2(x)/(x^2+a^2)^2 dx = -[2a i_{l+1}(a)k_l(a) - \pi/(2a) + (2l+1) i_l(a) k_l(a)]/2(a) \;, \tag{B3}$$

$$\begin{aligned}\int_0^\infty x^2 j_l^2(x)/(x^2+a^2)^3 dx &= -[2a i_{l+1}(a)k_l(a) - \pi/(2a) + (2l+1) i_l(a)k_l(a)]/(8a^3) \\ &\quad + \{4l i_{l+1}(a)k_l(a) - \pi l/a^2 + i_l(a)k_l(a)/a\,[2a^2+4(l+\tfrac{1}{2})^2-2l-1] \\ &\quad - 2a i_{l+1}(a)k_{l+1}(a)\}/(8a^2) \;.\end{aligned} \tag{B4}$$

Substituting (B3) and (B4) in (B2) and after some simplification Eq. (20) is obtained.

APPENDIX C: DERIVATION OF PHASE SHIFT FOR STATIC POTENTIAL IN BORN APPROXIMATION

Substituting $V_s(r)$ [Eq. (17)], in Eq. (5) and making use of the standard integral[78]

$$\int_0^\infty r \exp(-zr) j_l^2(kr) dr = (2k^2)^{-1} Q_l[1+z^2/(2k^2)] \;, \tag{C1}$$

where Q_l is the Legendre function of the second kind, Eq. (22) is obtained. The argument of the Q_l function, $1+z^2/(2k^2)$, is greater than 1 and therefore the recurrence relation cannot be used for the generation of the functions for increasing l. One convenient way to evaluate a Q_l function is to write it in terms of Gaussian hypergeometric function $F(a,b;c;x)$ as[76]

$$Q_l(x)=\frac{\pi^{1/2}\Gamma(l+1)}{2^{l+1}\Gamma(l+\frac{3}{2})}\frac{1}{x^{l+1}}F(1+l/2,\tfrac{1}{2}+l/2;l+\tfrac{3}{2};1/x^2), \quad x>1 \tag{C2}$$

where the hypergeometric function can be evaluated by summing the following series:

$$F(a,b;c;x)=1+\frac{ab}{c\times 1}x+\frac{a(a+1)b(b+1)}{c(c+1)\times 1\times 2}x^2+\frac{a(a+1)(a+2)b(b+1)(b+2)}{c(c+1)(c+2)\times 1\times 2\times 3}x^3+\cdots \;. \tag{C3}$$

The higher-order derivatives of Q_l with respect to z can be carried out easily using Eq. (C2) and the relation

$$\frac{d^n}{dx^n}F(a,b;c;x)=\frac{\Gamma(a+n)\Gamma(b+n)\Gamma(c)}{\Gamma(c+n)\Gamma(a)\Gamma(b)}F(a+n,b+n;c+n;x) \;. \tag{C4}$$

[1] C. Ramsauer, Ann. Phys. (Leipzig) **66**, 546 (1921).

[2] W. E. Kauppila and T. S. Stein, Can. J. Phys. **60**, 471 (1982); T. S. Stein and W. E. Kauppila, Adv. At. Mol. Phys. **18**, 53 (1982).

[3] G. M. A. Hyder, M. S. Dababneh, Y.-F. Hsieh, W. E. Kauppila, C. K. Kwan, M. Mahdavi-Hezaveh, and T. S. Stein, Phys. Rev. Lett. **57**, 2252 (1986).

[4] G. M. Webb, Phys. Rev. **47**, 379 (1935).

[5] W. Aberth, G. Sunshine, and B. Bederson, *Abstracts of the Third International Conference on the Physics of Electronic and Atomic Collisions, London, 1963*, edited by M. R. C. McDowell (North-Holland, Amsterdam, 1964), p. 53.

[6] D. E. Golden and H. W. Bandel, Phys. Rev. **149**, 58 (1966).

[7] W. E. Kauppila, T. S. Stein, G. Jesion, M. S. Dababneh, and V. Pol, Rev. Sci. Instrum. **48**, 822 (1977).

[8] R. W. Wagenaar and F. J. de Heer, J. Phys. B **13**, 3855 (1980).

[9] R. W. Wagenaar and F. J. de Heer, J. Phys. B **18**, 2021 (1985).

[10] W. E. Kauppila, T. S. Stein, J. H. Smart, M. S. Dababneh, Y. K. Ho, J. P. Downing, and V. Pol, Phys. Rev. A **24**, 725 (1981).

[11] J. C. Nickel, I. Imre, D. F. Register, and S. Trajmar, J. Phys. B **18**, 125 (1985).

[12] K. Jost, P. G. F. Bisling, F. Eschen, M. Felsmann, and L. Walther, in *Abstracts of Contributed Papers, Thirteenth Inter-*

national Conference on the Physics of Electronic and Atomic Collisions, Berlin, 1983, edited by J. Eichler, W. Fritsch, I. V. Hertel, N. Stolterfoht, and W. Willie (North-Holland, Amsterdam, 1983), p. 91; A. K. Bhatia (private communication).
[13]J. Ferch, B. Granitza, C. Masche, and W. Raith, J. Phys. B **18**, 967 (1985).
[14]M. Charlton, T. C. Griffith, G. R. Heyland, and T. R. Twomey, J. Phys. B **13**, L239 (1980).
[15]Yu. K. Gus'kov, R. V. Savvov, and V. A. Slobodyanyuk, Zh. Tekh. Fiz. **48**, 277 (1978) [Sov. Phys.—Tech. Phys. **23**, 167 (1978)].
[16]J. Mehr, Z. Phys. **198**, 345 (1967).
[17]K. Schackert, Z. Phys. **213**, 316 (1968).
[18]J. P. Bromberg, J. Chem. Phys. **61**, 963 (1974).
[19]J. F. Williams and B. A. Willis, J. Phys. B **8**, 1670 (1975).
[20]R. H. J. Jansen, F. J. de Heer, H. J. Luyken, B. van Wingerden, and H. J. Blaauw, J. Phys. B **9**, 185 (1976).
[21]B. R. Lewis, J. B. Furness, P. J. O. Teubner, and E. Weigold, J. Phys. B **7**, 1083 (1974).
[22]L. Vušković and M. V. Kurepa, J. Phys. B **9**, 837 (1976).
[23]R. D. DuBois and M. E. Rudd, J. Phys. B **9**, 2657 (1976).
[24]S. C. Gupta, Ph.D. thesis, University of Liverpool, 1975 (the data are quoted in Ref. 31).
[25]S. C. Gupta and J. A. Rees, J. Phys. B **8**, 1267 (1975).
[26]J. F. Williams, J. Phys. B **12**, 265 (1979).
[27]S. K. Srivastava, H. Tanaka, A. Chutjian, and S. Trajmar, Phys. Rev. A **23**, 2156 (1981).
[28]D. Andrick (private communication).
[29]Zhou Qing, M. J. M. Beerlage, and M. J. van der Weil, Physica C **113**, 225 (1982).
[30]Dusan M. Filipović, M. Sci. thesis, Institute of Physics, Beograd, 1984.
[31]F. J. de Heer, R. H. J. Jansen, and W. van der Kaay, J. Phys. B **12**, 979 (1979).
[32]D. A. McPherson, R. K. Feeney, and J. W. Hooper, Phys. Rev. A **13**, 167 (1976).
[33]K. S. Golovanivsky and A. P. Kabilan, Phys. Lett. **80A**, 249 (1980).
[34]G. N. Haddad and T. F. O'Malley, Aust. J. Phys. **35**, 35 (1982).
[35]D. W. Walker, Adv. Phys. **20**, 257 (1971).
[36]M. Fink and A. C. Yates, At. Data **1**, 385 (1970).
[37]D. G. Thompson, Proc. R. Soc. London, Ser. A **294**, 160 (1966); J. Phys. B **4**, 468 (1971).
[38]A. Garbaty and R. W. LaBahn, Phys. Rev. A **4**, 1425 (1971).
[39]A. W. Yau, R. P. McEachran, and A. D. Stauffer, J. Phys. B **11**, 2907 (1978).
[40]A. Dasgupta and A. K. Bhatia, Phys. Rev. A **32**, 3335 (1985).
[41]W. C. Fon, K. A. Berrington, P. G. Burke, and A. Hibbert, J. Phys. B **16**, 307 (1983).
[42]K. L. Bell, N. S. Scott, and M. A. Lennon, J. Phys. B **17**, 4757 (1984).
[43]M. S. Pindzola and H. P. Kelly, Phys. Rev. A **9**, 323 (1974).
[44]M. Ya. Amusia, N. A. Cherepkov, L. V. Chernysheva, D. M. Davidović, and V. Radojević, Phys. Rev. A **25**, 219 (1982).
[45]I. E. McCarthy, C. J. Noble, B. A. Phillips, and A. D. Turnbull, Phys. Rev. A **15**, 2173 (1977).
[46]C. J. Joachain, R. Vanderpoorten, K. H. Winters, and F. W. Byron, Jr., J. Phys. B **10**, 227 (1977).
[47]C. J. Joachain, *Proceedings of the Tenth International Conference on the Physics of Electronic and Atomic Collisions, Paris, 1977,* edited by G. Watel (North-Holland, Amsterdam, 1977), p. 71.
[48]G. Staszewska, D. W. Schwenke, and D. G. Truhlar, Phys. Rev. A **29**, 3078 (1984).
[49]R. A. Berg, J. E. Purcell, and A. E. S. Green, Phys. Rev. A **3**, 508 (1971).
[50]S. K. Datta, S. K. Mandal, P. Khan, and A. S. Ghosh, in *Proceedings of the Seventh International Conference on Positron Annihilation (ICPA),* edited by P. C. Jain, R. M. Singru, and K. P. Gopinathan (World Scientific, Singapore, 1985), p. 387; Phys. Rev. A **32**, 633 (1985).
[51]S. P. Khare and P. Shobha, J. Phys. B **7**, 420 (1974).
[52]R. P. McEachran and A. D. Stauffer, J. Phys. B **16**, 4023 (1983).
[53]R. Haberland, L. Fritsche, and J. Noffke, Phys. Rev. A **33**, 2305 (1986).
[54]L. S. Frost and A. V. Phelps, Phys. Rev. **136**, A1538 (1964).
[55]H. B. Milloy, R. W. Crompton, J. A. Rees, and A. G. Robertson, Aust. J. Phys. **30**, 61 (1977).
[56]K. F. Canter, P. G. Coleman, T. C. Griffith, and G. R. Heyland, Appl. Phys. **3**, 249 (1974).
[57]B. Jaduszliwer and D. A. Paul, Can. J. Phys. **52**, 272 (1974); T. S. Stein (private communication).
[58]W. E. Kauppila, T. S. Stein, and G. Jesion, Phys. Rev. Lett. **36**, 580 (1976).
[59]P. G. Coleman, T. C. Griffith, G. R. Heyland, and T. R. Twomey, Appl. Phys. **11**, 321 (1976).
[60]T. C. Griffith, G. R. Heyland, and T. R. Twomey, as reported by T. C. Griffith and G. R. Heyland, Phys. Rep. **39**, 169 (1978).
[61]J-S. Tsai, L. Lebow, and D. A. L. Paul, Can. J. Phys. **54**, 1741 (1976).
[62]A. G. Brenton, J. Dutton, and F. M. Harris, J. Phys. B **11**, L15 (1978).
[63]G. Sinapius, W. Raith, and W. G. Wilson, J. Phys. B **13**, 4079 (1980).
[64]P. G. Coleman, J. D. McNutt, L. M. Diana, and J. T. Hutton, Phys. Rev. A **22**, 2290 (1980); T. S. Stein (private communication).
[65]T. S. Stein and W. E. Kauppila, in *Proceedings of the Fourteenth International Conference on the Physics of Electronic and Atomic Collisions,* edited by D. C. Lorents, W. E. Meyerhof, and J. R. Peterson (North-Holland, Amsterdam, 1986), p. 105.
[66]P. G. Coleman and J. D. McNutt, Phys. Rev. Lett. **42**, 1130 (1979).
[67]S. P. Khare, A. Kumar, and K. Lata, Indian J. Pure Appl. Phys. **20**, 379 (1982); Phys. Rev. A **33**, 2795 (1986).
[68]R. P. McEachran, A. G. Ryman, and A. D. Stauffer, J. Phys. B **12**, 1031 (1979).
[69]R. P. McEachran and A. D. Stauffer, in *Proceedings of the Third International Workshop on Positron (Electron)-Gas Scattering,* edited by W. E. Kauppila, T. S. Stein, and J. M. Wadehra (World Scientific, Singapore, 1986), p. 122.
[70]P. U. Arifov and G. I. Zhuravleva, in *Proceedings of the Seventh International Conference on Positron Annihilation (ICPA),* edited by P. C. Jain, R. M. Singru, and K. P. Gopinathan (World Scientific, Singapore, 1985), p. 425.
[71]E. Clementi and C. Roetti, At. Data Nucl. Data Tables **14**, 177 (1974).
[72]B. L. Jhanwar and S. P. Khare, Phys. Lett. **50A**, 201 (1974).
[73]M. E. Riley and D. G. Truhlar, J. Chem. Phys. **63**, 2182 (1975); J. B. Furness and I. E. McCarthy, J. Phys. B **6**, 2280 (1973); B. H. Bransden, M. R. C. McDowell, C. J. Noble, and T. Scott, *ibid.* **9**, 1301 (1976).
[74]See, for example, E. W. McDaniel and E. A. Mason, *The Mobility and Diffusion of Ions in Gases* (Wiley, New York, 1973).

[75]J. M. Wadehra, T. S. Stein, and W. E. Kauppila, Phys. Rev. A **29**, 2912 (1984).

[76]See, for example, *Handbook of Mathematical Functions*, edited by M. Abramowitz and I. A. Stegun (Dover, New York, 1970).

[77]See, for example, Yudell L. Luke, *Algorithms for the Computation of Mathematical Functions* (Academic, New York, 1977).

[78]See, for example, *Table of Integrals, Series, and Products*, edited by I. S. Gradshteyn and I. M. Ryzhik (Academic, New York, 1980).

PHYSICAL REVIEW A VOLUME 35, NUMBER 11 JUNE 1, 1987

Positronium formation from Li and Na atoms by use of pseudopotentials

Sultana N. Nahar and J. M. Wadehra
Department of Physics and Astronomy, Wayne State University, Detroit, Michigan 48202
(Received 29 December 1986)

The differential and total cross sections for the formation of positronium in its ground state from Li and Na atoms by the impact of intermediate-energy positrons are calculated in the first Born and distorted-wave Born approximations. Hellmann-type pseudopotentials are used to represent the alkali-metal ion cores. The difference in the use of pseudopotentials and the static potential for the core representation for evaluating various rearrangement cross sections is discussed.

I. INTRODUCTION

There has been a growing interest in the investigation of electron capture from alkali-metal atom. As an example, charge-transfer processes with Li have been suggested to be occurring in plasma diagnostic probes.[1] Also, alkali-metal atoms are many-electron systems that can be simplified to be one-electron systems due to a single valence electron. Theoretical calculations as well as experimental measurements have been carried out for ionization of and electron capture from alkali-metal atoms by proton impact (for some recent works see Refs. 1 and 2). The charge-transfer[3] and the total collisional[4] cross sections for positron impact on alkali-metal atoms have been calculated by several authors, and the total collisional cross sections have been measured for a potassium target by Stein *et al.*[5] In the present paper, the first Born approximation (FBA) and the distorted-wave Born approximation (DWBA) are used to calculate the cross sections for the ground-state positronium (Ps) formation from lithium and sodium by the impact of intermediate-energy positrons. Although the FBA cross sections are calculated and compared both in the post and the prior forms, DWBA cross sections are calculated, for computational convenience, only in the post form.

To compare the effects of different potentials (model potential versus pseudopotential) describing the ion cores, the first calculation[6] is done to calculate the cross sections for positronium formation from Li in the first Born approximation by using the static potential for the lithium ion core. The next calculations, employing FBA and DWBA, are for the positronium formation in both lithium and sodium using the pseudopotentials. In these calculations the alkali-metal ion cores have been represented by Hellmann-type pseudopotentials. A significant difference, in the values as well as in the shape, is observed for differential cross sections (DCS) in FBA using the pseudopotential and the static potential. A discussion about the formulation of various potentials representing the ion cores and the resulting differences in the shape of the DCS is presented in Secs. II B and III.

II. THEORY

A. Rearrangement cross sections

Let a positron of mass M_p with lab impact energy E and velocity $\mathbf{v}$ collide with a target alkali-metal atom at rest and form positronium in the ground state by electron capture from the target (T). Because of the single valence electron it is reasonable to treat the alkali-metal atom as a hydrogenic system by representing the ion core by a central potential, $V_p(r)$, which could either be a pseudopotential or a model potential. Then the initial and the final channel interactions are

$$V_i(\mathbf{r}_p,\mathbf{R})=V_{p\text{-}e}(\mathbf{r}_p)+V_{p\text{-}T}(\mathbf{R})=-e^2/r_p+V_p(R)\ , \tag{1a}$$

$$V_f(\mathbf{r}_T,\mathbf{R})=V_{T\text{-}e}(\mathbf{r}_T)+V_{p\text{-}T}(\mathbf{R})=V_p(r_T)+V_p(R)\ , \tag{1b}$$

respectively. The position vectors are shown in Fig. 1. The notation used is similar to that of Ref. 7. The interaction between the projectile and the valence electron is represented by $V_{p\text{-}e}$, that between the projectile and the target ion core is represented by $V_{p\text{-}T}$, and that between the target ion core and the electron is represented by $V_{T\text{-}e}$. In the present work $V_p(r)$ is chosen to be of the Hellmann or Yukawa type:[8]

$$V_p(r)=-\frac{e^2}{r}+\frac{e^2A}{r}\exp(-\zeta r)-\frac{e^2\alpha_d}{2(r^2+d^2)^2}-\frac{e^2\alpha_q}{2(r^2+d^2)^3}\ . \tag{2}$$

The parameters A and ζ for the valence electron in lithium and sodium atoms are listed in Ref. 8. α_d and α_q are the dipole and the quadrupole polarizability, respectively, of the alkali-metal ion core. Both the valence electron and the projectile positron experience the same interaction with the atomic core except that the signs of the first two terms of V_p change in the case of the positron interaction.

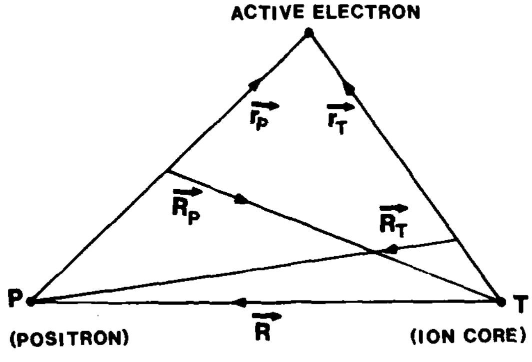

FIG. 1. Coordinate system.

This assumption is believed to be plausible for the following reasons. In the case of alkali-metal atoms the single valence electron is far removed from the alkali-metal ion core which contains the other tightly bound electrons and, therefore, the exchange effects in the valence-electron–ion-core interaction are expected to be small. Furthermore, the exchange interaction is, in general, a short-range and much weaker interaction compared to the static interaction. There are, of course, no exchange effects in positron–ion-core interactions. Thus, it appears reasonable to assume that in the energy range being considered here the valence electron and the incident positron experience similar interactions, apart from the sign of some terms, with the alkali-metal ion core. Defining the quantities

$$\alpha \equiv M_T/(m+M_T), \quad \beta \equiv M_p/(m+M_p), \tag{3}$$

where m is the electron mass and M_T is the mass of the alkali-metal ion core, the various position vectors of Fig. 1 are related as

$$\begin{aligned} \mathbf{R}_T &= \mathbf{R}_p-(1-\beta)\mathbf{r}_p, \\ \mathbf{r}_T &= \mathbf{R}_p+\beta\mathbf{r}_p, \\ \mathbf{R} &= \mathbf{R}_T+(1-\alpha)\mathbf{r}_T, \\ \mathbf{R}_p &= \beta\mathbf{R}_T+(1-\alpha\beta)\mathbf{r}_T, \\ \mathbf{r}_p &= -\mathbf{R}_T+\alpha\mathbf{r}_T. \end{aligned} \tag{4}$$

$\mathbf{R}_T$ is the position vector of the positron relative to the center of mass of the alkali-metal atom and $\mathbf{R}_p$ is that of the ion core relative to the center of mass of the final bound state, Ps. The reduced masses are

$$\begin{aligned} \mu_T &= mM_T/(m+M_T)=\alpha m, \\ \mu_p &= mM_p/(m+M_p)=\beta m, \\ \nu_i &= M_p(m+M_T)/(m+M_T+M_p), \\ \nu_f &= M_T(m+M_p)/(m+M_T+M_p). \end{aligned} \tag{5}$$

In the center-of-mass frame, the total energy of the system is

$$E=\hbar^2k_i^2/(2\nu_i)+\varepsilon_i=\hbar^2k_f^2/(2\nu_f)+\varepsilon_f, \tag{6}$$

where $\hbar\mathbf{k}_i=\nu_i\mathbf{v}$ is the initial relative momentum and $\hbar\mathbf{k}_f$ is the final relative momentum, ε_i is the internal energy of the $(e+T)$ system, and ε_f is the internal energy of the final bound Ps state. The average momentum transfer vectors are

$$\mathbf{K}=\beta\mathbf{k}_f-\mathbf{k}_i, \quad \mathbf{J}=\alpha\mathbf{k}_i-\mathbf{k}_f. \tag{7}$$

If Ψ_i^+ is the exact wave function of the complete system in the initial channel with outgoing wave boundary conditions, then the Schrödinger equation satisfied by Ψ_i^+ is

$$\left[-\frac{\hbar^2}{2\nu_i}\nabla^2_{\mathbf{R}_T}-\frac{\hbar^2}{2\mu_T}\nabla^2_{\mathbf{r}_T}+V_i+V_{Te}\right]\Psi_i^+=E\Psi_i^+, \tag{8}$$

which, for the purpose of using the two-potential theory, can be rewritten as

$$[H_D+(V_i-U_i)]\Psi_i^+=E\Psi_i^+, \tag{9}$$

where

$$H_D=H_0+U_i+V_{Te}, \quad H_0=-\frac{\hbar^2}{2\nu_i}\nabla^2_{\mathbf{R}_T}-\frac{\hbar^2}{2\mu_T}\nabla^2_{\mathbf{r}_T}, \tag{10}$$

and U_i is as yet an arbitrary distortion potential. The distorted wave χ_i^+, then, is

$$\chi_i^+=\psi_i^+\frac{1}{E-H_D+i\varepsilon}U_i\psi_i, \tag{11}$$

where χ_i^+ and ψ_i satisfy

$$H_D\chi_i^+=E\chi_i^+ \quad \text{and} \quad (H_0+V_{Te})\psi_i=E\psi_i. \tag{12}$$

Similar forms for the different wave functions (Ψ_f^-,χ_f^-,ψ_f, etc.) can be obtained for the final channel. Let $\phi_i(\mathbf{r}_T)$ represent the internal state of $(e+T)$ such that

$$\left[-\frac{\hbar^2}{2\mu_T}\nabla^2_{\mathbf{r}_T}+V_{Te}\right]\phi_i(\mathbf{r}_T)=\varepsilon_i\phi_i(\mathbf{r}_T). \tag{13}$$

A similar equation could be written for the final internal state $\phi_f(\mathbf{r}_p)$ of Ps. The initial and final channel wave functions are then

$$\psi_i=\exp(i\mathbf{k}_i\cdot\mathbf{R}_T)\phi_i(\mathbf{r}_T), \quad \psi_f=\exp(i\mathbf{k}_f\cdot\mathbf{R}_p)\phi_f(\mathbf{r}_p), \tag{14}$$

respectively. If χ_i^+ is chosen, following Ref. 7, to be of the form

$$\chi_i^+=\phi_i(\mathbf{r}_T)[\exp(i\mathbf{k}_i\cdot\mathbf{R}_T)+g_i^+(\mathbf{R}_T)], \tag{15}$$

then it follows from Eq. (11) that

$$g_i^+\phi_i(\mathbf{r}_T)=\frac{1}{E-H_D+i\varepsilon}U_i\psi_i. \tag{16}$$

Upon operating on both sides of Eq. (16) by (H_D-E), using Eq. (13) and then taking the Fourier transform of the resulting equation, it is seen that $\tilde{g}_i^+$ satisfies

$$\tilde{g}_i^+(\mathbf{K})\hbar^2(K^2-k_i^2-i\eta)/(2\nu_i)+\tilde{U}_i(\mathbf{K}-\mathbf{k}_i) +(2\pi)^{-3/2}\int\tilde{g}_i^+(\mathbf{p})\tilde{U}_i(\mathbf{K}-\mathbf{p})d^3p=0. \tag{17}$$

Here the tilde represents the Fourier transform. Similarly, for the final channel, if one writes

$$\chi_f^-=\phi_f(\mathbf{r}_p)[\exp(i\mathbf{k}_f\cdot\mathbf{R}_p)+g_f^-(\mathbf{R}_p)], \tag{18}$$

then an integral equation, similar to Eq. (17), can be obtained for $\tilde{g}_f^-$. The integral equations can be solved to first order in the distortion potentials U_i and U_f to give

$$\tilde{g}_i^+(\mathbf{K})=-\frac{2\nu_i}{\hbar^2}\frac{\tilde{U}_i(\mathbf{K}-\mathbf{k}_i)}{K^2-k_i^2-i\eta}, \tag{19}$$

and

$$\tilde{g}_f^-(\mathbf{K})=-\frac{2\nu_f}{\hbar^2}\frac{\tilde{U}_f(\mathbf{K}-\mathbf{k}_f)}{K^2-k_f^2+i\eta}. \tag{20}$$

The specific forms chosen for the distortion potentials are the static potentials

$$\begin{aligned} U_i(\mathbf{R}_T) &= \int|\phi_i(\mathbf{r}_T)|^2V_i(\mathbf{r}_p,\mathbf{R})d^3r_T, \\ U_f(\mathbf{R}_p) &= \int|\phi_f(\mathbf{r}_p)|^2V_f(\mathbf{r}_T,\mathbf{R})d^3r_p. \end{aligned} \tag{21}$$

Since U_i depends only on $\mathbf{R}_T$ and U_f depends only on $\mathbf{R}_p$, the T-matrix element for the transition from the initial state to the final state is given by[9]

$$T = \langle \chi_f^- \mid V_f - U_f \mid \Psi_i^+ \rangle , \tag{22a}$$

in the post form, and

$$T = \langle \Psi_f^- \mid V_i - U_i \mid \chi_i^+ \rangle , \tag{22b}$$

in the prior form. If the perturbations $(V_i - U_i)$ and $(V_f - U_f)$ are weak enough, Ψ_i^+ and Ψ_f^- can be replaced by χ_i^+ and χ_f^-. This approximation is the distorted-wave Born approximation (DWBA) used here, and the T-matrix element in this approximation is given by

$$T = \langle \chi_f^- \mid V_f - U_f \mid \chi_i^+ \rangle , \tag{23a}$$

in the post form, and

$$T = \langle \chi_f^- \mid V_i - U_i \mid \chi_i^+ \rangle , \tag{23b}$$

in the prior form. The present DWBA calculations for the positronium formation from alkali-metal atoms have been done in the post form only. The T-matrix element in the post form is

$$T = T_1 + T_2 + T_3 , \tag{24}$$

where

$$\begin{aligned} T_1 &= \langle \psi_f \mid V_f - U_f \mid \psi_i \rangle , \\ T_2 &= \langle \psi_f \mid V_f - U_f \mid g_i^+ \phi_i \rangle \\ &\quad + \langle g_f^- \phi_f \mid V_f - U_f \mid \psi_i \rangle \equiv T_2^+ + T_2^- , \\ T_3 &= \langle g_f^- \phi_f \mid V_f - U_f \mid g_i^+ \phi_i \rangle . \end{aligned} \tag{25}$$

Note, on using Eqs. (19) and (20), that T_1, T_2, and T_3 are first, second, and third order in the potential, respectively. Then keeping consistently terms up to third order in the potential, the differential cross section is

$$\left[\frac{d\sigma}{d\Omega} \right]_{\mathrm{DWBA}} = \frac{v_i v_f k_f}{4\pi^2 \hbar^4 k_i} \mid T \mid^2 , \tag{26}$$

where

$$\mid T \mid^2 = \{ \mid T_1 \mid^2 + 2[\mathrm{Re}(T_1)\mathrm{Re}(T_2) + \mathrm{Im}(T_1)\mathrm{Im}(T_2)] \} . \tag{27}$$

When distortion is excluded, the first Born approximation is obtained for which

$$T = \langle \psi_f \mid V_f \mid \psi_i \rangle , \tag{28a}$$

in the post form, and

$$T = \langle \psi_f \mid V_i \mid \psi_i \rangle , \tag{28b}$$

in the prior form. The cross sections for positronium formation in FBA have been calculated both in the post and the prior forms in order to check the accuracy of the trial wave functions for the valence electron of the alkali-metal atom. A better trial wave function, obtained by a lowering of the energy in the variational principle, results in a smaller post-prior discrepancy. The integrated cross section for positronium formation

$$\sigma = 2\pi \int_0^\pi \left[\frac{d\sigma}{d\Omega} \right] \sin\theta \, d\theta \tag{29}$$

is evaluated numerically.

Atomic units are used in the present calculations. In these calculations the pseudopotential, Eq. (2), has been reduced without losing much accuracy to

$$V_p(r) = -1/r + (A/r)\exp(-\zeta r) \tag{30}$$

for computational ease. The parameters A and ζ for the valence electron in lithium and sodium atoms are taken from Ref. 8. It was found that even without the polarization terms for the ion cores in $V_p(r)$ the use of Eq. (30) in Eq. (13) gives the energy ε_i of the valence electron in the alkali-metal atom very close to the observed values. The value of ε_i obtained in the present calculations is $-0.195\,895\,6$ a.u. compared to $-0.198\,162\,4$ a.u.[10] for the $2s$ valence electron of Li and $-0.182\,596$ a.u. compared to $-0.188\,864\,4$ a.u.[10] for the $3s$ valence electron of Na. The trial wave function for the s-state valence electron is expanded in terms of hydrogenic wave functions as

$$\phi_i(\mathbf{r}) = Y_{00}(\hat{\mathbf{r}}) \sum_{m=1}^{3} \sum_{i=1}^{2} c_{i+2m-2} r^{i-1} \exp(-\delta_m r) , \tag{31}$$

where c_i and δ_m are variational parameters. Writing the distortion potential as

$$U_i(\mathbf{R}_T) = \int \mid \phi_i(\mathbf{r}_T) \mid^2 V_{pe}(\mathbf{r}_p) d^3 r_T + V_p(R_T) , \tag{32}$$

where it is assumed that $\alpha = 1$ in the second term, the Fourier transform of the distortion potential can be written as

$$\tilde{U}_i(\mathbf{K}) = \frac{1}{\sqrt{2\pi}} \left[-\frac{A}{\zeta^2 + K^2} + \sum_{m=1}^{3} \sum_{n=1}^{3} \sum_{l=0}^{3} (-1)^l Q_{mnl} \frac{d^l}{dx^l} \frac{1}{x^2 + K^2} \right] ,$$

where

$$\begin{aligned} Q_{mn0} &= c_{2m-1} c_{2n-1} D_2 + (c_{2m-1} c_{2n} + c_{2n-1} c_{2m}) D_3 + c_{2m} c_{2n} D_4 , \\ Q_{mn1} &= c_{2m-1} c_{2n-1} D_1 + 2(c_{2m-1} c_{2n} + c_{2n-1} c_{2m}) D_2 + 3 c_{2m} c_{2n} D_3 , \\ Q_{mn2} &= (c_{2m-1} c_{2n} + c_{2m} c_{2n-1}) D_1 + 3 c_{2m} c_{2n} D_2 , \quad Q_{mn3} = c_{2m} c_{2n} D_1 , \quad x = \delta_m + \delta_n , \quad D_i = i!/x^{i+1} . \end{aligned} \tag{33}$$

The distortion potential in the final channel is

$$U_f(\mathbf{R}_p)=\int |\phi_f(\mathbf{r}_p)|^2[V_p(R)+V_p(r_T)]d^3r_p\ . \quad (34)$$

It vanishes when $\beta=\frac{1}{2}$ as in the case of Ps formation. Hence g_f^- also vanishes. The terms involved in calculating the cross sections in the post and prior forms of FBA and in the post form of the DWBA are given in the Appendix.

B. Pseudopotentials for rearrangement processes

Consider an N-electron open-shell atom with Z valence electrons. The general distinction between the valence and the core electrons is that the valence electrons determine many of the physical and chemical properties of the atom while the core electrons are relatively inert. Therefore, in a moderate-energy collision process it is a fairly good approximation to assume that the valence (or the outer electrons) take part in the interactions while the core electrons remain essentially inactive. However, for calculational purposes one needs to know the wave functions of the valence as well as the core electrons, that is, the total wave function of the atom which is antisymmetric with respect to the interchange of any pair of electrons. In the Hartree-Fock approximation this wave function is an $N\times N$ determinant of one-electron wave functions which are orthogonal to each other. In order to avoid the complications associated with the orthogonalization of N one-electron wave functions, one can utilize either a model or a pseudopotential approach. In the pseudopotential procedure the problem of N electrons is simplified by reducing it to a problem of Z electrons by introducing a repulsive potential $V(\mathbf{r})$ along with the ordinary Coulomb and exchange potentials for the valence electrons. This repulsive part represents the partially screened nucleus and simulates the orthogonality condition or Pauli principle by keeping the valence electrons out of the core. It may also contain implicitly the correlation between the valence and the core electrons which is generally expressed by the polarization potential. In its general form the radial part of $V(\mathbf{r})$ can be a Hellmann (or Yukawa) type, a Gaussian type, or a combination of various short-range potential terms. The difference between this choice of the potential for the core and the Hartree-Fock potential is that in the former case there are no energy eigenvalues corresponding to the core electrons, and the valence-electron wave functions are nodeless for s electrons, have one node for p electrons, etc. Hence the lowest Z eigenvalues correspond to the energies of the Z valence electrons.

The concept of the pseudopotential in atomic, molecular, nuclear, and condensed-matter physics has been known for quite a long time. Since the independent introductions of the pseudopotential, semiempirically by Hellmann,[11] and on the basis of the statistical model of the atom by Gombas,[12] the method of pseudopotential formulations has been developed by many investigators,[13] and several review articles[14] on this subject have been written. We will concentrate on determining the pseudopotential parameters for atoms with a single valence electron—for example, the alkali-metal atoms. Following the pseudopotential method as suggested by Hellmann, the Schrödinger equation for the valence electron (in a.u.) is

$$[-\tfrac{1}{2}\nabla^2+V_p(r)]\phi(\mathbf{r})=\varepsilon\phi(\mathbf{r})\ ,$$

where

$$V_p(r)=-1/r+(A/r)\exp(-\zeta r) \quad (35)$$

is the effective potential for the valence electron. A and ζ are variational parameters, ε is the binding energy of the valence electron, and $\phi(\mathbf{r})$ is the wave function of the valence electron, not necessarily orthogonal to the wave functions of the core electrons. Generally, $\phi(\mathbf{r})$ is approximated by a trial wave function of the form

$$\phi(\mathbf{r})\sim\sum_{m,n,l}R_{nl}(r)Y_{lm}(\hat{\mathbf{r}})\ , \quad (36)$$

where the radial part $R_{nl}(r)$ contains one or a few terms (depending on the atomic state it is representing) of hydrogenic functions with some adjustable parameters. The parameters A and ζ of the pseudopotential and the adjustable parameters of the wave function R_{nl} are varied until the lowest few eigenvalues, obtained using the Ritz variational principle, agree as well as possible with the observed energies of the ground and the first few excited states. This procedure for determining the potential can fail since on increasing the number of terms in the expansion for $R_{nl}(r)$, the energy eigenvalues ε of Eq. (35) continue to decrease and eventually can become much lower than the experimental values.

The alternate way to determine the values of the pseudopotential parameters is to solve Eq. (35) by direct numerical integration using the Numerov method. The radial part of the bound state $\phi(\mathbf{r})$ behaves as

$$\begin{aligned} &R_{nl}(r)\sim r^l \ \text{ for } r\to 0\ ,\\ &R_{nl}(r)\sim\exp(-\sqrt{F}r)/r \ \text{ for } r\to\infty\ , \end{aligned} \quad (37)$$

where $F=2(V_p-\varepsilon)$. Using the conditions of Eq. (37), the outward and the inward radial wave functions are generated and matched at a suitable matching radius. The first Kato cusp condition[15] can be used to start the outward function near the origin. The parameters A and ζ are varied until both the wave function and its derivative become continuous at the matching point. For a fixed energy ε of the valence electron a number of sets of parameter values may be obtained which will generate a smooth wave function for the ground state. Only that set of parameters is to be chosen which will reproduce as closely as possible a few low-lying energy levels of the same symmetry. In Ref. 8, from which the present values of A and ζ for the valence electron in Li and Na are taken, the parameters were chosen so that the lowest two energy levels were reproduced exactly. It is to be noted that a wave function which closely reproduces an energy eigenvalue may not necessarily generate expectation values of various powers of r which would agree with the previously known values[16] of these matrix elements. It is then possible that the transition matrix elements relevant to collisional processes could be affected which, in turn, would affect the related cross sections.

To illustrate the use of different potentials, the cross sections for positronium formation from Li by the impact of positrons have been calculated[6] using the static potential of the Li^+ core in the FBA. The static potential experienced by the valence electron is obtained by averaging the instantaneous interaction over the motion of the core electrons:

$$V_s(r) = \int |\Phi(\mathbf{r}_1,\mathbf{r}_2)|^2 \times \left[-\frac{1}{r} + \frac{1}{|\mathbf{r}-\mathbf{r}_1|} + \frac{1}{|\mathbf{r}-\mathbf{r}_2|} \right] d\mathbf{r}_1 d\mathbf{r}_2 \,. \quad (38)$$

$\Phi(\mathbf{r}_1,\mathbf{r}_2)$ is the antisymmetric Hartree-Fock wave function of Li^+ in terms of one-electron Slater-type orbitals given by Clementi and Roetti.[17] Since it is determined by the exact interaction and the Hartree-Fock functions, the static potential can be considered a model potential and not a pseudopotential. Unlike a pseudopotential, a model potential has bound states which may not correspond in energy to the observable states of the atom. Hence the lowest energy eigenvalue of the model Hamiltonian may not necessarily correspond to the energy of the valence electron. However, the wave function of the valence electron has the correct number of nodes, namely, $n-l-1$. The difference between the pseudopotential and the model-potential approaches has been discussed and elaborated on by Peach.[18] A six-term trial wave function for the 2s valence electron of the Li atom, similar to Eq. (31), which corresponds to an energy value of $-0.175\,867$ a.u. for the valence electron (that is, the second lowest eigenvalue of the Hamiltonian) in the static potential $V_s(r)$ of Li^+, is used for the calculations of the cross sections for positronium formation in FBA. The differential cross sections are shown in Fig. 2, and the integrated cross sections are given in Table I.

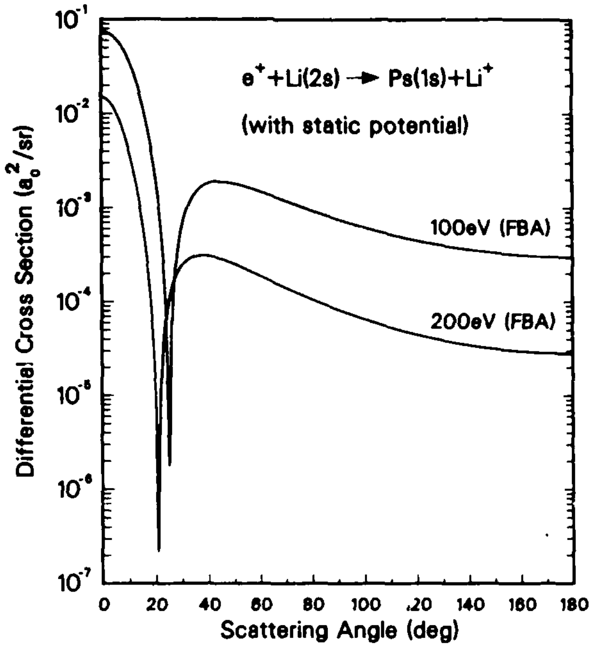

FIG. 2. Differential cross sections for the positronium formation from Li at positron impact energies of 100 and 200 eV using FBA.

III. RESULTS AND DISCUSSION

The differential cross sections (DCS), using the FBA, for the formation of positronium at positron impact energies of 100 and 200 eV from Li are shown in Fig. 2, and the integrated cross sections are presented in Table I. In these calculations, a static potential has been used to represent the alkali-metal ion core. The DCS and the integrated cross sections using both the FBA and the DWBA for the formation of positronium from Li and Na using pseudopotentials for the representation of the alkali-metal ion cores are also calculated. These DCS values for a Li target at positron impact energies of 100 and 300 eV are shown in Fig. 3, and for a Na target at positron impact energies of 75, 200, and 300 eV are shown in Fig. 4. The corresponding integrated cross sections are provided in Table I. In order to obtain the energy values and the wave function parameters for the valence electron of the alkali-metal atoms in Eq. (13), the variational principle as well as direct numerical integration using the Numerov method is used. The post-prior discrepancy for both the DCS and the integrated cross sections in the FBA is negligibly small in all cases. Hence only the post results in FBA are shown in Figs. 2–4. Some differences in the values of the cross sections, using the pseudopoten-

TABLE I. The integrated cross sections using FBA (σ_{FBA}) and DWBA (σ_{DWBA}) for Ps(1s) formation from Li and Na by the impact of positrons. The notations p and s following the target atom correspond to the use of pseudopotential and static potential, respectively. Numerical values of the form $a[b]$ mean $a \times 10^b$.

Target atom	Positron impact energy (eV)	σ_{FBA} (units of a_0^2) Post	Prior	σ_{DWBA} (units of a_0^2) Post
Li(p)	100	8.4317[−2]	8.430[−2]	2.8105[−1]
	300	1.8319[−3]	1.8334[−3]	2.254 65[−3]
Na(p)	75	3.5692	3.5676	1.3882[2]
	200	1.7259[−1]	1.7271[−1]	3.7385
	300	1.1783[−2]	1.1775[−2]	1.8342[−1]
Li(s)	50	6.3872[−2]	6.4361[−2]	
	100	1.9632[−2]	1.9704[−2]	
	200	2.5137[−3]	2.5023[−3]	

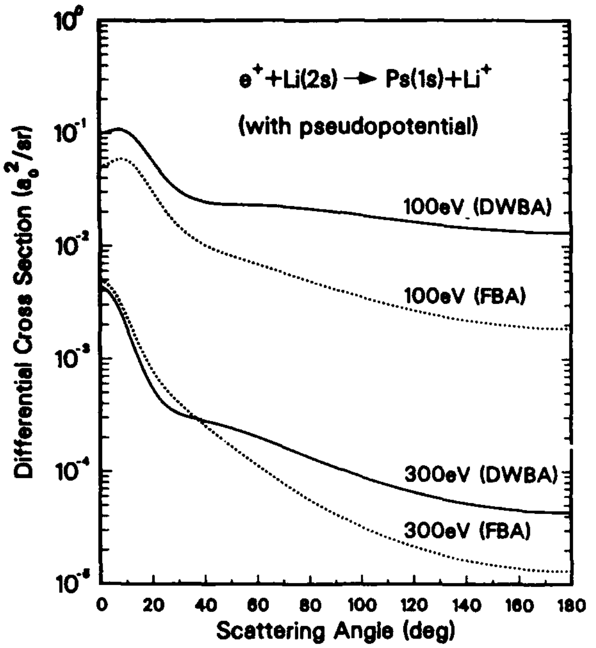

FIG. 3. Differential cross sections for the positronium formation from Li at positron energies of 100 and 300 eV using both the FBA and the DWBA.

tial and the static potential, are expected since the two potentials representing the Li^+ core do not correspond exactly to the same energy eigenvalue for the $2s$ valence electron. This difference is obvious in the values of Table I. Not only the values but also the shapes of the differential-cross-section curves, as shown in Figs. 2 and 3, are different. While with the static potential the DCS curves show a sharp minimum that moves toward the forward direction with increasing impact energy, with the pseudopotential these curves show a maximum, prominent at lower energies, near the forward direction. The total positron-atom interaction potential has both an attractive and a repulsive part. In the calculation employing the static potential, the contribution to the scattering amplitude arising from the repulsive part of the interaction almost equals that from the attractive part for a certain angle which results in a minimum in the DCS curve. This angle depends on the positron impact energy. This minimum in the DCS curve has also been obtained by Guha and Saha[3] (using FBA) and Mazumdar and Ghosh[3] (using FBA and the distorted-wave polarized orbital method). Guha and Saha have used a core model potential different from the one used here and their results (evaluated in the post form) for the positronium formation cross sections are much lower than the present results. Mazumdar and Ghosh[3] have used only the static potential for the Li^+ ion core. Their calculated positronium formation cross section at 50-eV impact energy, using FBA, is comparable with the present result but their cross section at 100-eV impact energy is lower than the present one.

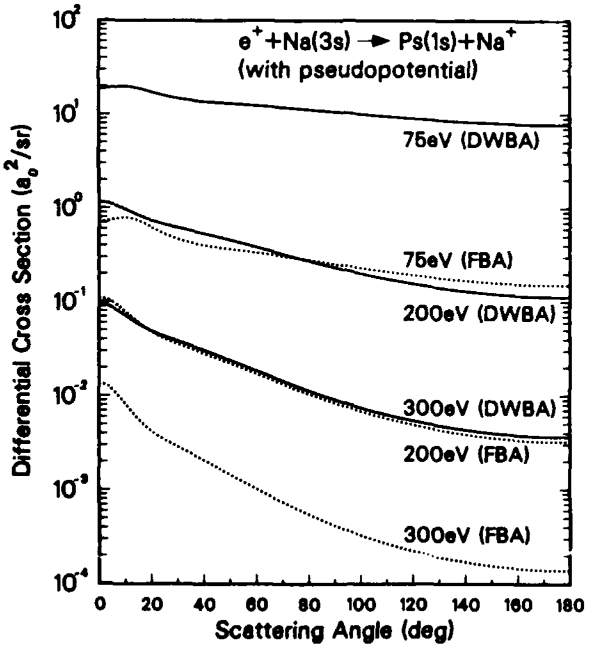

FIG. 4. Differential cross sections for the positronium formation from Na at positron impact energies of 75, 200, and 300 eV using both the FBA and the DWBA.

In the present calculations it is noticed that the contribution from the positron–ion-core interaction to the DCS values dominates at larger angles in all cases. Also in the present calculations, using the pseudopotential in DWBA, it is seen that the distortion contributes significantly to the positronium formation cross sections, especially for the Na target. No measured values for the corresponding cross sections with Li and Na targets are available at this moment, but such measurements may be feasible in the future.[19] Only when the experimental results become available in the future can a better justification for the use of different potentials be made. In spite of the availability of good wave functions containing the Slater-type orbitals[17] of alkali-metal atoms, the static potential formed by these wave functions does not provide the energy of the valence electron to a very good approximation. [See the energy values following Eqs. (30) and (38).] Furthermore, the form of these wave functions (having many terms) makes them computationally inconvenient for the evaluation of capture cross sections. In this respect the pseudopotentials are simpler to use, and the energy eigenvalues corresponding to these potentials can be made very close to the measured energy values of the alkali-metal atoms using adjustable parameters.

It is to be noted that, even though the model static potential and the pseudopotential do not reproduce the alkali-metal spectrum to the same degree of accuracy, a comparison between the positronium formation cross sections using these two potentials is still worthwhile. In the absence of any experimental information about cross sections for positronium formation in alkali-metal atoms, we can compare only with the previous theoretical results for these cross sections. The majority of these calculations[3] exhibited features in the positronium formation cross sections which were similar to the ones observed in Fig. 2 for the Ps formation in Li using the model static potential. We note that this potential did not reproduce the energies of the alkali-metal ground states very well. On the other hand, use of the pseudopotential, which reproduces the energies of the alkali-metal ground states quite well, in the present calculations provides Ps formation cross sections which differ markedly in shapes and magnitudes from the previous calculations.

In the present calculations terms up to third order in the potential are kept in the cross-section expression with the assumption that the higher-order terms contribute less significantly. The cross-section integrals are simplified by the fact that the positron mass is much smaller than that of the alkali-metal ions ($\alpha=1$). Several checks were made to ensure the correctness of the present computer codes.

(a) Both the FBA and DWBA cross sections for the process $e^+ + H(1s) \rightarrow Ps(1s) + H^+$ at a positron impact energy of 100 eV (Ref. 7) were reproduced.

(b) The DCS values in FBA for the process $e^+ + H(1s) \rightarrow Ps(1s) + H^+$ at a positron impact energy of 500 eV (Ref. 20) were reproduced.

(c) The DCS values in FBA for the process $H^+ + H(1s) \rightarrow H(1s) + H^+$ at a proton impact energy of 700 keV (Ref. 20) were reproduced.

(d) The DCS values in FBA for the process $H^+ + H(1s) \rightarrow H(1s) + H^+$ at a proton impact energy of 198.344 keV (Ref. 21) were reproduced.

(e) An attempt to reproduce the DCS values in FBA for the process $e^+ + Li(2s) \rightarrow Ps(1s) + Li^+$, as reported by Guha and co-workers,[3] did not meet with success. A small computer program which specifically made use of the wave function and potential of Guha *et al.* was written. This program reproduced the same values of the differential cross section as given by our general program.

Finally, we comment on two aspects of the present calculations for positronium formation from alkali-metal atoms. First, the shapes of the differential cross sections for positronium formation depend on the type of interaction potential used in the calculations. This is obvious on comparing Figs. 2 and 3. It is not yet possible to ascertain the correctness of either shape due to the absence of corresponding experimental cross sections. The second remark concerns the significant difference in the values of the cross sections, both differential and integrated, obtained by using the FBA and the DWBA. A rather large difference between the two values seems to suggest that the higher-order distortion terms in the DWBA may contribute significantly to the cross sections. The importance of including these terms can only be determined when the experimentally measured values of the cross sections for positronium formation become available.

ACKNOWLEDGMENTS

Support of the National Science Foundation (Grant No. PHY-83-11705) and the Air Force Office of Scientific Research (Grant No. AFOSR-84-0143) is gratefully acknowledged.

APPENDIX

In this appendix we present analytical forms for various terms in the cross sections for positronium formation. Note that U_f vanishes for the positronium formation. Various parts of the post form T-matrix elements, Eq. (25), using DWBA can be written as

$$T_1 = N_1 + N_2 , \tag{A1}$$

where

$$N_1 = -(2\pi)^{3/2} \int \tilde{\phi}_f^*(\mathbf{K}-\mathbf{t}) \tilde{V}_p(\mathbf{t}) \tilde{\phi}_i(-\mathbf{t}-\mathbf{J}) d^3t , \tag{A2}$$

$$N_2 = (2\pi)^{3/2} \tilde{\phi}_f^*(\mathbf{K}) \int \tilde{V}_p(\mathbf{t}) \tilde{\phi}_i(-\mathbf{t}-\mathbf{J}) d^3t , \tag{A3}$$

$$T_2^+ = L_1 + L_2 , \tag{A4}$$

where

$$L_1 = -\int \tilde{\phi}_f^*(-\mathbf{t}-\mathbf{q}+\beta\mathbf{k}_f) \tilde{V}_p(\mathbf{t}) \tilde{g}_i^+(\mathbf{q}) \times \tilde{\phi}_i(-\mathbf{t}-\alpha\mathbf{q}+\mathbf{k}_f) d^3t\, d^3q , \tag{A5}$$

$$L_2 = \int \tilde{\phi}_f^*(-\mathbf{q}+\beta\mathbf{k}_f) \tilde{V}_p(\mathbf{t}) \tilde{g}_i^+(\mathbf{q}) \times \tilde{\phi}_i(-\mathbf{t}-\mathbf{q}+\mathbf{k}_f) d^3t\, d^3q . \tag{A6}$$

In evaluating L_1, is it assumed that $\alpha=1$. T_2^- and T_3 vanish because of the vanishing of g_f^-. In the prior form of FBA, the T-matrix element (Eq. 28) is given by

$$T = N_1 + N_3 , \tag{A7}$$

where N_1 is same as in Eq. (A2) and

$$N_3 = -(2\pi)^{3/2} [K^2/(2\mu_p) - \varepsilon_f] \tilde{\phi}_f^*(\mathbf{K}) \tilde{\phi}_i(-\mathbf{J}) . \tag{A8}$$

In the post form of FBA, the T-matrix element of Eq. (28) is essentially T_1 of Eq. (A1). The integrals involved in evaluating these terms are of the form

$$I_1 = \int d^3p \frac{1}{(\mathbf{p}-\mathbf{A})^2+a^2} \frac{1}{(\mathbf{p}-\mathbf{B})^2+b^2} \frac{1}{p^2+z^2} , \tag{A9}$$

$$I_{1p} = \int d^3p \frac{1}{[(\mathbf{p}+\mathbf{A})^2+a^2]^2} \frac{1}{p^2+z^2} , \tag{A10}$$

$$I_2 = \int \int d^3p\, d^3q \frac{1}{(\mathbf{p}-\mathbf{A})^2+a^2} \frac{1}{(\mathbf{p}-\mathbf{B})^2+b^2} \frac{1}{p^2-v^2-i\eta} \frac{1}{[(\mathbf{p}+\mathbf{q}-\mathbf{D})^2+d^2]^2} \frac{1}{q^2+z^2} , \tag{A11}$$

$$I_3 = \int \int d^3p\, d^3q \frac{1}{(\mathbf{p}+\mathbf{q}-\mathbf{A})^2+a^2} \frac{1}{(\mathbf{p}+\mathbf{q}-\mathbf{B})^2+b^2} \frac{1}{p^2+c^2} \frac{1}{(\mathbf{q}-\mathbf{D})^2+d^2} \frac{1}{q^2-v^2-i\eta} . \tag{A12}$$

I_{1p} is integrated analytically and is given by

$$I_{1p} = \frac{\pi^2}{a} \frac{1}{A^2+(a+z)^2} . \tag{A13}$$

Using a Feynman identity, as in Ref. 7, the other integrals are reduced as follows:

$$I_1 = \pi^2 \int_0^1 dx \frac{1}{E[F^2+(E+z)^2]} ,$$

where

$$E^2=x(1-x)(\mathbf{A}-\mathbf{B})^2+xa^2+(1-x)b^2\ ,$$
$$\mathbf{F}=(\mathbf{A}-\mathbf{B})x+\mathbf{B}\ , \tag{A14}$$
$$I_2=\frac{\pi^4}{d}\int_0^1 dx\int_0^1 dy\, y\left[\frac{1}{2s^3T}+\frac{s-iv}{s^2T^2}\right],$$

where

$$E^2=x(1-x)(\mathbf{A}-\mathbf{D})^2+xa^2+(1-x)(d+z)^2\ ,$$
$$\mathbf{F}=(\mathbf{A}-\mathbf{D})x+\mathbf{D}\ ,$$
$$s^2=y(1-y)(\mathbf{F}-\mathbf{B})^2+yE^2+(1-y)b^2\ , \tag{A15}$$
$$T=-v^2-2ivs+y(E^2+F^2)+(1-y)(b^2+B^2)\ ,$$
$$I_3=\pi\int_0^1 dx\int_0^1 dy\frac{1}{Es[T^2+(s-iv)^2]}\ ,$$

where

$$E^2=x(1-x)(\mathbf{A}-\mathbf{B})^2+xa^2+(1-x)b^2\ ,$$
$$\mathbf{F}=x(\mathbf{A}-\mathbf{B})+\mathbf{B}\ ,$$
$$s^2=y(1-y)(\mathbf{F}-\mathbf{D})^2+y(E+c)^2+(1-y)d^2\ , \tag{A16}$$
$$\mathbf{T}=y\mathbf{F}+(1-y)\mathbf{D}\ .$$

Now the integrals are evaluated numerically. The one-dimensional integrals have been integrated using Simpson's rule, and the two-dimensional integrals are evaluated using a 9-point square formula[22] with an error proportional to the sixth power of the stepsize.

[1]R. D. DuBois and L. H. Toburen, Phys. Rev. A **31**, 3603 (1985).

[2]W. Fritsch and C. D. Lin, J. Phys. B **16**, 1595 (1983); W. Fritsch, Phys. Rev. A **30**, 1135 (1984).

[3]S. Guha and B. C. Saha, Phys. Rev. A **21**, 564 (1980); S. Guha and P. Mandal J. Phys. B **13**, 1919 (1980); P. Mandal and S. Guha, *ibid.* **13**, 1937 (1980); S. Guha and A. S. Ghosh, Phys. Rev. A **23**, 743 (1981); P. S. Mazumdar and A. S. Ghosh, *ibid.* **34**, 4433 (1986).

[4]S. P. Khare and Vijayshri, J. Phys. B **16**, 3621 (1983).

[5]T. S. Stein, R. D. Gomez, Y.-F. Hsieh, W. E. Kauppila, C. K. Kwan, and Y. J. Wan, Phys. Rev. Lett. **55**, 488 (1985).

[6]S. N. Nahar and J. M. Wadehra, in *Positron Annihilation*, edited by P. C. Jain, R. M. Singru, and K. P. Gopinathan (World Scientific, Singapore, 1985), p. 413.

[7]R. Shakeshaft and J. M. Wadehra, Phys. Rev. A **22**, 968 (1980).

[8]J. N. Bardsley, Chem. Phys. Lett. **7**, 517 (1970).

[9]See, for example, C. J. Joachain, *Quantum Collision Theory* (North-Holland, Amsterdam, 1975), p. 449.

[10]R. D. Cowan, *The Theory of Atomic Structure and Spectra* (University of California Press, Berkeley, 1981).

[11]H. Hellmann, J. Chem. Phys. **3**, 61 (1935).

[12]P. Gombas, Z. Phys. **118**, 164 (1941); **94**, 473 (1935).

[13]J. C. Phillips, Phys. Rev. **112**, 685 (1958); J. C. Phillips and L. Kleinmann, *ibid.* **116**, 287 (1959); **118**, 1153 (1960); L. Szasz and G. McGinn, J. Chem. Phys. **42**, 2363 (1965).

[14]J. D. Weeks, A. Hazi, and S. A. Rice, Adv. Chem. Phys. **16**, 283 (1969); J. N. Bardsley, Case Stud. At. Phys. **4**, 299 (1974).

[15]N. H. March, Phys. Rev. A **33**, 88 (1986).

[16]R. J. Boyd, Can. J. Phys. **55**, 452 (1977).

[17]E. Clementi and C. Roetti, At. Data Nucl. Data Tables **14**, 177 (1974).

[18]G. Peach, Comments At. Mol. Phys. **11**, 101 (1982).

[19]T. S. Stein and W. E. Kauppila (private communication).

[20]J. C. Y. Chen and P. J. Kramer, Phys. Rev. A **5**, 1207 (1972).

[21]D. R. Bates and A. Dalgarno, Proc. Phys. Soc. London, Sect. A **66**, 972 (1953).

[22]See, for example, *Handbook of Mathematical Functions*, edited by M. Abramowitz and I. A. Stegun (Dover, New York, 1972), p. 892.

PHYSICAL REVIEW A VOLUME 36, NUMBER 3 AUGUST 1, 1987

Simple model for the resonant vibrational excitation of molecules and its application to Li_2 and N_2

J. M. Wadehra and P. J. Drallos
Department of Physics and Astronomy, Wayne State University, Detroit, Michigan 48202
(Received 2 February 1987)

A simple model for the resonant vibrational excitation of a molecule by electron impact is proposed in which the potential curves of the electronic states of the molecule and its resonant anion are replaced by those of linear harmonic oscillators of arbitrary frequencies and equilibrium internuclear separations. A closed-form expression for the excitation amplitude is derived. Useful recursion relations among amplitudes are obtained which allow convenient evaluation of cross sections for any inelastic or superelastic vibrational transition. The model is used to generate the cross sections for vibrational excitation of Li_2 and N_2 by the impact of low-energy electrons.

I. INTRODUCTION

It has been well established that the phenomenon of vibrational excitation of a molecule by electron impact is dominated by resonance formation.[1] The direct (or nonresonant) contribution, which is quite important for the elastic scattering of electrons by a molecule, to the vibrational excitation is usually small. For example, the spectacular peaks in the cross sections for vibrational excitation of molecular nitrogen can be satisfactorily reproduced only by using a proper resonance model.[2] The purpose of this paper is to present a *closed-form expression for the* resonant contribution to the amplitude for vibrational excitation of a molecule by electron impact using a simple model. Furthermore, some useful recursion relations among the excitation amplitudes will be obtained which will permit a rapid evaluation of the resonant contribution to the cross sections for any inelastic or superelastic vibrational transition in a molecule.

In the model that we are proposing here, the potential curves of the electronic state of the molecule and of the resonant anion state are replaced by those of two simple harmonic oscillators of arbitrary frequencies, curvatures, and equilibrium internuclear separations. Moreover, the two oscillators have arbitrary energy separation. A similar (but not identical) model has been used in the past by other investigators[3,4] for vibrational excitation of a molecule by an electron. In these previous investigations the two linear harmonic oscillators were taken to have the same frequency. Also, a simple recursion relation among excitation amplitudes was obtained previously[4] and was valid only for the inelastic transitions. The results in the present paper represent a generalization of the previous results and indeed reduce to those previous results for the case of equal frequency oscillators.

Finally, the results of the present paper are used to obtain the cross sections for vibrational excitation of Li_2 and N_2 by electron impact. The model can successfully generate the experimentally observed[5] peaks in the cross sections for nitrogen and predicts the excitation cross sections for lithium dimers.

II. VIBRATIONAL EXCITATION AMPLITUDE

In the process of vibrational excitation, a molecule AB, initially in the vibrational level m, undergoes a transition under the impact of an electron of energy $\varepsilon=\hbar^2k_i^2/2m_e$, to the final vibrational level n, leaving behind an electron with energy $\varepsilon_f=\hbar^2k_f^2/2m_e$. This process,

$$e(k_i)+AB(m)\rightarrow AB^-\rightarrow e(k_f)+AB(n)\ ,$$

proceeds via the formation of an intermediate resonant state AB^-, whose nuclear wave function $\xi(\mathbf{R})$, in the local-width approximation, satisfies[1] (in atomic units),

$$[T_N+V^-+\Delta(\mathbf{R})-i\Gamma(\mathbf{R})/2-E]\xi(\mathbf{R}) = -[\Gamma/(2\pi)]^{1/2}\chi_m(\mathbf{R})\ . \quad (1)$$

Here, $V^-(\mathbf{R})$ is the real part of the potential curve of the anion state AB^-. $\Delta(\mathbf{R})$ and $\Gamma(\mathbf{R})$ are, respectively, the level shift and the resonance width. T_N is the nuclear kinetic energy, and $\chi_m(\mathbf{R})$ is the nuclear wave function of the initial rotationless vibrational level of AB. E is the total energy of the system, that is, $E=\varepsilon+E_m$, E_m being the initial vibrational energy of the target molecule. If $\chi_n(\mathbf{R})$ is the wave function of the final vibrational level of the molecule, the amplitude for vibrational excitation via resonance formation is[1]

$$A(m\rightarrow n;\varepsilon)=B\langle n\,|\,[\Gamma(\mathbf{R})/(2\pi)]^{1/2}\,|\,\xi(\mathbf{R})\rangle\ , \quad (2)$$

where $B=-4\pi^2/(k_ik_f)^{1/2}$. For brevity, we are using the bra and ket notation to denote the various vibrational wave functions of the molecule, namely, $\chi_m(\mathbf{R})=\langle\mathbf{R}\,|\,m\rangle$ and $\chi_n(\mathbf{R})=\langle\mathbf{R}\,|\,n\rangle$. Using Eq. (1) and introducing a complete set of vibrational wave functions $\langle\langle\mathbf{R}\,|\,v\rangle\rangle$ of the anion state, the transition amplitude can be written as

$$A(m\rightarrow n;\varepsilon)=-B\sum_v\langle n\,|\,[\Gamma(\mathbf{R})/2\pi]^{1/2}[E_v+\Delta(\mathbf{R})-i\Gamma(\mathbf{R})/2-E]^{-1}\,|\,v\rangle\rangle\langle\langle v\,|\,[\Gamma(\mathbf{R})/2\pi]^{1/2}\,|\,m\rangle\ , \quad (3)$$

where the sum over ν includes integration over the continuum nuclear functions of the resonant anion electronic state. E_ν is the energy of the νth vibrational level of the anion. In what follows, we will consistently use the doublet ket notation (such as $|\nu\rangle\rangle$) to denote the vibrational wave functions of the resonant state and a single ket notation (such as $|m\rangle$ or $|n\rangle$) to denote the vibrational wave functions of the neutral target state. Now, if the width Γ and the level shift Δ, which in general are energy dependent, are taken to be independent of the internuclear separation $\mathbf{R}$ and energy ε, then Eq. (3) can be written as

$$A(m\to n;\varepsilon)=-2\pi\left[\frac{\Gamma^2}{k_ik_f}\right]^{1/2}\sum_\nu \frac{\langle n|\nu\rangle\rangle\langle\langle\nu|m\rangle}{E-E_\nu+i\Gamma/2-\Delta}\ . \tag{4}$$

Note that $\langle n|\nu\rangle\rangle$ and $\langle\langle\nu|m\rangle$ are essentially the Franck-Condon overlap integrals between the vibrational levels of the initial electronic state of the target and those of the resonant anion state.

Now we introduce a simple model in which the potential curves of the initial electronic state of the target and the resonant anion state are taken to be those of simple linear harmonic oscillators of frequencies ω and ω_-, respectively. r is the separation between the equilibrium internuclear positions of the two oscillators. Figure 1 shows the two potential curves and their relative geometry. The overlap integrals, along with useful recursion relations, between vibrational levels of two off-center linear harmonic oscillators of different frequencies have been worked out in detail.[6] For the case of linear oscillators, Eq. (4) for the vibrational transition amplitude becomes

$$A(m\to n;\varepsilon)=-\frac{2\pi}{\omega_-}\left[\frac{\Gamma^2}{k_ik_f}\right]^{1/2}a(m\to n;\varepsilon)\ , \tag{5a}$$

where

$$a(m\to n;\varepsilon)=\sum_{\nu=0}^{\infty}\frac{\langle n|\nu\rangle\rangle\langle\langle\nu|m\rangle}{Q-\nu} \tag{5b}$$

and $Q=[\varepsilon-\delta E+m\omega+(\omega-\omega_-)/2-\Delta+i\Gamma/2]/\omega_-$. δE is defined in Fig. 1. Either one of the two overlap integrals appearing in Eq. (5b) can be written in a closed form as a finite sum.[6] Evaluation of $a(m\to n;\varepsilon)$ will then involve two finite sums and an infinite sum. As we will show now, $a(m\to n;\varepsilon)$ can be alternatively obtained, using the recursion relations which will be derived below, from the mere knowledge of $a(0\to 0;\varepsilon)$ and $a(0\to 1;\varepsilon)$. Furthermore, $a(0\to 0;\varepsilon)$ and $a(0\to 1;\varepsilon)$ can each be written as simple one-dimensional integrals which can be evaluated rapidly on a computer for any electron impact energy ε. To begin with, we define a few convenient relations:

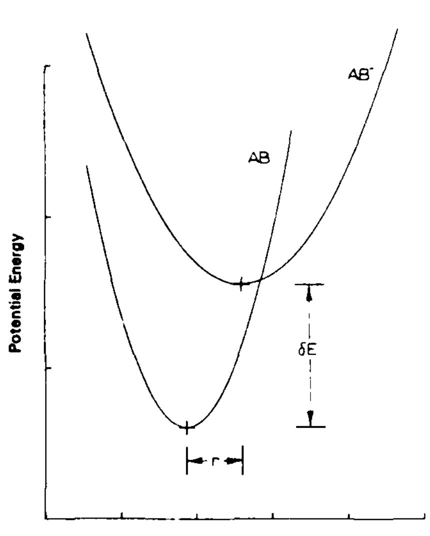

FIG. 1. Schematic representation of the potential energy curves of the molecule AB and its resonant anion AB^- by linear harmonic oscillators.

$$\gamma=\frac{\omega-\omega_-}{\omega+\omega_-},\quad \omega_0=\hbar/(\mu r^2),\quad \alpha^2=\omega\omega_-^2/[\omega_0(\omega_-^2-\omega^2)]\ ,$$
$$\beta^2=\omega^2\omega_-/[\omega_0(\omega^2-\omega_-^2)]\ , \tag{6}$$

where μ is the reduced mass of the nuclei in the molecule AB. Now the Franck-Condon overlap integral $\langle m|\nu\rangle\rangle$, using the two-center harmonic oscillator wave functions, is[6]

$$\langle m|\nu\rangle\rangle=N(2^{m+\nu}m!\nu!)^{-1/2}\sum_{k=0}^{[m,\nu]}\begin{bmatrix}m\\k\end{bmatrix}\begin{bmatrix}\nu\\k\end{bmatrix}\gamma^{(\nu-k)/2}(-\gamma)^{(m-k)/2}(1-\gamma^2)^{k/2}k!H_{m-k}(\alpha)H_{\nu-k}(-\beta)2^k\ , \tag{7}$$

where

$$N=\left[\frac{2(\omega\omega_-)^{1/2}}{\omega+\omega_-}\right]^{1/2}\exp\left[\frac{-\omega\omega_-}{2\omega_0(\omega+\omega_-)}\right]\ ,$$

H_m are the Hermite polynomials and $[m,\nu]$ denotes the smaller of the two integers m and ν. Substituting Eq. (7) into Eq. (5) and interchanging the order of the sums, one obtains

$$\begin{aligned}a(m\to n;\varepsilon)=N^2(2^{m+n}m!n!)^{-1/2}&\sum_{k=0}^{m}\begin{bmatrix}m\\k\end{bmatrix}\gamma^{-k/2}(-\gamma)^{(m-k)/2}(1-\gamma^2)^{k/2}k!2^kH_{m-k}(\alpha)\\&\times\sum_{l=0}^{n}\begin{bmatrix}n\\l\end{bmatrix}\gamma^{-l/2}(-\gamma)^{(n-l)/2}(1-\gamma^2)^{l/2}l!2^lH_{n-l}(\alpha)\\&\times\sum_{\nu=\{k,l\}}^{\infty}\begin{bmatrix}\nu\\k\end{bmatrix}\begin{bmatrix}\nu\\l\end{bmatrix}\gamma^\nu[2^\nu\nu!(Q-\nu)]^{-1}H_{\nu-k}(-\beta)H_{\nu-l}(-\beta)\ ,\end{aligned} \tag{8}$$

where $\{k,l\}$ denotes the larger of the two integers k and l. Using Eq (A4), $a(m\to n;\varepsilon)$ can be written as

$$a(m\to n;\varepsilon)=N^2(2^{m+n}m!n!)^{-1/2}\sum_{k=0}^{m}\begin{bmatrix}m\\k\end{bmatrix}\gamma^{-k/2}(-\gamma)^{(m-k)/2}(1-\gamma^2)^{k/2}H_{m-k}(\alpha)$$
$$\times\sum_{l=0}^{n}\begin{bmatrix}n\\l\end{bmatrix}\gamma^{-l/2}(-\gamma)^{(n-l)/2}(1-\gamma^2)^{l/2}H_{n-l}(\alpha)\left[\frac{\partial}{\partial x}\right]^k_{x=-\beta}\left[\frac{\partial}{\partial y}\right]^l_{y=-\beta}A_{00}(x\ y)\ , \tag{9}$$

where

$$A_{00}(x,y)=\sum_{\nu=0}^{\infty}\frac{\gamma^\nu H_\nu(x)H_\nu(y)}{2^\nu \nu!(Q-\nu)}\ . \tag{10}$$

On using the integral representation,

$$\int_0^\infty \exp[i(Q-\nu)t]dt=\frac{i}{Q-\nu},\quad \mathrm{Im}Q>0 \tag{11}$$

and the bilinear generating function for the Hermite polynomials, Eq. (A3), $A_{00}(x,y)$ can be rewritten as

$$A_{00}(x,y)=-i\int_0^\infty\frac{dt\,z^{Q+1}}{(z^2-\gamma^2)^{1/2}}\exp\left[\frac{\gamma^2(x^2-2xyz/\gamma+y^2)}{\gamma^2-z^2}\right]. \tag{12}$$

Here, for convenience, we have introduced $z=\exp(it)$. Now the derivatives in Eq. (9) can be carried out explicitly and using Eqs. (12) and (A2), we find

$$\left[\frac{\partial}{\partial x}\right]^k_{x=-\beta}\left[\frac{\partial}{\partial y}\right]^l_{y=-\beta}A_{00}(x,y)=-i\int_0^\infty\frac{dt\,z^{Q+1}}{(z^2-\gamma^2)^{1/2}}\exp\left[\frac{2\beta^2\gamma}{z+\gamma}\right]$$
$$\times\sum_{p=0}^{[k,l]}\begin{bmatrix}k\\p\end{bmatrix}\begin{bmatrix}l\\p\end{bmatrix}\left[\frac{2\gamma z}{z^2-\gamma^2}\right]^p p!\left[\frac{\gamma}{(z^2-\gamma^2)^{1/2}}\right]^{k+l-2p}$$
$$\times H_{k-p}\left\{-\left[\beta^2\left[\frac{z-\gamma}{z+\gamma}\right]\right]^{1/2}\right\}H_{l-p}\left\{-\left[\beta^2\left[\frac{z-\gamma}{z+\gamma}\right]\right]^{1/2}\right\}. \tag{13}$$

Substituting from Eq. (13) into Eq. (9) and interchanging the sums again, one obtains

$$a(m\to n;\varepsilon)=-iN^2(2^{m+n}m!n!)^{-1/2}\int_0^\infty\frac{dt\,z^{Q+1}}{(z^2-\gamma^2)^{1/2}}\exp\left[\frac{2\beta^2\gamma}{z+\gamma}\right]\sum_{p=0}^{[m,n]}\left[\frac{2\gamma z}{z^2-\gamma^2}\right]^p p!$$
$$\times\sum_{k=p}^{m}\begin{bmatrix}m\\k\end{bmatrix}\begin{bmatrix}k\\p\end{bmatrix}(-\gamma)^{(m-k)/2}\left[\frac{1-\gamma^2}{\gamma}\right]^{k/2}H_{m-k}(\alpha)\left[\frac{\gamma}{(z^2-\gamma^2)^{1/2}}\right]^{k-p}H_{k-p}\left\{-\left[\beta^2\left[\frac{z-\gamma}{z+\gamma}\right]\right]^{1/2}\right\}$$
$$\times\sum_{l=p}^{n}\begin{bmatrix}n\\l\end{bmatrix}\begin{bmatrix}l\\p\end{bmatrix}(-\gamma)^{(n-l)/2}\left[\frac{1-\gamma^2}{\gamma}\right]^{l/2}H_{n-l}(\alpha)\left[\frac{\gamma}{(z^2-\gamma^2)^{1/2}}\right]^{l-p}H_{l-p}\left\{-\left[\beta^2\left[\frac{z-\gamma}{z+\gamma}\right]\right]^{1/2}\right\}. \tag{14}$$

Finally, using Eq. (A5) twice to carry out the k and l sums and then applying Eq. (A6), the final result is obtained:

$$A(m\to n;\varepsilon)=\frac{-iBN^2}{2\omega_{-}\pi}\left[\frac{\Gamma^2}{2^{m+n}m!n!}\right]^{1/2}\sum_{p=0}^{[m,n]}\begin{bmatrix}m\\p\end{bmatrix}\begin{bmatrix}n\\p\end{bmatrix}p!2^p$$
$$\times\int_0^\infty\frac{dt\,z^{Q+1}}{(z^2-\gamma^2)^{1/2}}\exp\left[\frac{2\beta^2\gamma}{z+\gamma}\right]\left[\frac{1-\gamma z}{z-\gamma}\right]^p\left[\frac{\gamma(1-z^2)}{z^2-\gamma^2}\right]^{(m+n-2p)/2}$$
$$\times H_{m+n-2p}\left[\left[\alpha^2\frac{(z-1)(z-\gamma)}{(z+1)(z+\gamma)}\right]^{1/2}\right]. \tag{15}$$

Equation (15) reduces to a single term for the case in which either m or n is zero. For example, the two important special cases, $A(0\to0;\varepsilon)$ and $A(0\to1;\varepsilon)$, are

$$A(0\to0;\varepsilon)=\frac{-iBN^2\Gamma}{2\omega_{-}\pi}\int_0^\infty\frac{dt\,z^{Q+1}}{(z^2-\gamma^2)^{1/2}}\exp\left[\frac{2\beta^2\gamma}{z+\gamma}\right], \tag{16}$$

$$A(0\rightarrow 1;\varepsilon)=\frac{-iBN^2\Gamma}{2\omega_-\pi}\int_0^\infty \frac{dt\, z^{Q+1}}{(z^2-\gamma^2)^{1/2}}\exp\left[\frac{2\beta^2\gamma}{z+\gamma}\right]\left[\frac{z-1}{z+\gamma}\right]\left[\frac{(1-\gamma^2)\omega_-}{2\omega_0}\right]^{1/2} . \tag{17}$$

For the case in which both m and n are equal to one, we obtain

$$A(1\rightarrow 1;\varepsilon)=\frac{-iBN^2\Gamma}{4\omega_-\pi}\int_0^\infty \frac{dt\, z^{Q+1}}{(z^2-\gamma^2)^{1/2}}\exp\left[\frac{2\beta^2\gamma}{z+\gamma}\right]\left[\frac{z(1-\gamma^2)}{z+\gamma}\right]\left[\frac{2}{z-\gamma}+\frac{\omega_-(z-1)^2}{z\omega_0(z+\gamma)}\right] . \tag{18}$$

From these amplitudes [Eqs. (16) through (18)], and from the recursion relations to be derived below, the entire matrix for vibrational excitation amplitudes can be obtained (see Sec. III).

For the case in which the oscillator frequencies of both the neutral state and the resonant state are the same (that is, $\omega=\omega_-$), the integral in Eq. (15) can be carried out. The resulting expression for the vibrational amplitude in this case becomes

$$A(m\rightarrow n;\varepsilon)=\frac{-BN^2\Gamma}{\pi 2\omega(m!n!)^{1/2}}\sum_{p=0}^{[m,n]}\begin{bmatrix} m\\ p\end{bmatrix}\begin{bmatrix} n\\ p\end{bmatrix}p!\left[\frac{\omega}{2\omega_0}\right]^{(m+n-2p)/2}\frac{\Gamma(p-Q)\Gamma(m+n-2p+1)}{\Gamma(m+n-p-Q+1)}$$
$$\times\Phi(p-Q,m+n-Q-p+1;\omega/(2\omega_0)) . \tag{19}$$

Here, Φ is the confluent hypergeometric function. This expression was obtained earlier for the case $m=0$ and n arbitrary by Golubkov *et al.*,[3] and in the alternative form of continued fractions for the case $m=n=0$ by Domcke and Cederbaum.[7]

III. RECURSION RELATIONS

For the special case in which the frequencies of the two oscillators are equal ($\omega=\omega_-$), a three-term recursion relation among the vibrational amplitudes was derived by Domcke and Cederbaum.[7] More general recursion relations among the amplitudes, for the case in which the oscillator frequencies are not the same ($\omega\neq\omega_-$), are obtained below. The recursion relation of Domcke and Cederbaum is a special case of these general recursion relations.

The vibrational amplitude can be written as a sum of Franck-Condon overlap integrals as in Eq. (4) if the width and the level shift are taken to be independent of **R**. Recursion relations among these Franck-Condon integrals have been obtained previously[6,8] and can be written as

$$(n+1)^{1/2}(\omega+\omega_-)\langle n+1\,|\,\nu+1\rangle\rangle-2[\omega\omega_-(\nu+1)]^{1/2}\langle n\,|\,\nu\rangle\rangle$$
$$+n^{1/2}(\omega_--\omega)\langle n-1\,|\,\nu+1\rangle\rangle-\omega_-(2\omega/\omega_0)^{1/2}\langle n\,|\,\nu+1\rangle\rangle=0 , \tag{20}$$

$$[2(\nu+1)]^{1/2}\langle n\,|\,\nu+1\rangle\rangle=\left[\frac{n}{2\omega\omega_-}\right]^{1/2}(\omega+\omega_-)\langle n-1\,|\,\nu\rangle\rangle-\left[\frac{n+1}{2\omega\omega_-}\right]^{1/2}(\omega-\omega_-)\langle n+1\,|\,\nu\rangle\rangle$$
$$-\left[\frac{\omega_-}{\omega_0}\right]^{1/2}\langle n\,|\,\nu\rangle\rangle . \tag{21}$$

Using Eq. (21), the terms containing $|\,\nu+1\rangle\rangle$ in Eq. (20) can be eliminated, resulting in a five-term recursion relation in which the index ν stays constant. Thus,

$$[2n(\omega^2+\omega_-^2)-4\omega\omega_-(\nu+1)+(\omega+\omega_-)^2+2\omega\omega_-^2/\omega_0]\langle n\,|\,\nu\rangle\rangle$$
$$-2\omega_-^2(2\omega/\omega_0)^{1/2}[(n+1)^{1/2}\langle n+1\,|\,\nu\rangle\rangle+n^{1/2}\langle n-1\,|\,\nu\rangle\rangle]$$
$$-(\omega^2-\omega_-^2)\{[(n+1)(n+2)]^{1/2}\langle n+2\,|\,\nu\rangle\rangle+[n(n-1)]^{1/2}\langle n-2\,|\,\nu\rangle\rangle\}=0 . \tag{22}$$

Equation (22) can be used to obtain recursion relations for the vibrational excitation amplitudes. Multiply Eq. (22) by $\langle m\,|\,\nu\rangle\rangle/(Q-\nu)$ and sum over ν to get

$$\sum_{\nu=0}^{\infty}\langle m\,|\,\nu\rangle\rangle\langle n\,|\,\nu\rangle\rangle\left[2n(\omega^2+\omega_-^2)+4\omega\omega_-(Q-\nu)-4\omega\omega_-(Q+1)+(\omega+\omega_-)^2+\frac{2\omega\omega_-^2}{\omega_0}\right]\Big/(Q-\nu)$$
$$-2\omega_-^2\left[\frac{2\omega}{\omega_0}\right]^{1/2}\left[(n+1)^{1/2}\sum_{\nu=0}^{\infty}\frac{\langle m\,|\,\nu\rangle\rangle\langle\langle\nu\,|\,n+1\rangle}{Q-\nu}+n^{1/2}\sum_{\nu=0}^{\infty}\frac{\langle m\,|\,\nu\rangle\rangle\langle\langle\nu\,|\,n-1\rangle}{Q-\nu}\right]$$
$$-(\omega^2-\omega_-^2)\left[[(n+1)(n+2)]^{1/2}\sum_{\nu=0}^{\infty}\frac{\langle m\,|\,\nu\rangle\rangle\langle\langle\nu\,|\,n+2\rangle}{Q-\nu}+[n(n-1)]^{1/2}\sum_{\nu=0}^{\infty}\frac{\langle m\,|\,\nu\rangle\rangle\langle\langle\nu\,|\,n-2\rangle}{Q-\nu}\right]=0 , \tag{23}$$

where $4\omega\omega_-Q$ has been added and subtracted in the numerator of the first term. This first term can be rewritten as

$$\sum_{\nu=0}^{\infty} \langle m \mid \nu\rangle\rangle\langle\langle \nu \mid n\rangle \left[2n(\omega^2+\omega_-^2)+4\omega\omega_-(Q-\nu)-4\omega\omega_-(Q+1)+(\omega+\omega_-)^2+\frac{2\omega\omega_-^2}{\omega_0}\right]\Big/(Q-\nu)$$

$$=\left[2n(\omega^2+\omega_-^2)-4\omega\omega_-(Q+1)+(\omega+\omega_-)^2+\frac{2\omega\omega_-^2}{\omega_0}\right]\sum_{\nu=0}^{\infty}\frac{\langle m \mid \nu\rangle\rangle\langle\langle \nu \mid n\rangle}{Q-\nu}+4\omega\omega_-\sum_{\nu=0}^{\infty}\langle m \mid \nu\rangle\rangle\langle\langle \nu \mid n\rangle \; . \tag{24}$$

Using the completeness relation on the second term in Eq. (24) and using Eq. (5) we obtain the following recursion relation:

$$\left[2n(\omega^2+\omega_-^2)-4\omega\omega_-(Q+1)+(\omega+\omega_-)^2+\frac{2\omega\omega_-^2}{\omega_0}\right]a(m\to n;\varepsilon)+4\omega\omega_-\delta_{m,n}$$
$$-2\omega_-^2(2\omega/\omega_0)^{1/2}[(n+1)^{1/2}a(m\to n+1;\varepsilon)+n^{1/2}a(m\to n-1;\varepsilon)]$$
$$-(\omega^2-\omega_-^2)\{[(n+1)(n+2)]^{1/2}a(m\to n+2;\varepsilon)+[n(n-1)]^{1/2}a(m\to n-2;\varepsilon)\}=0\; . \tag{25}$$

Note that in this five-term recursion relation among vibrational excitation amplitudes, the initial vibrational level m and the incident electron energy ε is fixed in each term. This, of course, implies that the total energy $E=\varepsilon+E_m$ is the same in each term as it should be. It is possible to obtain an alternative recursion relation among the amplitudes in which the final vibrational level n is fixed in each term. Such a relationship can be obtained by replacing n by m in Eq. (22), multiplying the resulting equation by $\langle n \mid \nu\rangle\rangle/(Q-\nu)$, and summing over ν. Additional care must be taken in this case because the factor Q in the denominator contains m. The resulting recursion relation is

$$\left[2m(\omega^2+\omega_-^2)-4\omega\omega_-(Q+1)+(\omega+\omega_-)^2+\frac{2\omega\omega_-^2}{\omega_0}\right]a(m\to n;\varepsilon)+4\omega\omega_-\delta_{m,n}$$
$$-2\omega_-^2(2\omega/\omega_0)^{1/2}[(m+1)^{1/2}a(m+1\to n;\varepsilon-\omega)+m^{1/2}a(m-1\to n;\varepsilon+\omega)]$$
$$-(\omega^2-\omega_-^2)\{[(m+1)(m+2)]^{1/2}a(m+2\to n;\varepsilon-2\omega)+[m(m-1)]^{1/2}a(m-2\to n;\varepsilon+2\omega)\}=0\; . \tag{26}$$

Note that the initial vibrational level m is different in various terms but the final level n is fixed. Furthermore, the incident electron energy is different, although the total energy E is the same in each term of the recursion relation.

The principle of detailed balancing relates the amplitude of the m-to-n transition to the amplitude of the n-to-m transition, albeit at different incident electron energy (but at the same total energy), as

$$A(m\to n;\varepsilon)=A(n\to m;\varepsilon+(m-n)\omega)\; . \tag{27}$$

It is easy to see that Eq. (27) also follows from Eq. (5) almost by inspection.

From the mere knowledge of the two vibrational amplitudes, $A(0\to 0;\varepsilon)$ and $A(0\to 1;\varepsilon)$ at all energies, and using the recursion relation of Eq. (25), the entire first row ($m=0$) of the vibrational amplitude matrix can be obtained. Equation (27) can then be applied to obtain the first column ($n=0$). With the additional knowledge of $A(1\to 1;\varepsilon)$, the next row (or column) can be obtained using Eq. (25) [or Eq. (26)]. Here, it should be noted that there are two alternative methods for completing the amplitude matrix. First, the rows and columns of the entire matrix can be obtained by successive use of the recursion relations of Eqs. (25) and (26). Second, using the principle of detailed balancing, Eq. (27), each column (or row) can be obtained from its corresponding row (or column). Thus only half of the matrix needs to be built up via the recursion relations.

IV. DISCUSSION

In the preceding sections we have obtained a summation expression, Eq. (5), and an integral expression, Eq. (15), for the amplitude for resonant vibrational excitation of a molecule. Useful five-term recursion relations among these amplitudes are obtained in Eqs. (25) and (26) which, from a mere knowledge of amplitudes for transitions to only three low-lying levels, would permit a rapid evaluation of vibrational excitation cross sections for any transition, inelastic or superelastic, for any molecule.

The summation expression of Eq. (5) proved to be more useful than the integral expressions of Eqs. (16) and (17) when used for evaluation of the amplitudes. This is because the integrands in Eqs. (16) and (17) for $A(0\to 0;\varepsilon)$ and $A(0\to 1;\varepsilon)$ are rapidly oscillating and require a prohibitive number of evaluations in order to obtain sufficient accuracy to be used with the recursion relations. The summation expression, Eq. (5), on the other hand, achieves similar accuracy after typically including only 25 terms in the sum, and is to be preferred *numerically*. Although the integral expression may not appear useful numerically, it can be seen from Eq. (9) that if $A_{00}(x,y)$ could be evaluated analytically, then all of the higher-order transition amplitudes can be determined exactly by merely taking derivatives of A_{00}. The recursion relations, Eqs. (25) and (26), can be used for generating the amplitudes for excitation of higher vibrational levels if $a(0\to 0;\varepsilon)$, $a(0\to 1;\varepsilon)$, and $a(1\to 1;\varepsilon)$ are known either from the summation expression, Eq. (5), or from the integral expression, Eq. (15). These recursion relations become especially useful for the integral expressions because the real and imaginary parts of the integrals representing the lowest-order transition amplitudes ($0\rightarrow0$, $0\rightarrow1$, and $1\rightarrow1$) are easily separable. Furthermore, use of complex algebra and evaluation of Hermite polynomials can be avoided in obtaining the higher-order transition amplitudes. It should be noted that use of the recursion relations [Eq. (26), in particular] requires that the step size in electron-impact energy should be some proper fraction of the oscillator excitation energy $\hbar\omega$.

For the case when the frequencies of the two oscillators representing the potential curves of the molecule and its anion are equal, the recursion relation, Eq. (25), reduces to a three-term relation and is identical to the one obtained by Domcke *et al.*[4] This three-term recursion relation among amplitudes is essentially equivalent to a recursion relation among confluent hypergeometric functions[9] since for the case of equal-frequency oscillators the excitation amplitude is related to a confluent hypergeometric function as seen in Eq. (19). As far as we know, the second recursion relation, Eq. (26), that we have obtained, in which the *final* vibrational level is fixed, has not been obtained earlier in the literature for either equal or unequal frequency oscillators. In obtaining Eq. (4) for the excitation amplitude it was assumed that the width of the resonance is independent of the internuclear separation. This assumption led to the Franck-Condon overlap integrals in Eq. (4) and to the recursion relations in Eqs. (25) and (26) which are merely extensions of the recursion relations among the Franck-Condon integrals. If, however, the width Γ depends on the internuclear separation, more general recursion relations among excitation amplitudes can still be obtained by using the recursion relations among two-center harmonic-oscillator matrix elements.[6]

In order to illustrate the utility of the recursion relations derived above, we have numerically evaluated the vibrational excitation amplitudes for Li_2 and N_2 using Eqs. (5), (7), and (25). The vibrational excitation cross sections obtained from these amplitudes are displayed in Figs. 2 and 3, respectively. The parameters for the potential curves of the ground and the resonant anion states for the two molecules[10–12] used in these calculations are listed in Table I. Note that the width of the resonance Γ is taken to be energy independent. The level shift Δ is taken to be zero. It is easy to verify that the first five vibrational levels of the above simple harmonic oscillators have the same energy levels, within 5%, as the actual vibrational energy levels of the ground electronic states of the molecules. This indicates that the harmonic-oscillator approximation is reasonable for these levels. The parameters ω, ω_-, r, and δE of the lithium system are taken from the recent *ab initio* calculations[12] of the structure of the ground and excited states of Li_2 and Li_2^- using the optimized configuration-interaction (CI) wave functions. Following Wigner's threshold law, the width $\Gamma(R)$ of the resonant state is taken to be of the form $\Gamma(R)=ck(R)$, where $k(R)$ is the wave number of the electron autodetaching at internuclear separation R. The constant c is determined[12] by, first, smoothly extrapolating the fully optimized orbital

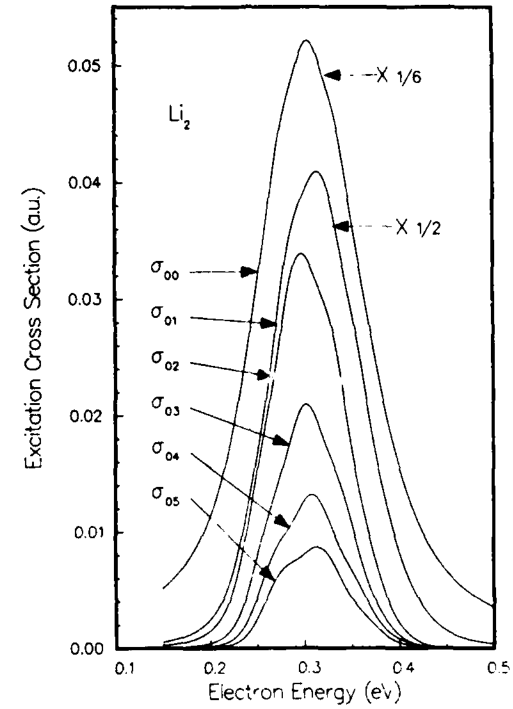

FIG. 2. Cross sections for the resonant vibrational excitation of Li_2 by the impact of low-energy electrons.

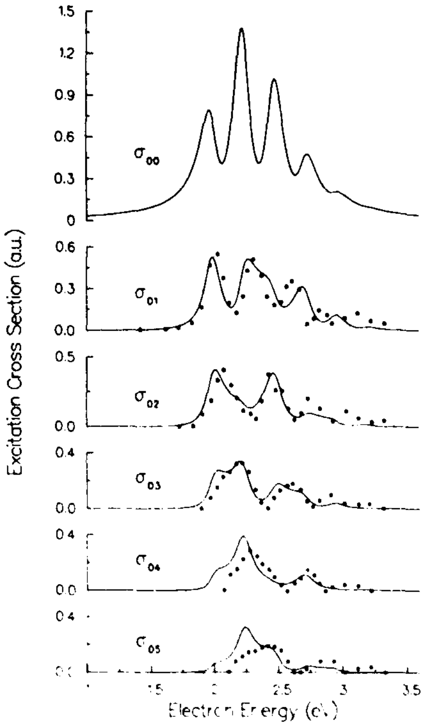

FIG. 3. Cross sections for the resonant vibrational excitation of N_2 by the impact of low-energy electrons. Solid circles represent the experimental values of the respective cross sections from Ref. 5.

TABLE I. Potential curve parameters in atomic units. The numbers in square brackets represent powers of ten.

Parameter	Li_2	N_2
ω	1.5983[−3]	1.073[−2]
ω_-	1.0519[−3]	8.82[−3]
r	8.0623[−1]	1.638[−1]
μ	6.426[+3]	1.2852[+4]
δE	9.4979[−3]	7.38699[−2]
Γ	2.273[−3]	6.5[−3]

exponents of the CI wave functions from the variationally stable region into the autodetaching region. This procedure yields estimates of the matrix elements coupling the discrete resonant state and the continuum states which, in turn, are related to the resonance width via Fermi's golden rule. In the present calculations, $\Gamma(R_0)$, where R_0 is the equilibrium internuclear separation of Li_2, is taken as the constant width of the resonant state of Li_2^-. The values of the parameters ω, ω_-, and δE for the molecular nitrogen system are taken from the *ab initio* calculations as listed in Ref. 11. The parameters r and Γ were adjusted by starting from the initial values of Golubkov *et al.*,[3] such that the calculated vibrational excitation cross sections agreed as best with the experimental values as possible.

Figure 2 shows the cross sections for vibrational excitation of Li_2 by the impact of low-energy electrons. Molecular lithium is isovalent with molecular hydrogen and is known to exhibit characteristics similar to those of molecular hydrogen in regard to the process of dissociative attachment, which is another resonant process.[13] The lowest resonant state of Li_2^- is the $A\,^2\Sigma_g^+$ state. In the case of molecular hydrogen it is known[14] that the contribution of the $^2\Sigma_g^+$ resonant state to the vibrational excitation cross sections shows a structureless peak for any inelastic transition. It is thus not surprising, based on the similarities between Li_2 and H_2, that the inelastic excitation cross sections for Li_2 as shown in Fig. 2 are also almost structureless. All of the cross sections show only one peak, and the location of the peak is roughly the same for all transitions. Also, there is the possible development of a second peak in the higher-order transitions $[A(0\rightarrow 4;\varepsilon)$ and $A(0\rightarrow 5;\varepsilon)]$. Figure 3 shows the cross sections for the vibrational excitation of molecular nitrogen by the impact of low-energy electrons dominated by the $^2\Pi_g$ resonance of N_2^-. Because of the boomerang nature of this resonance, the vibrational excitation cross sections exhibit a series of spectacular peaks.[5] It is to be noticed that the present model can successfully account for occurrence and locations of these peaks in the cross sections for low-lying transitions. The present model is not expected to reproduce the cross sections for excitations to higher vibrational levels[15] due to the effects of anharmonicity.

The assumption of constant Γ in the present calculations is made for convenience only. Even if Γ depends on the internuclear separation R in some simple analytical manner, it might be possible[6] to carry out the two-center harmonic-oscillator matrix elements analytically. At first sight, the assumption of constant Γ may appear quite drastic since in the case of N_2 it has been well established,[11] using the boomerang model, that features of the excitation cross sections are best obtained when the resonance width is taken as a decreasing function of the internuclear separation. Then, a strong interference between the single incident and a single reflected nuclear wave packet leads to peaks in the vibrational excitation cross sections of N_2 which shift to larger energies for excitation to higher levels. However, since the present model is expected to be accurate only for low-lying vibrational levels, the convenient (but not necessary) assumption of constant Γ is reasonable. Furthermore, since all of the results are analytic, it is hoped that the present model with recursion relations could be useful for calculations of excitation cross sections in polyatomic molecules for which *ab initio* calculations are relatively tedious.

Finally, we comment on the applicability of the present model for obtaining resonant contributions to the vibrational excitation of a molecule. The starting point of the present model is the local equation, Eq. (1), which implies that the model is valid for energies not too close to the threshold. Use of a harmonic oscillator to represent the potential curves implies that the present model would work best for obtaining cross sections for vibrational transitions among low-lying levels only. For transitions to higher vibrational levels where the effects of anharmonicity become important, a similar useful model using Morse oscillators could possibly be developed.

ACKNOWLEDGMENT

The support of the U.S. Air Force Office of Scientific Research through Grant No. AFOSR-84-0143 is gratefully acknowledged.

APPENDIX

Some of the useful properties of Hermite polynomials that have been used in various derivations are collected here.[9] From the linear generating function of Hermite polynomials,

$$\sum_{n=0}^{\infty} H_n(x)t^n/n! = \exp(-t^2+2xt) , \tag{A1}$$

the following representation for Hermite polynomials is obtained:

$$H_n(B/A) = A^{-n}(\partial/\partial t)^n_{t=0}\exp(-A^2t^2+2Bt) . \tag{A2}$$

The bilinear generating function of Hermite polynomials is

$$(1-z^2)^{-1/2}\exp\left[y^2-\frac{(y-zx)^2}{1-z^2}\right] = \sum_{n=0}^{\infty}\frac{H_n(x)H_n(y)z^n}{2^n n!} . \tag{A3}$$

The derivatives of the Hermite polynomials are given by

$$\frac{d}{dx}H_n(x) = 2nH_{n-1}(x) . \tag{A4}$$

A couple of useful sums of these polynomials are

$$\sum_{m=j}^{s} \binom{s}{m} \binom{m}{j} \alpha_1^{m-j} H_{m-j}(x_1) \alpha_2^{s-m} H_{s-m}(x_2) = (\alpha_1^2+\alpha_2^2)^{(s-j)/2} H_{s-j} \left[\frac{\alpha_1 x_1 + \alpha_2 x_2}{(\alpha_1^2+\alpha_2^2)^{1/2}} \right] \binom{s}{j} \tag{A5}$$

and

$$\sum_{p=0}^{[m,n]} \binom{m}{p} \binom{n}{p} p! g^p H_{m-p}(x) H_{n-p}(x) = \sum_{p=0}^{[m,n]} \binom{m}{p} \binom{n}{p} p!(2+g)^p H_{m+n-2p}(x) \ . \tag{A6}$$

[1]J. M. Wadehra, in *Nonequilibrium Vibrational Kinetics*, edited by M. Capitelli (Springer-Verlag, Heidelberg, 1986), p. 191.

[2]B. I. Schneider, Phys. Rev. A **14**, 1923 (1976).

[3]G. V. Golubkov, F. I. Dalidchik, and G. K. Ivanov, Zh. Eksp. Teor. Fiz. **73**, 439 (1977) [Sov. Phys.—JETP **46**, 230 (1977)].

[4]W. Domcke, L. S. Cederbaum, and F. Kasper, J. Phys. B **12**, L359 (1979).

[5]G. J. Schulz, Phys. Rev. **135**, A988 (1964).

[6]P. J. Drallos and J. M. Wadehra, J. Chem. Phys. **85**, 6524 (1986).

[7]W. Domcke and L. S. Cederbaum, J. Phys. B **13**, 2829 (1980); **14**, 149 (1981).

[8]F. Ansbacher, Z. Naturforsch., Teil A **14**, 889 (1959).

[9]W. Magnus, F. Oberhettinger, and R. P. Soni, *Formulas and Theorems for the Special Functions of Mathematical Physics* (Springer-Verlag, New York, 1966).

[10]K. P. Huber and G. Herzberg, *Constants of Diatomic Molecules* (Van Nostrand, New York, 1979).

[11]L. Dube and A. Herzenberg, Phys. Rev. A **20**, 194 (1979); A. U. Hazi, T. N. Rescigno, and M. Kurilla, *ibid.* **23**, 1089 (1981).

[12]H. H. Michels, R. H. Hobbs, and L. A. Wright, Chem. Phys. Lett. **118**, 67 (1985); H. H. Michels (private communication).

[13]J. M. Wadehra, in *Proceedings of the Fourth International Symposium on the Production and Neutralization of Negative Ions and Beams*, edited by J. Alessi (AIP, New York, 1987).

[14]J. N. Bardsley and J. M. Wadehra, Phys. Rev. A **20**, 1398 (1979).

[15]M. Allan, J. Phys. B **18**, 4511 (1985).

Contributions of higher partial waves to the elastic scattering amplitude for various long-range interactions

J. M. Wadehra and Sultana N. Nahar
Department of Physics and Astronomy, Wayne State University, Detroit, Michigan 48202
(Received 29 January 1987)

The contributions of higher partial waves to the elastic scattering amplitude are dominated by long-range interactions which fall off as r^{-n} as $r \to \infty$. Closed-form expressions for the contributions of higher partial waves ($2l > n-3$) to the scattering amplitude for various long-range interactions (n ranging from 3 to 8) are presented.

When the interaction between a projectile and a target is central, it is convenient to use the method of partial waves to obtain the elastic scattering amplitude and the corresponding differential and integrated cross sections. Each partial wave corresponds to a definite angular momentum of the system. For a fixed incident energy of the projectile, the higher partial waves correspond to larger impact parameters of the incoming projectile. If the impact parameter is larger than the range of the interaction, the contribution of the corresponding partial wave to the scattering amplitude, for this particular energy, is zero. Thus for short-range interactions between projectile and target only a finite number of partial waves make contributions to the scattering amplitude. Moreover, the number of contributing partial waves increases as the impact energy increases. If the projectile-target interaction has a long-range tail, then, in principle, an infinite number of partial waves will contribute to the amplitude. In practice, the phase shifts of the first few (say, L) partial waves are computed exactly by solving for the asymptotic radial part of the wave function and the phase shifts of the higher partial waves (from $L+1$ to infinity) are estimated by the Born approximation using only the long-range interaction. (For some recent examples see Refs. 1 and 2.) The purpose of this work is to provide closed-form expressions for the contributions of the higher partial waves to the scattering amplitude for various long-range interactions. As far as we are aware, such a closed-form expression has been obtained previously only for the $1/r^4$ potential;[3] the results for other long-range interactions are new in the present work.

Consider the elastic scattering of a projectile of mass μ and energy $E=\hbar^2k^2/2\mu$ by a central potential $V(r)$ which results in a change in momentum from $\hbar\mathbf{k}_i$ to $\hbar\mathbf{k}_f$ for the projectile ($k_i=k_f=k$). The momentum transfer $\hbar\mathbf{q}=\hbar(\mathbf{k}_f-\mathbf{k}_i)$ is related to the scattering angle θ by $q=2k\sin(\theta/2)$. For later convenience we define a quantity z as $z=\sin(\theta/2)=q/2k$. The partial-wave expansion for the elastic scattering amplitude can be written as

$$f(\theta)=\frac{1}{k}\sum_{l=0}^{\infty}(2l+1)T_lP_l(\cos\theta)\,, \tag{1}$$

where the transition matrix elements T_l are related to the phase shifts δ_l by

$$T_l=\exp(i\delta_l)\sin(\delta_l)\,. \tag{2}$$

If the quantities T_l for $l>L$ are approximated by T_{lB} which are obtained by using the Born approximation, then $f(\theta)$ can be rewritten as

$$f(\theta)=\frac{1}{k}\sum_{l=0}^{L}(2l+1)T_lP_l(\cos\theta)+\Delta f\,, \tag{3a}$$

where

$$\Delta f=\frac{1}{k}\sum_{l=L+1}^{\infty}(2l+1)T_{lB}P_l(\cos\theta) \tag{3b}$$

$$=f_B(\theta)-\frac{1}{k}\sum_{l=0}^{L}(2l+1)T_{lB}P_l(\cos\theta)\,. \tag{3c}$$

Here $f_B(\theta)$ is the complete scattering amplitude in the Born approximation, that is,

$$f_B(\theta)=-\frac{2\mu}{\hbar^2}\int_0^{\infty}dr\,V(r)r^2\frac{\sin(qr)}{qr} \tag{4a}$$

$$=-\frac{2\mu}{\hbar^2}\int_0^{\infty}dr\,V(r)r^2\sum_{l=0}^{\infty}(2l+1)j_l^2(kr)P_l(\cos\theta) \tag{4b}$$

$$=\frac{1}{k}\sum_{l=0}^{\infty}(2l+1)T_{lB}P_l(\cos\theta) \tag{4c}$$

and T_{lB} is the Born approximation for T_l, namely,

$$T_{lB}=-\frac{2\mu k}{\hbar^2}\int_0^{\infty}dr\,V(r)r^2j_l^2(kr)\,. \tag{5}$$

Now, since only the long-range part of the interaction contributes to phase shifts of higher partial waves, it is reasonable to take for $V(r)$, in Eq. (5), a general spherically symmetric potential of the form

$$V(r)=C_na_0^{n-1}e^2/r^n\,. \tag{6}$$

Here $a_0=\hbar^2/me^2$ is the Bohr radius, $-e$ and m are the charge and mass of an electron, and C_n are dimensionless coefficients. For certain values of n the two terms on the right-hand side of Eq. (3c) could be individually singular but the difference, namely, Δf is always finite and nonsingular. Substituting from (6) into (5) and using Eq. 6.574.2 of Ref. 4 one obtains

$$T_{lB}=-\frac{C_n}{2}\frac{\mu}{m}\sqrt{\pi}(ka_0)^{n-2}\frac{\Gamma\left[l-\frac{n}{2}+\frac{3}{2}\right]\Gamma\left[\frac{n}{2}-\frac{1}{2}\right]}{\Gamma\left[\frac{n}{2}\right]\Gamma\left[l+\frac{1}{2}+\frac{n}{2}\right]}. \tag{7}$$

The conditions of validity for this expression are

$$n>1\ ,\quad l>(n-3)/2\ . \tag{8}$$

Table I shows explicit expressions for T_{lB} for values of n from 3 to 8. The corresponding long-range interactions, along with their possible applications in atomic and molecular physics, are now discussed individually.

(i) $n=3$. A potential of the form $1/r^3$ appears as the leading retardation term (that is, the effect of the finiteness of the speed of light) for electron-electron interactions.[5,6] In a different context, when two identical neutral atoms, excited to different degrees, exchange a photon it leads[7] to a "resonance interaction" of the form $1/r^3$. Using the expression for T_{lB} for $n=3$ in Table I and the sum

$$S_3=\sum_{l=1}^{\infty}\frac{(2l+1)P_l(\cos\theta)}{l(l+1)}=-1-2\ln(z) \tag{9a}$$

where $z=\sin(\theta/2)$, we obtain the following closed-form expression

$$\Delta f=\frac{\mu a_0 C_3}{m}\left[1+2\ln(z)+\sum_{l=1}^{L}\frac{(2l+1)P_l(\cos\theta)}{l(l+1)}\right]. \tag{9b}$$

(ii) $n=4$. The case of $1/r^4$ potential, perhaps the most well known in atomic physics, arises as the leading term, in the adiabatic approximation, in interactions of a charged projectile (electron, ion, positron) with a neutral polarizable target. Again using the relevant entry in Table I for T_{lB} and

$$S_4=\sum_{l=0}^{\infty}\frac{P_l(\cos\theta)}{(2l+3)(2l-1)}=-\frac{z}{2}\ , \tag{10a}$$

the closed form expression for Δf becomes

$$\Delta f=\frac{2\pi\mu k a_0^2 C_4}{m}\left[\frac{z}{2}+\sum_{l=0}^{L}\frac{P_l(\cos\theta)}{(2l+3)(2l-1)}\right], \tag{10b}$$

with $z=\sin(\theta/2)$. This expression has previously been obtained by Thompson.[3]

(iii) $n=5$. When retardation effects are taken into account for interactions between a structureless charged projectile in motion and a neutral polarizable target, the leading correction term behaves[8] asymptotically as $1/r^5$. The $1/r^5$ retardation effect also appears when applied to an electron-ion system with the electron bound in a high Rydberg state.[9,10] This term, which is an addition to the $1/r^4$ polarization potential, vanishes in the nonrelativistic limit. Again using the results in Table I and

$$S_5=\sum_{l=2}^{\infty}\frac{(2l+1)P_l(\cos\theta)}{(l+2)(l+1)l(l-1)}=\frac{1}{3}-\frac{z^2}{6}+2z^2\ln(z)\ , \tag{11a}$$

the closed form expression for Δf in this case can be written as

$$\Delta f=-\frac{2\mu k^2 a_0^3 C_5}{3m}\left[\frac{1}{3}-\frac{z^2}{6}+2z^2\ln(z)-\sum_{l=2}^{L}\frac{(2l+1)P_l(\cos\theta)}{(l+2)(l+1)l(l-1)}\right], \tag{11b}$$

where $z=\sin(\theta/2)$.

(iv) $n=6$. A long-range potential of the form $1/r^6$ appears in various applications in atomic and molecular physics. First, the nonrelativistic van der Waals interaction between two neutral atoms, each in its lowest energy state, behaves as $1/r^6$ for separations much larger than the Bohr radius.[11] Next, the second term in the interaction energy between a charged projectile and a neutral polarizable target behaves, in the adiabatic approximation, as $1/r^6$. Third, the leading nonadiabatic correction to the dipole term in the interaction between a charged projectile and a neutral polarizable target behaves asymptotically as $1/r^6$.[12] In these cases one can use

$$S_6=\sum_{l=0}^{\infty}\frac{P_l(\cos\theta)}{(2l+5)(2l+3)(2l-1)(2l-3)}=\frac{z^3}{18} \tag{12a}$$

and the results of Table I to obtain the following closed-form expression for Δf,

$$\Delta f=\frac{6\pi\mu k^3 a_0^4 C_6}{m}\times\left[-\frac{z^3}{18}+\sum_{l=0}^{L}\frac{P_l(\cos\theta)}{(2l+5)(2l+3)(2l-1)(2l-3)}\right], \tag{12b}$$

where, as before, $z=\sin(\theta/2)$.

TABLE I. Explicit expressions for T_{lB} for various long-range interactions.

n	$-\frac{m(ka_0)^{2-n}}{\mu C_n}T_{lB}$	Condition of validity
3	$1/[l(l+1)]$	$l\geq 1$
4	$2\pi/[(2l+3)(2l+1)(2l-1)]$	$l\geq 1$
5	$2/[3(l+2)(l+1)l(l-1)]$	$l\geq 2$
6	$6\pi/[(2l+5)(2l+3)(2l+1)(2l-1)(2l-3)]$	$l\geq 2$
7	$8/[15(l+3)(l+2)(l+1)l(l-1)(l-2)]$	$l\geq 3$
8	$20\pi/[(2l+7)(2l+5)(2l+3)(2l+1)(2l-1)(2l-3)(2l-5)]$	$l\geq 3$

(v) $n=7$. When retardation effects are taken into account the interaction between two neutral atoms in their lowest energy states behaves as $1/r^7$ for extremely large atom-atom separations.[10,13] This interaction is a replacement for and not an additive correction to the nonrelativistic van der Waals interaction. Using the appropriate entry from Table I and

$$S_7=\sum_{l=3}^{\infty}\frac{(2l+1)P_l(\cos\theta)}{(l+3)(l+2)(l+1)l(l-1)(l-2)}$$

$$=\frac{43}{240}z^4-\frac{z^2}{5}+\frac{1}{80}-\frac{z^4}{2}\ln(z)\ , \tag{13a}$$

the closed-form expression for Δf becomes

$$\Delta f=\frac{8\mu k^4 a_0^5 C_7}{15m}\left[\frac{-43}{240}z^4+\frac{z^2}{5}-\frac{1}{80}+\frac{z^4}{2}\ln(z)+\sum_{l=3}^{L}\frac{(2l+1)P_l(\cos\theta)}{(l+3)(l+2)(l+1)l(l-1)(l-2)}\right], \tag{13b}$$

where $z=\sin(\theta/2)$.

(vi) $n=8$. In investigations of the Rydberg states of helium it is noted that terms up to $1/r^8$ in the polarization potential arising in the ion-core–electron interaction contribute significantly to the energy levels.[14,15] With the anticipation that interaction terms behaving asymptotically as $1/r^8$ might also contribute significantly to scattering processes, we provide the following closed-form expression for Δf for this case,

$$\Delta f=\frac{20\pi\mu k^5 a_0^6 C_8}{m}\left[\frac{z^5}{450}+\sum_{l=0}^{L}\frac{P_l(\cos\theta)}{(2l+7)(2l+5)(2l+3)(2l-1)(2l-3)(2l-5)}\right], \tag{14a}$$

with $z=\sin(\theta/2)$, using the results in Table I and the sum

$$S_8=\sum_{l=0}^{\infty}\frac{P_l(\cos\theta)}{(2l+7)(2l+5)(2l+3)(2l-1)(2l-3)(2l-5)}$$

$$=-\frac{z^5}{450}\ . \tag{14b}$$

The closed-form expressions [Eqs. (9b), (10b), (11b), (12b), (13b), and (14a)] for Δf for various long-range potentials depend crucially on the evaluation of sums S_i, $i=3,\ldots,8$ [Eqs. (9a), (10a), (11a), (12a), (13a), and (14b)]. These sums can be obtained as follows. On multiplying both sides of the generating function

$$\sum_{l=0}^{\infty}t^l P_l(\cos\theta)=(1-2t\cos\theta+t^2)^{-1/2} \tag{15}$$

by t^m $(m=-3,-2,-1,0,1,2,3)$ and integrating with respect to t from 0 to 1, one can establish the following sums:

$$\sum_{l=0}^{\infty}\frac{P_l(\cos\theta)}{(l+4)}=(20z^5-10z^4-\tfrac{70}{3}z^3+10z^2+6z-\tfrac{11}{6})+(-20z^6+30z^4-12z^2+1)\times\ln(1+1/z)\ , \tag{16a}$$

$$\sum_{l=0}^{\infty}\frac{P_l(\cos\theta)}{(l+3)}=(-6z^3+3z^2+4z-\tfrac{3}{2})+(6z^4-6z^2+1)\ln[(1+z)/z]\ , \tag{16b}$$

$$\sum_{l=0}^{\infty}\frac{P_l(\cos\theta)}{(l+2)}=(2z-1)+(-2z^2+1)\ln[(1+z)/z]\ , \tag{16c}$$

$$\sum_{l=0}^{\infty}\frac{P_l(\cos\theta)}{(l+1)}=\ln[(1+z)/z]\ , \tag{16d}$$

$$\sum_{l=1}^{\infty}\frac{P_l(\cos\theta)}{l}=-\ln[z(1+z)]\ , \tag{16e}$$

$$\sum_{l=2}^{\infty}\frac{P_l(\cos\theta)}{(l-1)}=(2z^2-2z)+(2z^2-1)\ln[z(1+z)]\ , \tag{16f}$$

$$\sum_{l=3}^{\infty}\frac{P_l(\cos\theta)}{(l-2)}=(-7z^4+6z^3+5z^2-4z)-(6z^4-6z^2+1)\ln[z(1+z)]\ , \tag{16g}$$

where $z=\sin(\theta/2)$. Now the sums S_3, S_5, and S_7 can be easily evaluated by first doing the partial fractions of the summand and then using the sums of Eq. (16). The sums S_4, S_6, and S_8 are evaluated by first doing the partial fractions of the summand, then using

$$[P_{l+1}(\cos\theta)-P_{l-1}(\cos\theta)]/(2l+1)=\frac{\sin\theta\, dP_l(\cos\theta)}{l(l+1)d\theta} \tag{17}$$

[and similar lengthy relations for $(P_{l+2}-P_{l-2})/(2l+1)$ and $(P_{l+3}-P_{l-3})/(2l+1)$] and eventually utilizing the sums of Eq. (16). It is rather remarkable that after many pages of algebra the sums S_4, S_6, and S_8 turn out to be as simple as in Eqs. (10a), (12a), and (14b), which suggests that there could be an easier and perhaps more general procedure (which obviously eluded us) of evaluating sums of this kind.

Finally we comment that in the present work the contributions of higher partial waves to the elastic scattering amplitude for various long-range interactions are taken into account via the first Born approximation. It is now possible to include, in principle, the additional correction terms via the second Born approximation since an exact analytical expression for the second Born contribution to the transition matrix elements T_l for any long-range interaction has been obtained recently by Wadehra.[16]

It is a pleasure to thank Professor Larry Spruch for a helpful conversation. This research has been supported, in part, by the Air Force Office of Scientific Research under Grant No. AFOSR-84-0143.

[1]R. K. Nesbet and S. Geltman, Phys. Rev. A **33**, 3815 (1986).
[2]W. L. van Wyngaarden and H. R. J. Walters, J. Phys. B **19**, 1817 (1986).
[3]D. G. Thompson, Proc. R. Soc. London Ser. A **294**, 160 (1966).
[4]I. S. Gradshteyn and I. M. Ryzhik, *Table of Integrals, Series, and Products* (Academic, New York, 1965).
[5]T. Fulton and P. Martin, Phys. Rev. **95**, 811 (1954).
[6]L. Spruch, Phys. Today **39**(11), 37 (1986).
[7]H. Margenau and W. W. Watson, Rev. Mod. Phys. **8**, 22 (1936).
[8]J. Bernabeu and R. Tarrach, Ann. Phys. (N.Y.) **102**, 323 (1976).
[9]E. J. Kelsey and L. Spruch, Phys. Rev. A **18**, 15 (1978).
[10]L. Spruch and E. J. Kelsey, Phys. Rev. A **18**, 845 (1978).
[11]F. London, Z. Phys. **63**, 245 (1930).
[12]C. J. Kleinman, Y. Hahn, and L. Spruch, Phys. Rev. **165**, 53 (1968).
[13]H. B. G. Casimir and D. Polder, Phys. Rev. **73**, 360 (1948).
[14]R. J. Drachman, Phys. Rev. A **26**, 1228 (1982).
[15]C. K. Au, Phys. Rev. A **34**, 3568 (1986).
[16]J. M. Wadehra, J. Phys. B **19**, L761 (1986).

B-5 Dissociative Attachment in Low-Energy e + Li_2 Collisions, H. H. MICHELS* and J. M. WADEHRA**, AFWAL/APL, Wright-Patterson AFB, OH, 45433--A study of dissociative attachment (DA) in e + Li_2 collisions has been initiated based on *ab initio* calculations of the pertinent potential energy curves and capture widths. For collision energies less than 1.4 eV, DA occurs only on the lowest $^2\Sigma_g^+$ state of Li_2^-. We find that this state crosses the ground $^1\Sigma_g^+$ state at R_x = 3.45 Å, close to the sixth vibrational level of Li_2. The imaginary part of the $^2\Sigma_g^+$ potential has been calculated by analytic continuation of a discrete representation of e + Li_2 and the autoionizing region of this potential has been treated using the stabilization method. This resonant state of Li_2^- is of the Feshbach type. Our preliminary studies indicate that DA should increase for vibrationally excited Li_2, a result similar to that found for e + H_2.

Permanent addresses: *UTRC, East Hartford, CT, 06108; **Wayne State U., Detroit, MI, 48202. Work supported in part by AFOSR under Contract F49620-83-C-0094.

Thirty-seventh Annual

Gaseous Electronics Conference

October 9-12, 1984

Program and Abstracts

Presented at the Fourteenth International Conference on the Physics of Electronic and Atomic Collisions, Palo Alto, California, July 24-30, 1985

DISSOCIATIVE ELECTRON ATTACHMENT TO MOLECULAR LITHIUM

J. M. Wadehra* and H. H. Michels+

*Department of Physics, Wayne State University, Detroit, Michigan 48202 USA
+United Technologies Research Center, East Hartford, Connecticut 06108 USA

The fact that both molecular lithium (Li_2) and molecular hydrogen (H_2) are isoelectronic in the valence shell suggests that the rates of electron attachment to these two molecules might also be quite similar. In fact, preliminary results of recent experiments[1] indicate that the maximum rate for electron attachment to Li_2 is about 10^{-8} cm^3 sec^{-1} which is comparable to the corresponding value[2] for H_2.

Both experimental observations as well as theoretical calculations for H_2 indicate[2] that rovibrational excitation of the molecule can enhance the electron attachment rate by several orders of magnitude. The aim of present studies is to investigate whether a similar strong enhancement of the attachment rates occurs for Li_2 on increasing the temperature.

Figure 1 shows the potential curves of some low lying electronic states of Li_2 and Li_2^-. The lowest two states of anion Li_2^-, namely the X $^2\Sigma_u^+$ and the A $^2\Sigma_g^+$ states, possess the same electronic symmetry as the lowest two states of H_2^-. However, due to large polarizability and weak bond strength, the X $^2\Sigma_u^+$ state of Li_2^- is a true bound state for all internuclear separations. The A $^2\Sigma_g^+$ state, on the other hand, is bound only for $R \geq 6.51$ a.u. For smaller internuclear separations, this state is the lowest resonance of Li_2^-.

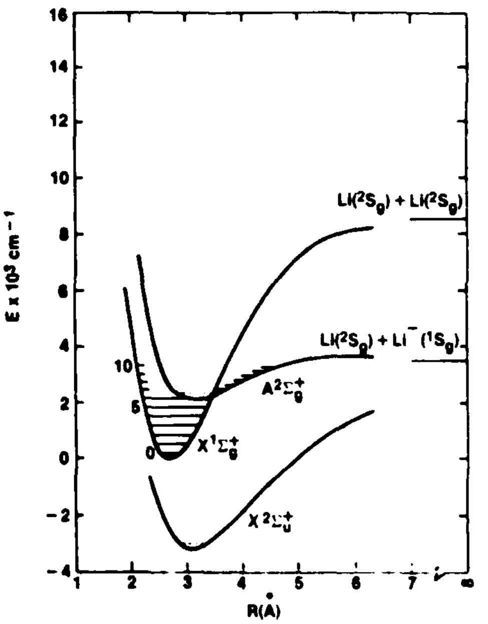

FIGURE 1 Potential energy curves for dissociative electron attachment to Li_2.

A semiclassical approach utilizing the local-width resonance model is used to obtain the cross sections and rates for dissociative attachment to Li_2. The resonance width for the A $^2\Sigma_g^+$ state is parametrized in atomic units as $\Gamma(R) = 0.0143\, k(R)$, where $k(R)$ is the local wave number of the attached electron. The behavior of the attachment cross section is investigated both as a function of the incident electron energy for a given rovibrational state of the molecule Li_2 and as a function of the internal energy of the molecule for a fixed incident electron energy.

This research is supported by AFOSR under Grant AFOSR-84-0143 and Contract F49620-83-C-0094.

References

1. M. W. McGeoch and R. E. Schlier, in Proceedings of the Third International Symposium on the Production and Neutralization of Negative Ions and Beams, edited by K. Prelec (American Institute of Physics, New York, 1984), p. 291.
2. J. M. Wadehra, Phys. Rev. A29, 106 (1984).

CA-5 Vibrational Excitation of Diatomic Molecules (N_2, CO, Li_2) during Resonance Scattering of Electrons,*

J.M. WADEHRA and P.J. DRALLOS, Wayne State University--
A one dimensional integral expression is obtained for the cross section for resonant vibrational excitation of diatomic molecules. The potential energy curves for both the neutral molecule as well as the resonant state are approximated by one dimensional harmonic oscillators having arbitrary curvatures and equilibrium positions. Results of the computations are obtained for the molecules N_2 and CO, and are in good agreement with experiment. Results for resonant vibrational excitation cross sections for Li_2 are also presented.

*Work supported by AFOSR Grant 84-0143

Thirty-eighth Annual

Gaseous Electronics Conference

October 15-18

Program and Abstracts

A Topical Conference of the American Physical Society

Thirty-Ninth Annual Gaseous Electronics Conference

GEC86

October 7–10, 1986
Madison, Wisconsin

•

Program and Abstracts

LC-6 Dissociative Electron Attachment to the Isotopes of Molecular Hydrogen,* J. M. WADEHRA, Wayne State U.-- Using a local width model, the cross sections for dissociative electron attachment to rovibrationally excited isotopes (HD, HT, D_2, DT and T_2) of H_2 are obtained. For a given rovibrational level, the factor by which the peak attachment cross section alters on isotope substitution, varies from about 10 to 65000. For a given isotope, the factor by which the peak attachment cross section is altered on exciting the molecule vibrationally from v=0 to v=1, varies from about 39 to 61. For a given isotope, the factor by which the peak attachment cross section is altered on exciting the molecule rotationally from J=0 to J=10, varies from about 12 to 6. The reasons for these observations will be given.

*Supported by AFOSR Grant Number 84-0143.

Presented at the Fifteenth International
Conference on the Physics of Electronic
and Atomic Collisions, Brighton,
United Kingdom, July 22-28, 1987.

ELASTIC SCATTERING OF POSITRONS FROM ARGON

J. M. Wadehra and Sultana N. Nahar

Department of Physics and Astronomy , Wayne State University, Detroit, MI 48202, USA

Differential and integrated cross sections for the elastic scattering of low- and intermediate-energy (3 - 300 eV) positrons and electrons by argon atoms are calculated. Model potentials are used to represent the interactions between positrons or electrons and argon atoms. For each impact energy, the phase shifts of the lower partial waves are obtained exactly by numerical integration of the radial equation. The Born approximation is used to obtain the contribution of the higher partial waves to the scattering amplitude.

The model potential for positron argon interaction contains the static potential of the target atom and Buckingham type polarization potential with an adjustable parameter d. The electron argon interaction is represented by the target static potential (with proper sign), Buckingham type polarization potential with the parameter d and exchange potential. The value of d, which depends on the projectile impact energy, is determined by fitting the calculated electron-argon scattering cross sections (i.e., differential, integrated and momentum transfer cross sections) and phase shifts with the measured values of the same for a particular energy. Then the same value of d is used for the calculation of cross section for positron scattering from argon. When normalized at 90°, the relative values of the differential cross sections for the elastic scattering of positrons from argon measured by Hyder et al.[1] agree well with the present calculations as shown in Fig. 1. Presently the group of Kauppila and Stein[2] is making measurements for positron scattering from argon at lower impact energies. Their preliminary results are showing encouraging agreement with the present calculations.

Suppport of NSF and AFOSR is gratefully acknowledged.

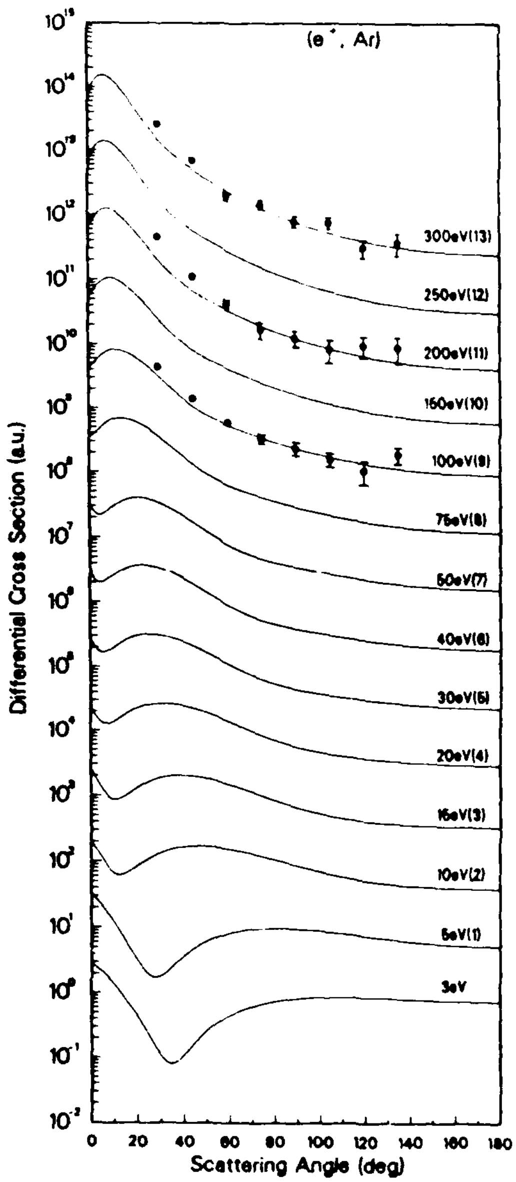

Fig. 1. Differential cross sections for the elastic scattering of positrons by argon at various impact energies. Solid lines are the present theoretical curves. The number in parenthesis following an energy value indicates the power of ten by which the cross section values are multiplied. The experimental values are from Ref. (1)

Reference

1. G.M.A. Hyder, M.S. Dababneh, Y.-F. Hsieh, W.E. Kauppila, C.K. Kwan, M. Mahdavi-Hezaveh and T.S. Stein, Phys. Rev. Lett. 57, 2252(1986).

2. W.E. Kauppila and T.S. Stein (private communication).

A SIMPLE MODEL FOR THE RESONANT VIBRATIONAL EXCITATION OF MOLECULES

Presented at the Fifteenth International Conference on the Physics of Electronic and Atomic Collisions, Brighton, United Kingdom, July 22-28, 1987.

P.J. Drallos and J.M. Wadehra

Department of Physics and Astronomy, Wayne State University
Detroit, Michigan 48202

It has been well established that the phenomenon of vibrational excitation of a molecule by electron impact is dominated by resonance formation[1]. The nonresonant contribution to the vibrational excition is usually small. Here we present a closed-form expression for the resonant contribution to the amplitude for vibrational excitation of a molecule by electron impact using a simple model. Also, simple recursion relations among the excitation amplitudes are obtained which are valid for both inelastic and superelastic transitions.

In the model we are proposing here, the potential curves of the electronic states of the molecule and of the resonant anion state are replaced by those of two simple harmonic oscillators of arbitrary frequencies, curvatures, and equilibrium internuclear separations. The resonance width Γ and the level shift Δ are taken to be independent of the internuclear separation $\vec{R}$. The nuclear wave function of the intermediate resonant state, by which the process of vibrational excitation proceeds, is obtained in the local-width approximation. This implies that the model is valid for energies not too close to the threshold. The use of harmonic oscillators to represent the potential curves implies that the present model would be best suited for vibrational transitions among low-lying levels only.

With the above approximations, the vibrational transition amplitude can be written as

$$A(m\rightarrow n;\varepsilon) = -\frac{2\pi}{\omega_-}\left(\frac{\Gamma^2}{k_i k_f}\right)^{1/2} a(m\rightarrow n;\varepsilon) \qquad (1a)$$

where

$$a(m\rightarrow n;\varepsilon) = \sum_{v=0}^{\infty}\frac{\langle n|v\rangle\rangle\langle\langle v|m\rangle}{Q-v} \qquad (1b)$$

and Q is a constant that depends on the electron impact energy ε. Note that $\langle n|v\rangle\rangle$ and $\langle\langle v|m\rangle$ are Franck-Condon overlap integrals between vibrational levels of the initial electronic state of the target and those of the resonant anion state. Each of these Franck-Condon integrals can be written as a finite sum[2]. Evaluation of Eq. (1) will then involve two finite sums and one infinite sum which can be reduced to a single finite sum and a one-dimensional integral:

$$A(m\rightarrow n;\varepsilon) = \frac{-iBN^2}{2\omega_-\pi}\left(\frac{\Gamma^2}{2^{m+n}m!n!}\right)\sum_{p=0}^{1/2[m,n]}\binom{m}{p}\binom{n}{p}p!2^p$$

$$\cdot\int_0^{2\pi}\frac{dt\; z^{Q+1}}{(z^2-\gamma^2)^{1/2}}\exp\left(\frac{2\beta^2\gamma}{z+\gamma}\right)\left(\frac{1-\gamma z}{z-\gamma}\right)^p\left[\frac{\gamma(1-z^2)}{z^2-\gamma^2}\right]^{(m+n-2p)/2}$$

$$\cdot H_{m+n-2p}\left\{\left[\alpha^2\frac{(z-1)(z-\gamma)}{(z+1)(z+\gamma)}\right]^{1/2}\right\}. \qquad (2)$$

where $z=\exp(it)$ and B, N, α, β, γ and ω_- are constants. As we will show, knowledge of only three low-lying transitions is required to obtain the entire matrix for vibrational excitation amplitudes.

Recursion relations among the Franck-Condon integrals[2] allow us to write recursion relations among the vibrational excitation amplitudes. These recursion relations are:

$$[2n(\omega^2+\omega_-^2)-4\omega\omega_-(Q+1)+(\omega+\omega_-)^2+\frac{2\omega\omega_-^2}{\omega_0}]\,a(m\rightarrow n;\varepsilon)+4\omega\omega_-\delta_{m,n}$$
$$-2\omega_-^2(2\omega/\omega_0)^{1/2}\left[(n+1)^{1/2}a(m\rightarrow n+1;\varepsilon)+n^{1/2}a(m\rightarrow n-1;\varepsilon)\right]$$
$$-(\omega^2-\omega_-^2)\left\{[(n+1)(n+2)]^{1/2}a(m\rightarrow n+2;\varepsilon)\right.$$
$$\left.+[n(n-1)]^{1/2}a(m\rightarrow n-2;\varepsilon)\right\}=0, \qquad (3a)$$

$$\left[2m(\omega^2+\omega_-^2)-4\omega\omega_-(Q+1)+(\omega+\omega_-)^2+\frac{2\omega\omega_-^2}{\omega_0}\right]a(m\rightarrow n;\varepsilon)+4\omega\omega_-\delta_{m,n}$$
$$-2\omega_-^2(2\omega/\omega_0)^{1/2}\left[(m+1)^{1/2}a(m+1\rightarrow n;\varepsilon-\omega)+m^{1/2}a(m-1\rightarrow n;\varepsilon+\omega)\right]$$
$$-(\omega^2-\omega_-^2)\left\{[(m+1)(m+2)]^{1/2}a(m+2\rightarrow n;\varepsilon-2\omega)\right.$$
$$\left.+[m(m-1)]^{1/2}a(m-2\rightarrow n;\varepsilon+2\omega)\right\}=0. \qquad (3b)$$

As an illustration of the utility of the recursion relations derived above, we have numerically evaluated the vibrational excitation amplitudes for Li_2 and N_2 using Eqs. (1) and (3a). The inelastic excitation cross sections for Li_2 show characteristics similar to those of molecular hydrogen as expected. The present model also successfully accounts for the experimentally observed spectacular peaks in the cross sections for low lying transitions of N_2.

The support of the Air Force Office of Scientific Research through Grant Number AFOSR-84-0143 is gratefully acknowledged.

References

1. J.M. Wadehra, in Nonequilibrium Vibrational Kinetics, ed. M. Capitelli (Springer-Verlag, Heidelberg 1986).

2. P.J. Drallos and J.M. Wadehra, J. Chem. Phys. 85, 6524 (1986).

Presented at the NATO Advanced Research Workshop on Atomic Physics with Positrons, University College London, United Kingdom, July 15-17, 1987.

ELASTIC SCATTERING OF POSITRONS FROM ARGON

J. M. Wadehra and Sultana N. Nahar

Department of Physics and Astronomy, Wayne State University

Detroit, Michigan 48202, USA

Differential and integrated cross sections for the elastic scattering of low- and intermediate-energy (3 - 300 eV) positrons and electrons by argon atoms are calculated using partial wave method. Model potentials are used to represent the interactions between positrons or electrons and argon atoms. For each impact energy, the phase shifts of the lower partial waves are obtained exactly by numerical integration of the radial part of the Schrodinger equation. The Born approximation is used to obtain the contribution of the higher partial waves to the scattering amplitude.

The model potential for positron-argon interaction contains the static potential of the target atom and a Buckingham type polarization potential with an adjustable parameter d. The electron-argon interaction is represented by the target static potential (with proper sign), the Buckingham type polarization potential with parameter d and an exchange potential. The value of the parameter d, which depends on the projectile impact energy, is determined by fitting the calculated electron-argon scattering cross sections (i.e., differential, integrated and momentum transfer cross sections) and the phase shifts with the measured values of the same for a particular energy. Then the same value of d is used for the calculation of cross sections for positron scattering from argon at the same impact energy. When normalized at 90°, the relative values of the differential cross sections for the elastic scattering of positrons from argon at impact energies of 100, 200 and 300 eV measured by Hyder et al.[1] agree well with the present calculations as shown in Fig. 1 on the next page. Presently the group of Kauppila and Stein[2] is making measurements for positron scattering from argon at lower impact energies. Their preliminary results are showing encouraging agreement with the present calculations.

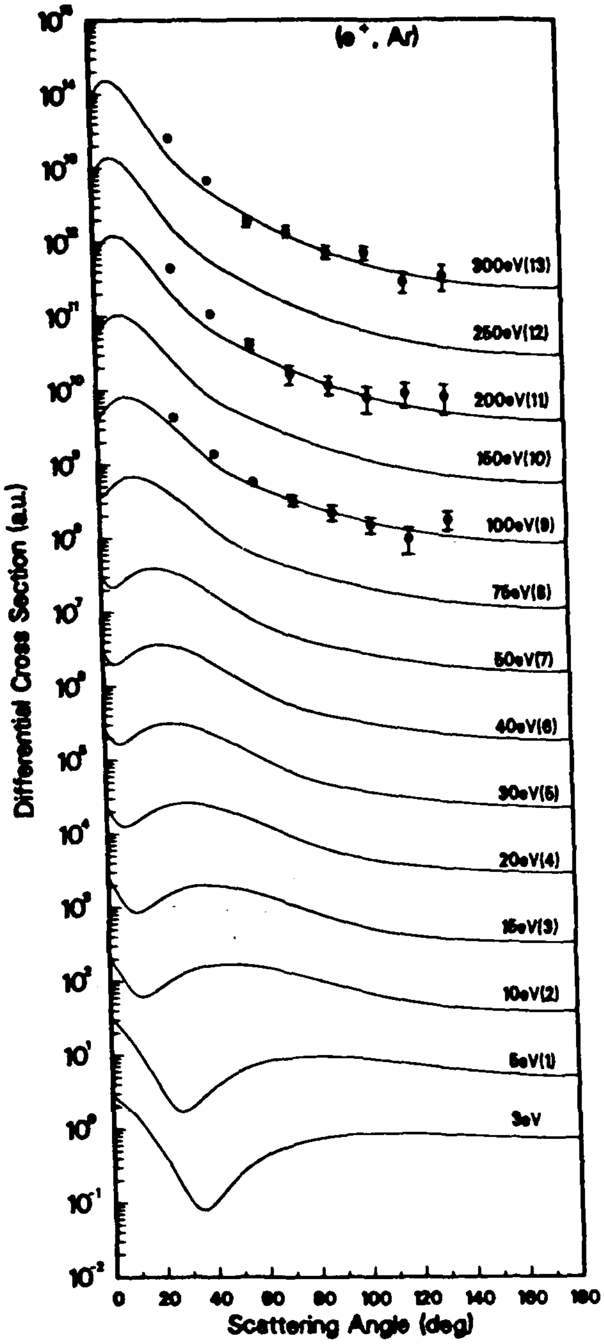

Fig. 1. Differential cross sections for the elastic scattering of positrons by argon at various impact energies. Solid lines are the present theoretical curves. The number in parenthesis following an energy value indicates the power of ten by which the cross section values are multiplied. The experimental values are from Ref. 1.

Support of NSF and AFOSR is gratefully acknowledged.

1. G.M.A. Hyder, M.S. Dababneh, Y.-F. Hsieh, W.E. Kauppila, C.K. Kwan, M. Mahdavi-Hezaveh and T.S.Stein, Phys. Rev. Lett. 57, 2252 (1986).
2. W.E. Kauppila and T.S. Stein (private communication).

Presented at the NATO Advanced
Research Workshop on Atomic Physics
with Positrons, University College London,
United Kingdom, July 15-17, 1987

POSITRONIUM FORMATION FROM ATOMIC HYDROGEN

J. M. Wadehra and Sultana N. Nahar

Department of Physics and Astronomy, Wayne State University

Detroit, Michigan 48202, USA

The first Born approximation and the distorted wave Born approximation are used to calculate the cross sections for positronium (Ps) formation in all bound states by the impact of intermediate energy (20 - 500 eV) positrons on atomic hydrogen. Differential and integrated cross sections for the formation of Ps(1s), Ps(2s), Ps($2p_0$) and Ps($2p_1$) are calculated individually and the $1/n^3$ behavior (n being the principal quantum number) for charge transfer cross sections is used for $n \geqslant 3$ to obtain the total cross sections for positronium formation. The formation of Ps in s-state is evaluated using formulation of the distorted wave Born approximation similar to that described in Ref. 1. All calculations are carried out using the prior form of the interaction. The p-state wave functions of Ps, unlike spherically symmetric s-state wave functions, are angle dependent and introduce complexity in the calculations of capture cross sections. The complexity is reduced by expressing the angle dependent part of the wave function in terms of an exponential factor. It is observed in the present calculations that the cross section for Ps formation in n = 1 state dominates significantly over that for n = 2 state. No experimental values of cross sections for Ps formation from atomic hydrogen are available at present. The present results for the formation of Ps(1s) compare[2] favorably with some of the other theoretical investigations. The features of the present differential cross section curves for Ps formation showing a large maximum in the forward direction followed by a minimum also agree well with works of other investigators. The total cross sections for the formation of Ps in all bound states at various impact energies are shown in Fig. 1 on the next page.

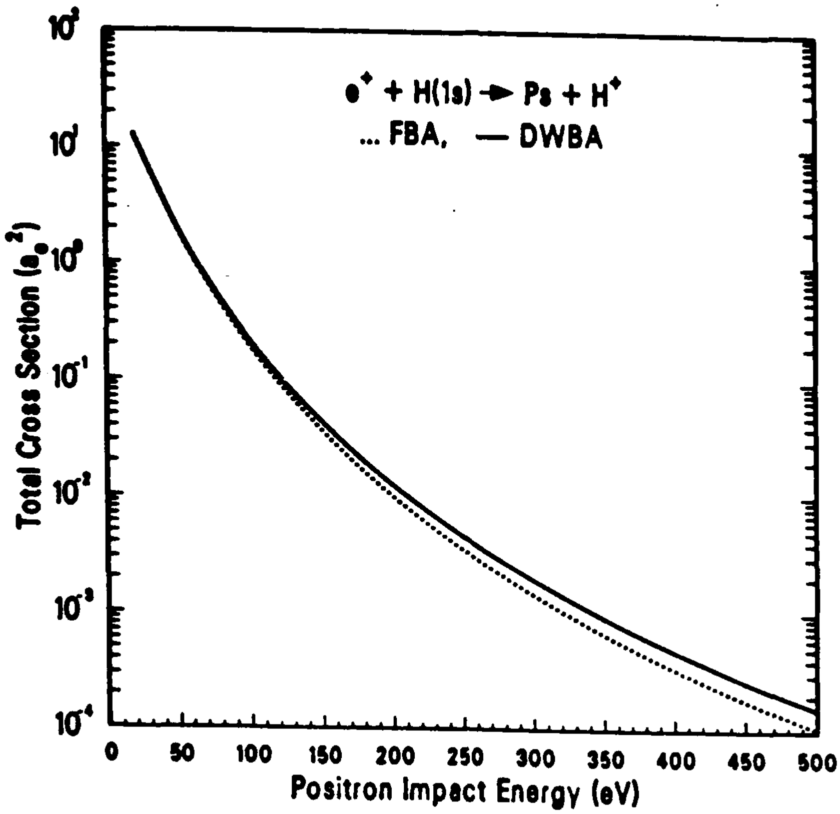

Fig. 1. Total integrated cross sections for positronium formation from atomic hydrogen at various positron impact energies.

Support of NSF and AFOSR is gratefully acknowledged.

1. R. Shakeshaft and J.M. Wadehra, Phys. Rev. A22, 968 (1980); Sultana N. Nahar and J.M. Wadehra, ibid, A35, XXXX (1987).
2. Sultana N. Nahar, Ph.D. Thesis, Wayne State University (1987).

Presented at the Satellite Meeting on Electron-molecule Scattering and Photoionisation, Daresbury, United Kingdom, July 18-19, 1987.

A SIMPLE MODEL FOR THE RESONANT VIBRATIONAL EXCITATION OF MOLECULES

P.J. Drallos and J.M. Wadehra
Department of Physics and Astronomy, Wayne State University
Detroit, Michigan 48202

It has been well established that the phenomenon of vibrational excitation of a molecule by electron impact is dominated by resonance formation[1]. The nonresonant contribution, which is important for the elastic scattering of electrons by a molecule, to the vibrational excitation is usually small. For example, the spectacular peaks in the cross sections for vibrational excitation of molecular nitrogen can be satisfactorily reproduced only by using a proper resonance model. Here we present a closed-form expression for the resonant contribution to the amplitude for vibrational excitation of a molecule by electron impact using a simple model. Also, simple recursion relations among the excitation amplitudes are obtained which are valid for both inelastic and superelastic transitions.

In the model we are proposing here, the potential curves of the electronic state of the molecule and of the resonant anion state are replaced by those of two simple harmonic oscillators of arbitrary frequencies, curvatures, equilibrium internuclear separations and energy separation. The resonance width Γ and the level shift Δ are taken to be independent of the internuclear separation $\vec{R}$. The nuclear wave function of the intermediate resonant state, by which the process of vibrational excitation proceeds, is obtained in the local-width approximation. This implies that the model is valid for energies not too close to the threshold. The use of harmonic oscillators to represent the potential curves implies that the present model would be best suited for obtaining cross sections for vibrational transitions among low-lying levels only.

From the approximations above, the vibrational transition amplitude can be written as

$$A(m\rightarrow n;\varepsilon) = -\frac{2\pi}{\omega_-}\left(\frac{\Gamma^2}{k_i k_f}\right)^{1/2} a(m\rightarrow n;\varepsilon) \tag{1a}$$

where

$$a(m\rightarrow n;\varepsilon) = \sum_{\nu=0}^{\infty}\frac{<n|\nu>><<\nu|m>}{Q-\nu} \tag{1b}$$

and Q is a constant that depends on the electron impact energy ε. Note that $<n|\nu>>$ and $<<\nu|m>$ are Franck-Condon overlap integrals between vibrational levels of the initial electronic state of the target and those of the resonant anion state. Each of these Franck-Condon integrals can be written in closed form as a finite sum[2]. Evaluation of Eq. (1) will then involve two finite sums and one infinite sum which can be reduced to a single finite sum and a one-dimensional integral. As we will show, knowledge of only three low-lying transition amplitudes, in particular $a(0\rightarrow0;\varepsilon)$, $a(0\rightarrow1;\varepsilon)$ and $a(1\rightarrow1;\varepsilon)$, is required to obtain the entire matrix for vibrational excitation amplitudes. Explicit expressions for these amplitudes are:

$$A(0\rightarrow0;\varepsilon) = \frac{-i\beta N^2 T}{2\omega_-\pi}\int_0^{\infty}\frac{dt\; z^{Q+1}}{(z^2-\gamma^2)^{1/2}}\exp\left(\frac{2\beta^2\gamma}{z+\gamma}\right) \tag{2a}$$

$$A(0\rightarrow 1;\varepsilon)=\frac{-iBN^2\,\Gamma}{2\omega_-\pi}\int_0^{2\pi}\frac{dt\;z^{Q+1}}{(z^2-\gamma^2)^{1/2}}\exp\left(\frac{2\beta^2\gamma}{z+\gamma}\right)\left(\frac{z-1}{z+\gamma}\right)\left[\frac{(1-\gamma^2)\omega_-}{2\omega_0}\right]^{1/2}. \tag{2b}$$

$$A(1\rightarrow 1;\varepsilon)=\frac{-iBN^2\,\Gamma}{4\omega_-\pi}\int_0^{2\pi}\frac{dt\;z^{Q+1}}{(z^2-\gamma^2)^{1/2}}\exp\left(\frac{2\beta^2\gamma}{z+\gamma}\right)\left[\frac{z(1-\gamma^2)}{z+\gamma}\right]\left[\frac{2}{z-\gamma}+\frac{\omega_-(z-1)^2}{z\omega_0(z+\gamma)}\right]. \tag{2c}$$

where z=exp(it) and B, N, α, β, γ and ω_- are constants.

Recursion relations among the Franck-Condon integrals[2] allow us to write recursion relations among the vibrational excitation amplitudes. These recursion relations are:

$$\begin{aligned}&\left[2n(\omega^2+\omega_-^2)-4\omega\omega_-(Q+1)+(\omega+\omega_-)^2+\frac{2\omega\omega_-^2}{\omega_0}\right]a(m\rightarrow n;\varepsilon)+4\omega\omega_-\delta_{m,n}\\&-2\omega_-^2(2\omega/\omega_0)^{1/2}\left[(n+1)^{1/2}a(m\rightarrow n+1;\varepsilon)+n^{1/2}a(m\rightarrow n-1;\varepsilon)\right]\\&-(\omega^2-\omega_-^2)\left\{[(n+1)(n+2)]^{1/2}a(m\rightarrow n+2;\varepsilon)+[n(n-1)]^{1/2}a(m\rightarrow n-2;\varepsilon)\right\}=0.\end{aligned} \tag{3a}$$

$$\begin{aligned}&\left[2m(\omega^2+\omega_-^2)-4\omega\omega_-(Q+1)+(\omega+\omega_-)^2+\frac{2\omega\omega_-^2}{\omega_0}\right]a(m\rightarrow n;\varepsilon)+4\omega\omega_-\delta_{m,n}\\&-2\omega_-^2(2\omega/\omega_0)^{1/2}\left[(m+1)^{1/2}a(m+1\rightarrow n;\varepsilon-\omega)+m^{1/2}a(m-1\rightarrow n;\varepsilon+\omega)\right]\\&-(\omega^2-\omega_-^2)\left\{[(m+1)(m+2)]^{1/2}a(m+2\rightarrow n;\varepsilon-2\omega)+[m(m-1)]^{1/2}a(m-2\rightarrow n;\varepsilon+2\omega)\right\}=0.\end{aligned} \tag{3b}$$

Note that in Eq. (3a) the initial vibrational level m and the incident electron energy ε are fixed in each term. In Eq. (3b), however, the initial vibrational level m is different in various terms but the final level n is fixed. Furthermore, the incident electron energy is different although the total energy is the same in each term of the recursion relation.

As an illustration of the utility of the recursion relations derived above, we have numerically evaluated the vibrational excitation amplitudes for Li_2 and N_2 using Eqs. (1) and (3a). The inelastic excitation cross sections for Li_2 show characteristics similar to those of molecular hydrogen as expected. Experimentally the vibrational excitation cross sections for N_2 exhibit a series of spectacular peaks. The present model can successfully account for occurence and locations of these peaks in the cross sections for low lying transitions.

The support of the Air Force Office of Scientific Research through Grant Number AFOSR-84-0143 is gratefully acknowledged.

References

1. J.M. Wadehra, in Nonequilibrium Vibrational Kinetics, ed. M. Capitelli (Springer-Verlag, Heidelberg 1986) p. 191-232.

2. P.J. Drallos and J.M. Wadehra, J. Chem. Phys. 85, 6524 (1986).

40th ANNUAL GASEOUS ELECTRONICS CONFERENCE

13-16 October 1987

ATLANTA, GEORGIA

PLEASE TYPE NAME, ADDRESS & TELEPHONE NUMBER	AUTHORS PLEASE NOTE	DO NOT WRITE IN THIS SPACE
Paul J. Drallos Dept. of Physics and Astronomy, Wayne State University, Detroit, MI 48202 (313)-577-2745	Indicate topic(s) covered in the paper by selecting a letter and a digit from the attached list. If more than one, present in order of importance. Indicate preferred mode of presentation ☒ Poster ☐ Lecture ☐ Either Letter / Digit: F 1; K 2	Serial No. ____ Accepted: Yes ____ No ____ Session ____ Number ____ Date. Conf. ____

TYPE ABSTRACT ENTIRELY WITHIN THE BLUE RECTANGLE BELOW AND ACCORDING TO RULES OF AMERICAN PHYSICAL SOCIETY. SEE BULLETIN OF THE AMERICAN PHYSICAL SOCIETY FOR DETAILS.

DO NOT TYPE IN THIS BLOCK

THIS SPACE 12.0 x 10.5 CM

TYPE ABSTRACT ENTIRELY WITHIN THIS RECTANGLE

Time Evolution of Electron and Positron Swarms ~~in Neon~~*. P.J. Drallos and J.M. Wadehra, Wayne State University - The time evolution of swarm parameters in gaseous neon are calculated using a finite difference solution of the Boltzmann Equation. The finite difference method provides a more accurate representation of the distribution function[1] than does the more commonly used two-term expansion method. However, this method normally leads to strong instabilities due to derivatives which must be evaluated numerically. In the present work we use a novel algorithm for evaluation of the derivatives in which they can be obtained simply and exactly, thus eliminating the instability problems normally associated with this method. Swarm parameters for electrons and positrons in neon are calculated for various values of E/N.

* Research supported by the U.S. Air Force Office of Scientific Research through Grant No. AFOSR 84-0143.

1 H. Tagashira et al., J. Phys. D 11, 283 (1978).